Microbial-Induced Calcium Carbonate Precipitation: from Micro to Macro Scale

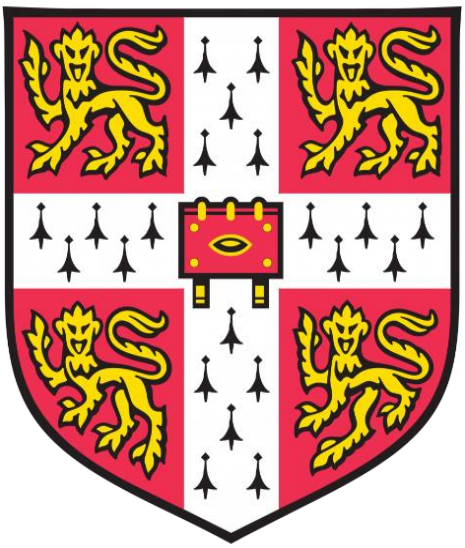

Yuze Wang

Department of Engineering

University of Cambridge

This dissertation is submitted for the degree of

Doctor of Philosophy

Queens' College

September 2018

Abstract

Yuze Wang

Microbial-Induced Calcium Carbonate Precipitation: from micro to macro scale

Microbial-Induced Calcium Carbonate ($CaCO_3$) Precipitation (MICP) is a biological process in which microbial activities alter the surrounding aqueous environment and induce $CaCO_3$ precipitation. Because the formed $CaCO_3$ crystals can bond soil particles and improve the mechanical properties of soils such as strength, MICP has been explored for potential engineering applications such as soil stabilisation. However, it has been difficult to control and predict the properties of $CaCO_3$ precipitates, thus making it very challenging to achieve homogeneous MICP-treated soils with the desired mechanical properties. This PhD study investigates MICP at both micro and macro scales to improve the micro-scale understandings of MICP which can be applied at the macro-scale for improving the homogeneity and mechanical properties of MICP-treated sand.

A microfluidic chip which models a sandy soil matrix was designed and fabricated to investigate the micro-scale fundamentals of MICP. The first important finding was that, during MICP processes, phase transformation of $CaCO_3$ can occur, which results in smaller and less stable $CaCO_3$ crystals dissolving at the expense of growth of larger and more stable $CaCO_3$ crystals. In addition, it was found that bacteria can aggregate after being mixed with cementation solution, and both bacterial density and the concentration of cementation solution affect the size of aggregates, which may consequently affect the transport and distribution of bacteria in a soil matrix. Furthermore, bacterial density was found to have a profound effect on both the growth kinetics and characteristics of $CaCO_3$. A higher bacterial density resulted in a quicker formation of a larger amount of smaller crystals, whereas a lower bacterial density resulted in a slower formation of fewer but larger crystals.

Based on the findings from micro-scale experiments, upscaling experiments were conducted on sandy soils to investigate the effect of injection interval on the strength of MICP treated soils and the effects of bacterial density and concentration of cementation solution on the

uniformity of MICP treated soils. Increasing the interval between injections of cementation solution (from 4 h to 24 h) increased the average size of $CaCO_3$ crystals and the resulting strength of MICP-treated sand. An optimised combination of bacterial density and cementation solution concentration resulted in a relative homogeneous distribution of $CaCO_3$ content and suitable strength and stiffness of MICP-treated sand.

This thesis study revealed that a microfluidic chip is a very useful tool to investigate the micro-scale fundamentals of MICP including the behaviour of bacteria and the process of $CaCO_3$ precipitation. The optimised MICP protocols will be useful for improving the engineering performance of MICP-treated sandy soils such as uniformity and strength.

Declaration

I hereby declare that this dissertation is the result of my own work and includes nothing which is the outcome of work done in collaboration except as declared in the Preface and specified in the text.

I also declare that it is not substantially the same as any that I have submitted, or, is being concurrently submitted for a degree or diploma or other qualification at the University of Cambridge or any other University or similar institution except as declared in the Preface and specified in the text. I further state that no substantial part of my dissertation has already been submitted, or, is being concurrently submitted for any such degree, diploma or other qualification at the University of Cambridge or any other University or similar institution except as declared in the Preface and specified in the text.

I confirm that this dissertation contains less than 65,000 words including appendices, bibliography, footnotes, tables and equations and has less than 150 figures, as required by the Engineering Degree Committee.

Yuze Wang

September 2018

Acknowledgements

First and foremost, I would like to express my sincere gratitude to my supervisors Professor Kenichi Soga and Dr Alexandre Kabla for supervising this PhD project and for providing me with help, support, advice and motivation throughout the course my PhD. Professor Kenichi Soga has been an inspiring role model not only in his profound knowledge and admirable work, but also in the way that he works with his students. Even after he moved to Berkeley in the US, he continued constantly supporting my research in every way possible. Dr Alexandre Kabla was my PhD advisor during my first two years and became my primary supervisor after Professor Kenichi Soga moved to Berkeley. He is an expert in microfluidics and gave me a lot of useful advice at the start of my PhD. He also greatly supported me as a supervisor during the final year of my PhD. I really consider myself privileged to have worked with them. I have learned a lot from them, and for this, I am most grateful.

I would also like to deliver my special thanks to Professor Jason DeJong of the University of California at Davis for the chance to work with him during the second year my PhD during his visit to Cambridge. Professor Jason DeJong is an expert in MICP and has a lot of experience in it. He gave me many useful suggestions for my research, and I feel that his visit greatly influenced my research. In addition, I would also like to thank Prof Douglas C. Nelson for giving lots of suggestions regarding my research whilst I was vising UC Davis in December 2017.

My special thanks also go to all of the other people who have been providing me with a lot of help with my research over the years of my PhD. I would like to thank Dr Ningjun Jiang and Dr Osama Dawoud for helping me a lot at the start of my PhD; Mr Charalampos Konstantinou and Mr Christopher Wilkes for helping me with my soil experiments whenever I needed help; Professor Tuomas Knowles for granting access to his laboratory in the Chemistry Department, University of Cambridge; Dr Thierry Savin and Dr Jerome Charmet for teaching me how to fabricate a microfluidic chip; Dr Giovanna Biscontin, Dr Xiaomin Xu, Dr Fei Jin and Dr Livia Ribeiro de Souza for giving me advice on my research; Dr Xiang Sun for teaching me how to use COMSOL to simulate fluid transport; Prof Toshiro Hata, Dr Chaosheng Tang, Dr

Kazuyuki Hayashi and Mr Tsubasa Sasaki for discussing MICP techniques; Prof Gopal Santana Phani Madabhushi for his feedback on my first year report and Prof Malcolm Bolton for his insightful suggestions during seminars.

I would also like to deliver my thanks to my officemates and friends at GRO, colleagues in the Geotechnical group and lab mates in the biolabs. They provided a pleasant working environment and spending the spare time with them is always enjoyable.

My appreciation also goes to my college tutor Dr Laurence Tiley for his support over the past few years. I would like to thank laboratory technicians Mr Chris Knight, Mr Alex Casabuena-Rodriguez, Mr Len Howlett, administrative staff Mrs Jennifer Fusiello, and IT officer Mr Tim Ablett for being friendly, professional and supportive. I would also like to thank my examiners for their time looking through my thesis and my viva.

I am also extremely grateful to the Chinese Scholarship Council and Cambridge Trust Scholarship Council for funding my PhD in Cambridge; Cambridge Philosophical Society and Great Britain-China Centre for financially supporting me during the last five months of my research; Cambridge Philosophical Society, Cambridge Trust Scholarship Council, Queens' College Cambridge and the Engineering Department for providing me with financial support to attend conferences.

Last but certainly not least, I would like to express all my love and gratitude to my parents, my boyfriend, my aunts and cousin for giving me endless love, support and encouragement throughout every stage of this PhD.

Table of Contents

List of Figures

List of Tables

List of Abbreviations

°C	Degree Celcius
[−]	Concentration
µm	Micron or micrometres [L]
μm^2	Square micrometres [L^2]
μm^3	Cubic micrometres [L^3]
µl	Microliters
µS	Microsiemens
1-D	One dimensional
2-D	Two dimensional
3-D	Three dimensional
%	Percent
$-CH_3$	Methyl groups
-Si-O-H	Silanol groups
ε_f	Axial strain at failure
A	Area [L^2]
A	Arrhenius constant
A	Aggregated
ACC	Amorphous calcium carbonate
ATCC	American Type Culture Collection
ASTM	American Society for Testing and Materials
BA	Bacterial aggregates
BS	Bacterial suspension
C	Concentration [M L^{-3}]
C	Calcite
CA	$CaCO_3$ aggregates
C_{urea}	Concentration of urea [M L^{-3}]
$C_{bacteria}$	Bacterial density
C_{Ca2+} *or* [Ca^{2+}]	Concentration of Ca^{2+}
Ca	Calcium
Ca^{2+}	Calcium ion
$CaCl_2$	Calcium chloride

$CaCl_2\ 2H_2O$	Calcium chloride dihydrate
$CaCO_3$	Calcium carbonate
CCS	Carbon capture and storage
CO_3^{2-}	Carbonate ions
CFU	Colony-forming units
cm	Centimetre(s) [L]
cm^2	Square centimetre(s) [L^2]
CO_2	Carbon dioxide
$CO(NH_2)_2$	Urea
CS	Cementation solution
d	Day(s)
D	Diameter [L]
D_{10}	Sieve size passed through by the first 10 % by weight of soil
D_{50}	Sieve size passed through by the first 50 % by weight of soil
D_{90}	Sieve size passed through by the first 90 % by weight of soil
Da	The ratio of reaction rate to transport rate
Dd	Diffusion coefficient [$L^2\ T^{-1}$]
DO	Dissolved oxygen
DI	Deionised
DSMZ	Deutsche Sammlung von Mikroorganismen und Zellkulturen
E_{act}	Activation energy
EPS	Extracellular polymeric substances
F	Force
g	Gram [M]
g/g	grams of $CaCO_3$ per gram of soil
H	Height [L]
H^+	Hydrogen ion
HCl	Hydrochloric acid
H_2O	Water
hr or h	Hour(s) [T]
i	Hydraulic gradient [unitless]
ISP	Irregular-shaped precipitates
k	Hydraulic conductivity (water permeability) [LT^{-1}]
[K]	Product constant

K_{sp}	Equilibrium $CaCO_3$ solubility product
K_m	The substrate concentration at which the reaction rate is half of Vmax (The Michaelis constant)
kg	Kilogram [M]
kN	Kilo Newton(s) [MLT^{-2}]
kPa	Kilo Pascal(s)
l	Litre(s)
L	Length
m	Metre(s)
mM	Millimolar [ML^{-3}]
M	Molar (mole/litre) [ML^{-3}]
m^2	Square meter [L^2]
m^3	Cubic meter [L^3]
mg	Miligrams(s) [M]
ml	Millilitre(s) [L^3]
min	Minute(s) [T]
mm	Millimetre(s)
MPa	Mega Pascal(s)
MICP	Microbially-Induced carbonate precipitation
mS	Millisiemen (s)
n	Porosity [dimensionless]
n	Reaction order
n	The number of times each measurement was repeated
Na_2CO_3	Sodium carbonate
$NaHCO_3$	Sodium bi-carbonate
NH_4^+	Ammonium ion
NH_4Cl	Ammonium chloride
$(NH_4)_2SO_4$	Ammonium sulphate
NH_4-YE	Ammonium-yeast
nm	Nano meter
OD	Optical density
OD_{600}	Optical density at 600 nanometres
OH^-	Hydroxyl ion
PV	Pore volume

PDMS	Polydimethylsiloxane
PVC	Polyvinyl chloride
Q	Volumetric flow [L^3T^{-1}]
r	Radius [L]
R	Gas constant [$L^3M^{-1}\theta^{-1}$]
R	Rhombohedral
R^2	Correlation coefficient
r_u	Ureolysis rate
r_p	Precipitation rate
rpm	Rotations per minute
S	Spherical
(s)	(solid)
S. pasteurii	*Sporosarcina pasteurii*
Sec	Second(s)
SEM	Scanning Electron Microscopy
t	Time
T	Temperature
TEM	Transmission electron microscopy
U	μmol of urea hydrolyzed per minute
UCS	Unconfined Compressive Strength
UV	Ultraviolet
v	Velocity [LT^{-1}]
V_{max}	Maximum ureolysis rate (mMT^{-1}) in Michaelis-Menten model
V	Vaterite
XRD	X-Ray Diffraction

Chapter 1 Introduction

1.1 Research background

1.1.1 Bio-considerations in the field of geotechnical engineering

Studies of soil behaviour in the field of geotechnical engineering in the 19^{th} - 20^{th} century considered soils as an inert construction material and had been primarily focussed on mechanical principles, geological processes, mineralogy and colloidal chemistry (Mitchell and Santamarina, 2005). However, there are an estimated 10^9 to 10^{12} organisms in a kilogram of soil near the ground surface (Mitchell and Santamarina, 2005), and the variability and changes in properties of ground due to the effect of microbial activities over time mean that engineering mechanics alone are insufficient to address many practical problems (DeJong et al., 2013). In the past one to two decades, some biological processes such as bio-mineralization, biofilm generation and biogas production have been suggested as potential soil improvement techniques (DeJong et al., 2010). The consideration of soil as a living ecosystem was addressed in the field of geotechnical engineering (DeJong et al., 2013). **Figure 1.1** shows an overview of the bio-mediated soil improvement techniques which use biological activity to manage and control chemical reactions within soils and produce by-products that alter the engineering properties of soil (DeJong et al., 2010).

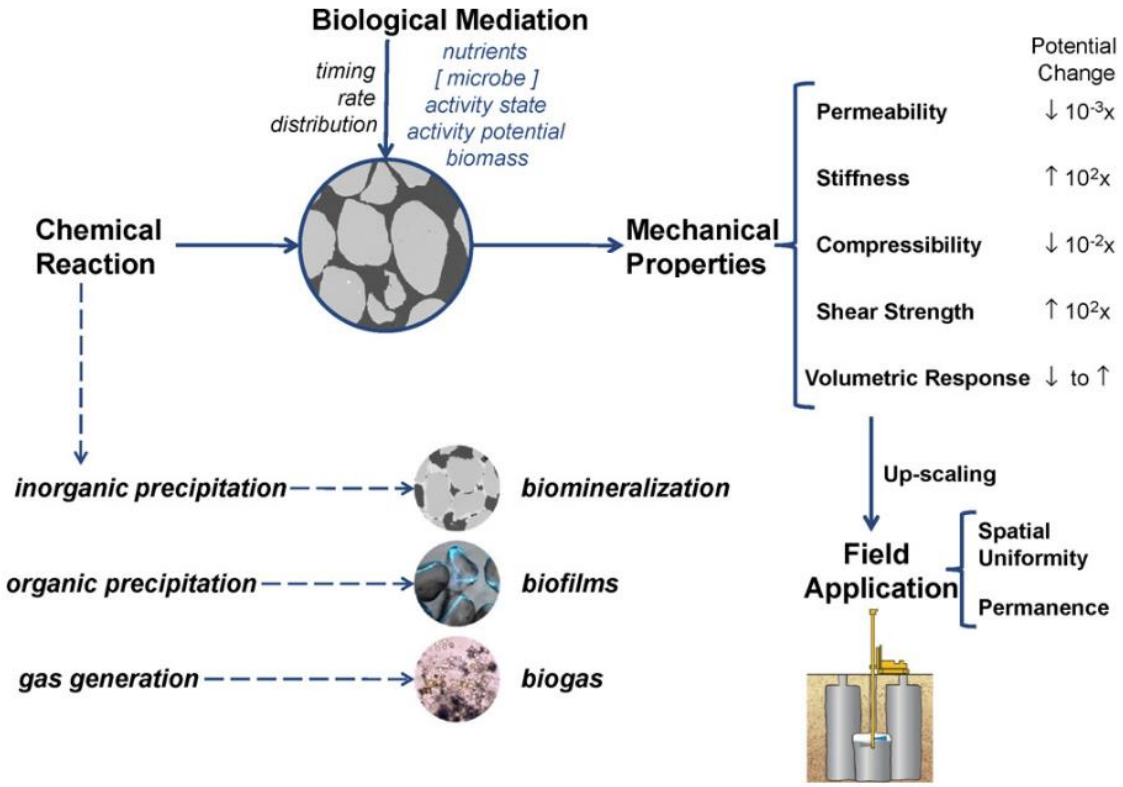

Figure 1.1 Overview of bio-mediated soil improvement systems (DeJong et al., 2010)

1.1.2 Microbial-Induced Calcium Carbonate Precipitation (MICP)

Microbial-Induced Calcium Carbonate Precipitation (MICP) is a bio-mediated soil improvement technique in which subsurface microbes are employed to create a supersaturated environment conducive to the desired carbonate precipitation (Stocks-Fischer et al., 1999). Several possible bio-mediated processes such as ureolysis (urea hydrolysis), denitrification and sulfate reduction (DeJong et al., 2010), could be used to induce MICP. Among these, ureolysis has been the most widely explored MICP treatment process due to its ease of control, high chemical conversion efficiency and short amount of time required (Dhami et al., 2013). During the ureolysis-driven MICP process, bacteria with ureolytic activity express a urease enzyme which catalyses the hydrolysis of urea (*Equation 1.1*); the addition of calcium (Ca^{2+}) to this system induces the precipitation of calcium carbonate ($CaCO_3$) as the CO_3^{2-} ions produced by the hydrolysis of urea react with the supplied Ca^{2+} (*Equation 1.2*) (van Paassen et al., 2010; Al Qabany and Soga, 2013):

$$CO(NH_2)_2 + 2H_2O \xrightarrow{Urease} 2NH_4^+ + CO_3^{2-} \quad 1.1$$

$$Ca^{2+} + CO_3^{2-} \rightarrow CaCO_3(s) \quad 1.2$$

The $CaCO_3$ crystals formed can bond soil particles together, thus increasing the strength of soils (DeJong et al., 2006, 2010), whilst maintaining the permeability (Al Qabany and Soga, 2013). Therefore, MICP has many potential applications including soil stabilization, liquefaction prevention, dam safety, erosion prevention, slope stabilization and hydraulic control (van Paassen et al., 2010; DeJong et al., 2013; Montoya et al., 2013; Jiang et al., 2017). However, it is worth noting that the application of MICP is not limited to soil improvement, as it can also be applied in concrete remediation (Kim et al., 2013; Joshi et al., 2017) and soil environmental-remediation (Warren et al., 2001; Fujita et al., 2010).

1.2 Research challenges

Although a large body of research has been conducted on ureolysis-driven MICP for its potential application in soil stabilization, many challenges still remain. Due to a lack of available methods to visualise and study the process of $CaCO_3$ precipitation occurring at the conditions that can simulate real MICP applications, the micro-scale mechanisms of MICP are largely unknown. Therefore, it has so far been very challenging to control and predict the micro-scale properties of $CaCO_3$ precipitates which affect the mechanical properties of MICP-treated soils. Therefore, because the micro-scale MICP process remains unclear, it is extremely challenging to control and predict $CaCO_3$ precipitation temporally and spatially at macro-scale.

1.3 Research objectives

This PhD project focuses on developing a better understanding of the MICP process for soil stabilization at micro-scale which can be used to improve the engineering properties of MICP-treated soils at macro-scale. At the micro-scale, this study is to investigate the fundamental mechanisms of MICP, such as the behaviour of bacterial cells and $CaCO_3$ crystals, the processes of $CaCO_3$ precipitation and the kinetics and characteristic of $CaCO_3$ crystal growth

during MICP. In addition, at the macro-scale, this study also aims to improve the engineering properties of MICP-treated sand, including mechanical properties and homogeneity, by applying the improved understanding of micro-scale mechanisms in upscaling experiments. The specific objectives of this study are:

- To develop a micro-scale testing procedure for MICP which enables bacterial cells and $CaCO_3$ crystals to be observed and characterised at particle-scale throughout the entire MICP process
- To investigate the process of $CaCO_3$ precipitation during MICP and to determine the effect of modifying the MICP treatment procedure on the relationship between $CaCO_3$ precipitation and the final size of $CaCO_3$ crystals formed
- To investigate the effect of bacterial density on the growth rate (kinetics) and the micro-scale properties of $CaCO_3$ crystals
- To perform an upscaling study to investigate the effect of varying the MICP treatment procedure on the strength of MICP-treated soil samples
- To perform and upscaling study to investigate the effect of bacterial density and the concentration of cementation solution on the uniformity of MICP-treated soil samples

1.4 Structure of the thesis

The schematic of the thesis structure is shown in **Figure 1.2**. This thesis contains nine chapters.

Chapter 2 presents a literature review on MICP which includes the kinetics and process of ureolysis and $CaCO_3$ precipitation; micro-scale mechanisms of MICP and the investigation method which might be useful for studying the fundamental processes occurring during MICP at micro-scale; the macro-scale engineering properties of MICP-treated soils, and their relationships with the micro-scale properties of $CaCO_3$ precipitates.

Chapter 3 describes the materials and methods used for this research, including cultivating bacteria, measurement of bacterial density and activity, and assessment of ureolysis kinetics in liquids. This chapter also presents the setup of microscope slide experiments and microfluidic

chip experiments for MICP micro-scale studies, as well as small and long soil column experiments for MICP macro-scale studies.

Chapter 4 presents the design and fabrication of a micro-scale porous medium which can model the porous structure of a soil matrix. A series of MICP tests were conducted to investigate the utility of this porous medium to study MICP under conditions which mimic fluid flow through soil matrices and enable the number of bacterial cells and the size of $CaCO_3$ crystals to be determined.

Chapters 5 and *6* describe two micro-scale experimental studies which investigate the process and kinetics of $CaCO_3$ precipitation during MICP. In the 'process' experiment, the MICP process in terms the behaviour of both bacterial and $CaCO_3$ crystals and their changes with time was investigated. In the 'kinetics' experiment, the effects of bacterial density on the kinetics of $CaCO_3$ crystals growth and the properties of $CaCO_3$ crystals formed were addressed.

Based on the results obtained in *Chapters 4-6*, *Chapters 7* and *8* present two upscaling experimental studies conducted in soil columns to increase the strength and homogeneity of MICP-treated soils. In *Chapter 7*, different treatment procedures were conducted in an attempt to establish a correlation between the $CaCO_3$ precipitation process and the final size of $CaCO_3$ crystals formed, after which small soil column tests were conducted to study the effect of these different treatment procedures on the strength of MICP-treated soils. In *Chapter 8*, another macro-scale experiment was conducted using 1.2-metre long soil columns in attempt to optimise the biological properties and chemical reactants of MICP, the density of the bacterial suspension and the concentration of cementation solution, to increase the homogeneity of MICP-treated soils.

Finally, *Chapter 9* contains a summary of the main results of this study, the limitations and the implications of this study, as well as recommendations for future work.

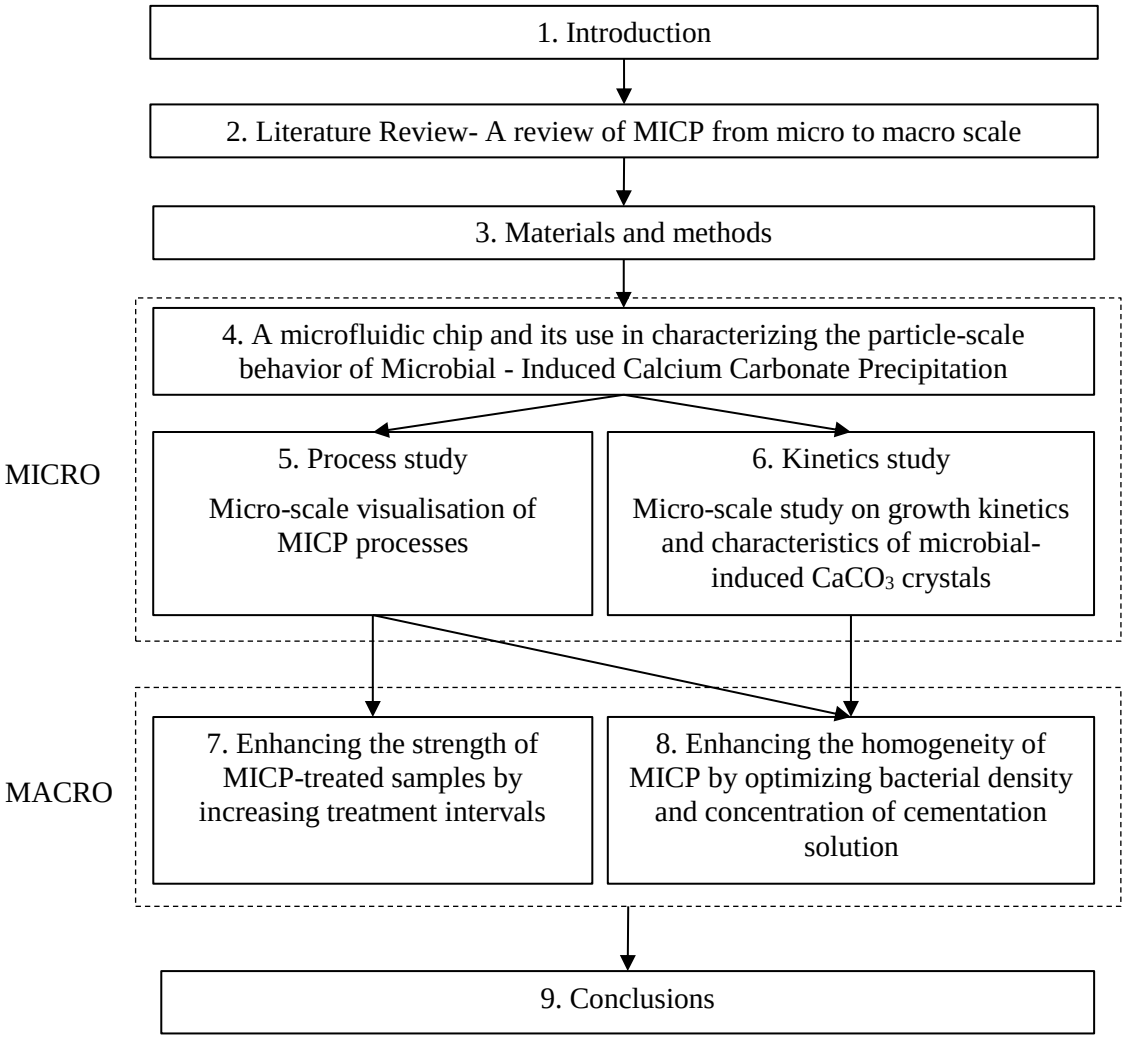

Figure 1.2 Schematic of the thesis structure

Chapter 2 Literature review

2.1 Introduction

Microbial-Induced Calcium Carbonate ($CaCO_3$) Precipitation (MICP) is a natural biomineralisation process in which microbial activity alters the surrounding aqueous environment and produces $CaCO_3$ (Stocks-Fischer et al., 1999; DeJong et al., 2006). The $CaCO_3$ precipitates formed in soil porous matrixes have been shown to be able to bond soil particles and fill soil pores, which consequently increases the strength and stiffness of the soils. As a result, MICP has been proposed as a promising soil stabilization technique.

Compared with traditional soil stabilization materials such as synthetic cement which is highly alkaline and may contaminate the groundwater, $CaCO_3$ is one of the main natural components of many soils, therefore is more environmental friendly (DeJong et al., 2006; Zhang et al., 2018). In addition, the bacterial suspensions and chemical solutions used in MICP have much lower viscosities (similar to water) than cement slurry, and therefore they can be delivered a longer distance from the injection point (up to 5 meter by Whiffin et al., 2007) or penetrate small fractures (Phillips et al., 2013a) where it is difficult for cement to penetrate. The low-viscosity liquids also cause less pressure within the subsurface (Phillips et al., 2013a). Furthermore, unlike cement, a ureolysis-driven MICP process enables the amount of $CaCO_3$ to be controlled by varying the amount of reactants such as urea and $CaCl_2$ that are injected into soils, thus allowing soils to be strengthened whilst maintaining adequate permeability (van der Ruyt et al., 2009; Burbank et al., 2011). This is very useful for avoiding the pore water pressure increasing and therefore can be used in applications such as slope liquefaction or dam erosion control (van der Ruyt et al., 2009). Apart from being proposed for soil stabilization, MICP has also been considered for alternative applications such as surface treatment (De Muynck et al., 2011), repairing cracks in concrete or building materials (Achal et al., 2013; Joshi et al., 2017),

pore plugging in carbon capture and storage (CCS) (Mitchell et al., 2010) and environmental remediation of heavy metal contaminated soils (Lauchnor et al., 2013).

Despite the extensive studies that have been conducted, there are still many challenges in the research field of MICP, such as the control and prediction of the properties of $CaCO_3$ spatially and temporally at both micro-scale (soil particle-scale) and macro-scale (soil matrix-scale). However, this is crucially important because both the micro-scale properties of $CaCO_3$, such as size, number and distribution, and the macro-scale content of $CaCO_3$ may significantly affect the engineering properties of MICP-treated soils (DeJong et al., 2010; Al Qabany and Soga, 2013; Cheng et al., 2017).

At the micro-scale, the properties of $CaCO_3$ mainly refer to the type, size, number, and distribution of $CaCO_3$ crystals, which directly affect the ability of $CaCO_3$ crystals to bond soil particles or fill soil pores, thus affecting the extent to which MICP is able to improve the strength and permeability of the soil matrix at the macro-scale (DeJong et al., 2010; Al Qabany and Soga, 2013; Cheng et al., 2017). The properties of $CaCO_3$ crystals may change both spatially and temporally at the micro-scale during their formation process. Understanding the process of $CaCO_3$ crystal formation under different conditions would be useful for engineers to design MICP treatment protocols that can produce the desired properties of $CaCO_3$ crystals for different applications. In addition, the growth rate of $CaCO_3$ crystals is another factor that needs to be considered. For given properties of $CaCO_3$ crystals, a faster growth rate will reduce the time taken for the $CaCO_3$ precipitation process to become complete, which would be beneficial for large-scale engineering applications of MICP (van Paassen, 2009). Both the process and rate of $CaCO_3$ crystal formation might be affected by the amount of bacterial cells in the soil pores at the micro-scale, which in turn may be affected by the initial density and transport behaviour of bacteria with flow (Tobler et al., 2014), as well as by the attachment of bacteria to soil particles (Dunne, 2002; Persat et al., 2015). In addition, chemicals such as Ca^{2+} have also been reported to cause bacterial aggregation (EI Mountassir et al., 2014), and the formation of bacterial aggregates might affect the amount of bacteria in the pores and hence the process and rate of $CaCO_3$ crystal formation. Furthermore, the formation process and growth rate of $CaCO_3$ crystals may also be affected by the concentrations and distribution of

urea and Ca^{2+} (Al Qabany and Soga, 2013), as well as by environmental factors such as temperature, pH and oxygen concentration (Cheng et al., 2017).

At the macro-scale, the properties of $CaCO_3$ normally refer to $CaCO_3$ content, which is the mass or volume of $CaCO_3$ relative to the mass or volume of soil particles or soil matrix (Whiffin et al., 2007; van Paassen, 2009; Al Qabany and Soga, 2013). $CaCO_3$ content has been suggested to affect the engineering properties of MICP-treated soils (Whiffin et al., 2007; van Paassen, 2009; Al Qabany and Soga, 2013). Ideally, the $CaCO_3$ content needs to be homogenously distributed throughout the whole volume of soil matrix being used for MICP treatment. However, treatment homogeneity remains the most critical component to date (Mujah et al., 2017). In theory, the local $CaCO_3$ content can be predicted as long as the local amount of chemicals, urea, Ca^{2+} and the chemical reaction efficiency (the percentage of urea and Ca^{2+} that transform into $CaCO_3$ precipitates, Al Qabany et al., 2012) are known. However, the injection of bacteria and chemicals inside a soil matrix is a reactive-transport process in which the biochemical reactions involving bacteria occur during and after the transport of bacteria and chemicals through the soil matrix (Phillips et al., 2013b). Therefore, to predict the $CaCO_3$ content spatially and temporally, it is essential to understand how bacteria and chemicals are transported through a soil matrix and the factors affecting their transport, how the bio-chemical reaction occurs during or after transport, and how the transport and reaction affect each other. To understand these, micro-scale fundamentals such as the interactions between bacterial cells with soil particles, interactions between bacteria and chemicals and interactions between flow rate and reaction rate need to be considered.

Therefore, understanding MICP from both micro-scale fundamentals to macro-scale engineering properties and the correlations between them is essential for designing robust and effective MICP treatment protocols. This chapter focusses on reviewing MICP in terms of its micro-scale mechanisms and macro-scale properties. To begin with, basic principles associated with MICP via the urea hydrolysis pathway, including the kinetics of ureolysis and precipitation and the process of $CaCO_3$ precipitation, will be reviewed (*Section 2.2*). Ureolysis-driven MICP studies at both micro- and macro-scales will also be reviewed (*Sections 2.3* and *2.4*). At the micro-scale, this review focusses on: 1) the properties of bacteria used in MICP, such as morphology, their interactions with chemicals, solid surfaces and flow, and the effect

of bacteria on $CaCO_3$ formation; 2) the properties of $CaCO_3$ observed in MICP-treated samples along with the parameters that affect them; and 3) the current understanding of the micro-scale process of $CaCO_3$ crystal formation during MICP. At the micro-scale, a microfluidic technique as a novel method that could be used to investigate the micro-scale properties and processes of MICP under the conditions which represent the real MICP conditions is also reviewed. At the macro-scale, this review focusses on the engineering properties of MICP-treated soils such as strength, uniformity, and efficiency.

2.2 Process and kinetics of ureolysis and carbonate precipitation

Ureolysis and $CaCO_3$ precipitation are the two key processes involved in the ureolysis-driven MICP process, and understanding the kinetics and process of these two process is essential for designing a MICP protocol. When MICP is applied for soil stabilization, the $CaCO_3$ content produced in the soil matrix is controlled by the amount of urea and Ca^{2+} (volume multiplied by concentration) injected and the chemical transform efficiencies of urea hydrolysis and $CaCO_3$ precipitation (*Equations 1.1* and *1.2*). To produce the desired $CaCO_3$ content, it is essential to know how much urea and Ca^{2+} to inject and the amount of time required for the reactions (*Equations 1.1* and *1.2*) to complete. The time needed for the reactions to complete is dependent on both the ureolysis rate and precipitation rate. Understanding the kinetics of these two reactions is important for predicting and controlling the time needed for MICP, which is useful for designing an appropriate MICP protocol for its engineering applications. Studies relating to the kinetics of ureolysis and $CaCO_3$ precipitation are reviewed in *Sections 2.2.1* and *2.2.2*, respectively.

2.2.1 Kinetics of ureolysis

Ureolysis kinetics are determined by the rate of ureolysis and the factors that affect this rate. The ureolysis rate (r_u) is defined as the rate of decrease in the concentration of urea (C_{urea}) with time (t) (*Equation 2.1*).

$$r_u = -\frac{dC_{urea}}{dt} \qquad 2.1$$

The rate of ureolysis is influenced by several factors such as the concentration of urea, bacterial density, Ca^{2+} concentration, temperature, pH and oxygen concentration (Stocks-Fischer et al., 1999; Ferris et al., 2003; Dupraz et al., 2009; van Paassen, 2009; Tobler et al., 2011; Mortensen et al., 2011; Lauchnor et al., 2015) (*Equation 2.2*):

$$r_u = -\frac{dC_{urea}}{dt} = f(C_{urea}, C_{bacteria}, C_{ca^{2+}}, temperature, pH, oxygen, ...) \quad 2.2$$

2.2.1.1 Influence of urea concentration on ureolysis rate

The ureolysis reaction (*Equation 1.1*) is a reaction that is catalysed by the urease enzyme. When only urea and urease are present in a urease-urea reaction system, the ureolysis rate is affected by the concentration of urea and the specific activity of the urease enzyme. The Michaelis-Menten model, a common model used to describe the kinetics of enzyme-catalysed reactions, can be used to describe the correlation between ureolysis rate and urea concentration. In this model, the activity of urease is assumed to be constant. Based on the Michaelis- Menten model, the ureolysis rate r_u is calculated using *Equation 2.3*:

$$r_u = \frac{V_{\max} C_{urea}}{K_m + C_{urea}} \quad 2.3$$

where C_{urea} is the urea concentration (mM), V_{max} (mM/h) represents the maximum ureolysis rate and K_m (mM/L) represents the urea concentration at which the initial reaction rate is half maximal (Stocks-Fischer et al., 1999). The typical Michaelis-Menten curve is shown in **Figure 2.1.**

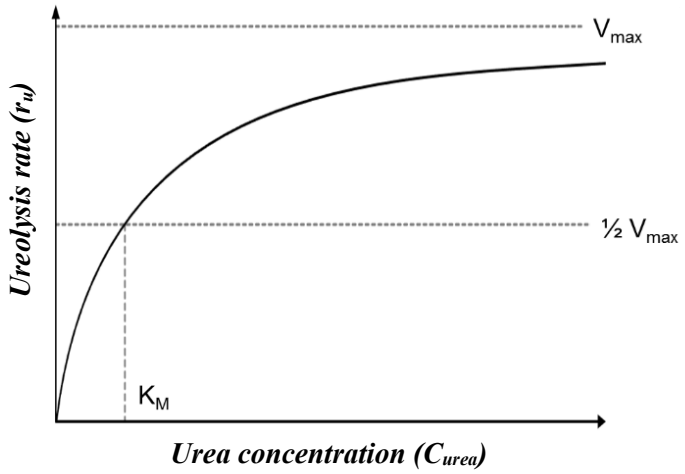

Figure 2.1 Michaelis-Menten curve for ureolysis showing the relationship between the urea concentration (C_{urea}) and ureolysis rate (r_u). K_m represents the urea concentration at which the initial reaction rate is half maximal ($1/2 V_{max}$)

The typical method for determining the constants K_m and V_{max} involves running a series of liquid batch tests at varying urea concentrations whilst keeping all the other experimental variables constant and measuring the ureolysis rate shortly after the mixing of urease and urea solution. In the case of testing the ureolysis rate of ureolytic bacteria, an ureolytic bacterial suspension is mixed with urea solution (Tobler et al., 2011; Mortensen et al., 2011; Lauchnor et al., 2015). A conductivity method has been widely used to determine ureolysis rate (Whiffin, 2004; Whiffin et al., 2007; van Paassen, 2009; Al Qabany and Soga, 2013). In this method, the conductivity change of a mixture of bacterial suspension and urea solution over a certain period of time is recorded, so as to calculate the ureolysis rate. This is because bacteria with an ureolysis activity hydrolyse the non-ionic substrate urea into ionic produces thus generating a proportionate increase in conductivity, and because the increase of conductivity change is linearly correlated with the change of the concentration of ionic products, the concentration of urea hydrolyzed can be calculated (Whiffin, 2004). Lauchnor et al. (2015) investigated the effect of urea concentration on the rate of ureolysis using the ureolytic bacteria *Sporosarcina pasteurii*. The range of urea concentrations investigated was 1.1 to 722 mM and the concentration of bacterial suspension was kept constant at an optical density of 0.1 when tested at 600 nm wavelength (OD_{600}- a more detailed description of bacterial density is reviewed in *Section 2.2.1.2*). Lauchnor and colleagues found that the ureolysis rate increased as the

concentration of urea increased up to 423 mM, beyond which the ureolysis rate stayed approximately constant.

2.2.1.2 Reported density and activity of *S. pasteurii* and their influence on ureolysis rate

There are many bacterial strains with urease activity which could be used in MICP studies, such as *Sporosarcina pasteurii (S. pasteurii*) (Whiffin et al., 2007; van Paassen et al., 2010), *Bacillus megaterium* (Soon et al., 2014) and *Bacillus sphaericus* (De Muynck et al., 2008). Among these bacterial strains, *S. pasteurii* is the most commonly used bacterial strain due to its high urease activity (Whiffin et al., 2007; van Paassen et al., 2010). However, even for the same bacterial strain, environmental factors such as cultivation and storage procedures may substantially affect ureolysis activity. This section summarises the reported density and activity of *S. pasteurii* and then reviews studies related to the influence of bacterial density on the rate of ureolysis.

There are normally two different ways of reporting bacterial density. The first one involves reporting the optical density (or absorbance) by measuring the proportion of light absorbed by a sample at a wavelength of 600 nm (OD_{600}). Optical density indicates the turbidity of the bacterial suspension, which is correlated with both bacterial concentration and bacterial size (Zapata and Ramirez-Arcos, 2015). A schematic illustrating how the optical density of a bacterial culture was measured is shown in **Figure 2.2**. The intensity of the light that reaches the photoelectric cell after passing through a clear sterile medium in a cuvette is taken as the reference intensity (zero extinction or zero OD). When the liquid medium contains bacterial cells, a significant portion the light is scattered and no longer reaches the photoelectric cell. Therefore, the weaker electrical signal obtained when bacterial cells are present in the cuvette is converted to an extinction or OD value. When bacterial size is the same, optical density is linearly correlated with bacterial concentration, although this correlation tends to deviate from linearity at high ODs (Widdel, 2007). Optical density does not have a unit.

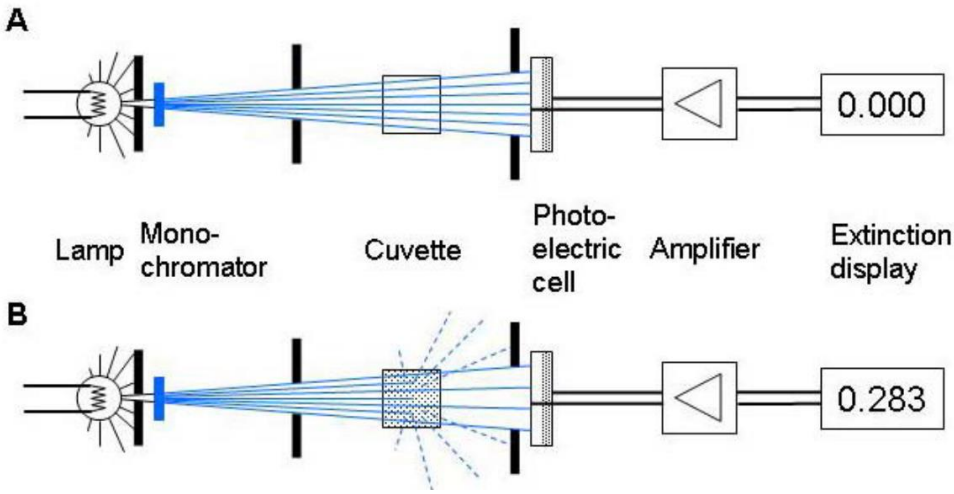

Figure 2.2 Schematic showing how the optical density (OD) of a culture is measured using a spectrophotometer (Widdel, 2007)

The second measure is bacterial density which is reported as the number of bacterial cells or colony-forming units (CFU) per millilitre of cell suspension. Bacterial density in the unit of cells/ml is normally obtained by counting the number of bacteria observed under a light microscope in a given area. However, bacterial concentration in the unit of CFU/ml is obtained by culturing the bacteria on an agar plate and counting the number of colonies that appear on the dish. Although a linear correlation between OD and cell density has been proposed (Widdel, 2007; Kim et al., 2012), different cell densities have previously been linked to the same OD value. For example, Lin et al. (2017) reported that an OD_{600} of 0.8-1.0 corresponds to a bacterial density of 1.5×10^7 cells/mL, whereas Cardoso et al. (2018) reported that an OD_{600} of 1.0 corresponds to 1.0×10^9 cells/mL - a difference of nearly two orders of magnitude. The discrepancy between OD_{600} values of the bacterial suspension and bacterial cell counts on agar plates in these studies might, on one hand, be due to the fact that the OD_{600} value accounts for both dead and live bacteria within the suspension, whereas only live bacteria are counted on agar plates. Because the ratio of live and dead bacteria in the bacterial suspensions might be different in these two studies, there would therefore be a difference in the correlations between these two values. On the other hand, as the optical density of the bacterial suspension is dependent on bacterial size (Zapata and Ramirez-Arcos, 2015) and the size of bacteria used in these studies might be different, this might cause different suspensions to have the same optical density but different bacterial densities.

There are normally two ways of reporting the urease activity of bacteria - total bacterial activity (in mM/h or U/ml) or specific bacterial activity (in mM/h/OD). The conversion of total bacterial activity from the unit of U/ml to mM/h is given as

$$1\ \text{U}=1\ \mu\text{mol of urea hydrolyzed per minute} \qquad 2.4\ a$$

$$1\ \text{U/ml}=1\mu\text{mol/minute/ml}=1\ \text{mM/min}=60\ \text{mM/h} \qquad 2.4\ b$$

Due to the fact that many factors such as cultivation, storage and testing methods (such as the bacterial density used for measuring activity and urea concentration) may affect the ureolysis activity of bacteria, different ureolysis activities for the same type and density of *S. pasteurii* bacteria have been reported in the literature. In addition, the bacterial density used in previous MICP studies also varied significantly. For comparison, a summary of the activities and densities of *S. pasteurii* reported in the literature is presented in **Table 2.1** and **Figure 2.3**. Optical density is used to indicate the bacterial density, whilst bacterial activity is stated in the unit of mM/h. Because the bacterial density and activity are tested before commencing MICP treatment, and because they may change with time during the ureolysis process, they are sometimes referred to as the initial bacterial density and initial bacterial activity. The range of bacterial activity reported for MICP is very large (2-3000 mM/h), with normal values ranging from 2 to 300 mM/h (**Figure 2.3a**). In addition, the range of bacterial densities is also large (OD_{600} values between 0.02 and 2.5), with normal values ranging between 0.2 and 1.2 (**Figure 2.3b**).

Table 2.1 Bacterial density, activity, cultivation and storage reported for ureolysis-driven MICP

OD_{600}	Bacterial activity (mM/h)	Reference
1.5	1050 (17.5 U/mL)	Sarda et al., 2009
-	Up to1100[1]	van Paassen et al., 2010
0.8–1.2	2–30[2]	Al Qabany, 2011
0.8–1.2	5–20	Al Qabany et al., 2012
0.3	-	Cuthbert et al., 2012
8×10^4 cell per ml	36	DeJong et al., 2014
0.02-0.15[3]	50-300	Lauchnor et al., 2015
0.2-0.8	-	Rowshanbakht et al., 2016
2-2.5	600 (10 U/L)	Cheng et al., 2017
1.1-11	300-3000 (5-50 U/L) [4]	Cheng et al., 2017
0.8-1(1.5×10^7 cells/mL)	-	Lin et al., 2017
0.22	*125 mM/h/OD[5]	Jiang et al., 2017
1 (~10^9 cells/mL)	-	Cardoso et al., 2018
0.8–1.0(10^7 cells/mL)	84-120	Omoregie et al., 2017[6]

Note: BA-bacterial activity. The activity reported by van Paassen (2009) (up to 1100 mM/h)[1] is relatively high, which may be because the composition of the cultivation medium (20 g/L yeast extract, 0.17 M ammonia sulphate, and 0.1 mM $NiCl_2$, with a pH value of 9.25) was different compared to the cultivation medium used in other studies. The bacterial activity reported by Al Qabany (2011) (2 mM/h) [2] was considered to be relativity low and was attributed to sub-optimal bacterial growth conditions due to the absence of an incubator and lack of proper shaking. The optical density tested was 0.02-0.15[3], lower than the other studies, which might be because the testing method involved using a Synergy HT reader (Biotek Instruments, Inc., Winooski, VT) in a 96-well plate with 100 μl per well is different than the others. The bacterial activity was extremely high in this range (3000 mM/h) [4], which is likely to be mainly due to a high bacterial density (OD_{600}=11) being used. This high bacterial density was obtained by concentrating bacterial cells by centrifugation. The specific activity was reported[5]. Bacteria isolated from soil was used in the study of Omoregie et al. (2017) [6], with the activity in the normal range as reported for the bacterial strains purched commerically.

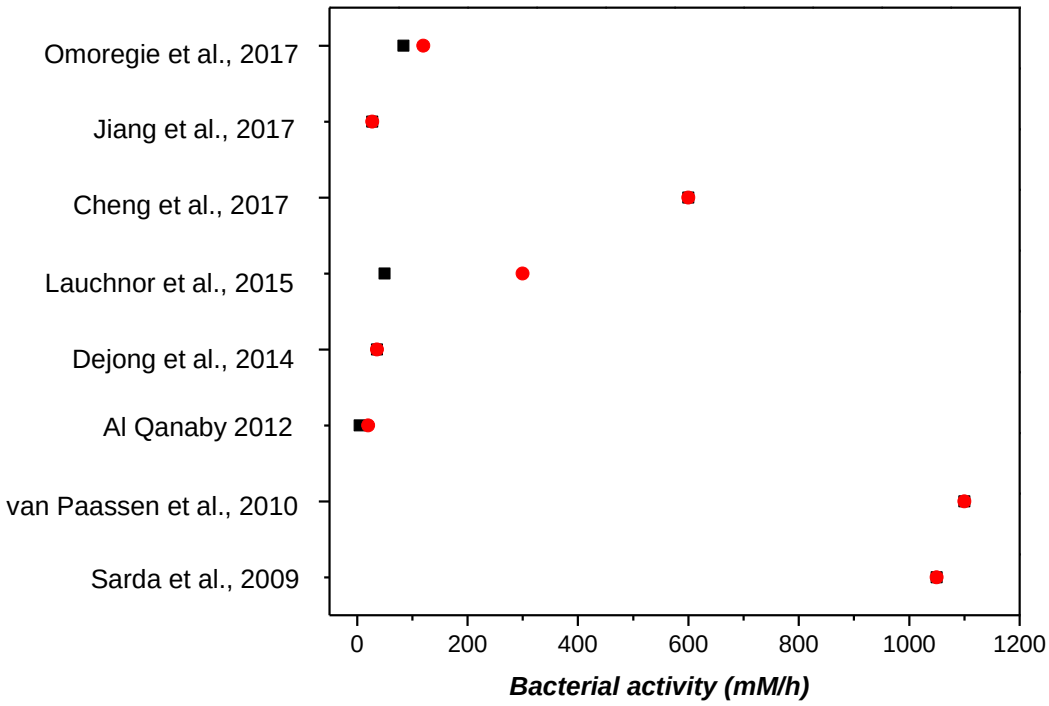

(a)

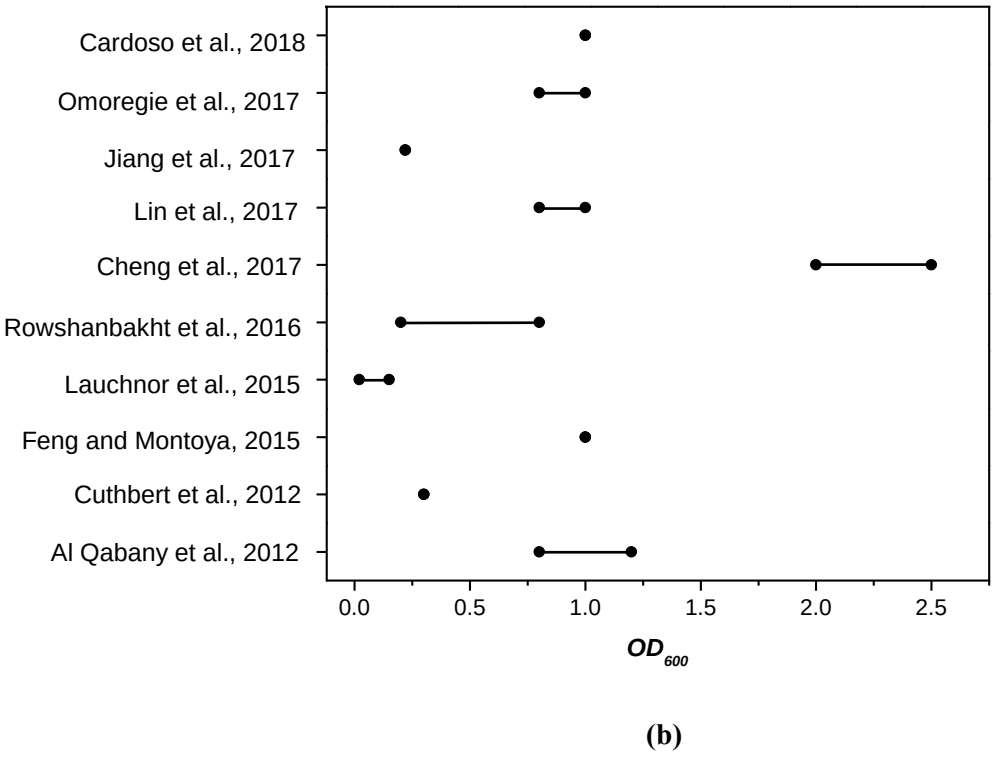

(b)

Figure 2.3 Bacterial activity and density reported for ureolysis-driven MICP: **(a)** activity; **(b)** density

The effect of bacterial density on ureolysis rate was studied in liquid batch tests by Lauchnor et al., (2015). The rate of ureolysis linearly increased from 50 mM/h to 300 mM/h with an increase in cell density from 1×10^7 to 2×10^8 colony-forming units per millilitre of cell suspension (CFU/ml), corresponding to optical densities between 0.02 and 0.15 (**Figure 2.4**) (Lauchnor et al., 2015). However, it is also suggested that at very high bacterial cell densities, saturation kinetics with respect to cell concentration might be observed, even though no experimental data was presented to confirm this (Lauchnor et al., 2015).

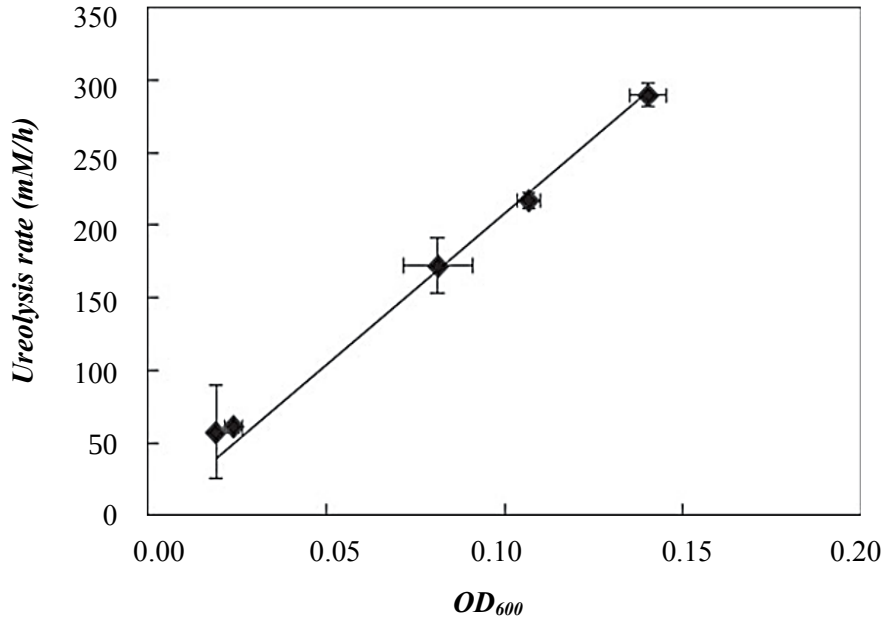

Figure 2.4 Increase in ureolysis rate with the increase in the density of *S. pasteurii* at urea concentration of 330 mM (Lauchnor et al., 2015)

2.2.1.3 Influence of other factors (Ca^{2+} concentration, temperature, pH and oxygen concentration) on ureolysis rate

In addition to the concentration of urea and the density/activity of bacterial cells, the potential effects of factors such as Ca^{2+} concentration, temperature, pH and oxygen levels on ureolysis rate have also been studied. It was found that increasing the calcium concentration up to 1.5 M resulted in a decrease in ureolytic activity to a point at which ureolysis was almost completely inhibited (van Paassen, 2009). By contrast, other studies found that the rate of ureolysis was not affected by calcium concentration up to 50 mM (Whiffin, 2004) and that Ca^{2+} concentration

in the range of 50 to 500 mM did not inhibit the ureolytic activity of *S. pasteurii* (Tobler et al., 2011). Therefore, the precise effect of Ca^{2+} concentration on the rate of ureolysis remains unclear.

Temperature has been reported to affect the rate of urea hydrolysis. For example, a previous study reported that the ureolysis rate of *S. pasteurii* was stable between 15 and 25°C and exhibited a linear increase between 25 and 60°C, reaching an optimum at 70°C, above which the urease activity quickly decreased (Whiffin, 2004). However, van Paassen (2009) reported that a rise of 10°C within the temperature range of 5-35°C causes the urease activity to increase by a factor of 3.4 (**Figure 2.5**).

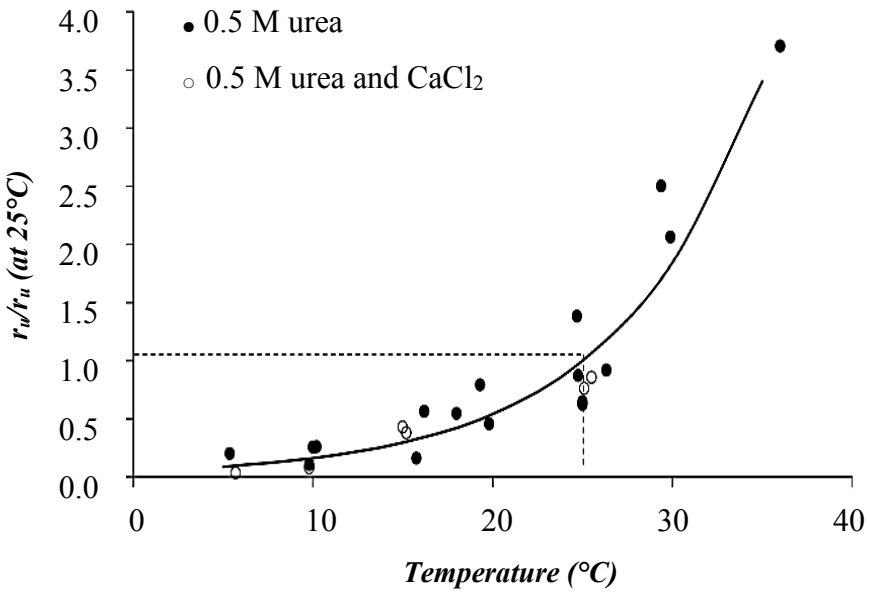

Figure 2.5 Influence of temperature on urease activity of *S. pasteurii* (van Paassen, 2009)

In terms of the influence of pH, it was found that ureolysis rate by *S. pasteurii* measured in a batch system was not strongly pH-dependent within the range of pH 6-9, and only a slight pH dependence was observed in the pH range 5-10 (Whiffin, 2004, Lauchnor et al., 2015). It was found that rate of the ureolysis rate by *S. pasteurii* decreases with the increase of pH from 9 to 11, and decreases with the decrease of pH from 6 to 4 (Whiffin, 2004).

The influences of oxygen concentration on urease activity of *S. pasteurii* have been studied. It was suggested that an anoxic environment does not impair urease activity of *S. pasteurii*, with anaerobic cultures in fact showing an approximately 1.5-2 greater increase in the rate of ureolysis than aerobic cultures over the same period of time (Mortensen et al., 2011). Similarly, zero oxygen levels did not inhibit the ureolytic activity of *S. pasteurii* (Tobler et al., 2011). Martin et al. (2012) found that *S. pasteurii* is unable to grow anaerobically and that the ureolytic activity previously shown under anoxic conditions is a consequence of the urease enzyme already present in the cells of the aerobically grown inoculum (Martin et al., 2012). It was suggested that *S. pasteurii* could still be used as a source of enzyme in the anoxic subsurface, but ureolysis may decline over time as the urease degrades or becomes inhibited (Martin et al., 2012).

2.2.2 Process and kinetics of $CaCO_3$ precipitation

The process and kinetics of $CaCO_3$ precipitation have been investigated in many research fields such as chemistry, biology and geology because it is a common chemical reaction which occurs in natural water systems, biochemical-mediated processes and during the evolution of the Earth-atmosphere-ocean system (Stumm and Morgan, 1981). Despite substantial theoretical and experimental investigations, the precise mechanisms involved in $CaCO_3$ precipitation are still highly debated and not fully understood. This section reviews the current understanding of the process and kinetics of $CaCO_3$ precipitation.

2.2.2.1 Crystal nucleation and nucleation rate

Based on classic nucleation theory, the process of $CaCO_3$ precipitation occurs when Ca^{2+} and CO_3^{2-} ions in a supersaturated solution interact to form a cluster of crystals whose size overcomes the free-energy barrier required for nucleation to occur (Stumm and Morgan, 1981). A supersaturated state is required for $CaCO_3$ precipitation to occur, meaning the solution has to contain more Ca^{2+} and CO_3^{2-} ions than could normally be dissolved by the solvent. The supersaturation ratio S has been used to quantify the level at which supersaturation induces $CaCO_3$ precipitation, which is defined in *Equation 2.5*:

$$S = \frac{[Ca^{2+}] \times [CO_3^{2-}]}{K_{sp}} \quad 2.5$$

where $[Ca^{2+}]$ and $[CO_3^{2-}]$ are the concentrations of calcium and carbonate ions, and K_{sp} is the equilibrium $CaCO_3$ solubility product for each experimental temperature (Stumm and Morgan, 1996). A supersaturation ratio that is higher than 1 is required for precipitation to occur. $CaCO_3$ precipitates can exist as several polymorphs, each of which have different K_{sp} values at different temperatures. For example, at 25 °C, the K_{sp} values of the four main polymorphs of $CaCO_3$ (calcite, aragonite, vaterite, and amorphous $CaCO_3$) are $10^{-8.48}$ M^2, $10^{-8.34}$ M^2, $10^{-7.91}$ M^2 and $10^{-6.40}$ M^2, respectively (Plummer and Busenberg, 1982; Brečevic and Nielsen, 1990).

The supersaturation ratio affects the nucleation rate which is defined as the number of nuclei formed per unit time per unit volume [m^{-3} s^{-1}]. In addition, other factors such as temperature and tension between the crystalline surface and the supersaturated solution also affect the nucleation rate. The nucleation rate is expressed in the form of the Arrhenius Equation (Mullin 2001):

$$\frac{dN}{dt} = A\exp(-\Delta G / \mathbf{k}T) = A\exp(-\frac{16\pi\gamma^3 v^2}{3\mathbf{k}^3 T^3 (\ln S)^2}) \quad 2.6$$

where A is Arrhenius constant [$m^{-3}s^{-1}$]; ΔG is the activation energy [J]; $\mathbf{k}$ is the Boltzmann constant, 1.3805×10^{-23} J K^{-1}; ν is the number of ions per mole of solute (in the case of $CaCO_3$, ν = 2); T is temperature in [K]; γ is the interfacial tension in [J m^{-2}], and S is the supersaturation ratio.

However, it was found that using only this equation is not enough to predict the nucleation rate in many cases, as nucleation occurs either homogeneously and spontaneously from the solution itself or heterogeneously from the presence of other substances in the solution, such as surfaces, dispersed particles or crystals (Cöelfen and Antonietti, 2008). The nucleation rates of calcite crystals for different values of γ and T reported in the literature were summarised by van Paassen (2009) (shown in **Figure 2.6**). It was found that as the effect of the substance that causes the heterogeneous nucleation, the nucleation rate is difficult to predict.

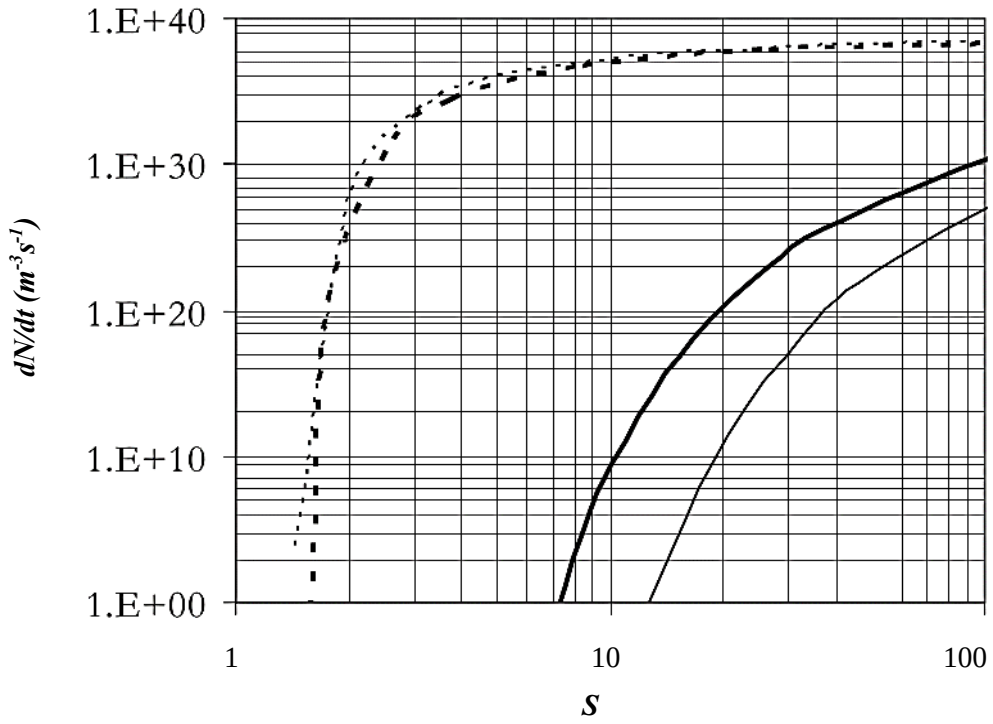

Figure 2.6 The correlation between the nucleation rate of calcite and the supersaturation ratio, *S*, in a pure solution (solid lines, $\gamma = 0.098$ J m^{-2} by Söhnel and Mullin, 1982) and in the presence of a substrate (dashed lines, $\gamma = 0.029$ J m^{-2} by Dalas et al., 1988). Thick lines are for T = 283 K and thin lines for T = 298 K (summarized by van Paassen, 2009)

These observations have therefore challenged the classical nucleation theory that has been widely used to analyse nucleation phenomena. As shown in **Figure 2.6**, the wide range of theoretical nucleation rates illustrates the difficulty of predicting the rate of precipitation in the case of spontaneous nucleation. In addition, very big deviations between classical nucleation theories and the experimental findings have been observed, especially in regions far from the equilibrium, which indicates that the actual crystallisation process is more complicated than a description based on single molecules only (Cöelfen and Antonietti, 2008). Moreover, a recent study found that the measured free Ca^{2+} concentration was lower than the dosed Ca^{2+} concentration even in under-saturated conditions (Gebauer et al., 2008). Therefore, it was suggested that stable pre-nucleation ion clusters even exist in under-saturated solutions (Gebauer et al., 2008). Because the nucleation process depends critically on many parameters such as temperature, pH, and crystal type, the process of nucleation and growth of $CaCO_3$ crystals remains subject to debate. In addition, during MICP processes, the $CaCO_3$ precipitation

in a soil porous medium, the existence of bacteria, and the surfaces of soil particles may greatly affect the nucleation rate. However, the exact effects of these parameters on $CaCO_3$ precipitation are so far largely unknown.

2.2.2.2 Crystal growth and growth rate

Classical nucleation theory suggests that $CaCO_3$ crystals grow from the nuclei after nucleation is complete. According to the experimental data obtained by Kralj and colleagues (1990, 1994 and 1997), the growth rate of vaterite and calcite, two of the main $CaCO_3$ polymorphs, can be described as:

$$\frac{dr}{dt} = k(S-1)^2 = k(\frac{[Ca^{2+}]\times[CO_3^{2-}]}{K_{sp}} - 1)^2 \qquad 2.7$$

where r is the crystal radius, S is the supersaturation ratio for the specific mineral phase and k is the growth rate constant. Based on the experimental data of Kralj and colleagues (1990; 1997), k increases with temperature in the range of 10 °C to 55 °C, and at 25 °C, the k values of vaterite and calcite are 0.56 nm/s and 0.014 nm/s, respectively. Based on *Equation 2.7*, at the same temperature, crystal grow rate is affected by k, K_{sp} and the concentration of Ca^{2+} and CO_3^{2-}. As described in the previous section, at 25 °C, the K_{sp} values of vaterite and calcite, are $10^{-7.91}$ and $10^{-8.48}$ M^2, respectively (Plummer and Busenberg, 1982; Brečevic and Nielsen, 1990). Based on the experimental data and *Equation 2.7*, the growth rate of vaterite and calcite crystals can be plotted against $[Ca^{2+}]\times[CO_3^{2-}]$ as shown in **Figure 2.7**.When $[Ca^{2+}]\times[CO_3^{2-}]$is between the K_{sp} of calcite and vaterite, only calcite can precipitate. When $[Ca^{2+}]\times[CO_3^{2-}]$ is higher than the K_{sp} of vaterite, both calcite and vaterite can precipitate. However, the precipitation rate of these two forms of $CaCO_3$ crystals varies. When $[Ca^{2+}]\times[CO_3^{2-}]$ is between the K_{sp} of vaterite and about 2.5×10^{-8} M^2, the growth rate of calcite crystals is higher than vaterite, whereas when $[Ca^{2+}]\times[CO_3^{2-}]$ is higher than 2.5×10^{-8} M^2, the precipitation rate of vaterite is higher than that of calcite.

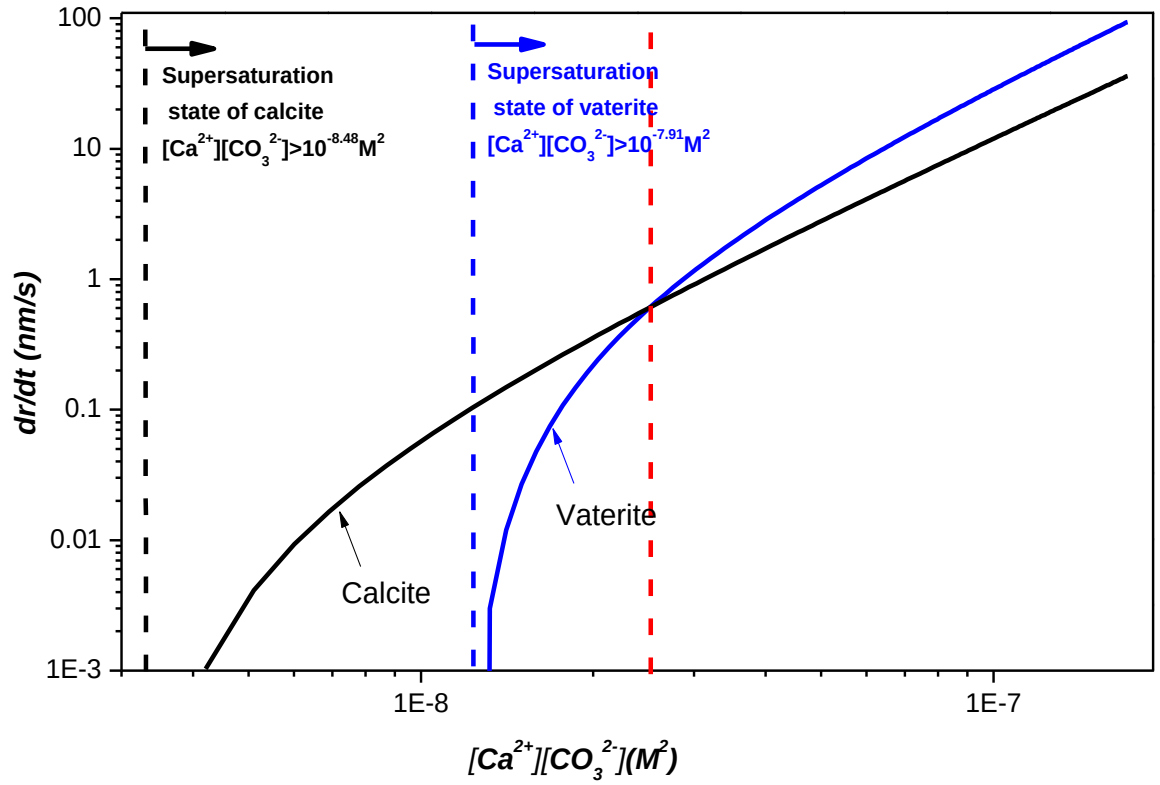

Figure 2.7 Correlation between *dr/dt* and $[Ca^{2+}]\times[CO_3^{2-}]$ for calcite and vaterite, based on *Equation 2.7*. *k* values of vaterite and calcite are 0.56 nm/s and 0.014 nm/s, respectively (Kralj et al., 1990 and 1997), K_{sp} values of vaterite and calcite are $10^{-7.91}$ and $10^{-8.48}$ M^2, respectively (Plummer and Busenberg, 1982; Brečevic and Nielsen, 1990).

The crystal growth rate calculated using *Equation 2.7* revealed that crystal growth is complex, as the $[Ca^{2+}]\times[CO_3^{2-}]$ in the solution is normally changing with time. The different K_{sp} values of the calcite and vaterite also indicate that vaterite is less stable compared with calcite, as when the $[Ca^{2+}]\times[CO_3^{2-}]$ is lower than the K_{sp} of vaterite, vaterite would dissolve while calcite can still growth as long as $[Ca^{2+}]\times[CO_3^{2-}]$ is higher than the K_{sp} of calcite. In addition, vaterite can grow and dissolve during the $CaCO_3$ precipitation process (Kralj et al., 1994; 1997).

2.2.2.3 Polymorphs and phase transformations

Vaterite and calcite are two of the main polymorphs of $CaCO_3$. In addition, two other $CaCO_3$ polymorphs have also been observed during $CaCO_3$ precipitation, namely aragonite at high temperatures (>35°C) and amorphous calcium carbonate (ACC) nanoparticles. These $CaCO_3$ polymorphs vary in their shapes, such as rhombohedral calcite (Kawano et al., 2002; Lian et al., 2006; Dhami et al., 2013), spherical vaterite (Kawano et al., 2002; Lian et al., 2006; van Paassen 2009; Dhami et al., 2013), aragonite which normally crystallizes as clustered needles (Morse et al., 2007; Dhami et al., 2013) (Ogino et al., 1987; Carteret et al., 2009), and non-crystalline amorphous calcium carbonate (ACC) nanoparticles which have a complex hybrid structure (Kawano et al., 2002; Bots et al., 2012; Dhami et al., 2013; Rodriguez-Navarro et al., 2011). Four images showing the polymorphs of $CaCO_3$ reported in the literature are summarised in **Figure 2.8**.

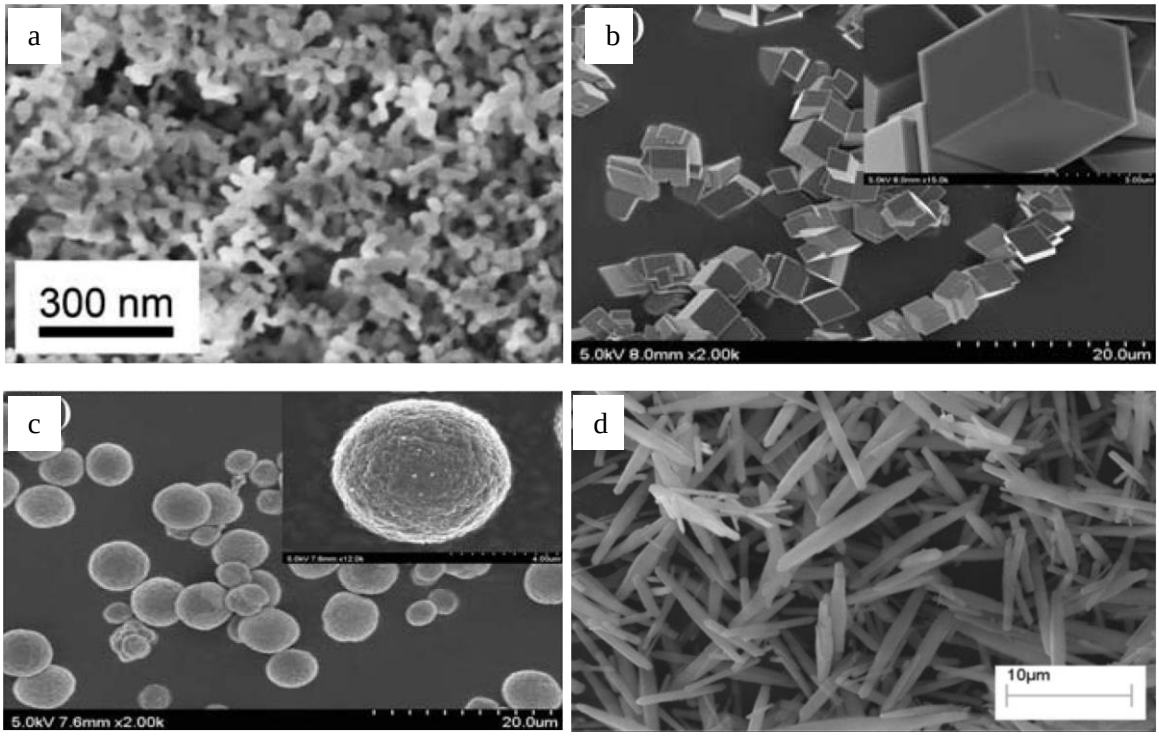

Figure 2.8 Polymorphs of $CaCO_3$. **(a)** Amorphous calcium carbonate (ACC) (Rodriguez-Blanco et al., 2011); **(b)** calcite (Chu et al., 2013); **(c)** vaterite (Chu et al., 2013); **(d)** aragonite (Zhou et al., 2004)

The polymorphs of $CaCO_3$ not only vary in their morphology, but also vary in their stability and precipitation rate. Consistent with the prediction of crystal growth rate based on *Equation 5.7* and the dissolution of vaterite reported by (Kralj et al., 1994; 1997), Wei et al. (2003) observed the transformation from vaterite to calcite (**Figure 2.9a**). However, others have also reported that ACC forms first and subsequently transforms to vaterite and calcite (**Figure 2.9b**, Kawano et al., 2002) or subsequently transforms to calcite via the intermediate formation of vaterite (**Figure 2.9c**, Rodriguez-Blanco et al. 2011). These phase transformations of $CaCO_3$ during precipitation processes are consistent with the Ostwald's step rule, which suggests that, usually, the least dense phase is formed first and transforms to the next dense phase until finally, the densest (which is usually also the most stable phase) is formed (reviewed by Cöelfen and Antonietti, 2008). It should be mentioned that not all $CaCO_3$ polymorphs show up along such lines. Aragonite is normally not observed along this sequence as it is notoriously hard to nucleate (reviewed by Cöelfen and Antonietti, 2008). How far the metastable intermediates are stable or transform to the next stable species according to Ostwald's step rule depends on the solubility of minerals and on the free energies of the activation of nucleation in different environments, all of which are strongly influenced by other substances such as minerals or other solids present in the system.

The phase transformations reported by Kawano et al. (2002), Wei et al. (2003) and Rodriguez-Blanco et al. (2011) were based on the chemical precipitation of $CaCO_3$ in aqueous solutions containing $CaCl_2$ and Na_2CO_3 rather than on bacterial-induced $CaCO_3$ precipitation. As described in *Section 2.2.2.1*, the $CaCO_3$ precipitation during the MICP process might be more complex due to the presence of bacteria and a porous medium. In the next section, the micro-scale understanding of MICP processes, including the properties of bacteria, will be addressed.

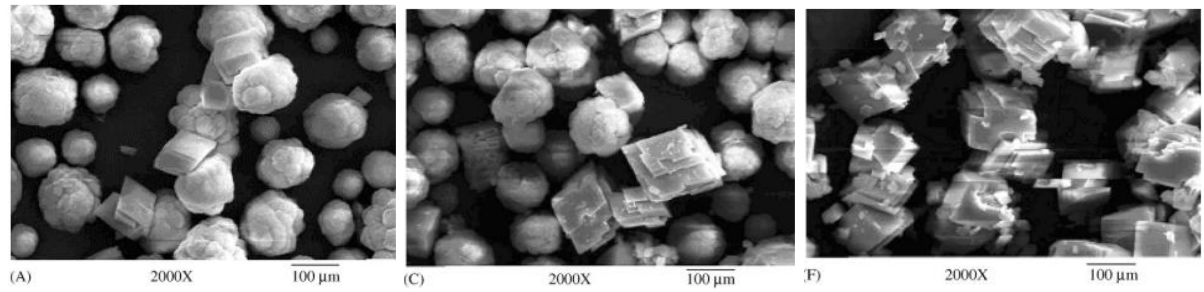

(a)

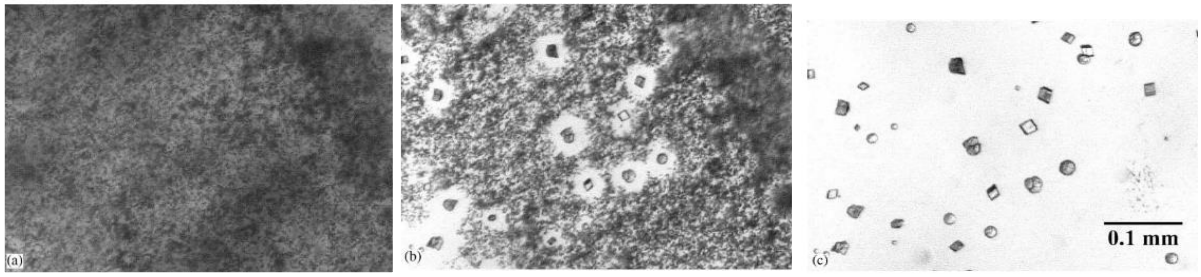

(b)

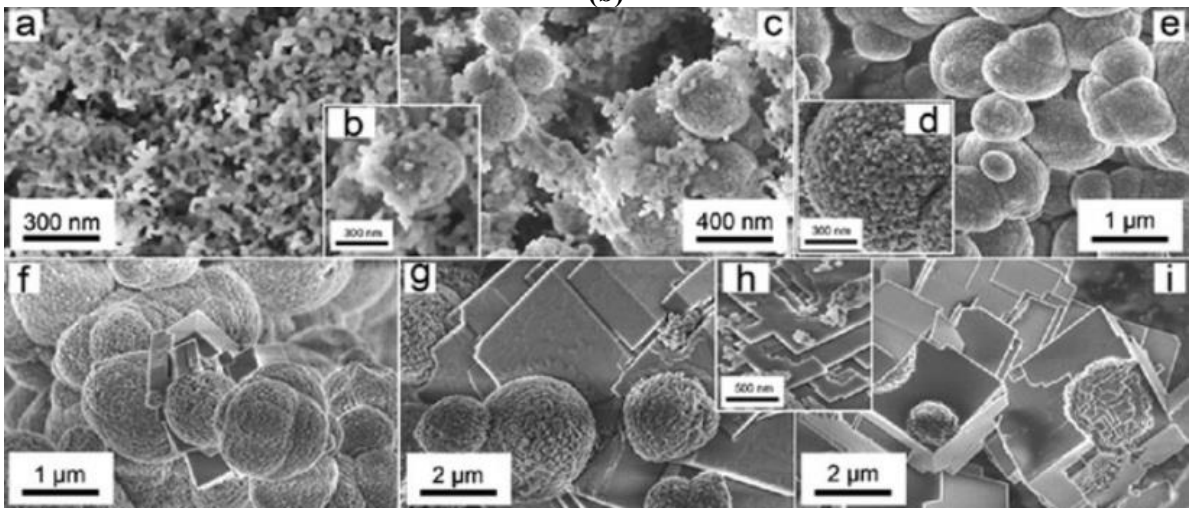

(c)

Figure 2.9 Phase transformation of $CaCO_3$ crystallisation pathways reported in literature. **(a)** transformation from vaterite to calcite (Wei et al., 2003); **(b)** transformation from ACC to vaterite and calcite (Kawano et al., 2002); **(c)** transformation from ACC to vaterite and then to calcite (Rodriguez-Blanco et al., 2011)

2.3 Micro-scale study of MICP

At the micro-scale, the properties of individual bacterial cells such as distribution and number may affect the local supersaturation zone, thus affecting the kinetics and process of MICP

which in turn affects the properties of $CaCO_3$ crystals. In addition, the formed $CaCO_3$ modifies the sandy soil matrix via processes such as coating on the surfaces of soil particles, filling in the pores, or bonding soil particles together, and therefore improves the engineering properties of the soils.

2.3.1 Properties of *Sporosarcina pasteurii*

2.3.1.1 Bacterial growth

Bacterial growth experiments in a laboratory have shown that under optimized conditions, bacterial growth follows six phases - lag phase, the starting phase, exponential phase, slow-down phase, stationary phase and death phase (Widdel, 2007). After an initial lag phase, a rapid increase in bacterial population occurs during the exponential growth phase (Widdel, 2007). During rapid growth, bacteria consume the surrounding nutrients from the bulk fluid (Widdel, 2007). During MICP studies, bacteria are normally grown in the lab until the bacterial cells reach the exponential phase (Whiffin, 2004), and are then injected into the soil matrix. The bacterial density reported in the literature to date was tested after cultivation before commencing the MICP experiments. However, *in situ* growth of bacteria within the soil matrix after the injection has not previously been studied.

2.3.1.2 Morphology of *Sporosarcina pasteurii*

Bacterial cells are too small to be visualised without a microscope. Transmission electron microscopy (TEM), scanning electron microscopy (SEM) and high resolution optical microscope have been used to observe bacterial cells (Fujita et al., 2000; Yoon et al., 2001; Bang et al, 2001; Warren et al., 2001; Keykha et al., 2013; Zhang et al., 2018). Exemplar micro-scale images of *S. pasteurii* reported in the literature are presented in **Figure 2.10**. It is shown in **Figure 2.10** that *S. pasteurii* are of rod-shaped and have a length of about 1.5 to 10 μm. *S. pasteurii* cells are motile due to the presence of a single polar flagellum in each of these bacterial cells (Yoon et al., 2001).

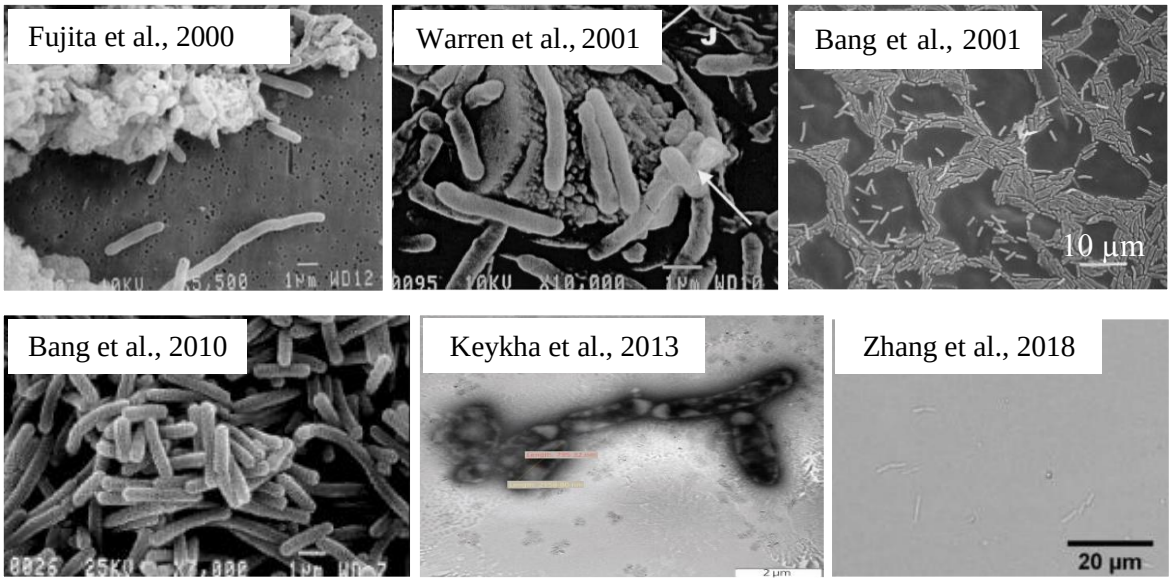

Figure 2.10 *S. pasteurii* cells with different sizes (Fujita et al., 2000; Bang et al, 2001; Warren et al., 2001; Bang et al., 2010; Keykha et al., 2013; Zhang et al., 2018)

2.3.1.3 Movement of *Sporosarcina pasteurii* in liquid

Transport of bacteria in a porous medium with flow is governed by advection and dispersion (Tufenkji, 2007; Liu et al., 2011). At high flow rates, bacteria migrated mainly by advection and bacteria were most likely to travel along with the convective flow. However, as *S. pasteurii* bacteria are motile due to the presence of a single polar flagellum in each of these bacterial cells (Yoon et al., 2001), when the flow rate is low, especially when the flow rate is comparable with the average bacterial swimming speed, bacteria are able to approach solid surfaces via their own motility (Liu et al., 2011). In addition, when the bacterial size is larger than 1 μm, gravity should also be taken into account (Chen et al., 2010). As the size of *S. pasteurii* is larger than 1 μm, they may settle at the bottom substrate within the soil pores.

2.3.1.4 Attachment to and detachment from a solid surface

Previous research has shown that bacteria tend to secrete structures such as flagella, pili, exopolysaccharides, and other matrix components to attach to solid surfaces and live at the solid-liquid interface (Dunne, 2002). This process results in an adhesive force between bacteria and solid surfaces (Persat et al., 2015, see **Figure 2.11**). Because bacterial adhesion might be

one of the most important mechanisms that enables bacterial cells to be retained inside a soil matrix, understanding the interactions between bacterial cells and the surface of soil particles is very important for designing MICP procedures. However, to date, due to a lack of suitable methods, very few studies have investigated the interactions between soil particles and bacteria such as *S. pasteurii* which are commonly used in MICP.

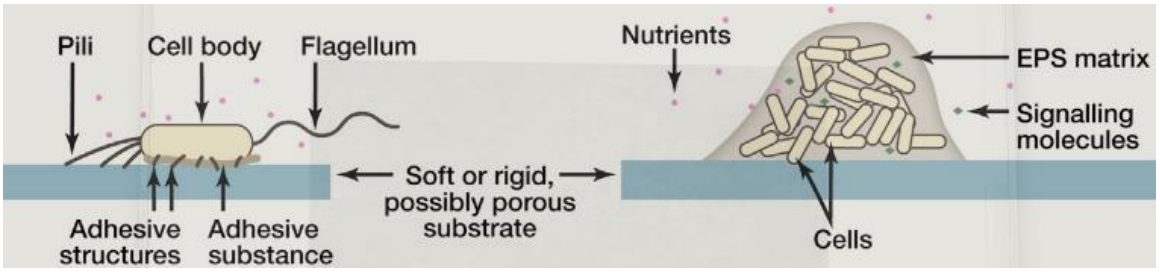

Figure 2.11 Two mechanisms through which bacteria can adhere to a solid substrate. **(a)** Flagella, pili, and adhesive substances are useful for attachment of individual bacterial cells to surfaces. **(b)** Extracellular polymeric substances (EPS) aid in maintaining the integrity of community structures composed of multiple cells (Persat et al., 2015)

Apart from being adhered to the surfaces, where a bacterial cell is subject to a local adhesive force (F) in the direction normal to the surface, bacterial cells also experience a variety of other mechanical effects on surfaces. Shear stresses due to fluid flow generate a force (F) on the cell that is parallel to the surface (**Figure 2.12**). If the shear force is higher than the friction force, such as under the condition of flow, the attached bacterial become unattached again.

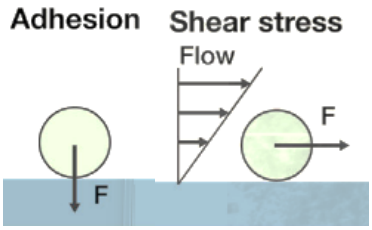

Figure 2.12 The forces on bacteria. A cell attaching to a surface is subject to a local adhesive force (F) in the direction normal to the surface; Shear stresses due to fluid flow generate a force (F) on the cell that is parallel to the surface (Persat et al., 2015)

2.3.1.5 Aggregation of *Sporosarcina pasteurii*

S. pasteurii cells have been shown being able to aggregate when bacterial cells are mixed with $CaCl_2$ solution (**Figure 2.13**, El Mountassir et al., 2014), and the bacterial aggregates were applied for producing MICP. However, the study conducted by El Mountassir and colleagues did not focuses on the effect of bacterial aggregates on the MICP properties, to date the precise effects of bacterial aggregates on $CaCO_3$ precipitation and growth were studied.

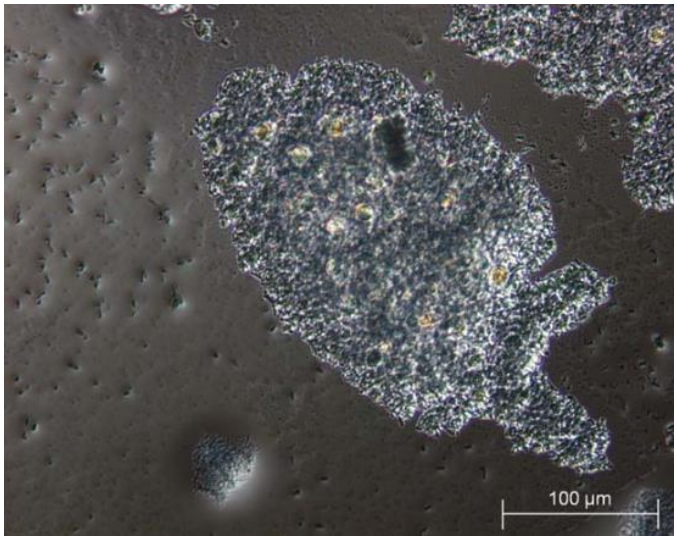

Figure 2.13 Microbial floc formed by mixing *S. pasteurii* with $CaCl_2$ solution (El Mountassir et al., 2014)

2.3.2 Properties of $CaCO_3$ precipitates formed during MICP

Scanning electronical microscopy (SEM) has been applied to visualise MICP-treated soil specimens at the particle scale of sandy soils to observe the micro-scale properties of $CaCO_3$ crystals such as shape, size and their distribution on the surface of the soil particle or inside soil pores. The type of $CaCO_3$ crystals formed can be determined by observing the shape of $CaCO_3$ crystals or by performing an X-Ray Diffraction (XRD) test. A summary of the observed properties of $CaCO_3$ reported in the literature is presented in **Table 2.2**. Crystal sizes were obtained either from the relevant literature or by measuring crystal size using GetData Graph Digitizer 2.26.

Table 2.2 Summary of $CaCO_3$ properties in MICP-treated samples

	$CaCO_3$ Properties			Experimental parameters				$CaCO_3$
	Shape/ Type	Size (μm)	Distribution	C (M)	BA (mM/)	T (°C)	Sample condition	content
Al Qabany, 2011	R	5	Coating	0.25	2-30	20	Silica	80 kg/m^3
	R	3-10		0.5				100 kg/m^3
	R	10-150		1				65 kg/m^3
	S	3-40		1				60 kg/m^3
Van Paassen, 2009	S	10-40	In pores	0.5	130	20 ± 2	Siliceous	-
	R	2-5	Coating	-	-		Calcareous	-
	-	-	-	1	9-180		Batch I	-
	S-H	3-30	-	1	60		Batch II	-
	S-H	S-H: 20-40	-	1	170		glass-slide	-
	R	R: 2-6						
	RA	RA:20-40						
Cheng et al., 2017	S	2-5		1	3000	25	Silica	0.061 g/g
	A	20-50			300			0.039 g/g
	S	2-5			600	4		0.021 g/g
	A	20-50			600	25		0.028 g/g
	R	2-5			600	50		0.034 g/g
Zhang et al., 2018	C &V	5-20	-	0.025	25	-	Bacteria-inclusive solution	-
	CA	1-10	-	0.025	25	-	Bacteria-free solution	-

Note: S-Spherical; R- Rhombohedral; A-Aggregated; H-Hollow; Batch I- Unstirred Batch; Batch II- Stirred batch; C- Calcite; V-Vaterite; g/g grams of $CaCO_3$ per gram of soils

2.3.2.1 Shapes and types of $CaCO_3$ crystals formed during MICP

Two types of $CaCO_3$ crystal have been reported to occur in MICP-treated samples, namely vaterite and calcite (van Paassen, 2009). Vaterite crystals are spherical, with both hollow and dense types being reported (van Paassen, 2009), whereas calcite crystals are rhombohedral.

Two factors have been suggested to influence the types and shapes of $CaCO_3$ crystals formed in MICP-treated soil samples, namely initial bacterial activity (van Paassen, 2009; Al Qabany 2011) and sand mineral type (van Paassen, 2009). The initial bacterial activity refers to the bacterial activity tested before MICP treatment and the two types of sand that have been reported to affect the type and shape of $CaCO_3$ crystals were siliceous sand and calcareous sand (van Paassen, 2009). By performing batch tests and X-Ray Diffraction (XRD) analyses, van Paassen (2009) reported that when the initial bacterial activity increased from 9 to 36 mM/h, the relative abundance of vaterite increased from 5 to 90 %. Spherical vaterite crystals were preferably formed when the bacterial activity was higher than 30 mM/h, whereas rhomboidal calcite crystals were preferably formed when bacterial activity was lower than 10 mM/h (**Figure 2.14**).

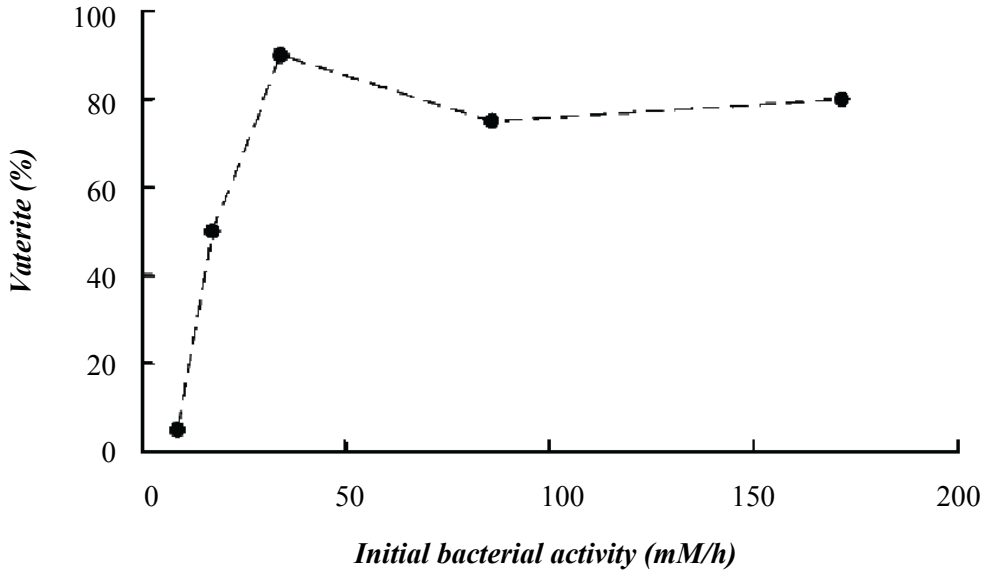

Figure 2.14 Relative abundance of vaterite as a function of bacterial activity (van Paassen, 2009)

By conducting soil tests and Scanning Electronic Microscopy analyses, Al Qabany (2011) also suggested that high bacterial activities may result in the precipitation of vaterite, whereas low activities may result in the precipitation of calcite (**Figure 2.15**). However, although the activity range in this study was reported to be 2-30 mM/h, the exact values of the activities for each sample were not reported (Al Qabany, 2011).

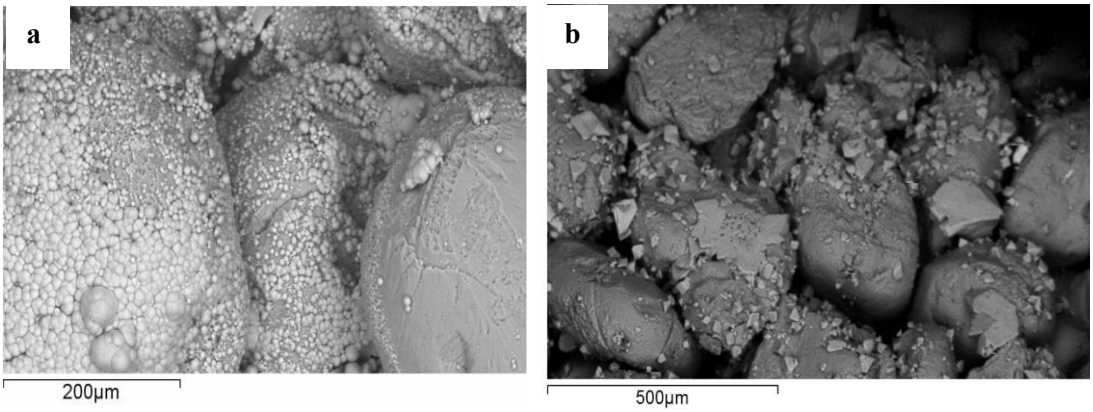

Figure 2.15 Representative SEM images of spherical vaterite crystals **(a)** or rhomboidal calcite crystals **(b)** in a MICP-treated sand specimen. Vaterite crystals preferentially formed when the bacterial activity was high **(a)**, whereas rhomboidal calcite crystals formed when the bacterial activity was low **(b)** (Al Qabany, 2011)

2.3.2.2 Size and number of $CaCO_3$ crystals formed during MICP

The sizes of $CaCO_3$ crystals formed in MICP-treated samples varied significantly from 2 µm to 150 µm (**Table 2.2**). Three factors that have been suggested to influence the size of $CaCO_3$ crystals formed in MICP-treated soil samples are (i) concentration and injection interval of cementation solution, (ii) bacterial activity and (iii) temperature.

Al Qabany et al. (2012) concluded that the size of $CaCO_3$ crystals formed was smaller when soil samples were treated more frequently with a lower concentration of cementation solution compared with soil samples that were treated less frequently with a higher concentration of cementation solution (**Figure 2.16**). However, the exact reason behind this finding remain largely unknown.

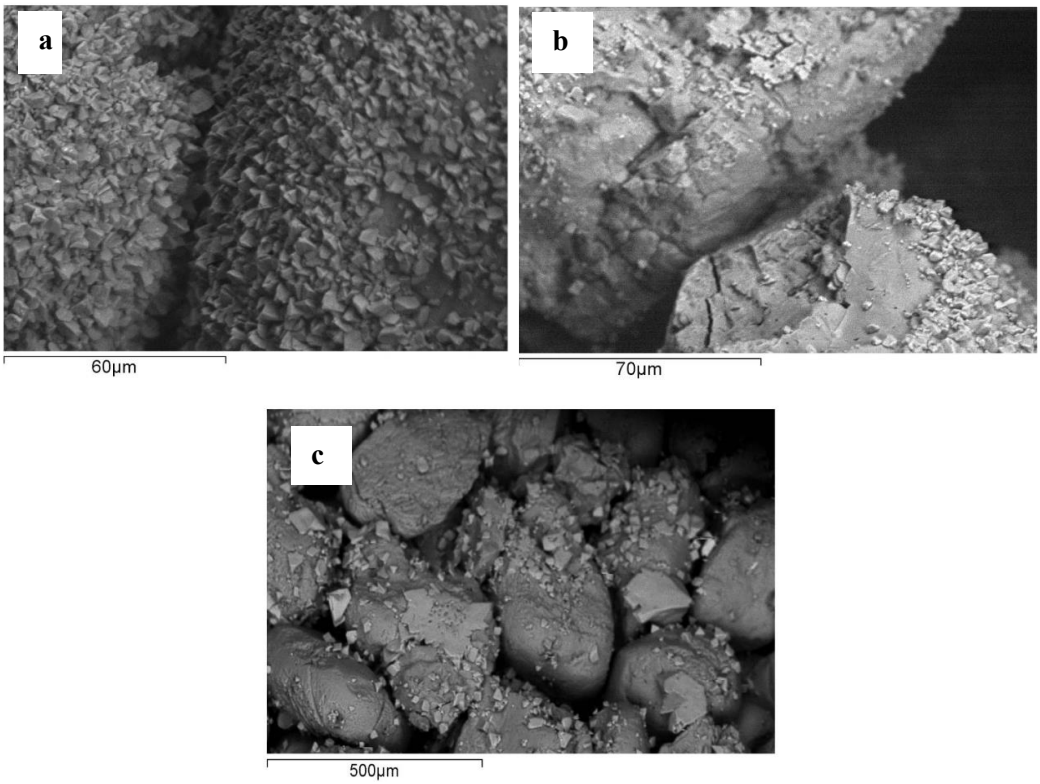

Figure 2.16 Representative SEM images of $CaCO_3$ crystals observed in MICP-treated sandy soils after injecting cementation solution with a concentration and injection interval between cementation solution injection. **(a)** 0.25 M and 6 h; **(b)** 0.5 M and 12 h; **(c)** 1 M and 24 h (Al Qabany et al., 2012)

In terms of the effect of bacterial activity on the characteristics of $CaCO_3$ crystals, based on the observation that larger carbonate crystals were generated in the presence of ureolytic bacterial cells, whereas smaller ones developed in the absence of ureolytic bacterial cells, it was proposed that higher bacterial concentrations may generate larger carbonate crystals (Mitchell and Ferris, 2006). However, on the contrary, Cuthbert et al. (2012) and Cheng et al. (2017) found that ureolysis rate affects the average size of $CaCO_3$ crystals. As the rate of ureolysis increased from 0.1 to 10 mM/d, indicated by the rate of ammonia production, Cuthbert et al. found that the average size of $CaCO_3$ crystals decreased from 100 μm to 10 μm. Similarly, Cheng et al. (2017) found that the crystal sizes in MICP-treated soils varied significantly as the ureolysis rate was different, with the ureolysis rate decreasing from 50 U/L to 5 U/L, the crystal sizes increased from 2-5 μm to 20-50 μm (**Figure 2.17**). It has been proposed that the initial ureolysis rate appears to govern the final distribution of crystal sizes, which might be because nucleation rate increases with the degree of saturation, as indicated by the Arrhenius equation

(Mullin, 2001). The higher the ureolysis rate, the higher the nucleation rate, thus resulting in the formation of a larger number of smaller crystals.

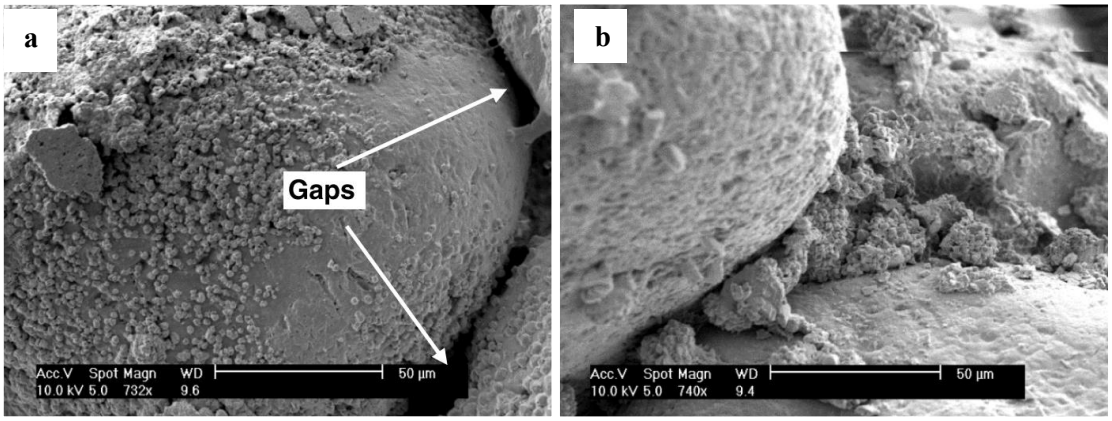

Figure 2.17 $CaCO_3$ crystals observed in MICP-treated sandy soils with different bacterial activities: 50 U/mL **(a)** and 5 U/mL **(b)** (Cheng et al., 2017)

Temperature is the third factor that has been reported to affect both the size and number of $CaCO_3$ crystals in MICP-treated soil samples. The size of $CaCO_3$ crystals was found to be 2-5 µm after MICP treatment at 0°C or 50°C, and 20-50 µm after MICP treatment at 20°C (**Figure 2.18** by Cheng et al., 2017). It was suggested that higher temperatures reduce the activation energy required for nucleation to proceed and increase the rate of nucleation and $CaCO_3$ precipitation (Wojtowicz, 1998). Therefore, this concept was used to explain the reason why more crystals formed at 50°C than at 20 °C. However, this does not explain why fewer crystals formed at 20°C than at 4°C. In addition, it was suggested that the competition between the formation of new crystals and the growth of existing crystals affects crystal size (Cheng et al., 2017). However, as neither the formation of new crystals nor crystal growth were observed in this study, this suggestion appears to be speculative. To date, the exact effects of temperature on the size of $CaCO_3$ crystals formed during MICP and the reason behind this remain largely unknown.

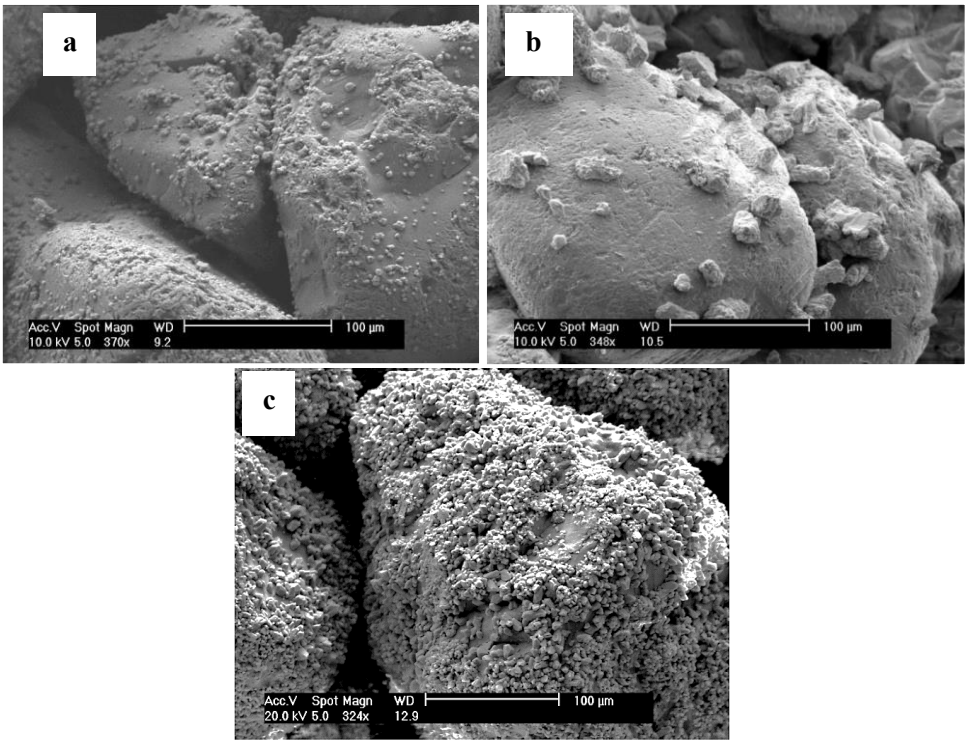

Figure 2.18 SEM images of $CaCO_3$ crystals observed in MICP-treated sandy soils when MICP treatment was performed at 4°C **(a)**, 25°C **(b)** or 50°C **(c)** (Cheng et al., 2017)

2.3.2.3 Spatial distribution of $CaCO_3$ crystal formed during MICP

The effectiveness of the MICP technique for soil stabilisation is directly dependent on the spatial distribution of the $CaCO_3$ precipitates (DeJong et al., 2010). In theory, the precipitates that are produced at particle contacts rather than uniformly distributing on the surfaces of soil particles (help to) bind sand particles together (**Figure 2.19)** (DeJong et al., 2010).

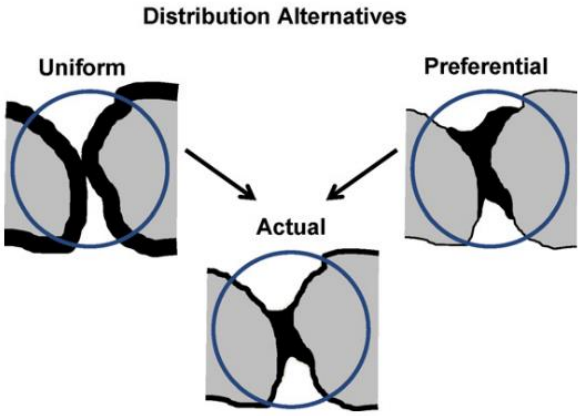

Figure 2.19 Illustration of calcite distribution alternatives within pore space (DeJong et al., 2010)

However, in reality, SEM images of the distribution of $CaCO_3$ precipitates have shown that $CaCO_3$ crystals can coat particle surfaces, deposit at particle contacts, and even grow within pores. In addition, in most cases, these three distribution patterns coexist. It is important to note that in most cases $CaCO_3$ precipitates exist as individual crystals, even though they sometimes aggregate. The particle 'coating' pattern was usually described when the crystals were relative small and covered most of the surface area of the soil particles, as shown in **Figure 2.16a, Figure 2.17a and Figure 2.18c**. When the particles deposit at particle contacts, this is sometimes referred to as a bonding pattern, with the preferential distribution described in **Figure 2.19.** In this pattern, the crystals are normally large enough to bond soil particles at soil particle contacts and if the particles are large, $CaCO_3$ crystals can also precipitate on the soil particle surface away from any particle contacts, as shown in **Figure 2.17b** and **Figure 2.18b**. Therefore, the spatial distribution of $CaCO_3$ crystals should be considered together with other crystal parameters such as size and number. To date, the reasons why these different $CaCO_3$ crystal precipitation patterns form remain largely unknown.

2.3.3 Micro-scale ureolysis-driven MICP processes and microfluidics

2.3.3.1 Current understanding of ureolysis-driven MICP processes at the micro-scale

The theories behind $CaCO_3$ nucleation and precipitation processes reviewed in *Section 2.2.2* are all based on chemical reactions between Ca^{2+} and CO_3^{2-} rather than on bacteria-driven MICP processes. Similar to classic nucleation and crystal growth theory, a widely believed assumption of the $CaCO_3$ precipitation process during MICP is that bacterial cells serve as nucleation sites for $CaCO_3$, and that once the nucleation sites are formed, the $CaCO_3$ crystals continue growing from them (Stocks-Fischer et al., 1999; Hammes et al., 2002; DeJong et al, 2006; Siddique et al., 2011; Dhami et al., 2013; Ganendra et al., 2014). This is assumed because bacterial cell walls are negatively charged and can adsorb Ca^{2+} (Rodriguez-Navarro et al., 2011; EI Mountassir et al., 2014). Therefore, once the bacterial cells hydrolyse the urea, the released CO_3^{2-} ions precipitate with the Ca^{2+} cations which are attached to bacterial cell walls, forming the $CaCO_3$ nucleation sites required for $CaCO_3$ crystal growth.

By contrast, others have found the effect of bacterial cells on nucleation of $CaCO_3$ is very limited. By using a cellulose dialysis membrane to divide a cylinder containing urea and $CaCl_2$ into a bacterial free reaction part and a bacterial inclusive reaction part, it was found that $CaCO_3$ could precipitate in both the presence and the absence of bacterial cells (Mitchell and Ferris, 2006). More recently, using the same membrane to separate bacterial cells from an agar plate containing urea and $CaCl_2$, it was found that the $CaCO_3$ precipitates did not grow on bacterial cells (Zhang et al., 2018). Despite the studies that have been reported, the understanding of MICP process in real soils is still very limited because the experimental conditions such as liquid reactions in a cylinder or on agar plates cannot represent the real MICP conditions when MICP is applied in a porous soil matrix under the influence of flow. During an MICP process occurring in the pore fluid inside a porous soil matrix, the properties of the soil matrix itself might also affect the MICP process. In addition, in a MICP treatment procedure, a single injection or multiple injections of cementation solution are normally conducted, where the injection flow rate, injection volume and injection procedure significantly affects $CaCO_3$ precipitation processes. The experimental conditions in the liquid in a cylinder and on agar plates cannot represent the real MICP conditions at all. To date, the precise process of ureolysis-driven MICP especially in the real soils remains largely unknown.

As reviewed in *Section 2.3.2*, bacterial activity affects crystal type, bacterial density affects crystal size, and bacterial distribution may affect crystal distribution. Therefore, it is essential to know the factors affecting bacterial activity, density and distribution at the micro-scale. The density of bacteria inside the pores depends on the density of bacterial cells that were injected into the soil matrix, as well as on the transport of the bacteria during the injection, their interactions with soil particles, and the interactions between bacteria and ions such as Ca^{2+}. Therefore, to understand the micro-scale ureolysis-driven MICP process, it is essential to understand the behaviour of bacterial cells and the effect of bacterial cells on the process of $CaCO_3$ precipitation. However, as reviewed in *Section 2.3.1*, our understanding of *S. pasteurii* behaviour in a saturated porous medium is still very limited, and the precise nature of the processes implicated in $CaCO_3$ precipitation during MICP are largely unknown. Although SEM enables the $CaCO_3$ properties after the MICP treatment to be observed, SEM does not allow the actual MICP process to be observed. In addition, although the growth of $CaCO_3$ crystals in liquid contained in a petri dish or on an agar pad was observed (Zhang et al., 2018),

neither of these two methods can model fluid flow through a porous medium which occurs in real MICP processes. A suitable method which can observe both bacterial cells and $CaCO_3$ crystals during the entire MICP process under conditions that are relevant MICP treatment of real soils is therefore required.

2.3.3.2 Microfluidics as a potential useful way to study MICP processes at the micro-scale

Originating from micro-analytical methods and microelectronic circuits in the early 1990s (Whitesides, 2006), the field of microfluidics has expanded dramatically in the past decade. This is largely due to the introduction of soft lithography, an easily accessible fabrication technique which is used to create microfluidic chips based on patterned elastomeric polymers. This technique enables the fabrication of a master which contains channels with dimensions of tens to hundreds of micrometres. The master is used to mould the channels that are built into a small optically transparent device called a microfluidic chip. Polydimethylsiloxane (PDMS) is the most common material used to make a microfluidic chip which is due to its low cost, easy fabrication, flexibility and optical transparency (Sia and Whitesides, 2003; Weibel et al., 2007). In addition, the surface properties of microfluidic chips, such as wetting properties (hydrophobic and hydrophilic) and charges (positive and negative), can be varied using different surface treatment technologies (Bodas and Khan-Malek, 2007; Wong and Ho, 2009; Zhou et al., 2010, 2012).

Microfluidic chips can be used to manipulate small volumes of fluid transport through the channels and to study the micro-scale transport behaviour of fluids (Grate et al., 2013) and fluid components such as colloids, nanoparticles, bacteria or biofilms (Lanning and Ford, 2002; Auset and Keller, 2006; Durham et al., 2012; Drescher et al., 2013). In addition, microfluidic chips have also been used to study chemical reactions such as precipitation (Yoon et al., 2012; Jaho et al., 2015) or biological processes such as bacterial growth and motility (Mannik et al., 2009). Microfluidics has revolutionised fundamental and applied research to investigate and observe small-scale physical, chemical, and biological processes in the fields of chemical, biological, medical and environmental engineering (Tohidi et al., 2002; Sia and Whitesides, 2003; Jaho et al., 2015; Zhang et al., 2010; Long et al., 2013). Microfluidic platforms might

therefore be useful to study the particle-scale behaviour of Microbial-Induced Carbonate Precipitation (MICP) for applications in geotechnical engineering.

2.4 Macro-scale study of MICP

Research into MICP as an engineering technique is application-driven. The ultimate aim of MICP studies is to apply MICP in real projects to treat different *in situ* soils in different environmental conditions for different applications. This requires: (i) the ability to control and predict the properties of $CaCO_3$ crystals formed *in situ* and for these properties to be homogeneous, (ii) MICP-treated soils to be strong, and (iii) the treatment procedure to be efficient by using fewer chemicals to achieve better engineering properties such as strength.

2.4.1 Homogeneity of MICP

As mentioned in the introduction of this *Chapter*, one of the advantages of MICP over the traditional cementation method using cement is that MICP has the potential to treat larger volumes of soil because the injected bacterial suspension and cementation have much lower viscosities compared to cement. However, because the injection of bacterial suspension and cementation solution is a reactive transport process, it has been difficult to control and predict the amount and properties of $CaCO_3$ formed *in situ*. In many cases, $CaCO_3$ was found to be heterogeneously distributed within the soil matrix after MICP-treatment (Whiffin et al., 2007; van Paassen et al., 2010). The homogeneity of MICP in terms of the spatial distribution of $CaCO_3$ content within the soil matrix therefore became one of the key challenges associated with MICP. Before MICP can be used in industrial and environmental applications, calcium carbonate deposition must be shown to be controllable at a relevant scale while maintaining economic feasibility (Harkes et al., 2010). Ideally, calcium carbonate deposition should be uniform over the desired scale for the purpose of economic feasibility.

2.4.1.1 Effects of injection protocols on treatment homogeneity

A widely used MICP injection protocol, referred to as 'staged injection', in which a bacterial suspension is injected prior to injecting cementation solution in a subsequent step (Whiffin et

al., 2007; van Paassen et al., 2010) has been suggested to produce a more homogeneous distribution of $CaCO_3$ within a soil matrix compared with injecting a mixture of bacterial suspension and cementation solution (Tobler et al., 2012). This might be because mixing bacterial suspension with cementation solution produces bacterial aggregates (as reviewed in *Section 2.3.1*) which might be more difficult to be injected into the soil matrix and cause clogging at the injection point. However, homogeneity is still a big challenge even when using the staged injection protocol, as shown by the large variations in the $CaCO_3$ content formed in the soil matrix after MICP treatments (Whiffin et al., 2007; van Paassen et al., 2010).

2.4.1.2 Effects of bacterial distribution on homogeneity

The distribution of bacteria has been suggested to be an important factor that affects the distribution of $CaCO_3$ in MICP-treated soils (Martinez et al., 2013). As reviewed in *Section 2.2*, bacterial density affects the kinetics of the ureolysis reaction which produces CO_3^{2-}, which in turn affects the local supersaturation state of $CaCO_3$ and may thus affect the $CaCO_3$ precipitation process. Therefore, a homogeneous distribution of bacteria might be essential to achieve a uniform distribution of $CaCO_3$. As reviewed in *Section 2.3*, bacterial behaviour inside the soil matrix such as transport with flow, attachment to and detachment from the soil particles, and aggregation with chemicals such as Ca^{2+} might affect the distribution of bacteria in a soil matrix. However, neither these bacterial behaviours at the micro-scale nor the consequent effects of these behaviours on the distribution of bacteria inside a soil matrix at the macro-scale are fully understood yet.

2.4.1.3 Effects of flow rate and $CaCO_3$ precipitation rate on treatment homogeneity

As the injection of MICP reactants (bacterial suspension and cementation solution) is a reactive transport process, injection flow rate and $CaCO_3$ precipitation rate are thought to affect the uniformity of MICP treatment. It was suggested that a more homogeneous distribution could be achieved by increasing the flow rate of cementation solution or lowering the precipitation rate of MICP to deliver the reactants over larger distances. However, this hypothesis has not yet been proven. In addition, this hypothesis does not consider the effect of flow rate on the

number of bacteria remaining in the soil matrix. As reviewed in *Section 2.3.1.4*, increasing flow rate may increase the detachment of bacteria from solid surfaces and soil particles, which would consequently affect the number of bacteria remaining in the soil matrix. Because bacterial amount may affect both the process and kinetics of MICP, an optimised injection flow rate and $CaCO_3$ precipitation rate might be helpful for increasing the uniformity and maintaining the efficiency of MICP.

2.4.1.4 Effects of cementation solution concentration on treatment homogeneity

The concentration of cementation solution has also been found to affect the uniformity of MICP (Al Qabany et al., 2012; Dawoud et al., 2014 a, b), with a low concentration solution (0.1 M-0.5 M) resulting in a higher uniformity of $CaCO_3$ precipitation compared with a 1.0 M solution. However, as the experiments were conducted in a soil matrix without a way to monitoring the micro-scale effect of concentration of cementation solution on the MICP processes, the reason behind this is still largely unknown.

2.4.2 Strength of MICP-treated sandy soils

As mentioned in the introduction of this *Chapter*, another main advantage of MICP for soil stabilisation is that soil can be strengthened without interfering with the hydraulics of the treated soil. Therefore, natural aquifers are not interrupted by construction work, and maintain their function even at a local level. Furthermore, the soil can be strengthened without the need for excavation or replacement (van der Ruyt and van der Zon, 2009). The correlation between the hydraulic conductivity of MICP-treated soils and the $CaCO_3$ content, defined as the ratio of mass of $CaCO_3$ to the total volume of soil (Al Qabany and Soga, 2013; Cheng et al., 2017), reported in literature is summarised in **Figure 2.20**. Apart from the result of Martinez et al. (2012), where permeability decreased by a factor of 10^2 when the $CaCO_3$ content increased from about 3% to 8%, soil permeability in the other studies only decreased slightly as the $CaCO_3$ content increased from 0 to 14%. The reduction in permeability observed by Martinez et al. (2012) may be because the treatment processes including the injection type and flow rate of cementation solution varied between the six samples, which might explain the difference in

the micro-scale properties of $CaCO_3$ crystals formed in the soils after MICP treatment. However, as the effect of microscale properties of $CaCO_3$ crystals on the permeability was not investigated, the exact reason behind this remains unclear.

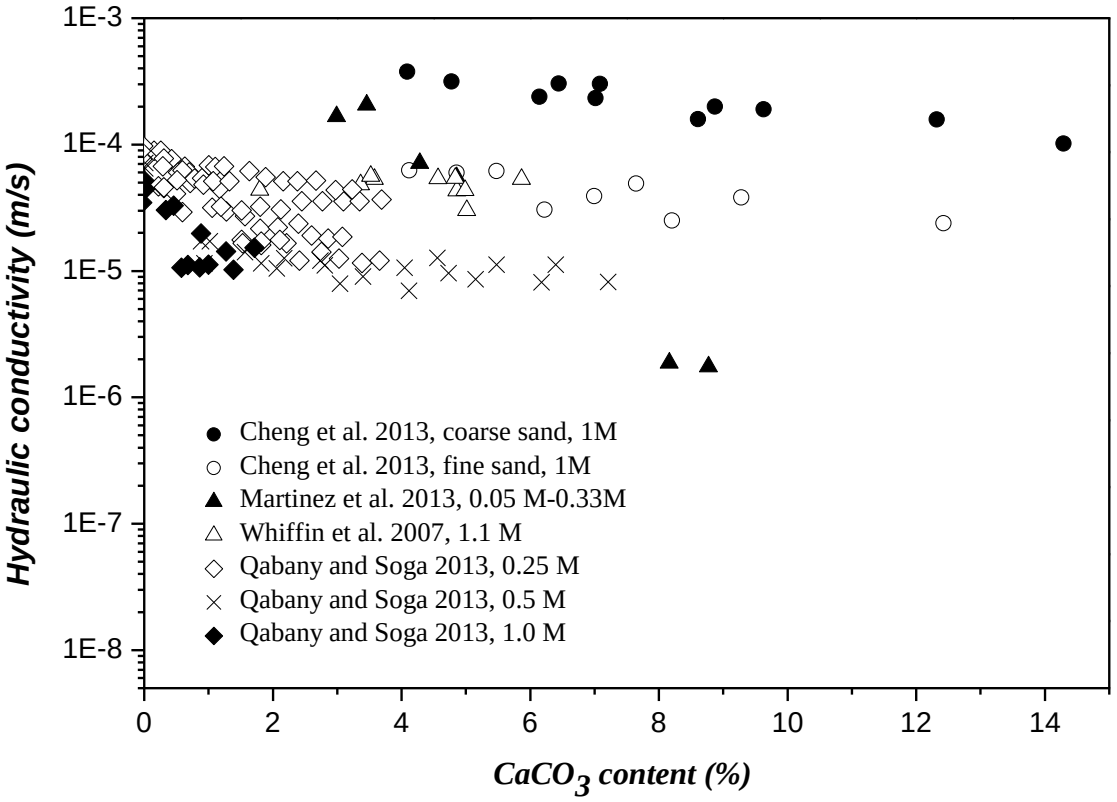

Figure 2.20 Relationship between hydraulic conductivity and precipitated $CaCO_3$ content. The concentration of cementation solution used in the studies are listed in the legend [unit: M (mol/L)]

2.4.2.1 Effects of $CaCO_3$ content on the strength of MICP-treated soils

Although the effect of $CaCO_3$ on reducing hydraulic conductivity is not obvious, research has shown that $CaCO_3$ can improve mechanical properties such as strength, stiffness and volumetric strain of sand. Research has also shown that these mechanical properties are affected by $CaCO_3$ content, sand gradation, relative density, and confining stress (Rebata-Landa, 2007; Chou et al., 2011; van Paassen et al., 2010; Al Qabany and Soga, 2013; Cheng et al., 2013). The correlations between $CaCO_3$ content in the MICP-treated soil specimen and the relative unconfined compressive strength (UCS) values of the MICP-treated soil specimen reported in literature, are summarized in **Figure 2.21**. An increase in UCS of MICP-treated

soils with increasing $CaCO_3$ content was found, while it is worth noting that different treatment strategies and methods create different correlations between UCS and $CaCO_3$ content.

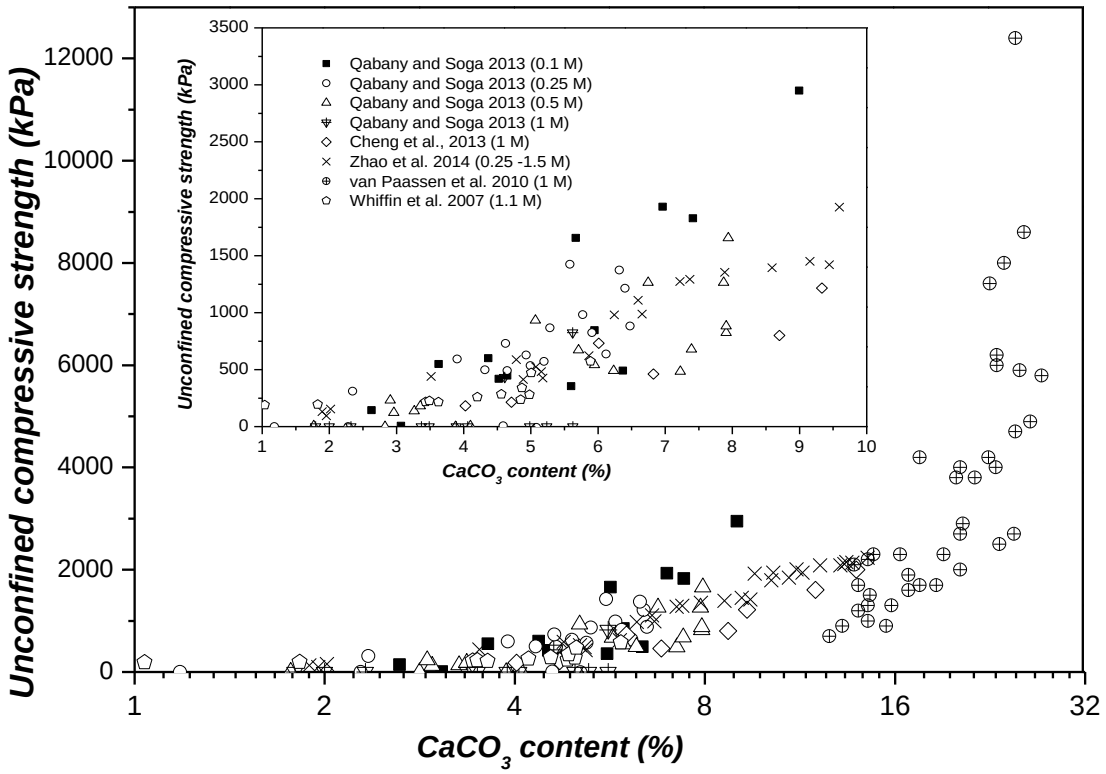

Figure 2.21 Correlation between UCS and precipitated $CaCO_3$ content ($CaCO_3$ content is based on the total weight of soil and $CaCO_3$ in the $CaCO_3$ range of 0-32%. The correlation between UCS and precipitated $CaCO_3$ content in the $CaCO_3$ content range of 0-10% is also shown in the figure.

2.4.2.2 Effects of sand gradation on the strength of MICP-treated soils

Another factor which affects the strength of MICP-treated soils is soil gradation (particle size). The content of $CaCO_3$ is shown as a function of grain size in **Figure 2.22**. Pictures of the different soils after MICP treatment are superimposed on the figure. Maximum carbonate deposition is observed on grains of 100 microns in size. The clay was un-cemented and coarse grains were readily disintegrated upon manipulation. All other intermediate cases exhibited a well-bonded fabric. Because the size of *S. pasteurii* is larger than 1 μm, for clay with grain sizes lower than 1 μm, the pore size may be too small for bacteria to pass through, which may have resulted in uncemented samples. On the other hand, because the size of $CaCO_3$ crystals

produced after MICP treatment is in the range of 2 - 150 µm, for coarse sands and gravel which have a grain size larger than 500 µm, the crystals may not be large enough to effectively bond the grains, thus resulting in poor cementation.

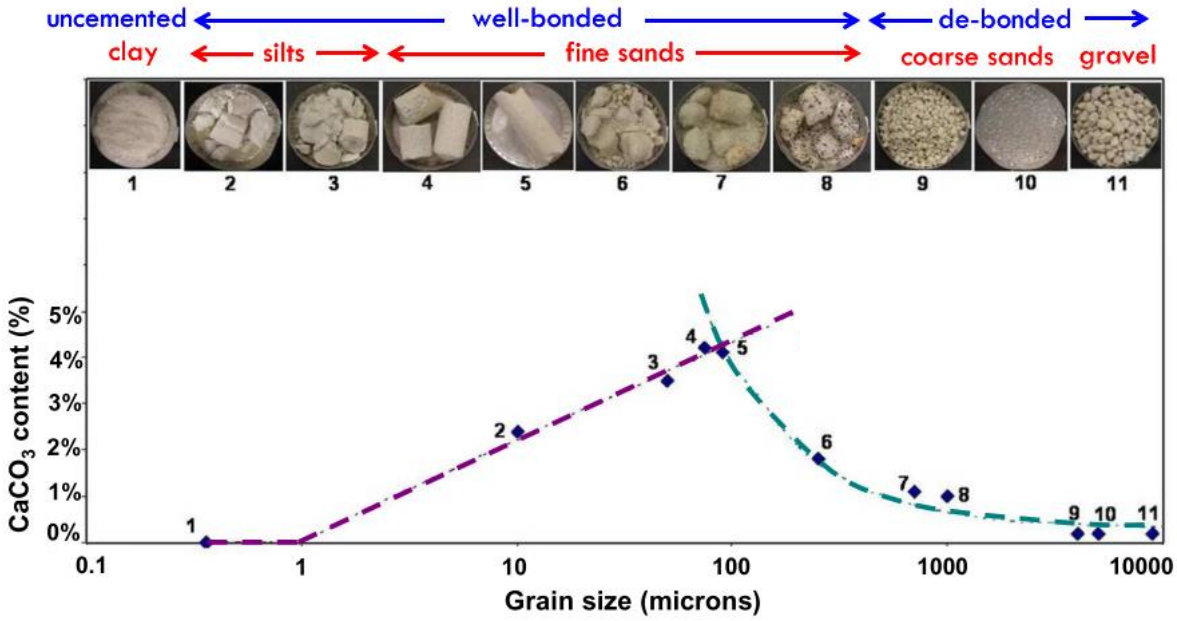

Figure 2.22 $CaCO_3$ content and models as a function of the grain size. Pictures correspond to each data point (Rebata-Landa, 2007).

2.4.2.3 Effects of bacterial number/activity and temperature on the strength of MICP-treated soils

The effect of bacterial number and total bacterial activity has previously been shown to affect the strength of MICP-treated sand (Shahrokhi-Shahraki et al., 2015; Cheng et al., 2017). It was found that the strength of MICP-treated sand decreased as the bacterial density was increased from 6×10^7 cells/ml to 4×10^8 cells/ml. (Shahrokhi-Shahraki et al., 2015). Similarly, when bacteria with an optical density ranging between 1.1 to 11 and activities between 300 to 3000 mM/h (5-50 U/L) were used, a low level of urease activity resulted in a more effective improvement in strength (Cheng et al., 2017).

Temperature was also shown to have an effect on the strength of MICP-treated sand. Strength improvement was higher at 25°C compared to either 4°C or 50°C. The crystals which formed at 50°C were the least efficient in terms of improving soil strength.

As reviewed in *Section 2.3.2.2*, both bacterial number/activity and temperature might have an effect on the formation and growth of crystals, which in turn affects the number and size of $CaCO_3$ crystals formed. Bacterial number/activity and temperature may thus have an effect on the strength of MICP-treated sand. However, because the micro-scale $CaCO_3$ formation process during MICP is still not fully understood, our current understanding of the effects of these parameters on the formation and growth of $CaCO_3$ crystals is very limited.

2.4.3 Chemical efficiency and performance efficiency of MICP

2.4.3.1 Chemical efficiency of MICP

The chemical efficiency (transformation efficiency) is defined as the percentage of injected urea and calcium chloride that precipitate as calcium carbonate (Al Qabany et al., 2012). Improving the precipitation efficiency of $CaCO_3$ is essential for avoiding excessive use of raw materials. Al Qabany et al. (2012) studied the effect of chemical treatment factors (i.e. cementation liquid concentrations, retention times and effective input rates) on precipitation efficiency. It was found that when the urea and $CaCl_2$ input rate was below 0.042 mol/L/h and the bacterial optical density was between 0.8 and 1.2, the reaction efficiency remained high and the amount of precipitation was not affected by the concentration of liquid medium for input concentrations up to 1 M. However, the study by Al Qabany and colleagues did not consider the effects of bacterial activity and bacterial number on chemical efficiency. As reviewed in *Section 2.2*, bacterial activity and density, as well as many environmental factors such as temperature and oxygen, affect the kinetics of ureolysis which in turn affects the kinetics of $CaCO_3$ precipitation and transformation efficiency.

2.4.3.2 Performance efficiency of MICP

The performance efficiency here refers to the efficiency with which $CaCO_3$ is added to improve the strength and other engineering properties of MICP-treated soils. As reviewed in *Section 2.4.2.1*, when the $CaCO_3$ content is kept constant, the increase in strength of MICP-treated soils varied significantly. This is partially because the soil properties varied between those different studies, but also because of the difference in the micro-scale properties of $CaCO_3$ crystals formed and variation in the percentage of $CaCO_3$ crystals that can bond soil particles. Therefore, it is important to understand the factors that affect the formation of the $CaCO_3$ crystals with different properties, as well as how to increase the amount of $CaCO_3$ crystals that can contribute to the increase of the strength of MICP-treated soils.

Micro-scale properties of $CaCO_3$ crystals such as type, size and distribution affect the macro-scale engineering properties of a soil matrix. The type of $CaCO_3$ is thought to affect the mechanical behaviour of MICP-treated soils. By comparing two samples containing a similar $CaCO_3$ content but different types of $CaCO_3$ (calcite and vaterite), the MICP-treated sample containing calcite was found to be relatively strong and maintained its shape, whereas the MICP-treated sample containing vaterite was extremely weak and almost turned into powder when held by hand (Al Qabany, 2011). This study suggested that the size and distribution of $CaCO_3$ crystals affects the strength of MICP-treated soils. It was suggested that crystals that are large enough and precipitate at soil-particle contacts are more efficient in bonding soil particles and therefore provide the greatest contribution to the increase in soil strength compared with smaller crystals that cannot bond soil particles, or with crystals which distribute on the surfaces of a soil particles which face away from the surfaces of neighbouring soil particles.

Chapter 3 Materials and Methods

3.1 Bacteria and chemicals

3.1.1 Bacterial strain and cultivation

Sporosarcina pasteurii (*S. pasteurii*) is a naturally-occurring strain of soil bacteria with ureolysis activity. *S. pasteurii* has been widely used in MICP studies (DeJong et al., 2006; Whiffin et al., 2007; van Paassen et al., 2010; Al Qabany and Soga, 2013; Dawoud, 2015, Zhang et al., 2018). As reviewed in *Chapter 2*, bacterial storage/cultivation procedure significantly affect bacterial activity. Two different strains of *S. pasteurii* were cultivated and stored in the lab under different conditions. The first strain was cultivated from a frozen *S. pasteurii* glycerol stock (ATCC 11859) prepared by Dawoud (2015). Once defrosted, cells from the glycerol stock were grown in ATCC 1376 NH_4-YE agar medium (20 g/L yeast extract, 10 g/L ammonium sulphate, 20 g/L agar, and 0.13 M Tris base) for 48 hours at 30°C. Subsequently, several colonies on the agar plate were picked and transferred to 100 mL of NH_4-YE liquid medium containing the same components without agar in a 250 mL flask and cultivated in a shaking incubator for 12 hours at 30°C and a shaking rate of 200 rpm to obtain a bacterial suspension with an optical density of around 1.0~2.0 measured at a wavelength of 600 nm (OD_{600}). Details regarding how bacterial density was measured is described in *Section 3.1.2*. This bacterial suspension was stored in a refrigerator at 4 °C for up to one month before cultivating bacteria in a fresh liquid medium by adding 1 ml of this bacterial suspension to 100 ml of freshly autoclaved liquid medium and repeating the same cultivation process mentioned above. Bacterial density and activity were measured prior to each experiment as described in *Sections 3.1.2* and *3.1.3*. Using this method, the bacterial activity observed in our study was in the range of 20-40 mM/h when the OD_{600} was 1.0.

To obtain a bacterial strain with a higher bacterial activity, the second strain of *S. pasteurii* was cultivated from a freeze-dried *S. pasteurii* stock (strain DSM 33, purchased from DSMZ, Germany) and activated according to the manufacturer's guidelines. After activation, glycerol stocks of the bacteria were prepared by adding 225 µl of 80 % glycerol (autoclaved) to 1 ml of overnight liquid culture in cryogenic vials, after which the liquid culture was immediately frozen at -80°C. Bacterial colonies and liquid medium were prepared in the same way as mentioned above. However, for each new experiment, a new frozen stock was used for cultivation on agar plates and in liquid medium. In addition, for each experiment, the plate cultures and liquid cultures were stored in the fridge for a maximum of two days before the experiment. In this way, the bacterial activity observed in our study was in the range of 200-300 mM/h when the OD_{600} was 1.0.

3.1.2 Bacterial density measurement

Bacterial density was measured using a spectrophotometer (Thermo Scientific Helios Zeta) at a fixed wavelength of 600 nm (OD_{600}) (**Figure 3.1)**. When the density of the bacterial suspension was high, the bacterial suspension was diluted using the same nutrient medium to optical density values between 0.05-0.4 when measuring the OD. When this was the case, the OD of the bacterial suspension was determined by multiplying the OD reading of the diluted suspension by the dilution factor.

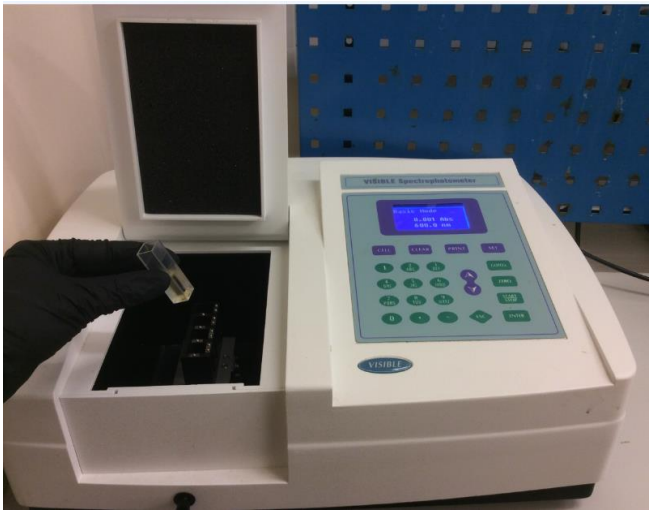

Figure 3.1 Photo of the spectrophotometer for bacterial optical density measurement

3.1.3 Bacterial activity measurement

The activity of bacterial cells in a liquid suspension of urea was measured as described in Whiffin (2004). Samples were prepared by mixing a urea solution with a bacterial suspension at 25°C at a volume ratio of urea solution to bacterial suspension of 9:1. The concentration of urea was 1.11 M and the bacterial density was 1.0 when measuring OD_{600}. The conductivity of the mixed content was assessed by using a conductivity meter (FiveGo, Meter Toledo) immediately after the mixing and five minutes after mixing. The concentration of hydrolysed urea during these five minutes and the relative ureolysis rate were calculated using equation 3.1 (Whiffin, 2004). Measurements were performed in triplicates for each of the different media tested, with data presented as mean ± standard error.

$$BA(mM/h) = \frac{\Delta Conductivity(\mu S/cm)}{\Delta t(\text{min})} \times (10^{-3} \times 11.11)(mM/(\mu S/cm)) \times 60(\text{min}/h) \qquad 3.1$$

3.1.4 Cementation solution

The cementation solution for MICP treatment was created using calcium chloride ($CaCl_2$), urea ($CO(NH_2)_2$), ammonium chloride (NH_4Cl), sodium bicarbonate ($NaHCO_3$), and Thermo Scientific™ Oxoid™ Nutrient Broth dissolved in deionised (DI) water. The cementation solution was not autoclaved. Urea and calcium chloride served as important ingredients for promoting calcium carbonate precipitation, and the nutrient broth served as an energy source for bacterial activity. Three concentrations of calcium chloride were used: 0.25 M, 0.5 M and 1.0 M. The concentration of urea was 1.5 times higher than the concentration of calcium chloride (0.375 M, 0.75 M and 1.5 M) and the concentration of nutrient broth was kept constant at 3 g/L.

3.2 Liquid batch test to assess ureolysis kinetics

A set of liquid batch experiments were conducted to examine the influence of bacterial density and urea concentration on ureolysis kinetics. The experiments were conducted by testing the change in the conductivity of the mixture of bacterial suspension with urea solution as described in Whiffin (2004). The experimental setup for assessment of ureolysis kinetics is

shown in **Figure 3.2**. Samples were prepared by mixing urea solution and bacterial suspension at 20°C at volume ratios between 9:1 and 1:1 to obtained desired bacterial density and urea concentration in the mixture. The change in the concentration of urea with time was measured using the same method described in *Section 2.2.1*, but over a wider time interval which ranged from immediately after to 1 hour after mixing. In addition, the mixed liquid culture was placed on a shaker shaking at a constant rate of 100 rpm at 20°C. Apart from when the activity of the liquid was tested, the mixed culture was constantly shaken to ensure that the bacterial cells and urea were fully mixed. Batch tests were performed in triplicates for each of the different media tested, with data presented as mean ± standard error.

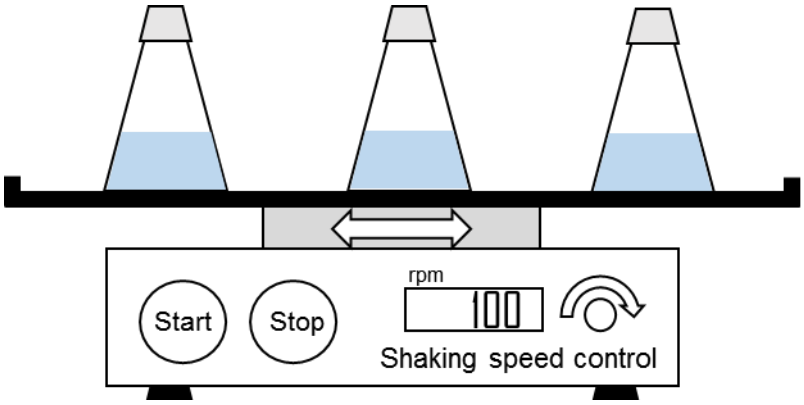

Figure 3.2 Schematic of a setup for ureolysis kinetics experiments

3.3 Micro-scale experimental setup

3.3.1 Microscope slide experiments

To observe the MICP processes including the behaviour of bacteria and the process of calcium carbonate crystal formation during the biochemical reactions at the micro-scale, the first micro-scale experimental setup-microscope slide experiments is shown in **Figure 3.3**. This experimental setup mainly contains a microscope slide sample made of a glass slide, a cover slip and a liquid sample, and a micro-scale visualisation and image quantification system. Microscope slide samples were prepared by placing either a single 10 µl drop or two successive 5 µl drops of liquid specimen at the centre of a microscope slide, after which a cover slip was

placed on top of the liquid specimen. The edges of the cover slip were sealed using nail varnish to avoid the drying of the samples on the microscope slide. Micro-scale visualisation and image quantification of the samples are described in *Section 3.3.3*. The microscope slide experiments were conducted at 20 °C.

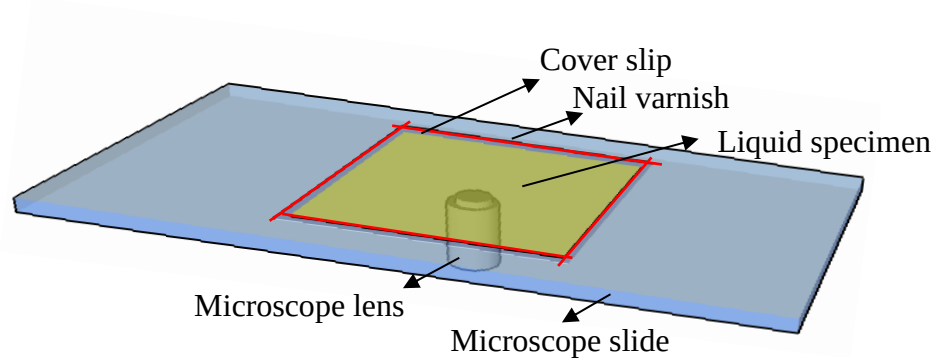

Figure 3.3 Schematic of the setup used for the microscope slide experiments

3.3.2 Microfluidic chip experiments

In the first micro-scale experimental setup-microscope slide experiments, the bacterial suspension and cementation solution have to be mixed first and after which the MICP process in mixture of bacterial suspension and cementation solution is observed. However, in real MICP treatment conditions, bacterial suspension and cementation solution are injected into a soil matrix. On the one hand, the injection flow rate, injection volume and injection procedure affect the MICP processes significantly. The speed and volume of the injection of bacterial suspension and cementation solution can be varied; the injection of bacterial suspension and cementation solution can be injected sequentially or together. In addition, the soil matrix as a porous medium also has effects on the MICP processes. This is because the structure of the porous medium affects the flow conditions including the distribution of flow rate, which consequently affects the transport of bacterial cells and chemical ions in the medium. The surface properties of soil particles also affect the interactions between bacterial cells and soil particles, which consequently affect the adsorption/desorption of bacterial cells. Therefore, to visualize the MICP process under the conditions that are equivalent to the real MICP conditions, a micro-scale porous medium with and flow manipulating system is necessary. As reviewed in *Chapter 2*, a microfluidic chip made by soft lithography can be made to contain

the porous channels. Therefore, the second micro-scale experimental setup was designed including the use of a microfluidic chip. **Figure 3.4** shows the schematic of the microfluidic chip experiments. The setup for a microfluidic chip experiment includes a microfluidic chip, a microscope, and a flow injection system which consists of a syringe, syringe pump and tubing. The designing and fabrication of the microfluidic chip will be described in *Chapter 4*. The microfluidic chip experiments were conducted at 20 °C.

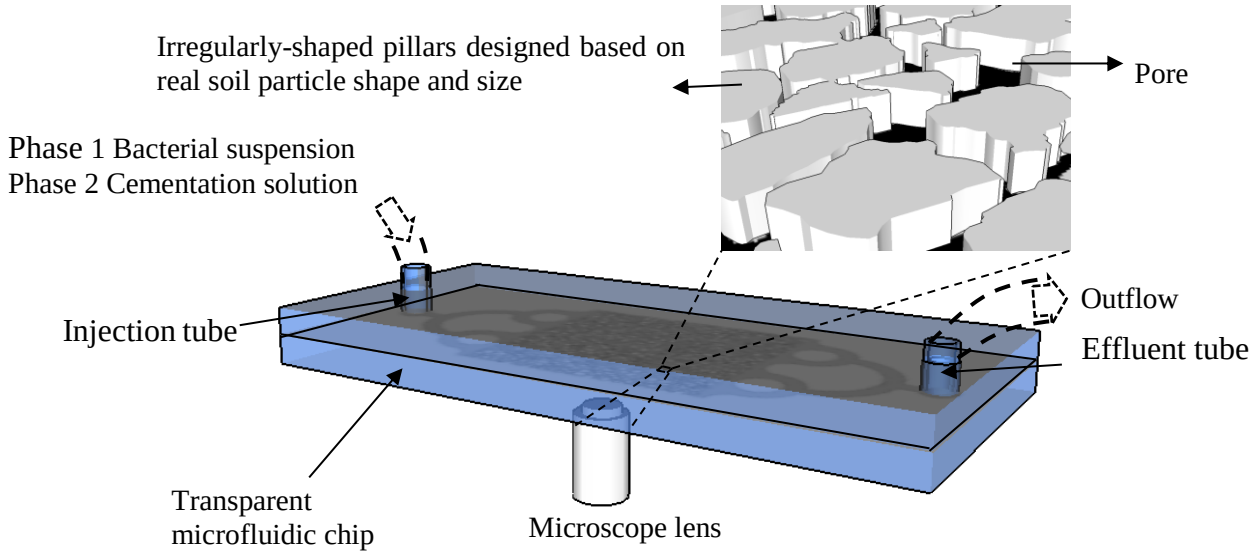

Figure 3.4 Schematic of the microfluidic chip experiments

3.3.3 Micro-scale visualization and image quantification

Images of samples were taken using an optical microscope (Zeiss Axio Observer Z1) to visualise the micro-scale MICP process in all of the experiments. The microscope is equipped with an automated stage (Prior Scientific Instruments), as well as a black and white camera (Hamamatsu C11440-22CU) connected to a computer. Images were taken at 100× magnification using phase field illumination with image resolution of 0.65 µm/pixel. For tests that investigate bacterial numbers, *S. pasteurii* were imaged at 100× magnification using a black and white camera and phase field illumination. For tests that investigate $CaCO_3$ size and amount, images were taken at 100× magnification using a black and white camera using either bright field illumination or phase field illumination. Images were analysed using Zeiss Axio Vision image analysis software to determine the areas of the corresponding crystals (will be

described later in the results of *Chapter 4*). The number of bacteria was counted manually at selected positions and time points during the injection process (will be described in *Chapter 4*).

3.4 Macro-scale experimental setup and materials

3.4.1 Sand

The sandy soil used in this study was fraction D silica sand (British standard, Sibelco, UK) (Al Qabany, 2011). This sand has a d_{50} value of 165 μm, with 50% of sand grains having a diameter of 165 μm or lower, and a d_{90} of 250 μm, with 90% of the grains having a diameter of 250 μm or less (Al Qabany, 2011). The density of the sand used was 2.65 g/cm^3. The sand contains 99.8 % SiO_2 and 0.005 % CaO. The full chemical composition of Sibelco sand is listed in **Table 3.1**.

Table 3.1 Chemical analysis of silica sand (%), provided by SIBELCO

Chemicals	Content （%）
SiO_2	99.80
Fe_2O_3	0.009
Al_2O_3	0.040
TiO_2	0.016
K_2O	0.006
CaO	0.005
Cr_2O_3	0.00005

3.4.2 Small soil column experiments

Based on experiments described in Al Qabany (2011), small soil column experiments were conducted by using plastic 100 mL syringes. The syringes were positioned vertically and packed with Fraction D sand to a dry density of 1.65 g/cm^3 (porosity of 0.37-0.38). The columns were positioned vertically with downward flow direction to avoid any settling of the

material inside the column or the generation of preferential flow paths that might have occurred if the column was positioned horizontally. The bottom of the column was fitted with filter material consisting of 2 layers of Whatman filter paper and the top of the column was fitted with 1 layer of filter paper. 180 g of sand was packed into the column ensuring that sand was compacted evenly to achieve at least 95 % of the maximum dry density to maintain consistency across experiments. After the dry sand was packed inside the column, at least 100 ml of DI water, equivalent to two times the total volume of the pores inside the soil column [2 Pore Volumes (PV)], were injected into the soil column to saturate the soil before performing MICP treatment. During the injection of bacterial suspension or cementation solution, a flexible tube that is connected to the outlet of the columns was put inside a flask to allow the liquid to be injected into the soil by gravity. After the completion of this injection, the tube was bent upwards up to keep the liquid inside the column for MICP reactions (**Figure 3.5**). After the MICP treatment, sand sample were taken out of the column for testing the $CaCO_3$ content, strength, stiffness and micro-scale properties of $CaCO_3$ by using an SEM. The small soil column experiments were conducted at 22 ± 2 °C.

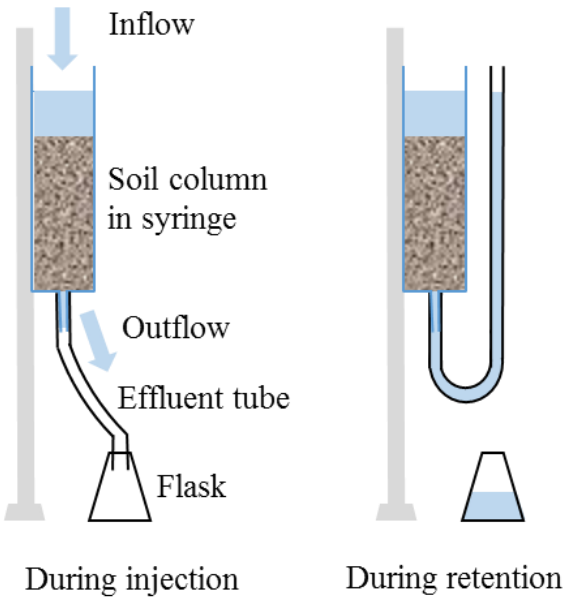

Figure 3.5 Schematic of setup for small soil experiments

3.4.3 1.2-meter column experiments

A 1.2-meter-long polyvinyl chloride (PVC) tube (internal diameter 75 mm) was positioned vertically and packed with Fraction D sand. A schematic of the setup of the long column experiment is shown in **Figure 3.6**. The columns were positioned vertically, with each end of the column being fitted with filter material consisting of 8 layers of filter paper. The sand was packed into the column in 6 consecutive layers, ensuring that each layer was compacted evenly to achieve at least 95% of the maximum dry density to maintain the consistency across experiments. The height of the soil samples placed in the columns were about 100 cm Same as the setup of small soil column experiment, during the injection of bacterial suspension or cementation solution, the tube was put down, to let them to be injected via gravity, while after injection during retention, the tube was put up to stop the flow; the liquid was always kept to be as high as the top of the columns either during injection or retention. After MICP-treatment, the specimen inside each column was taken out, and divided into about 10 pieces, to be tested of $CaCO_3$ content, strength and stiffness, and subsequently analysed of the pore-scale properties of $CaCO_3$ crystals using scanning electron microscopy (SEM). The 1.2-meter soil column experiments were conducted at 22 ± 2 °C

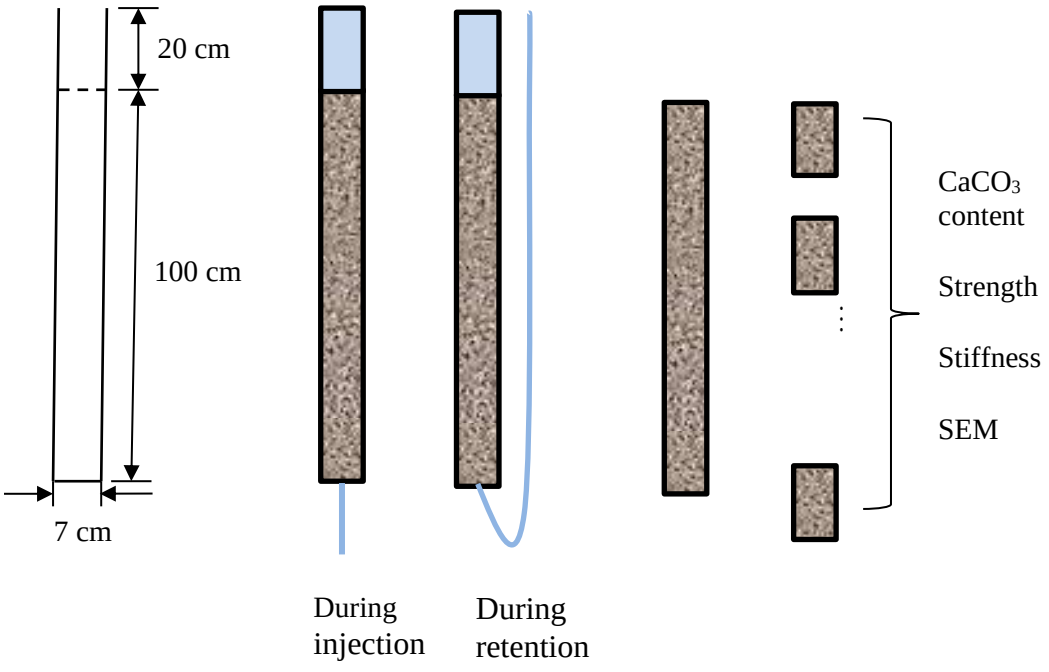

Figure 3.6 Schematic of setup for long column experiment

3.4.4 Flow rate measurement

The injection volume (V) and duration of injection (T) were measured during each of the injections where the treated soil samples were still intact inside the PVC column. The injection flow rate (Q) was calculated by dividing the volume of cementation solution injected (V) by the duration of the injection (T) (*Equation 3.2*). The permeability of soil samples (k) was tested using DI water before and after treatment and by using cementation solution during treatment where the treated soil samples were still intact inside the PVC column. The injection duration of water, bacterial suspension and cementation solution were recorded as for the permeability of the sand during the MICP treatment procedure following equations by *Equations 3.2* and *3.3*. It should be noticed that normally the permeability of soil is measured using water, while in this study, the permeability of the sand was measured by cementation solution.

$$Q = V / T \tag{3.2}$$

$$k = \frac{Q}{A \times n} \tag{3.3}$$

where A is the cross-sectional area of the soil columns and n is the porosity of the soil sample.

3.4.5 Unconfined compression strength (UCS) test

Unconfined compression strength (UCS) test has been applied extensively in the studies of MICP for testing the strength of MICP-treated soils (van Paassen, et al., 2010; Al Qabany and Soga, 2013; Cheng et al., 2017). UCS was chosen as an indicator for the strength of MICP-treated soil specimens. After MICP treatment, the treated sand samples were flushed with at least two pore volumes of DI water to wash away all excess soluble salts prior to drying the sand samples at 100.5°C for at least 24 hours. The top and bottom of the soil samples were treated to be flat and horizontal for Unconfined Compressive Strength (UCS) experiments conducted following the American Society for Testing and Materials (ASTM) standard D2938-86-standard test method for measuring unconfined compressive strength of an intact rock core specimen. The axial load was applied at a constant rate of 0.014 mm/min. The length of the sample was measured before UCS tests, and the height to diameter ratios were about 1: 2 because the exact height of the specimen varied when the specimen was taken out and prepared. The measured UCS values were computed to be the UCS values of an equivalent H/D=2

specimen based on *Equation 3.4* as suggested by the ASTM standard D2938-86-standard test method.

$$C = \frac{C_a}{0.88 + (0.24\,D/H)} \tag{3.4}$$

where C is the computed compressive strength of an equivalent H/D=2 specimen; C_a is the measured compressive strength of the specimen tested; D is the core diameter; and H is the core height.

3.4.6 Assessment of $CaCO_3$ content

The calcium carbonate ($CaCO_3$) content of MICP-treated soil samples was determined using the method described by Dawoud (2015) using a chamber connected to a gas pressure meter. After the UCS test, about 20-30 g of the soil specimen was ground, after which the exact mass of the ground specimen was measured before being placed in the chamber (**Figure 3.7a**). A container with 30 ml of HCl (2.5 M) was then placed in the chamber (**Figure 3.7b**). After the chamber was closed tightly (**Figure 3.7c**), it was shaken to mix the acid with the ground soil (**Figure 3.7b**). Because the $CaCO_3$ reacts with HCl and generates CO_2 (*Equation 3.5*), the gas pressure inside the chamber increases. The actual amount of $CaCO_3$ was calculated based on an established relationship (*Equation 3.6*) between the pressure of CO_2 gas and the amount of pure analytical grade $CaCO_3$ powder (Dawoud, 2015). Based on a calibrated pressure-$CaCO_3$ mass curve which is measured using mixtures of HCl and pure $CaCO_3$ powder, and the reading of the pressure in the experiments, the mass of $CaCO_3$ inside the ground soil can be calculated using *Equation 3.6*.

$$CaCO_3 + 2HCl \rightarrow CaCl_2 + CO_2 \uparrow + H_2O \tag{3.5}$$

$$CaCO_3\ content\,(g) = pressure \times 1.922 + 0.011 \tag{3.6}$$

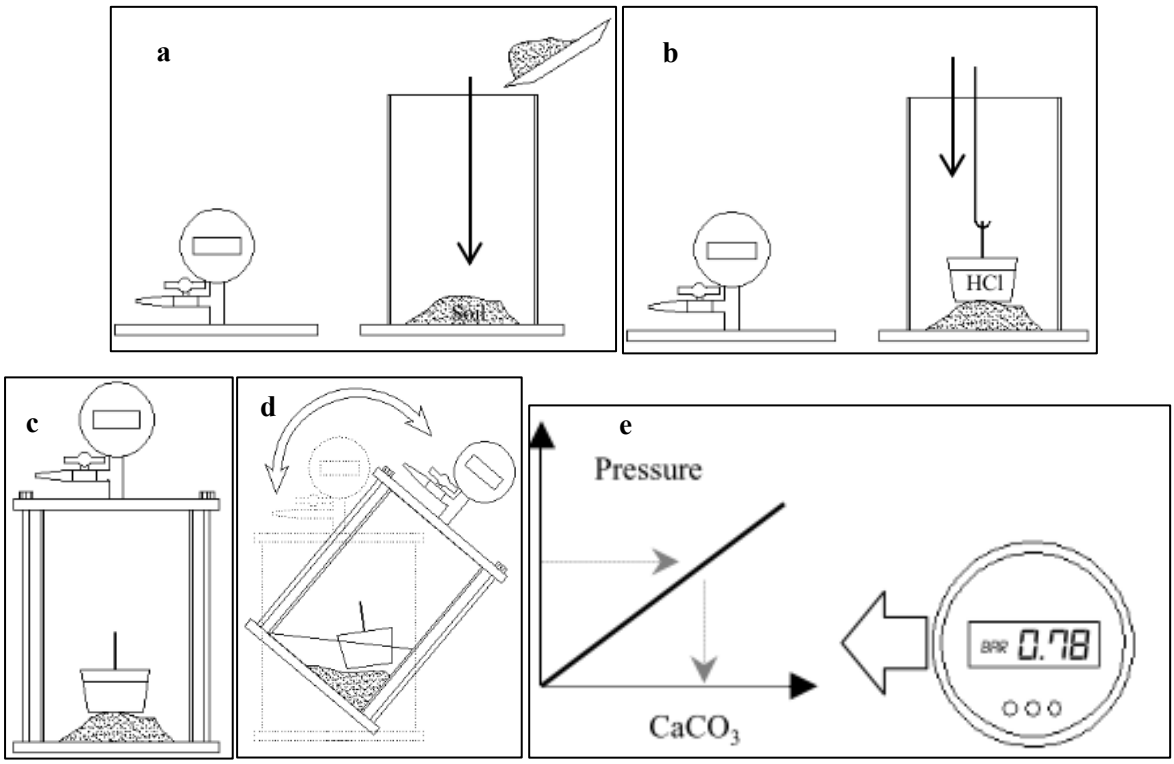

Figure 3.7 Calcium carbonate measurement chamber and measurement procedure. **(a)** Placing dry MICP-treated sand into the chamber; **(b)** placing HCl into the chamber; **(c)** close the chamber; **(d)** mixing sand with HCl; **(e)** pressure reading and $CaCO_3$ calculation by the correlation between pressure and $CaCO_3$ content (Dawoud, 2015).

3.4.7 Micro-scale properties of $CaCO_3$ crystals in MICP-treated sandy soils assessed by Scanning Electron Microscopy (SEM)

To characterise the shapes, size and distribution of precipitated $CaCO_3$ crystals inside the soil specimen, scanning electron microscope (SEM) images of MICP-treated soil samples were captured after the UCS test using a Philips XL20 scanning electron microscope (Philips Electron Optics, Eindhoven, The Netherlands). Samples were dried in an oven at 100.5°C for 24 hours. Before imaging, the surfaces of the samples were not gold-coated. Images were taken at 300× magnification.

Chapter 4 A microfluidic chip and its feasibility for characterising micro-scale properties of MICP

4.1 Research aims

Due to a lack of a micro-scale testing technique that could capture the behaviour of both bacteria and $CaCO_3$ crystals in the pore fluid of a soil matrix during Microbial-Induced Carbonate Precipitation (MICP) treatment procedures, MICP mechanisms such as its micro-scale process and kinetics have so far been poorly understood. As a result, it has been very challenging to control and predict the micro-scale properties of $CaCO_3$ precipitates which affect the macro-scale mechanical properties and uniformity of MICP-treated soils. Therefore, an appropriate testing technique that can be used to study the MICP fundamental mechanisms such as the behaviour of both bacteria and $CaCO_3$ crystals in the pore fluid of a soil matrix during MICP treatment procedures is needed.

As reviewed in *Chapter 2*, microfluidics techniques can be used to create a micro-scale porous medium that replicates the structure of a soil matrix and has surface properties equivalent to soil particles. In addition, microfluidics also allows the control of micro-scale flow conditions in the porous medium, including flow rate and volume, which can simulate the conditions of MICP treatment in real soils at the soil particle-scale.

Therefore, microfluidics has the potential to be used as an appropriate technique to study the micro-scale fundamental mechanisms of MICP. The research aim of this chapter was to design and fabricate a microfluidic chip which can model the porous structure of a soil matrix and can be used to study MICP under conditions which mimic fluid flow through soil matrices. In addition, a series of MICP tests were conducted in the fabricated microfluidic chips to

investigate their utility in characterising the micro-scale properties of MICP, including the quantification of bacteria and the sizes and shapes of $CaCO_3$ crystals. The content of this chapter has been accepted for publication in the Journal 'Géotechnique' as a general paper entitled 'A microfluidic chip and its use in characterising the particle-scale behaviour of Microbial-Induced Calcium Carbonate Precipitation (MICP)'.

4.2 Design of a mask for fabricating microfluidic chips

A microfluidic chip which represents a sandy soil matrix was designed based on a cross-sectional image of solidified and sectioned 3-D Ottawa 30-50 sandy soil specimen (**Figure 4.1a**). In a real sandy soil matrix, fluid flows through pores between soil particles even though the soil particles are in contact with each other. However, in the cross-sectional image of a soil specimen (presented by Yang, 2015) (**Figure 4.1a** and **b**), some of the particles are connected to each other, meaning that if this image was used to make a microfluidic chip with pillars, fluid would not be able to flow between these pillars. Therefore, contacts between the particles (**Figure 4.1 b**) were manually modified to create open channels that would allow flow between the pillars (**Figure 4.1c**). Most of the width of the opened channels were about 50 microns, which is roughly equivalent to the distances between narrow pore throats in the porous medium of the soil specimen. The depth of the microfluidic chip was designed to be 50 microns, which is also roughly equivalent to the distances between narrow pore throats in the porous medium of the soil specimen. The porous medium of the microfluidic chip is 15 mm in length and width and has a porosity approximately 0.40 (calculated by dividing the total pore area of the pores by the total area of the porous medium). The two-dimensional design of the microfluidic chip is shown in **Figure 4.1d.** The microfluidic chip also contains an inlet, upstream flow distribution channels, a porous medium, downstream flow distribution channels, and an outlet. The inlet and outlet enable solutions to be injected and flow out of the microfluidic chip. The flow distribution channels distribute the flow evenly into and out of the porous medium. The porous medium, in the middle of the microfluidic chip, represents the porous soil matrix. Autodesk® AutoCAD® 2015 was used to design the mask for fabricating the microfluidic

chips used in this study. The designed mask was printed by Micro Lithography Services (Chelmsford, UK) on a transparent film for the fabrication of the microfluidic chips.

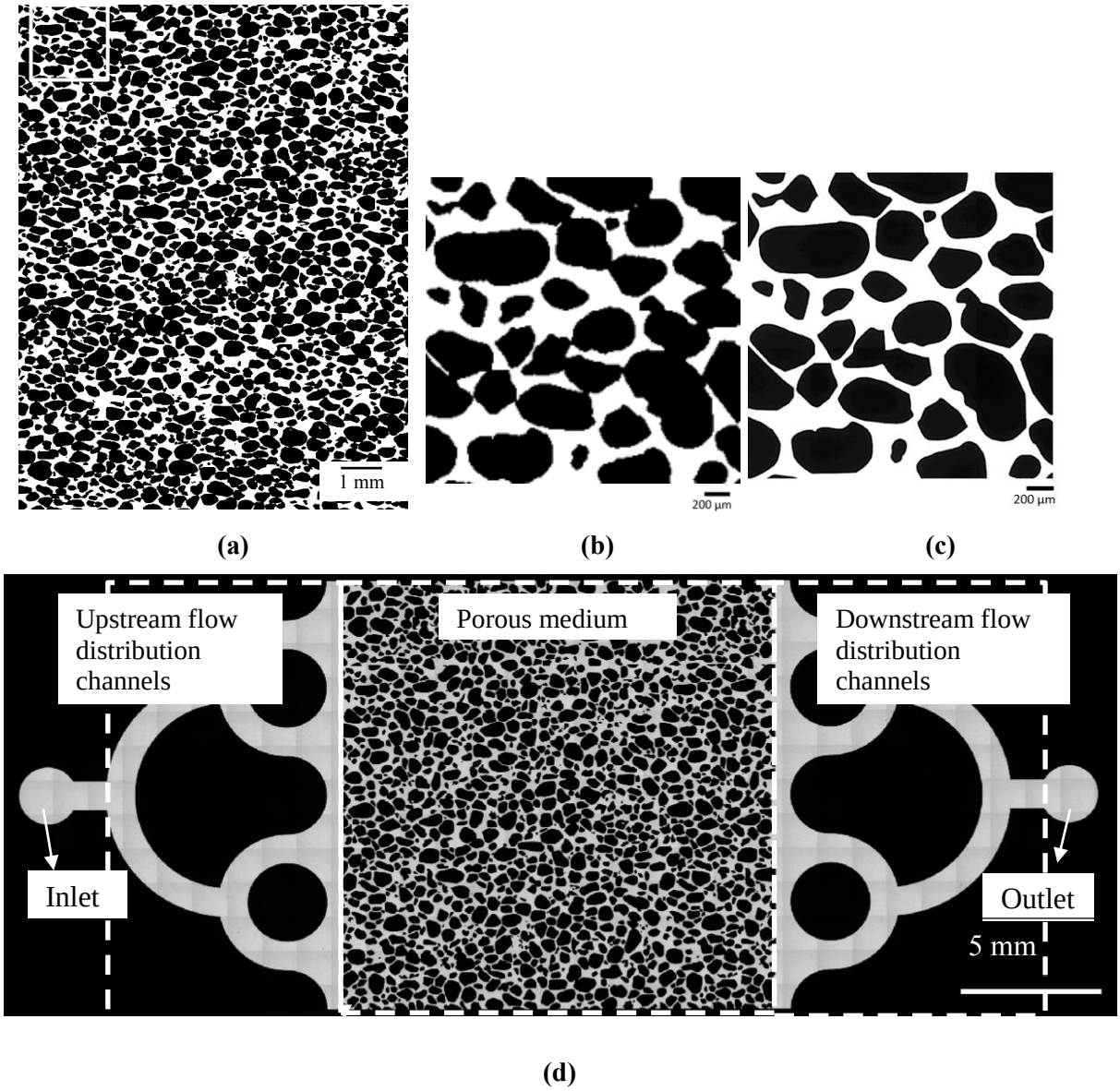

Figure 4.1 (a) Cross-sectional image of a solidified and sectioned 3-D Ottawa 30-50 sandy soil specimen by Yang (2015); **(b)** magnified image of top-left square in image; **(c)** AutoCAD image of the modified image of the image shown in (b). **(d)** Microscope image of a printed mask for making the microfluidic chip.

4.3 Fabrication of microfluidic chips

Standard photolithography techniques were used to fabricate the master for the microfluidic device, involving the use of a silicon wafer (MicroChemicals GmbH, Germany), SU-8 3025 photoresist (MicroChem, US) and EC solvent (Dow Chemical Company, Denmark). A schematic illustrating the main steps during the fabrication is shown in **Figure 4.2**. The silicon wafer was coated with SU-8 3025, which is a photoresist polymer. Coating was conducted using a spin coater, the speed and spinning duration of which controls the thickness of SU-8 (**Figure 4.2a**). The SU-8-coated silicon wafer was heated to be solid after coating (**Figure 4.2a**) and was then selectively exposed to UV light by placing the mask directly above the wafer (**Figure 4.2b**). The areas of the photoresist which were not exposed to UV light were weakened and removed by EC solvent (**Figure 4.2c**). The fabrication of the microfluidic device was conducted after the fabrication of the silicon master. A 10:1 v/v mixture of polydimethylsiloxane base (PDMS, Sylgard 184, Ellsworth Adhesives) and curing agent (Sylgard 184, Ellsworth Adhesives) was poured over the master and cured in an oven at 65 °C for 5 hours (**Figure 4.2d**), after which the cured PDMS stamp was peeled from the silicon master. After the inlet and the outlet hole were cut with a Harris Uni-Core 0.75 mm punch (Ted pella, Inc.), the PDMS chips were irreversibly sealed with clean PDMS bottom slips by exposing them to air plasma (Harrick Plasma) (**Figure 4.2e**). It is generally thought that PDMS consists of repeated units of $–O\text{-}Si(CH_3)_2\text{-}$, with methyl groups ($\text{-}CH_3$) being converted to silanol groups (-Si-O-H) after exposure to oxygen plasma (Zhou et al. 2010). The surface of PDMS was subjected to plasma treatment to make it hydrophilic and negatively charged. A photo of the fabricated master is shown in **Figure 4.3**.

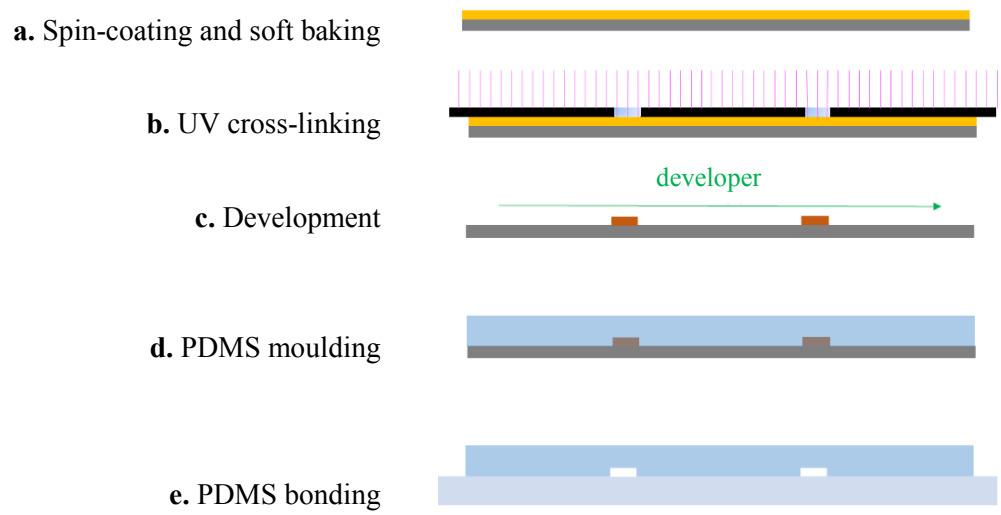

Figure 4.2 Schematic illustrating main steps of microfluidic chip fabrication.

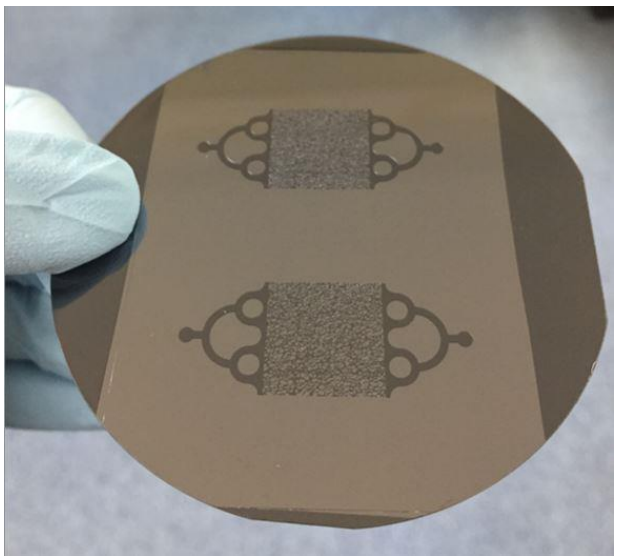

Figure 4.3 Photo of a fabricated silicon wafer master containing two microfluidic models. The wafer is 7.62 cm in diameter.

4.4 MICP microfluidic experiment

S. pasteurii [American Type Culture Collection (ATCC) 11859] was used in these experiments due to its ability to hydrolyse urea (Al Qabany et al., 2012). The bacterial cultivation procedure is described in *Section 3.1.1*. *S. pasteurii* cells were grown for 5.5 - 16 hours at 30°C to obtain

an optical density at 600 nm (OD_{600}) of 0.8 - 4.0. The cementation solution contained $CaCl_2 \cdot 2H_2O$ (0.25 M), $CO(NH_2)_2$ (0.375 M), NH_4Cl (0.187 M), $NaHCO_3$ (0.0252 M) and nutrient broth (3 g/L) (Al Qabany et al., 2012). The $NaHCO_3$ was added to stabilise the pH of the cementation solution (Al Qabany and Soga, 2013). The measured pH of the cementation solution was about 7.1 ± 0.1.

A staged-injection treatment procedure has been widely utilised in MICP for soil treatments due to its capability of delivering bacterial and chemical reactants over longer distances in soils (Whiffin et al., 2007; van Paassen et al., 2010; Al Qabany et al., 2012). To model this procedure in a MICP microfluidic chip experiment, the microfluidic chips were fully saturated with deionised (DI) water prior to the MICP treatment procedure. Bacterial suspension was injected into the microfluidic chips using a syringe pump at different flow rates over different periods of time. Bacteria were then given time to settle and attach to the PDMS surfaces within the chip. Subsequently, the syringe containing the bacterial suspension was displaced by a syringe containing cementation solution and, in the meantime, a new tubing was also replaced. The process of injecting the cementation solution was the same as the process of injecting bacteria, with different flow rates, volumes and numbers of injections being trialled. Images of the samples were taken at different time points.

PDMS microfluidic chips were fully saturated with deionized (DI) water prior to commencing microfluidic experiments to remove the effect of partial saturation on the transport of bacterial cells and chemicals in the porous medium which might have otherwise affected the $CaCO_3$ precipitation process. Bacterial suspension and cementation solution were injected into the microfluidic chips using a syringe pump which can be used to adjust injection flow rate. The bacterial cells and the $CaCO_3$ crystals formed within the microfluidic chip were observed under a light microscope as described in *Chapter 3*. Six tests were conducted to characterise the bacterial distribution during injection (Test 1), bacterial growth during bacterial settling (Test 2), bacterial detachment during the injection of cementation solution (Tests 3 and 4), and crystal growth during and after the injection of cementation solution (Tests 5 and 6). The bacterial, chemical and injection parameters associated with each test are summarised in **Table 4.1** and **Table 4.2**. The OD_{600} of the bacterial suspension was measured immediately before

the bacterial injection. The amount of fluid perfused through the microfluidic chip was measured by dividing the volume injected by the total pore volume (PV) of the device (**Table 4.1** and

Table 4.2). The settling time is the time interval between the completion of the injection of bacterial suspension and the start of the injection(s) of cementation solution (**Table 4.1**). In Tests 4 and 6, multiple injections of cementation solution were applied. The injection intervals between two successive injections are shown in **Table 4.2**. The injection flow rates of bacterial suspension and cementation solution were either 5.6 or 56 PV/h, corresponding to Darcy velocities of 4.6×10^{-5} m/s and 4.6×10^{-4} m/s, respectively. These values are within the range of values reported in the literature (Al Qabany and Soga, 2013; Martinez et al., 2013; Montoya et al., 2012). When observing bacterial transport during the bacterial injection, bacterial suspension was injected at a flow rate of 5.6 PV/h to allow enough time for images of the sample to be taken at different locations and at different time points during the injection.

Table 4.1 Bacterial properties of the experiments

Test No.	1	2	3	4	5	6
OD_{600}	4.0	0.8	1.6	1.6	0.8	1.6
Injection PV	1.5	1.5	1.25	1.25	1.5	1.25
Flow rate, PV/h	5.6	56	56	56	56	56
Settling time, h	-	4	3.5	4.5	4	3.5

Table 4.2 Chemical properties of the experiments

Test No.	1	2	3	4	5	6
Ca^{2+} concentration, M	-	-	0.25	0.25	0.25	0.25
Injection PV	-	-	1.25	1.25	6	1.25
Injection times	-	-	1	12	1	20
Flow rate, PV/h	-	-	5.6	5.6	5.6	5.6
Injection intervals, h	-	-	-	6	-	24

4.5 Observations of bacteria and calcium carbonate crystals during MICP processes

4.5.1 Observations during bacterial injection

A uniform distribution of bacteria is thought to be the most important factor for achieving uniform calcium carbonate precipitation (Martinez et al., 2013). During bacterial injection, the bacterial cells are transported through the porous medium by advection and dispersion. To enable bacteria to become perfused through the whole microfluidic chip, the volume of bacterial suspension injected into the microfluidic chip should at least be the same as the total volume of the microfluidic channels within the device (the pore volume, PV). Due to the inhomogeneous distribution of the pores and particles in the porous medium, some of the bacteria are transported through the chip faster than others during the injection of bacterial suspension. Even though dispersion can help to achieve a more homogenous distribution of bacteria in the porous medium, the injection volume should be higher than 1 PV to achieve this. Therefore, in Test 1, to check that flow is smooth and to check whether a uniform bacterial distribution can be obtained after the injection, the change in the number of bacteria with time and space in the porous medium during the injection of bacteria was investigated after saturating the microfluidic chip with DI water. The direction of the injection of bacterial suspension into the microfluidic chip was from left to right in the images presented in this thesis. Three areas were imaged - at the left, middle and right of the porous medium of the microfluidic chip (**Figure 4.4a**). Time-series images of these three areas were taken during the injection of 1.5 PVs of bacterial suspension and the number of bacteria present in two squares in each of these images was counted. Magnified images of squares A, C and E in **Figure 4.4a** showing intermediate stages during this injection (0.25, 0.5, 0.75, 1.0, 1.25 and 1.5 PVs) are shown **Figure 4.4b**. The bacterial density within the pores was greater closer to the injection side and increased at all measured locations as the number of pore volumes (PV) injected increased (**Figure 4.4b**).

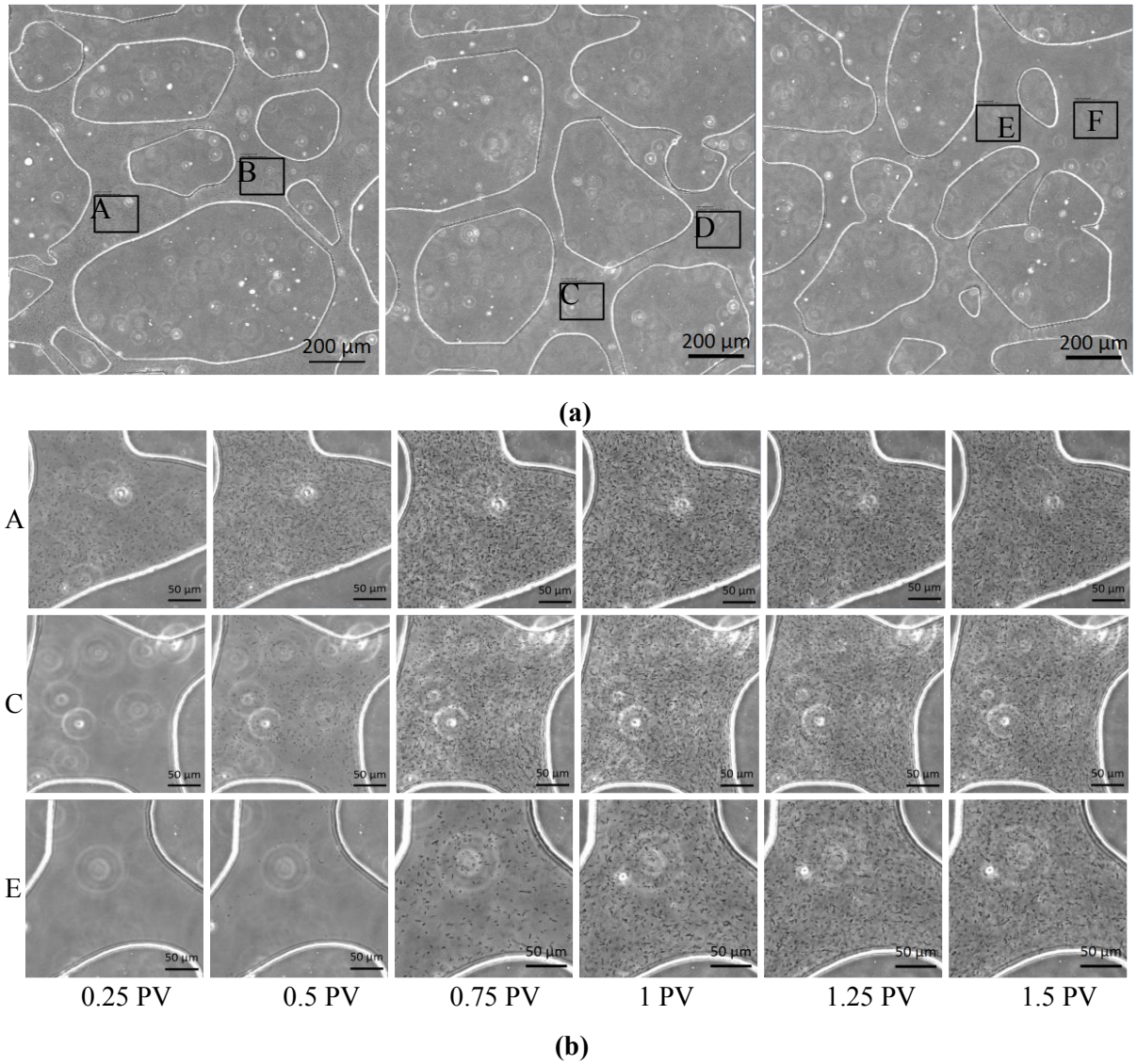

Figure 4.4 Observations during the bacterial injection: (**a**) images taken at the left, middle and right of the porous medium to enable counting of bacteria; (**b**) time series images of squares A, C and E in (a) taken at intermediate stages of 0.25 PV during the injection of 1.5 PV of bacterial suspension

Bacteria in the six squares (A-F in **Figure 4.4a**), were counted during the bacterial injection, with the results shown in **Figure 4.5**. Each data point represents the average number of bacteria counted across two areas (A and B for the left image, C and D for the middle image, and E and F for the right image in **Figure 4.4**), with error bars corresponding to standard errors. After injecting 1 PV of bacterial suspension, the number of bacteria on the left side of the porous medium was higher than in the middle, which in turn was higher than on the right-hand side of the porous medium closest to the outlet. The differences in the number of bacteria between

these three areas became smaller as the PV number of injected bacteria increased. The minimum pore volume of bacterial suspension required to achieve a relatively homogeneous distribution of bacteria inside the porous medium was between 1.0 and 1.25 PV. Therefore, in most of the experiments in this study, 1.25 PV of bacterial suspension was injected into the microfluidic chips to obtain a uniform distribution of bacterial cells. However, it should also be noted as that as bacterial cells contain flagella that enable them to move through fluids, a homogenous distribution of bacterial cells may also be achieved by allowing sufficient time for the bacteria to distribute within the media due to their motility.

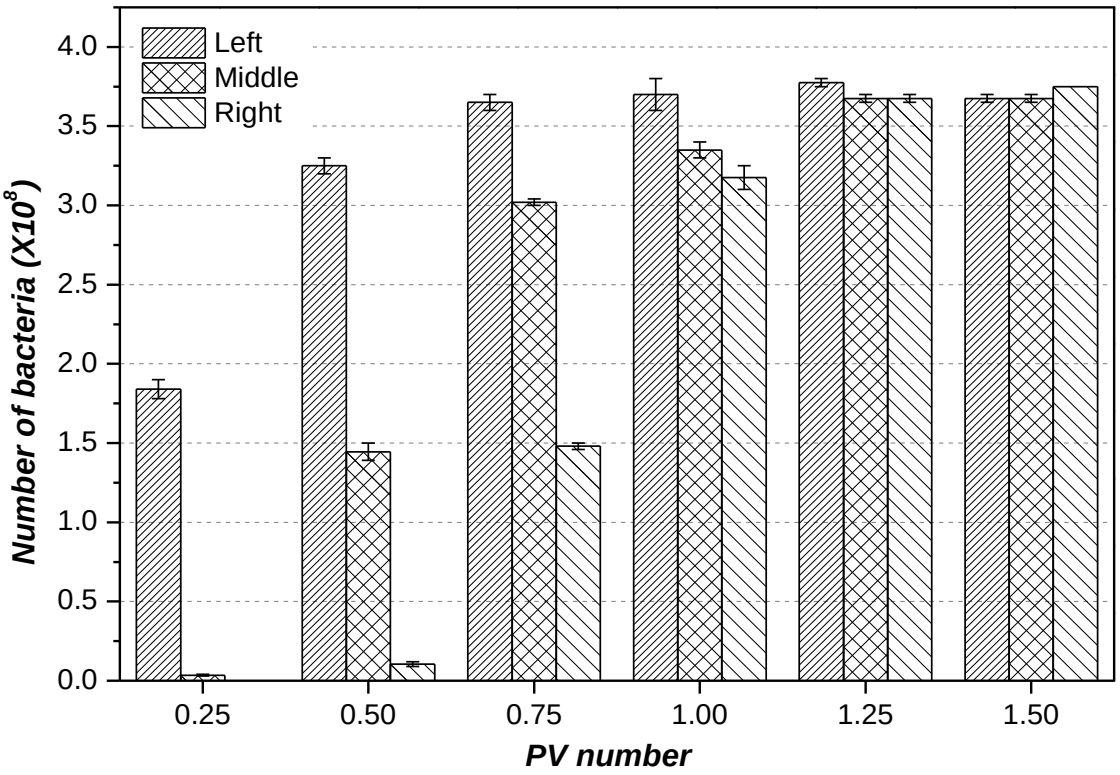

Figure 4.5 Number of bacteria counted at different time points during the bacterial injection, with each data point representing the mean number of bacteria present in two counting areas (A and B for the left image, C and D for the middle image, E and F for the right image in Figure 4.4a). Error bars correspond to standard errors.

4.5.2 Observations during bacterial settling

Before being injected into soil matrix, bacteria in MICP studies are normally cultivated in a laboratory to reach a certain density, concentration and biological activity, both of which depend on the application (Fauriel and Laloui, 2012). Bacterial growth experiments in a laboratory have normally shown that under optimised conditions, bacterial growth follows six phases - lag phase, the starting phase, exponential phase, slow-down phase, stationary phase and death phase (Widdel, 2007). In most studies, bacteria are cultivated to exponential phase (or early stationary phase) before being injected into the soil matrix, after which the bacterial number *in situ* is not assessed. In theory, bacteria exhibiting exponential growth still have the ability to increase in number even after being injected. Test 2 was therefore conducted to observe bacterial growth *in situ* during bacterial settling.

It is shown in Test 1 that the OD_{600} for *S. pasteurii* suspension can reach a value of 4.0. Because the OD_{600} of the bacterial suspension in this experiment was 0.8 prior to the injection of bacterial suspension and the growth medium was the same as that used in Test 1, it was assumed that the bacterial suspension contained sufficient nutrients for bacteria to grow further. To test this assumption, optical microscope images of bacteria in three pores of the microfluidic chip were taken at t_0, t_0 + 2 h and t_0 + 4 h during the settling of bacteria, as shown in **Figure 4.6a**. t_0 was about 10 minutes after the completion of the bacterial injection. The number of bacteria in each image depicted in **Figure 4.6a** was counted, with the results shown in **Figure 4.6b**. The number of bacteria at each time point represents the average number of bacteria present in the three counting areas (left, middle and right), with error bars corresponding to standard errors.

It is shown in **Figure 4.6** that the concentration of bacteria increased during the bacterial settling period due to *in situ* growth of bacteria. Bacteria with an OD_{600} of 0.8 were growing during bacterial settling, with the bacterial density increasing by 80% between t_0 and t_0 + 2 hours, and by another 80 % between t_0 + 2 hrs and t_0 + 4 hrs. The microfluidic chip was manufactured using polydimethylsiloxane (PDMS), a gas-permeable material which allows oxygen to diffuse into the porous medium of the chip (Leclerc et al., 2003). Based on the parameters given by Leclerc et al. (2003) and the thickness of the PDMS (5 mm) in this study, the estimated rate of oxygen diffusion into the porous medium of the chip is 4.8×10^{-5} mol per

day, which is considered to be sufficient for *S. pasteurii* to grow (Leclerc et al. 2003). However, it is important to note that since bacterial growth is affected by multiple factors such as temperature, dissolved oxygen (DO) content, availability of nutrients and pH (Garrett et al., 2008), the observations in this study may not fully mimic bacterial growth in real soils. Nevertheless, the direct observation of bacteria during the MICP process provides a possible way to investigate the effects of environmental factors on bacterial growth and the effects of bacterial amount on the properties of the calcium carbonate precipitates.

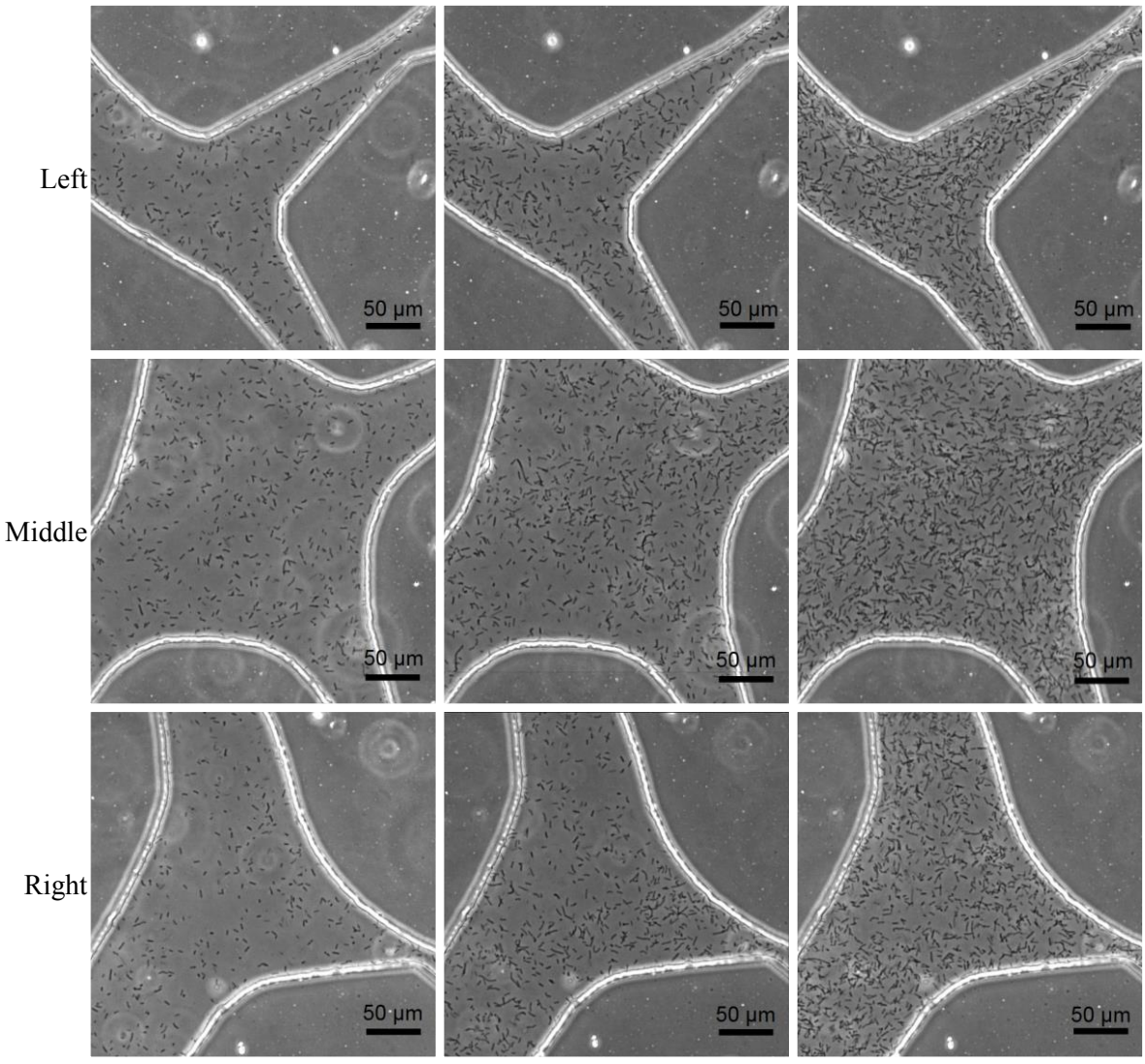

(a)

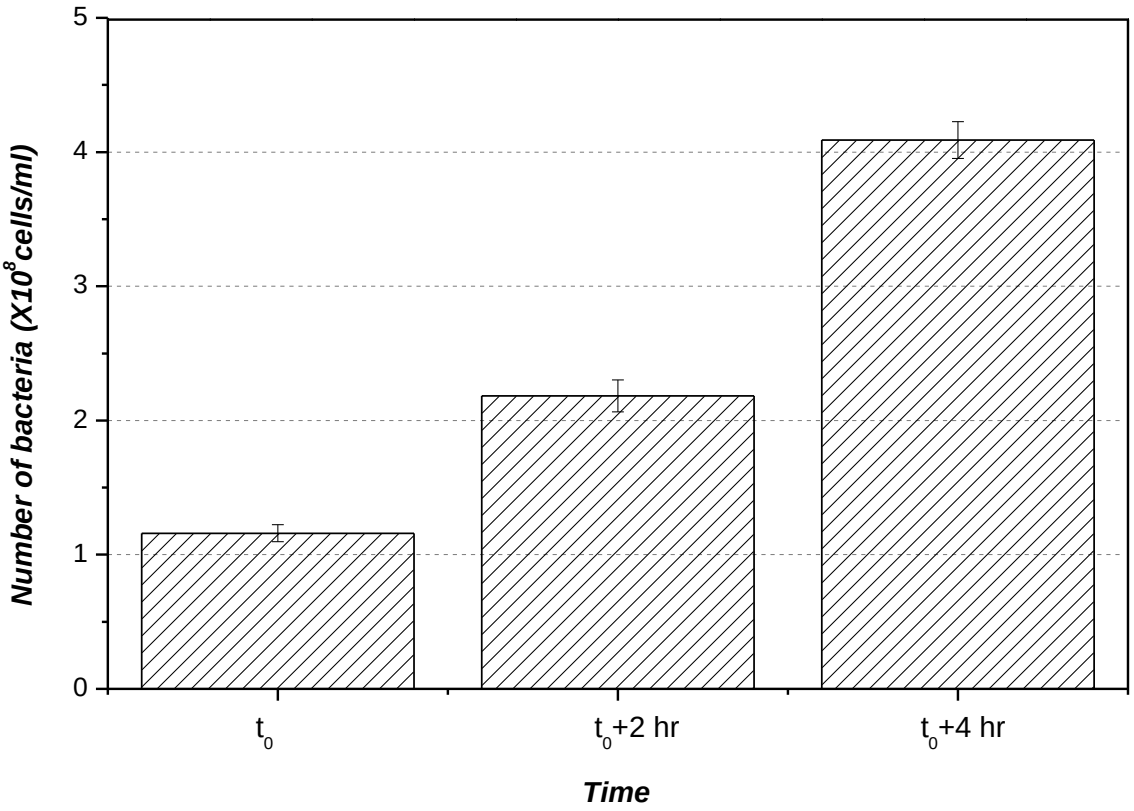

(b)

Figure 4.6 Observations during bacterial settling: **(a)** optical microscope images of bacteria in three pores of the microfluidic chip during bacterial settling at t_0, t_0 + 2 h and t_0 + 4 h after the bacterial injection. t_0 was about 10 minutes after the completion of the bacterial injection; **(b)** bacteria counted during bacterial settling, with each data point representing the average value of the three counting areas and error bars corresponding to standard errors

4.5.3 Observations during the injection of cementation solution

The settling period was followed by the injection of the cementation solution that will trigger the formation of calcium carbonate precipitates. Optical microscope images of bacteria inside three pores on the left-hand side, middle and right-hand side of the microfluidic chip during the 1.25 PV injection of cementation solution are shown in **Figure 4.7a**. Bacteria in three representative images at the left, middle and the right of the microfluidic chip at injection PV numbers of 0, 0.25, 0.5, 0.75, 1.0 and 1.25 were counted, and the average results are shown in **Figure 4.7b**. The number of bacteria in the pores on the left side of the microfluidic chip (close to the inlet where flow through the chip commences) continuously decreased throughout the

time course of the injection, while the number of bacteria in the pores in the middle and right-hand side of the chip (closer to the outlet) were increasing until around 0.25 to 0.5 PVs were injected, after which they began to decrease. This might be because during the injection of cementation solution, the bacterial cells at the left of the microfluidic chip were initially replaced by cementation solution which does not contain bacteria. Therefore, the bacterial density in the pores at the left-hand side decreased after the start of the injection. Meanwhile, during the injection of cementation solution, the bacterial cells which became detached on the left-hand side of the chip were flushed through the chip and accumulated on the right-hand side. Therefore, the bacterial density in the right-hand side of the chip increased during the first 0.5 PV injection of cementation solution. After the cementation solution reached the middle of the chip, some of the bacteria in the middle of the chip became displaced by the cementation solution, resulting in a decrease in bacterial density at this location. Bacteria in the pores in the left, middle and right of the microfluidic chip stopped decreasing after around 0.75, 1 and 1.25 PV were injected, respectively. The number of bacteria remaining in the microfluidic chip after the injection of 1.25 PV of cementation solution was about half of the initial amount.

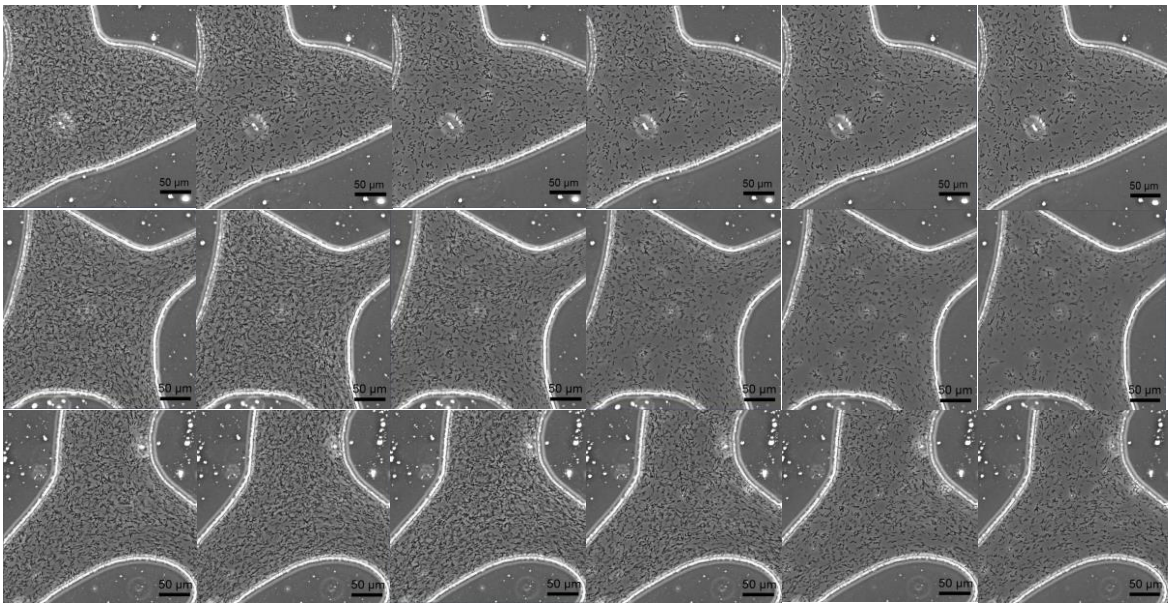

0 PV 0.25 PV 0.5 PV 0.75 PV 1 PV 1.25 PV

(a)

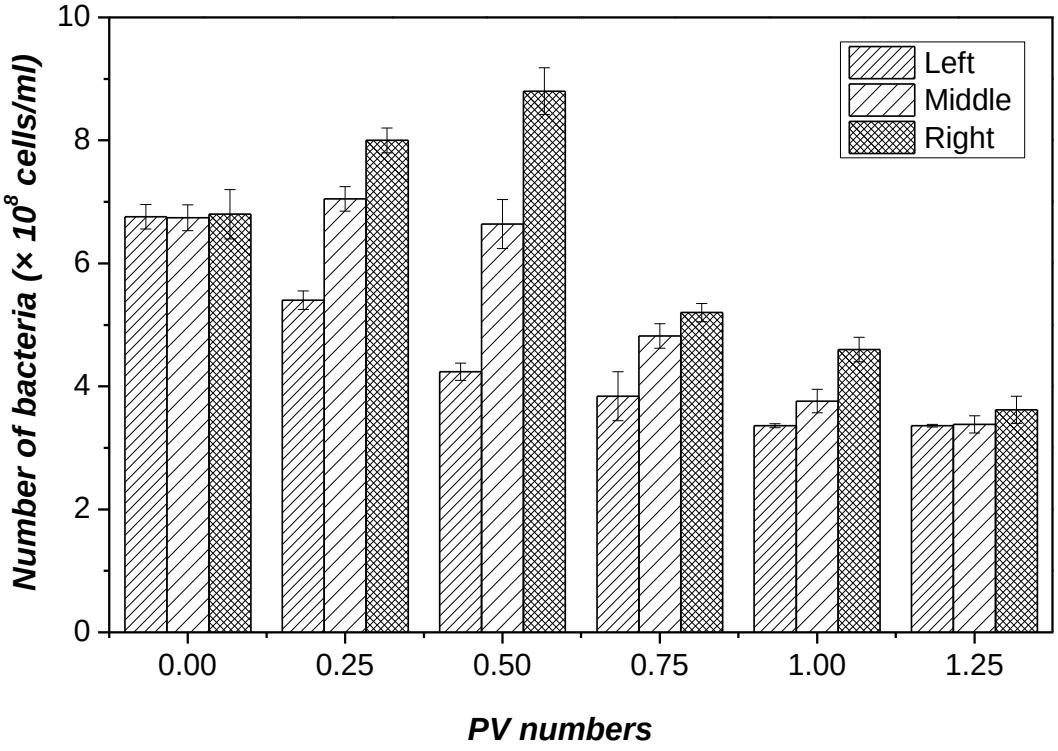

(b)

Figure 4.7 (a) Optical microscope images of bacteria inside three pores at the left (first row), middle (second row) and right (third row) of the microfluidic chip during the injection of 1.25 PV of cementation solution; **(b)** bacterial numbers during the injection of 1.25 PV of cementation solution, with each data point representing the average value of the three counting areas and error bars corresponding to standard errors

Optical microscope images of bacteria in one of the pores at the centre of the microfluidic chip taken after bacteria were allowed to settle for 4.5 hours (before the first cementation solution injection), and after the first, third and twelfth injection of cementation solution during twelve sequential injections are shown in **Figure 4.8a.** It is shown that the bacterial population decreased with continued injections of cementation solution, with the greatest reduction occurring during the first injection of cementation solution. Bacteria were counted (i) after the bacterial injection, (ii) after the bacteria were allowed to settle for 4.5 hours, and (iii) after each of the twelve injections of cementation solution (**Figure 4.8b**). About half of the bacteria were flushed out after the first 1.25 PV of the cementation solution was injected. The number of bacteria continued decreasing until around the seventh cementation solution injection, after

which the number of bacteria remained constant. The number of bacteria present at the end of the series of cementation solution injections was about 80% lower than the number of bacteria present immediately after settling.

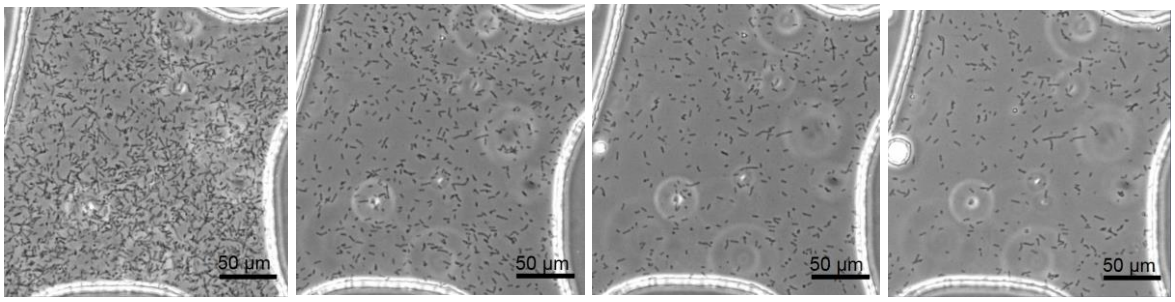

(a)

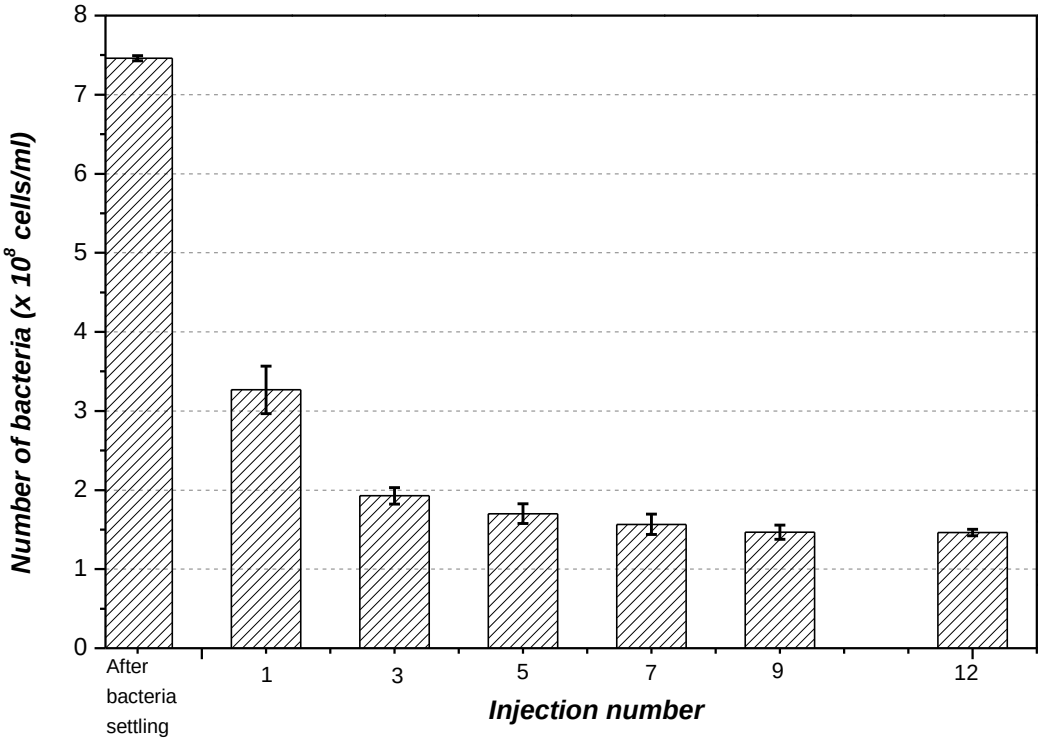

(b)

Figure 4.8 (a) Optical microscope images of bacteria taken during the injection of cementation solution (CS). From left to right, images were taken after bacterial settling for 4.5 hours (before the 1st CS injection), after the first CS injection, after the third CS injection, and after the twelfth CS injection; **(b)** Number of bacteria present after bacterial settling after the 1st, 3rd, 5th, 7th, 9th, and 12th injections of cementation solution, with each data point representing the average value of the three counting areas and error bars corresponding to standard errors

Previous research indicates that bacteria tend to secrete adhesive structures such as flagella, pili, exopolysaccharides and other matrix components to attach to the solid surface and live at the liquid-solid interface (Dunne, 2002). This process generates an adhesive force between bacterial and solid surfaces (Persat et al., 2015). During the injection of cementation solution, the viscosity of the cementation solution generates a hydrodynamic (shear) force on the cell that is tangential to the surface in the direction of the flow (Persat et al., 2015). Surface motility may produce a frictional force that is tangential to the cell wall and is localised at the interface with the substrate (Persat et al., 2015). When the forces on the cell are balanced, the cell attaches to the surface, whereas the cell detaches from the surface when the forces are not balanced. The shear stress generated by flow at a solid-liquid interface can easily overcome the adhesive forces which anchor cells to surfaces, thus potentially detaching them from the substrate. In this study, the cementation solution and the injection flow rate of the cementation solution were the same in each injection. Bacteria detached during the injections of cementation solution, possibly because the forces were not balanced. Bacterial attachment and detachment to and from the substrate is complex, and these forces also strongly depend on the chemical and mechanical properties of the substrate (Garrett et al., 2008; Licheter et al., 2008).

4.5.4 Formation of cementation with time

To observe the formation of cementation with time during a continuous injection of cementation solution, in Test 5, six PVs of cementation solution were continuously injected into one microfluidic chip at a flow rate of 0.05 ml/h, and optical microscope images were taken from the start of the first until the sixth PV injection of cementation solution (**Figure 4.9**). It is shown that the formation of cementation with time might occur during the injection of cementation solution. Bacterial aggregates were observed during this experiment (**Figure 4.9**, first row). Bacteria may have aggregated because that bacterial cell walls are negatively charged and could thus be bonded by the Ca^{2+} cations of $CaCl_2$ in the cementation solution (Rodriguez-Navarro et al., 2007 and EI Mountassir et al, 2014). Crystals appeared either at the narrow pore throat, next to the side wall or at the bottom of the inner surface of the microfluidic chip (**Figure 4.9**, second and third row). After being formed, the calcium carbonate crystals continued growing during the injection process.

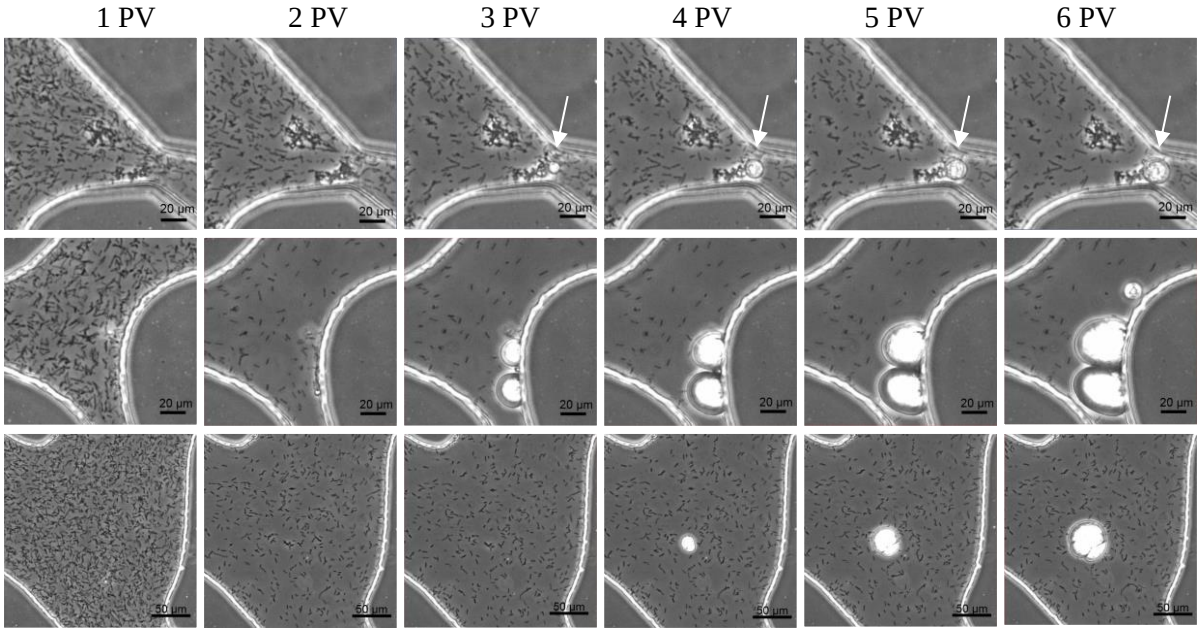

Figure 4.9 Time series microscope images taken from the start of the first until the sixth PV injection of cementation solution: bacterial aggregation and nucleation appear at a narrow pore throat (first row); crystals grow next to the side wall (second row); and a crystal growing out from the bottom of the inner surface of the microfluidic chip (third row)

To observe the formation of cementation with time during a staged injection of cementation solution procedure, in Test 6, 20 sequential 1.25 PV of cementation solution were injected into the microfluidic chip at an interval of about 24 hours between injections after the completion of bacterial settling. An image showing cementation throughout the whole porous medium of the microfluidic chip after the completion of the final cementation solution injection is presented in **Figure 4.10**. Representative images of crystals inside six pores of this porous medium at the completion of the final cementation solution injection are also shown in this figure. Pores A-C are narrow, whereas pores D-F are wide. The shape of the crystals was mainly prismatic, suggesting that the crystals might be calcite (Al Qabany et al., 2012; Zhao et al., 2014).

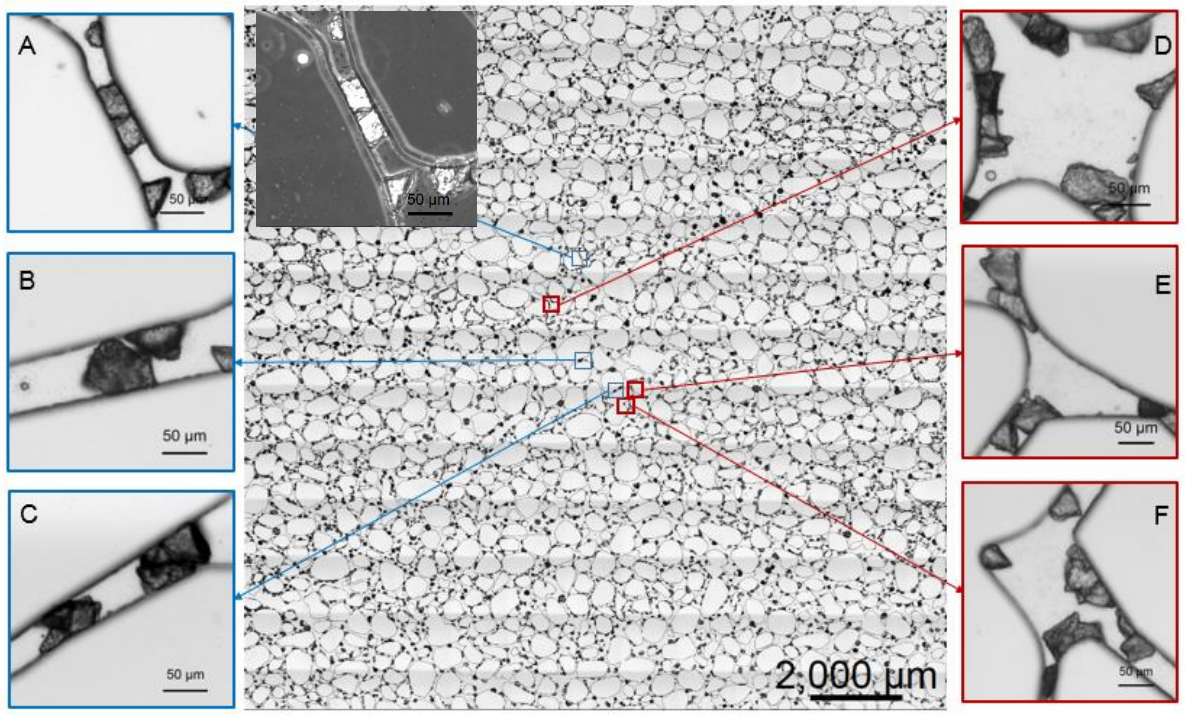

Figure 4.10 Image of the whole porous medium captured at the end of the final (20^{th}) injection of cementation solution and six magnified images of pores A-F

Images of pores A to F at the completion of the 4^{th}, 8^{th}, 12^{th}, 16^{th} and 20^{th} injection of cementation solution are shown in **Figure 4.11**. Most but not all crystals present after the final stage of the injection process were formed at the completion of the 4^{th} injection of cementation solution. Once the crystals were formed, they continued to grow with subsequent injections of cementation solution.

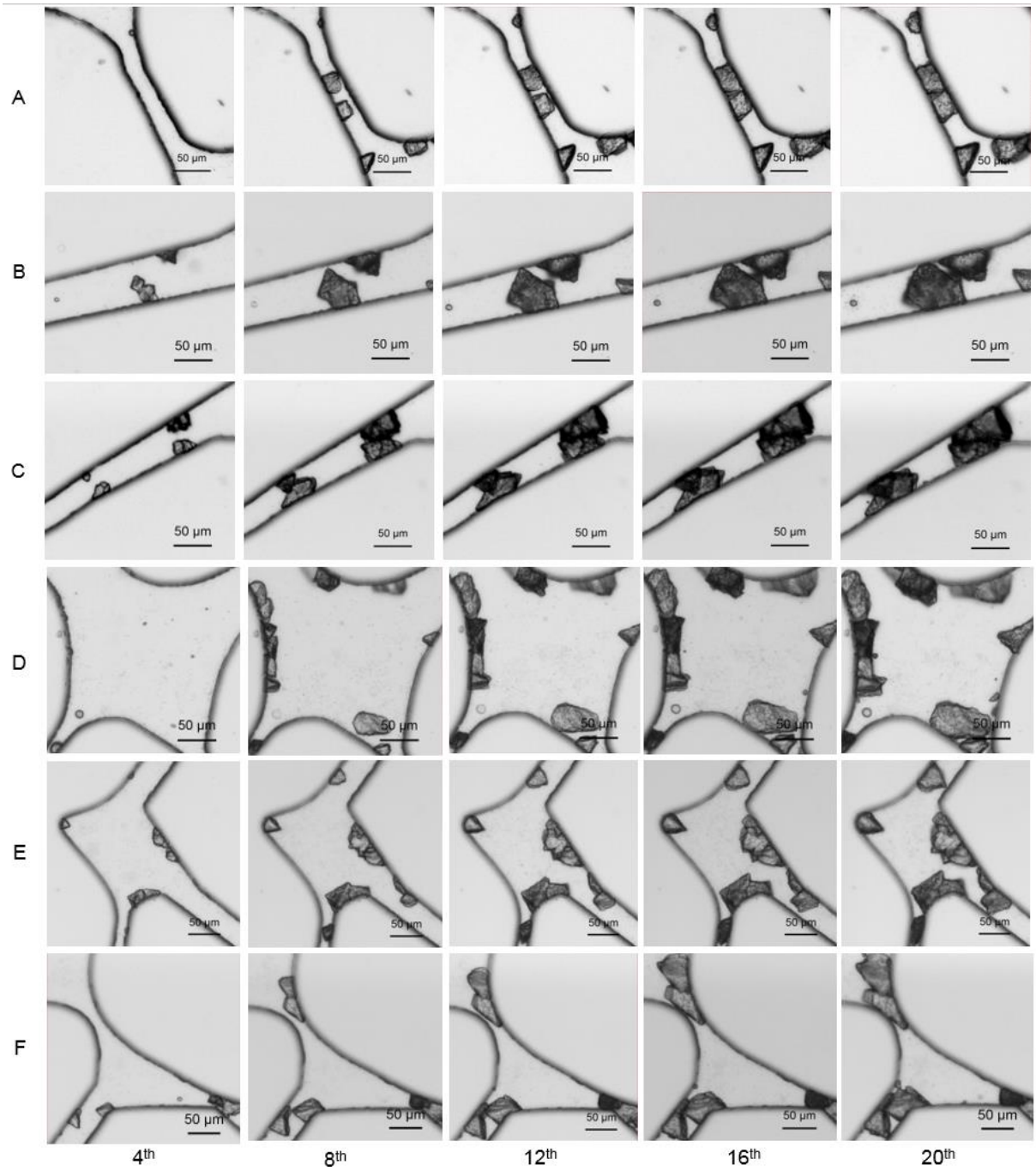

Figure 4.11 Images of pores A to F captured after the completion of the 4th, 8th, 12th, 16th and 20th injections

The sizes of the five crystals in pore A (quantified by measuring their areas) at the completion of the 4th, 8th, 12th, 16th and 20th injection of cementation solution are shown in **Figure 4.12**. Although crystal volumes could not be calculated from the two-dimensional images,

quantifying bacterial size by measuring the areas that they occupy in the microscope images could still be useful to study and compare their relative sizes and growth rates. At the completion of the 4th cementation solution injection, only one crystal was formed, whereas other crystals were formed between the 4th and the 8th injection of cementation solution (**Figure 4.12**). The sizes of the five crystals at the same time point were different, with all of these crystals continuing to grow during subsequent injections of cementation solution. Crystals that were smaller at earlier stages were also smaller at later time points.

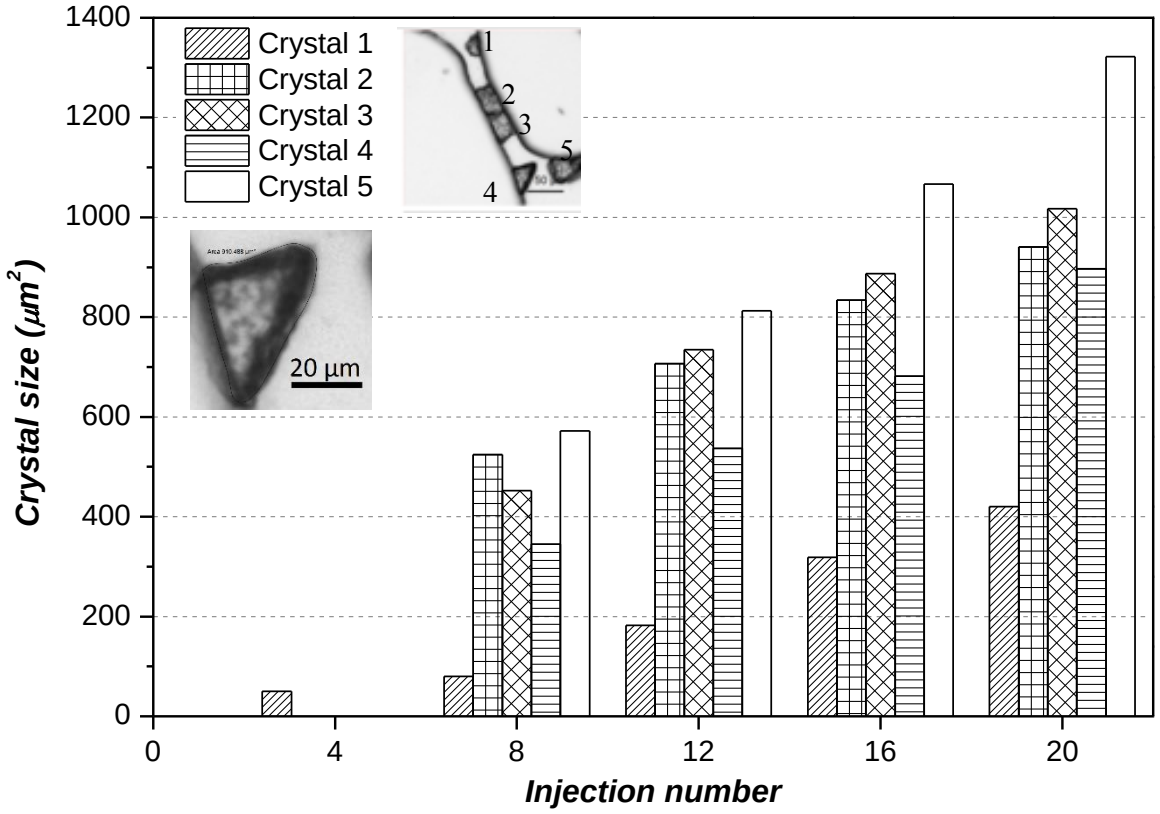

Figure 4.12 Quantification of the sizes of the five $CaCO_3$ crystals at position A in Figure 4.11 at the completion of the 4th, 8th, 12th, 16th and 20th injections

To quantify the micro-scale distribution of the crystals within the pores, the proportion of the total pore area occupied by the crystals in narrow and open pores after every 4th injection is shown in **Figure 4.13**. The ratio of crystal area to pore area in this study is not necessarily the same as the ratio of crystal volume to pore volume because the crystals might not occupy the whole height of the microfluidic chip. The crystal areas to pore area ratios in the narrow and

open pores at the completion of the 4th cementation solution injection were about 0.06 and 0.05, respectively. These ratios increased gradually to about 0.45 and 0.38, respectively, after the completion of the final (20th) injection of cementation solution. Cementation preferentially formed in narrow pore throats over open pore bodies. It should be noted that the proportion of the pore area occupied by crystals might vary if other pores were chosen.

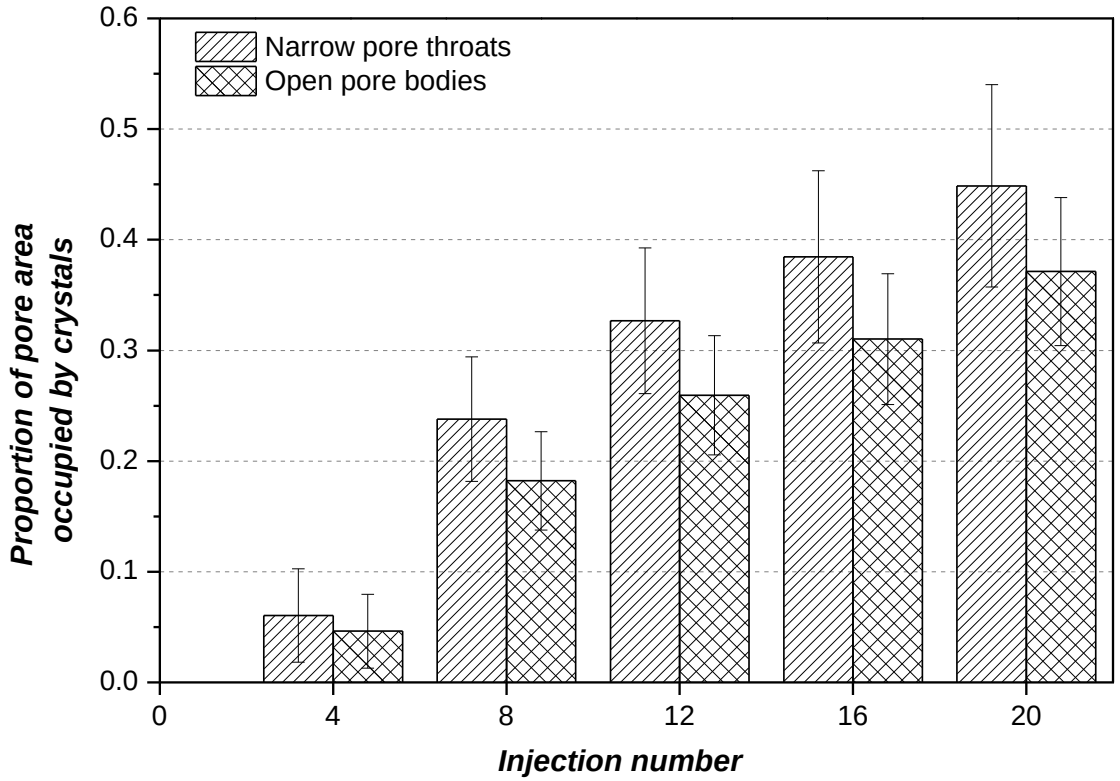

Figure 4.13 Ratios of the total area occupied by the crystals to the total area of pores in the narrow and open pores at the completion of the 4th, 8th, 12th, 16th and 20th injections, with each data point representing the average value of the three counting areas and error bars corresponding to standard errors

The cementation formed at narrow pore throats might represent the effective $CaCO_3$ required for increasing the strength and stiffness of soils (DeJong et al., 2010). Any cementation present inside soils decreases soil permeability, and large crystals at the open pore throat might correspond to the effective $CaCO_3$ required to reduce soil permeability (Al Qabany and Soga, 2013). The concentration of chemicals used during MICP treatment affects the size and distribution of crystals, which in turn affects the mechanical properties of MICP-treated

samples (Al Qabany and Soga, 2013). However, to date, no research has been conducted to explain the reason behind this. The observation of nucleation and crystal growth inside the porous medium can shed light on the mechanisms responsible for the spatial distribution of $CaCO_3$ at particle scale, as well as possible reasons for the formation of different shapes, sizes, and amounts of $CaCO_3$.

4.6 Conclusions

In this study, transparent microfluidic chips, which were designed based on a cross-sectional image of Ottawa 30-50 sandy soil, were fabricated using PDMS. Pore-scale MICP tests were conducted using the microfluidic chips and the behaviour of both bacteria and carbonate precipitates at different stages during the whole MICP process were investigated. The observations are summarised as follows:

Bacterial cells and calcium carbonate crystals inside the microfluidic chip can be observed under an optical microscope. The porous medium of a soil matrix can be simplified and simulated in a microfluidic chip. The PDMS microfluidic chip is impermeable to water and the injection flow rate of both bacterial suspension and cementation solution in the chip can be kept at the same level as in macro-scale soil column experiments. In contrast to sample preparation for SEM, samples do not need to be dried to be observed using an optical microscope, thus making it possible to observe bacteria and calcium carbonate crystals in a saturated condition. The image intensities of bacteria, water, PDMS chip, and crystals are different, which makes it very easy to distinguish them. The process of MICP inside the porous medium both during and after the MICP treatment can be observed without breaking the samples.

Flow of bacterial suspension and cementation solution through the microfluidic chip perfused the entire porous medium and the bacteria distributed homogeneously within the chip after 1.25 PV was injected. This observation supports the findings of Tobler et al. (2014) that the distribution of *S. pasteurii* in sandstone at a larger scale (1.8 - 7.5 cm) was fairly homogeneous after the initial bacterial injection when the bacterial optical density was either 0.5 or 1.0.

However, as the transport of bacteria through the porous medium might be affected by factors such as bacterial density, the size of the samples, the porosity of the porous medium, and the injection flow rate, further studies will be required to study the effects of these parameters on the transport of bacteria.

The microfluidic chip enabled the growth and distribution of bacteria to be monitored throughout the MICP treatment procedure. The early exponential growth of bacteria inside the porous medium during bacterial settling and the detachment of bacteria during the injection of cementation solution were observed. Because it is difficult to observe bacteria inside soils even by using a scanning electron microscope, the bacterial density reported in the literature was usually measured before injecting bacteria (Al Qabany et al., 2012; Montoya et al., 2013; Jiang et al., 2017). However, as the number of bacteria might change after the bacterial injection, the number of bacteria present by the time the cementation solution is injected might affect the precipitation rate and morphology of carbonate crystals. Using the microfluidic chip, further studies can be conducted to study the factors affecting bacterial growth properties and the relationship between the number of bacteria and the properties of carbonate crystals such as growth rate and morphology. In addition, as the distribution of bacteria might affect the distribution of carbonate precipitation, the microfluidic chip could also be used to investigate the correlation between the distributions of bacteria and carbonate crystals.

$CaCO_3$ crystal growth were observed during either one continuous injection or twenty sequential injections of cementation solution. The observation of $CaCO_3$ crystals during the MICP process using microfluidic chips has great advantages over traditional ways of studying MICP, by which only the $CaCO_3$ content at the end of the MICP treatment process can be measured (van Paassen, 2009; Al Qabany et al., 2012). The mechanisms responsible for the spatial distribution of $CaCO_3$ at the particle scale and the reasons for the formation of different shapes, sizes, and amount of $CaCO_3$ can be further explored. Furthermore, monitoring $CaCO_3$ size and amount during the MICP process can also be useful to study the rate of $CaCO_3$ precipitation, which might be helpful for optimising MICP treatment parameters.

Chapter 5 Micro-scale visualisation of MICP processes

5.1 Research aims

In real MICP applications such as soil stabilisation, bacterial suspension and cementation solution are injected into a soil matrix, resulting in $CaCO_3$ precipitation with time within the soil pores which bonds adjacent soil particles, thereby improving the engineering properties of the soil matrix such as stiffness and strength. It is essential to be able to better understand and control the MICP process in the soil pores so that MICP protocols can be designed accordingly to produce the $CaCO_3$ precipitates with desired properties (such as size, number and distribution) for different applications.

A MICP process in a soil pore starts with the bacteria in the pore fluid hydrolysing urea to form CO_3^{2-} ions, which react with the available Ca^{2+} cations in the pore fluid to form $CaCO_3$. A conventional belief is that bacteria serve as nucleation sites for $CaCO_3$ because the negative-charged cell walls of bacteria can adsorb Ca^{2+} for nucleation with the CO_3^{2-} ions (Stocks-Fischer et al., 1999; Hammes et al., 2002; DeJong et al, 2006; Siddique et al., 2011; Dhami et al., 2013; Ganendra et al., 2014). This conventional belief was challenged by a direct observation which showed that $CaCO_3$ crystals did not grow on bacterial cells which were immobilised on an agar pad containing urea and $CaCl_2$ (Zhang et al., 2018). Despite the studies that have been reported, the understanding of MICP processes in real soil pores is still very limited because the above conclusions were either obtained based on indirect observations using electron microscopy (Stocks-Fischer et al., 1999; Bang et al., 2010), or based on a direct observation under experimental conditions which do not mimic the flow of fluid through a porous medium in real MICP conditions (Zhang et al., 2018). In addition, the results of Test 5

presented in *Chapter 4* showed that bacterial aggregates and crystals can form within the narrow pore throat after the injection of cementation solution. Similarly, 0.05 M $CaCl_2$ solution was thought to be able to stimulate flocculation of *S. pasteurii* bacterial cells and increase the fixation of bacteria in a soil column (Harkes et al., 2010). During the MICP procedure, *S. pasteurii* cells can aggregate after bacterial cells are mixed with $CaCl_2$ solution (El Mountassir et al., 2014). This suggests that bacterial aggregates may affect $CaCO_3$ precipitation during MICP. However, the precise effects that bacterial aggregates have on $CaCO_3$ precipitation are largely known.

As reviewed in *Chapter 2*, $CaCO_3$ precipitates have a number of polymorphs with distinguished shapes, such as rhombohedral calcite, spherical vaterite, clustered needle-like aragonite and non-crystalline amorphous calcium carbonate (ACC) nanoparticles (Kawano et al., 2002; Lian et al., 2006; Dhami et al., 2013). Some of these polymorphs have also been observed in MICP studies, such as the $CaCO_3$ crystals with spherical and rhombohedral shapes observed in the experiments presented in *Chapter 4* and in a previous study by van Paassen (2009). The polymorphs varied in their stabilities, and during the formation of $CaCO_3$ in aqueous solutions as a result of chemical reactions between $CaCl_2$ and Na_2CO_3, less stable phases of $CaCO_3$ form first and transform to more stable phases according to Ostwald's step rule (Kawano et al., 2002; Bots et al., 2012). Because of the phase transformation of $CaCO_3$ during precipitation, the size and shape of $CaCO_3$ precipitates changes during the precipitation process (Kawano et al., 2002; Bots et al., 2012) even though the total $CaCO_3$ content remains the same. However, the phase transformation reported by Kawano et al. (2002) and Bots et al. (2012) was based on the chemical precipitation of $CaCO_3$ by $CaCl_2$ and Na_2CO_3, rather than on bacterial-induced $CaCO_3$ precipitation, with the similarities and differences between these two processes remaining largely unknown. It is therefore essential to understand if this transformation also occurs during ureolysis-driven MICP processes, as it is important to design MICP treatment protocols that produce stable $CaCO_3$ crystals for a permanent stable cementation (van Paassen, 2009).

As described in *Chapter 4*, a phase-contrast microscope can be used to observe both bacteria and $CaCO_3$ crystals. In addition, the designed and fabricated microfluidic chip can simulate the features of a real soil matrix and be used to manipulate the flow conditions based on real MICP conditions. In this chapter, micro-scale experiments were therefore designed and conducted to

improve the understanding the effects of bacterial cells/aggregates on $CaCO_3$ precipitation and the evolution of the shape and size of the $CaCO_3$ precipitates during the MICP process under the real MICP conditions. The experimental design and procedures in line with these research aims are described in the next section.

5.2 Experimental design and procedures

5.2.1 MICP processes which occur after mixing bacterial suspension with cementation solution

As shown in *Chapter 4*, bacterial aggregates can form during the injection of cementation solution. However, as it is difficult to predict when and where the bacterial aggregates are going to form in a microfluidic experiment during the injection of cementation solution, the capture of the whole MICP process from the formation of bacterial aggregates may be difficult. Therefore, to explore the effects of individual bacterial cells and bacterial aggregates on $CaCO_3$ precipitation and the changes in shape and size of the $CaCO_3$ precipitates during a MICP treatment procedure, the first micro-scale experiment was conducted by using glass slides as described in *Section 3.3*. This experiment was conducted based on the assumption that the interactions between bacterial cells and Ca^{2+} can be maximised during the mixing of bacterial suspension and cementation solution, which would enable large amounts of bacterial aggregates to be formed. To prove this assumption, a preliminary experiment was conducted before performing the glass slide experiment to examine whether large numbers of bacterial aggregates occur after mixing bacterial suspension with cementation solution. After the preliminary test, another glass slide sample was prepared which contained bacterial suspension with an OD_{600} of 2.5 mixed with an equal volume of cementation solution containing 1 M $CaCl_2$, 1.5 M urea, and 3 g/L nutrient broth. Immediately after preparing this mixture (which took about two minutes), time series images of this sample were taken at an imaging interval of five minutes over a period of twelve hours.

5.2.2 MICP processes occurring after the first and second injections of cementation solution

In the glass slide experiment, bacterial suspension and cementation solution can only be mixed once, whereas in real MICP applications the injection of cementation solution is normally repeated multiple times to increase the amount of $CaCO_3$ formed (van Paassen et al., 2010; Al Qabany et al., 2012). In addition, the glass slide experiment cannot simulate the flow of bacterial suspension and cementation solution through a porous soil matrix which may affect the distribution of bacterial aggregates and individual bacterial cells, and which in turn may affect the properties of MICP-treated soils. Therefore, after performing the glass slide experiment, a microfluidic chip experiment was conducted to further explore the MICP process under conditions that more closely mimic MICP conditions occurring in real soils. To achieve this, a staged injection MICP procedure (similar to the one described in *Chapter 4*) was conducted which involved a single injection of bacterial suspension after which bacteria were given time to 'settle' and attach to the inner surface of the porous medium before performing multiple injections of cementation solution in stages. However, some of the parameters of this experiment differ to the parameters of the staged injection procedure described in *Chapter 4*.

As shown in the results presented in *Chapter 4*, bacterial cells continued growing during the settling time. Therefore, the bacterial settling time may affect the number of bacteria present just before the injection of cementation solution. It was assumed that the presence of a larger number of bacterial cells would result in more bacterial aggregates being formed. Therefore, in this experiment the settling time was set at 24 hours to increase the number of bacterial cells present after the settling before the injection of cementation solution. In addition, whilst images were taken every 24 hours in Test 6 described in *Chapter 4*, images of the sample in this experiment were taken at 0, 1, 3, 6, 10 and 24 hours after the injections of cementation solution to visualise the effects of individual bacterial cells and bacterial aggregates on MICP processes and track changes in the shape and size of the crystals during MICP. The OD_{600} of the bacterial suspension measured prior to the injection of bacterial suspension was 1.0. Two injections of cementation solution were conducted to observe the MICP process occurring after each of these two injections. The flow rate and pore volume of bacterial suspension injection, as well as the

interval, flow rate and pore volume of cementation solution injection were the same as described in Test 6 in *Chapter 4*.

5.3 MICP processes in the mixtures of bacterial suspension and cementation solution

5.3.1 Bacterial aggregation

Before the glass slide experiment was conducted to study the effects of bacterial cells/aggregates on MICP processes, a preliminary glass slide experiment was conducted to test if both bacterial aggregates and individual bacterial cells are present after mixing bacterial suspension with cementation solution. Equal volumes of bacterial suspension (OD = 1.0) and cementation solution containing 1 M $CaCl_2$, 1.5 M urea and 3 g/L nutrient broth, were mixed on a glass slide sample. For comparison, a sample containing *S. pasteurii* suspension (OD =1.0) was also prepared. The images of the two samples are shown in **Figure 5.1.** Consistent with the results shown in *Chapter 4*, the *S. pasteurii* cells did not aggregate in the bacterial suspension (**Figure 5.1a**), but aggregated in the presence of cementation solution (**Figure 5.1b**). In addition, as expected, the size of the bacterial aggregate shown in **Figure 5.1b** was larger than the one observed in Test 5 presented in *Chapter 4* (shown in first row of **Figure 4.8**).

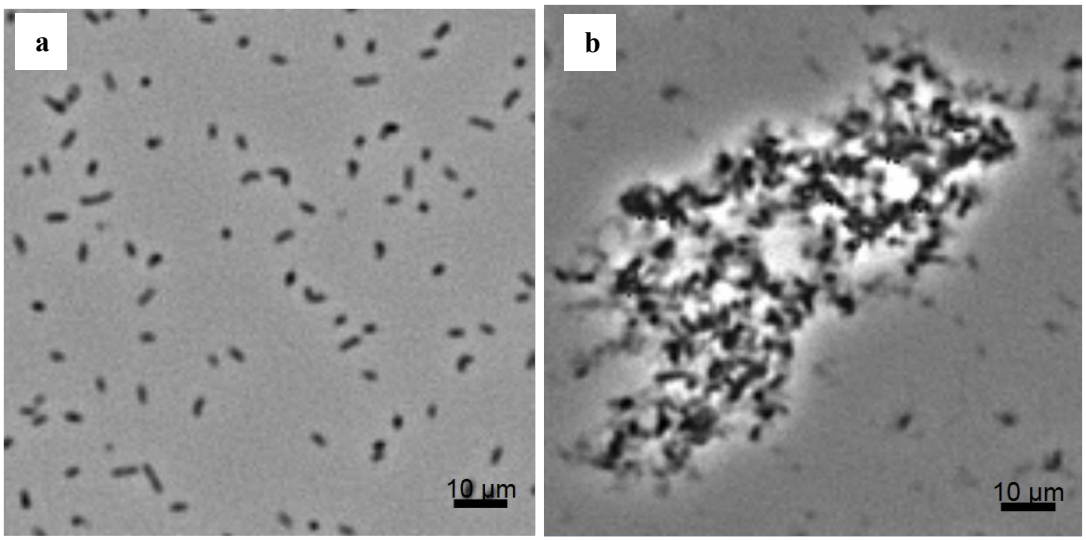

Figure 5.1 Optical microscope images of **(a)** a bacterial suspension (OD_{600} = 1.0), in which bacteria did not aggregate; **(b)** a bacterial aggregate observed after mixing bacterial suspension (OD_{600} = 1.0) with cementation solution (1 M). All images were taken immediately after the completion of the sample preparation, which took about 2 mins.

5.3.2 Overview of the MICP process after mixing bacterial suspension with cementation solution

To obtain an overview of the main stages of the MICP process after mixing bacterial suspension with cementation solution, 145 images of a 0.5 mm by 0.5 mm square of the sample were taken over a period of 12 hours after mixing to show the main stages of the precipitation process, with twelve of these images presented in **Figure 5.2**. Bacterial aggregation and $CaCO_3$ precipitation started immediately after the mixing (**Figure 5.2a**), which is consistent with the observation made by van Paassen (2009). The shapes of both bacterial aggregates and $CaCO_3$ precipitates at the initial stage were irregular (**Figure 5.2a**). By 30 min after mixing, more irregular-shaped $CaCO_3$ precipitates formed (**Figure 5.2b**), shown by more areas becoming lighter at 30 min compared with 0 min. The irregular-shaped $CaCO_3$ precipitates continued growing until 50 minutes when one spherical $CaCO_3$ crystal (Crystal A) appeared (**Figure 5.2c**). After that, the irregular-shaped $CaCO_3$ precipitates surrounding Crystal A started dissolving. The area containing dissolving irregular-shaped $CaCO_3$ became larger with the growth of Crystal A (**Figure 5.2e** compared with **Figure 5.2d**). In the meantime, several new crystals formed (**Figure 5.2e** compared with **Figure 5.2d**). It is worth noting that the zones

where the irregular-shaped $CaCO_3$ precipitates dissolved were not only increasing in size with the growth of the crystals, but also had a circular shape (**Figure 5.2f-h**). By 1 h and 45 minutes, some undissolved irregular-shaped $CaCO_3$ crystals (**Figure 5.2 i**) remained, but by 2 hours all irregular-shaped $CaCO_3$ precipitates dissolved (**Figure 5.2j**). Between 2 and12 hours, all of the existing $CaCO_3$ precipitates were regular-shaped crystals (**Figure 5.2j-l**). Therefore, in general, the overall MICP process between 0-12 hours after the mixing of bacterial suspension and cementation solution can be divided into the following three main stages: (1) bacterial aggregation occurred immediately after the mixing of bacterial suspension and cementation solution; (2) growth of irregular-shaped $CaCO_3$ crystals (0-1 hr); (3) dissolution of irregular-shaped $CaCO_3$ crystals (1-2 hr) at the expense of the growth and formation of regular-shaped $CaCO_3$ crystals (1-12 hr).

The irregular-shaped $CaCO_3$ precipitates which formed during the initial stage of $CaCO_3$ precipitation were not stable and dissolved easily with the precipitation of the regular-shaped $CaCO_3$ crystals, which is consistent with the observations made by Kawano et al. (2002). According to Ostwald's step rule, amorphous $CaCO_3$ (ACC), which is the most unstable form of $CaCO_3$, is the first to precipitate during $CaCl_2$- and Na_2CO_3-induced chemical precipitation of $CaCO_3$ (Rodriguez-Navarro et al., 2015). This is because ACC has the highest solubility among all the $CaCO_3$ precipitates and because the concentrations of Ca^{2+} and CO_3^{2-} in the mixed solution drop to the solubility for ACC during its precipitation, whilst still being high enough for more stable $CaCO_3$ crystals such as vaterite and calcite to nucleate and grow (Kawano et al., 2002). In this thesis study, the $CaCO_3$ precipitates that formed first were irregular-shaped and had a higher solubility compared with the crystal form of $CaCO_3$ precipitates, which is consistent with the parameters of amorphous phase $CaCO_3$ (Kawano 2002; Bots et al., 2012; Dhami et al., 2013; Rodriguez-Navarro et al., 2015). In addition, irregular-shaped $CaCO_3$ precipitates dissolved surrounding the crystals which formed, the shapes of the zones where the irregular-shaped $CaCO_3$ precipitates dissolved were circular, and these areas increased with the growth of the $CaCO_3$ crystals. This also suggests that the crystals grew at the expense of the dissolution of irregular-shaped $CaCO_3$ precipitates (Kawano 2002).

As the magnification level in the images shown in **Figure 5.2** is not high enough to observe the details of bacterial cells and $CaCO_3$ crystals, images taken at higher magnification levels (squares I and II in **Figure 5.2a**) are shown in the next two sections to observe more details regarding the effects of individual bacterial cells and bacterial aggregates on $CaCO_3$ precipitation and the evolution of $CaCO_3$ crystals.

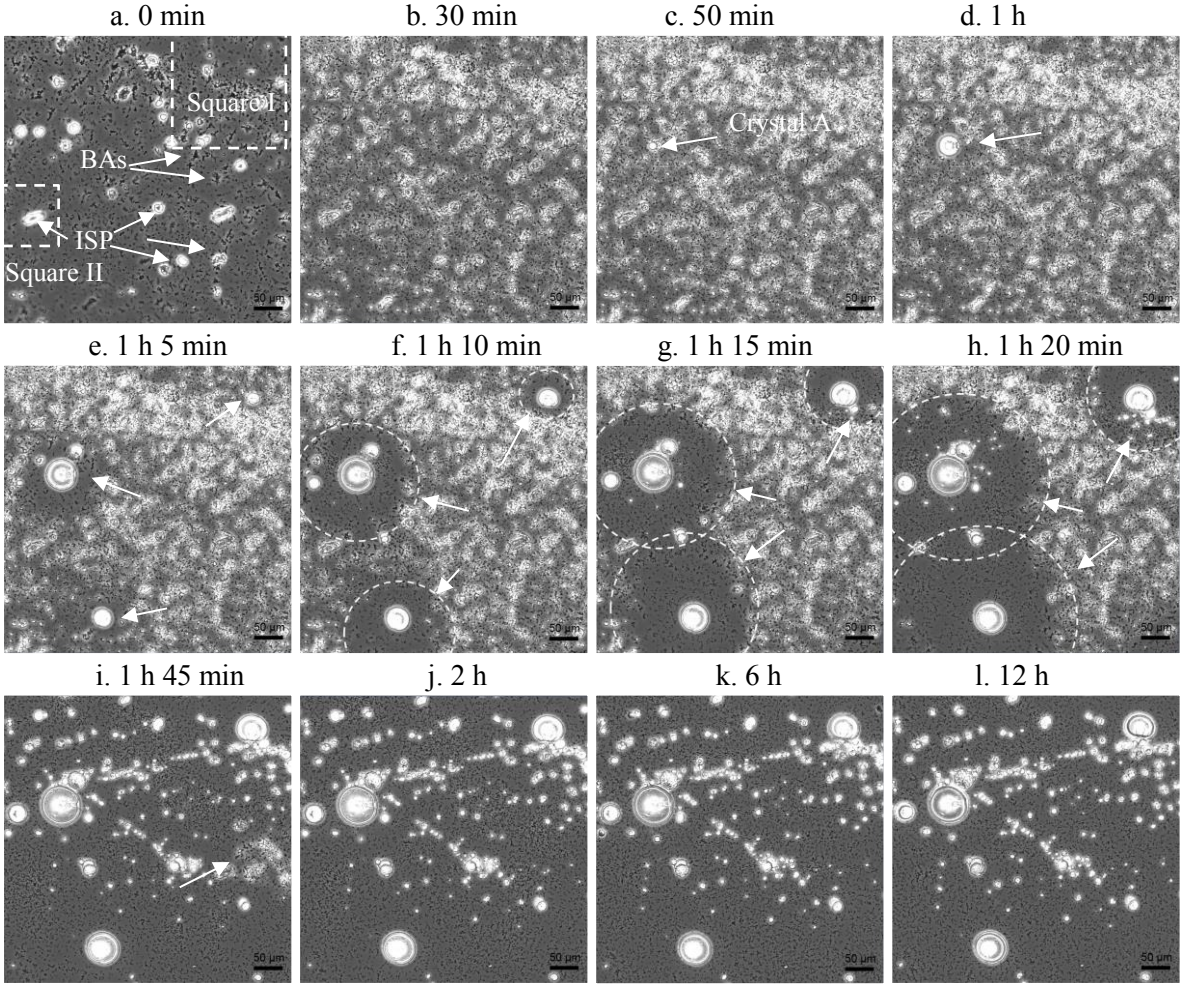

Figure 5.2 Time-lapse microscope images of microscope glass slides containing the mixture of bacterial suspension and cementation solution. **(a)** at 0 min bacterial aggregates (BAs) and irregular-shaped precipitates (ISP) formed; **(b)** by 30 mins more ISPs formed; **(c)** at 50 mins, crystal A formed (shown by the arrow) and ISPs became lighter compared with image **b**; **(d)** Crystal A became larger compared with image **c** and ISPs surrounding Crystal A dissolved; **(e)** at 1 h 5 min, new crystals formed (shown by arrows), crystal A continued growing and ISPs surrounding Crystal A continued dissolving; **(f-h)** circular zones where ISPs dissolved became larger with time as shown by the arrows; **(i)** undissolved ISPs (arrow); **(j-l)** only regular-shaped crystals remained after 2 hours.

5.3.3 Precipitation and dissolution of irregular shaped $CaCO_3$ precipitates

Magnified images of square I (shown in **Figure 5.2a**) at selected time points (0 min, 20 min and 50 min) are shown in **Figure 5.3a-c** to observe whether individual bacterial cells or bacterial aggregates have an effect on nucleation and growth of $CaCO_3$ precipitates. To observe the images in more detail, magnified images of the square in **Figure 5.3a-c** are shown in **Figure 5.3d-f**.

A large amount of the bacterial cells aggregated and irregular-shaped $CaCO_3$ precipitates started forming immediately after the start of the imaging process (**Figure 5.3 a**). The irregular-shaped $CaCO_3$ precipitates formed mostly on bacterial aggregates (**Figure 5.3 b**) and occasionally also formed on top of individual bacterial cells (arrows in **Figure 5.3 f**). The $CaCO_3$ precipitates continued to grow from 0 to 50 min, as shown by the image pixels becoming brighter (**Figure 5.3 b** compared with **a,** or **Figure 5.3 c** compared with **Figure 5.3 b**). The time at which the precipitates started forming varied, with some precipitates forming at 0 minutes, whereas others formed after 20 minutes (**Figure 5.3 d** and **e)**.

The images in **Figure 5.3** suggest that bacterial aggregation has great effects on the formation of irregular-shaped $CaCO_3$ precipitates. Based on *Equation 1.1 and 1.2* (in *Chapter 1*), bacteria hydrolyse urea and produce CO_3^{2-} which react with Ca^{2+} to form $CaCO_3$. Assuming that the ureolysis capacity of each bacterial cell is the same, bacterial aggregates containing a large number of bacteria are more effective at hydrolysing urea compared to individual bacterial cells. Therefore, the concentration of CO_3^{2-} surrounding the bacterial aggregates increases more quickly. In addition, the bacterial aggregates contained a large amount of Ca^{2+} surrounding the bacterial cells, thus causing $CaCO_3$ to precipitate on bacterial aggregates more quickly. As the local concentration of urea surrounding the bacterial aggregates decreases, more urea diffuses to them, thus resulting in the continued precipitation of $CaCO_3$ on the bacterial aggregates.

As reviewed in *Section 2.2.3*, the effects of ureolytic bacteria on the process of $CaCO_3$ precipitation have been debated. A widely believed assumption regarding the $CaCO_3$ precipitation process during MICP is that bacterial cells serve as nucleation sites for $CaCO_3$,

and that once the nucleation sites are formed, the $CaCO_3$ crystals continue growing from them (Stocks-Fischer et al., 1999; Hammes et al., 2002; DeJong et al, 2006; Siddique et al. 2011; Dhami et al., 2013; Ganendra et al., 2014). In contrast, some recent studies claimed that the effects of bacterial cells on the precipitation of $CaCO_3$ is very limited (Zhang et al., 2018). However, the observations made in this study suggest that, during the initial stage of $CaCO_3$ precipitation, bacterial aggregates formed and had an effect on $CaCO_3$ precipitation where the irregular-shaped $CaCO_3$ precipitates grew on top of the bacterial aggregates. In addition, the observations in this thesis study suggest that individual bacterial cells also have an effect on the precipitation of irregular-shaped $CaCO_3$ precipitates, but the effect of individual bacterial cells is less compared with the effect of bacterial aggregates.

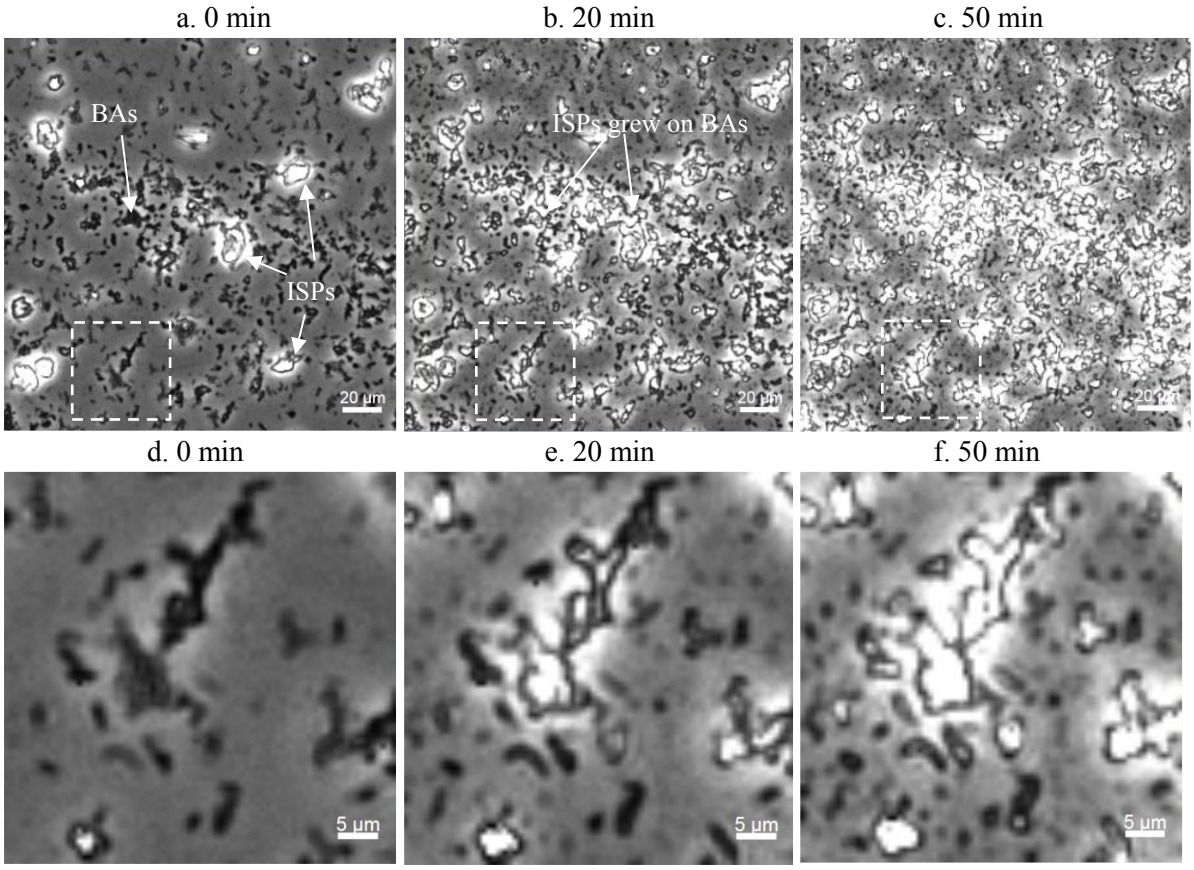

Figure 5.3 Microscope images showing the precipitation of irregular-shaped $CaCO_3$ crystals and the fixation of bacterial cells during the precipitation process. **(a)** at 0 min, bacterial aggregates (BAs) and irregular-shaped precipitates (ISP) formed; **(b** and **c)** ISPs formed on bacterial aggregates; **(d** and **e)** three bacterial cells shown by arrows; **(f)** at 50 mins, ISPs grew on the bacterial cells shown by the bottom two arrows but did not form on the bacterial cell shown by the top arrow

To observe the dissolution of irregularly-shaped $CaCO_3$ precipitates in more detail, magnified images of square II (shown in **Figure 5.2a**) at selected time points (between 30 min and 2 hrs) are shown in **Figure 5.4**. With the dissolution of the $CaCO_3$ precipitate, the bacterial cells become free to move. The mobility of *S. pasteurii* is consistent with that of Bacillus bacteria (Yoon et al. 2001). These observations suggest that bacterial aggregation and the formation of irregularly-shaped $CaCO_3$ precipitates encapsulate bacterial cells. By contrast, because the irregularly-shaped $CaCO_3$ precipitates were not stable, the dissolution of the irregularly-shaped $CaCO_3$ resulted in the bacterial cells becoming free to move again.

The fixation of bacteria in bacterial aggregates or irregular-shaped precipitates might affect the transport of bacterial cells as they are notably larger than individual bacterial cells and may therefore become more easily trapped at narrow pore throats of a soil matrix. In addition, as the bacterial aggregates encapsulate bacterial cells which later become released with the dissolution of the irregular-shaped precipitates, the distribution of aggregates/irregular-shaped precipitates in a soil matrix may affect the distribution of the bacterial cells in the matrix, which may consequently affect the MICP process. Further work is warranted to explore the factors affecting the size of the bacterial aggregates and their effect on the distribution of bacteria at the macro-scale and the resulting effects that this might have on the properties of the $CaCO_3$ formed.

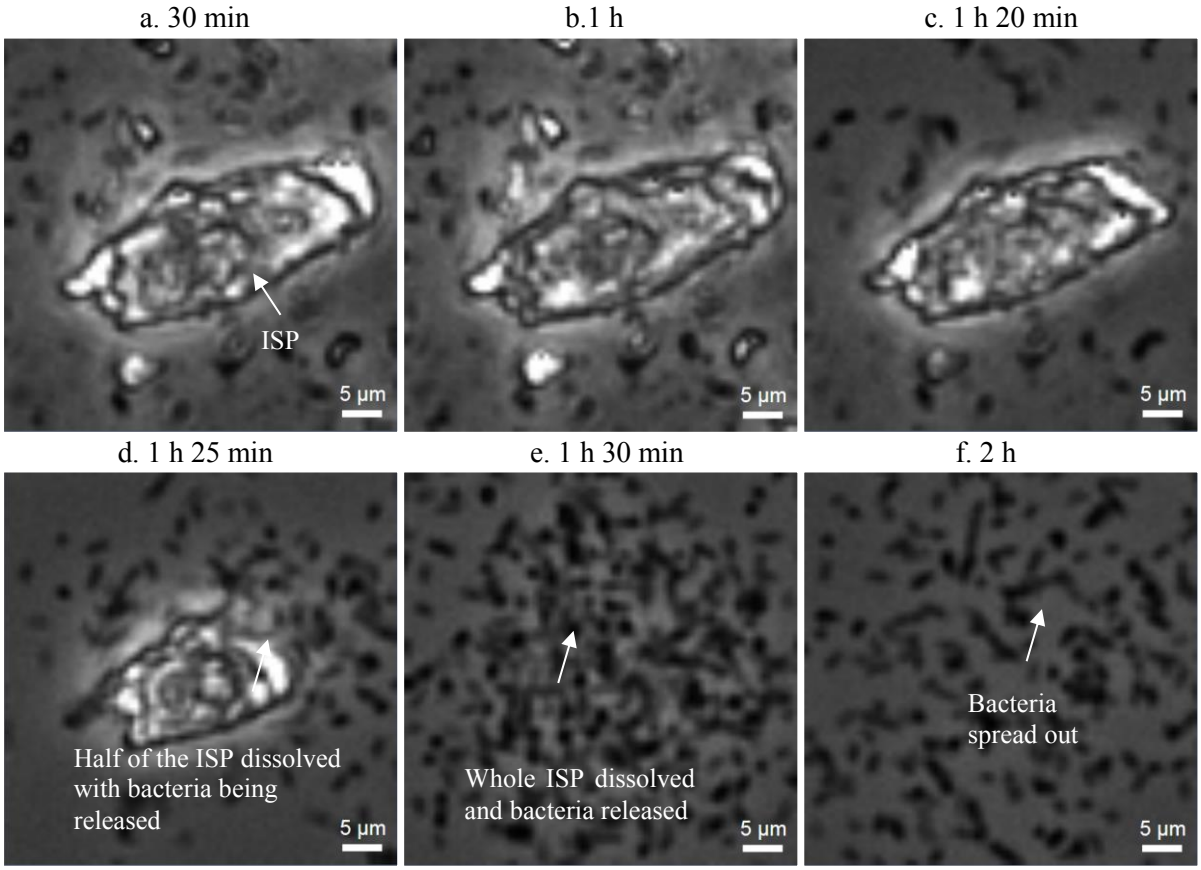

Figure 5.4 The dissolution of an irregular-shaped precipitate and the movement of bacterial cells after the dissolution. Bacterial aggregate (BA); Irregular-shaped precipitate (ISP)

5.3.4 Dissolution of irregularly-shaped $CaCO_3$ and re-precipitation of $CaCO_3$ crystals

To observe the precipitation process and stabilities of $CaCO_3$ crystals, magnified images of square I (shown in **Figure 5.2a**) at selected time points from 0 hr to 12 hrs are shown in **Figure 5.5**. As can be seen from this figure, $CaCO_3$ crystals grew with the dissolution of the irregular-shaped $CaCO_3$ precipitates. Most crystals were spherical, such as crystals A-F, or rhombohedral, such as crystals G-Q. Spherical crystals were not stable and dissolved later on. For example, Crystal B dissolved by 12 hrs and crystals C-F dissolved by 7 hrs. Rhombohedral crystals such as crystals G-Q were stable and did not dissolve after being formed.

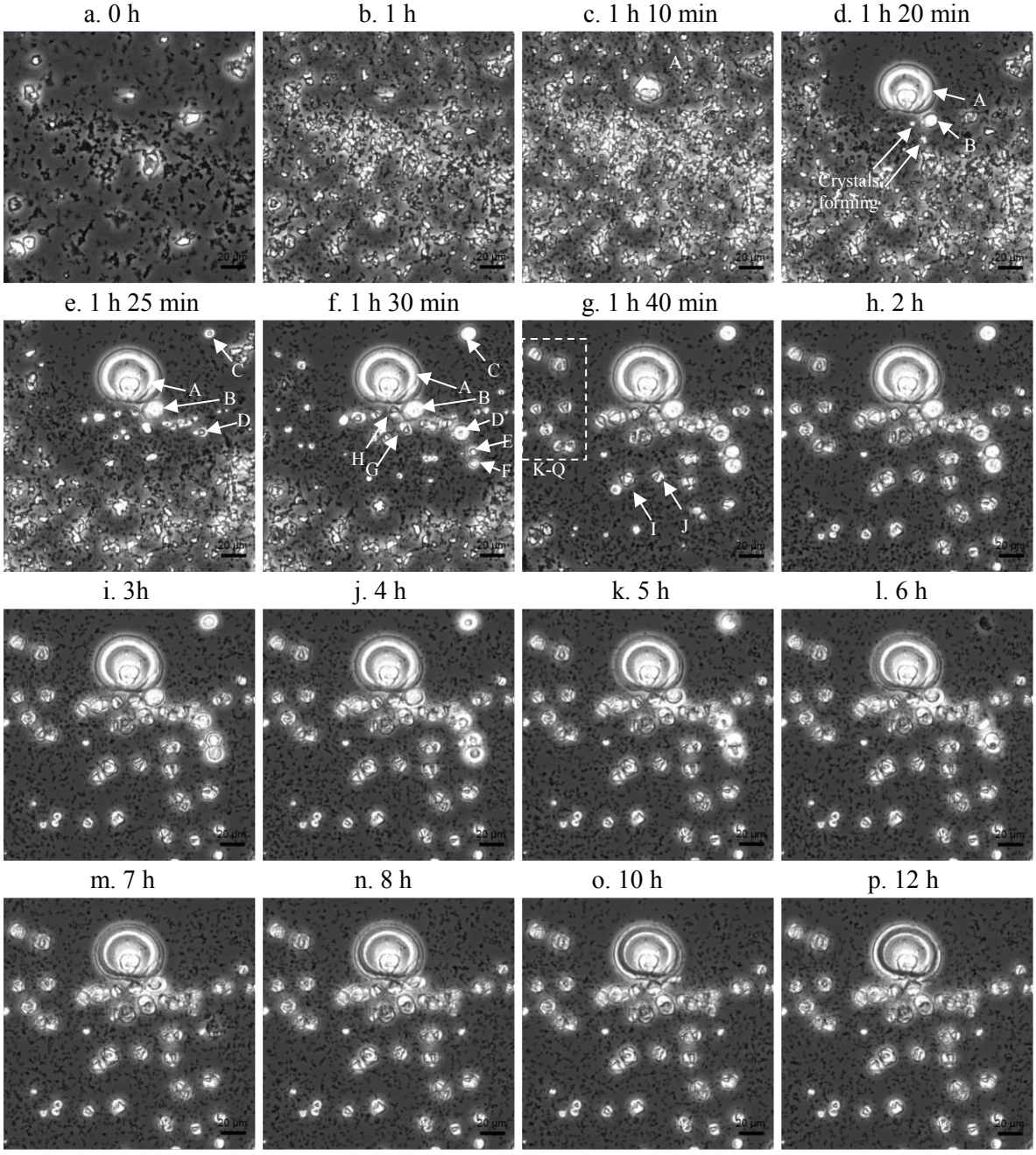

Figure 5.5 Microscope images showing the dissolution of spherical $CaCO_3$ crystals while rhombohedral $CaCO_3$ crystals continued to be stable. **(a-c)** growth of irregular-shaped $CaCO_3$ precipitates; **(c-h)** spherical $CaCO_3$ crystals and rhombohedral $CaCO_3$ crystals grow at the expense of the dissolution of irregular-shaped $CaCO_3$ precipitates; **(i-p)** rhombohedral $CaCO_3$ crystals stay stable, whereas spherical $CaCO_3$ crystals dissolved

To observe the formation of spherical $CaCO_3$ crystals and rhombohedral $CaCO_3$ crystals in more detail, such as changes in their shape and size with time, magnified images of crystals C and I, which are shown in **Figure 5.5,** were picked as representations and their shapes at selected time points are shown in **Figure 5.6** and **Figure 5.7**, respectively.

The spherical crystal (crystal C) started to form by 1 hr 25 min (**Figure 5.6d**), and then grew until 2 hrs (**Figure 5.6f**), after which it started to dissolve and was fully dissolved by 7 hrs. Therefore, spherical crystal C is relatively unstable. This dissolution of spherical crystals is consistent with the dissolution of vaterite according to Ostwald's step rule, as well as with the SEM images showing the dissolved vaterite (van Paassen 2009) taken 1 week after MICP treatment. By contrast, the rhombohedral crystal (crystal I) was stable after being formed (**Figure 5.7d-l**).

The growth of $CaCO_3$ crystals during an MICP process occurred on a soft agar or in liquid contained in a petri dish was observed by Zhang et al. (2018), and it was found that $CaCO_3$ crystals grew after formed without dissolution. However, the results presented in this thesis are the first direct observation of the process of dissolution of spherical $CaCO_3$ crystals and steady growth of rhombohedral crystals in the same sample during MICP. The rhombohedral crystals appear to be more stable than the spherical crystals, which in turn are more stable than the irregular-shaped precipitates. This is reminiscent of the transformation of irregular-shaped amorphous $CaCO_3$ precipitates to spherical vaterite and then to rhombohedral calcite (Rodriguez-Blanco et al., 2011). Together with the morphological aspects of these structures, this suggests that rhombohedral crystals are calcite, spherical crystals are vaterite, and irregular-shaped precipitates are amorphous $CaCO_3$ precipitates, as proposed by Rodriguez-Blanco et al. (2011) and Chu et al. (2013). In addition, these results are consistent with several studies in which the percentage of rhombohedral $CaCO_3$ crystals relative to all crystals increased at later stages during the precipitation process (Wei et al., 2003; Rodriguez-Blanco et al., 2011).

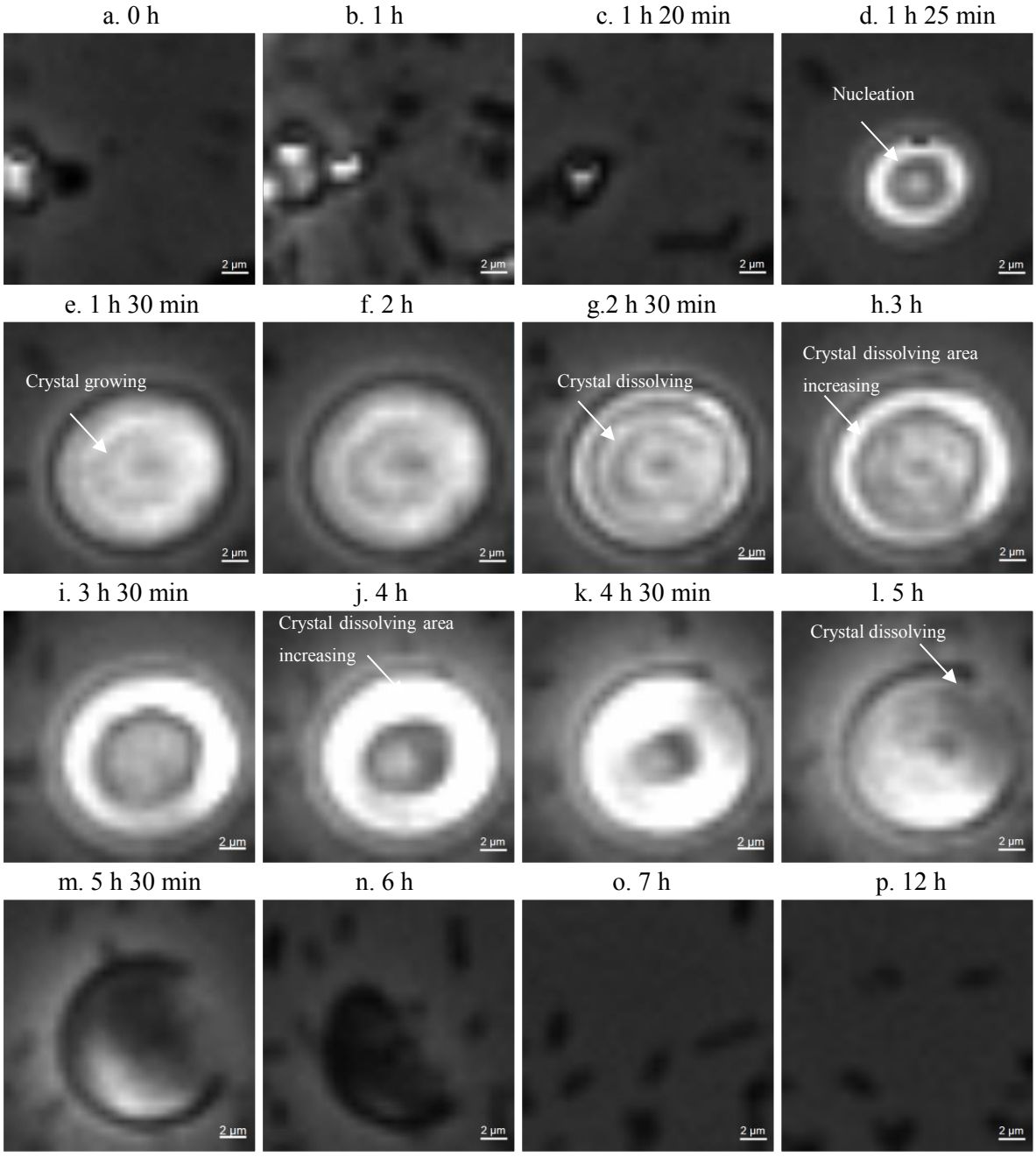

Figure 5.6 Microscope images showing the growth and dissolution of a spherical $CaCO_3$ crystal. **(a-c)** events preceding the formation of the crystal; **(d-g)** crystal growth phase; **(h-p)**, dissolution of the crystal.

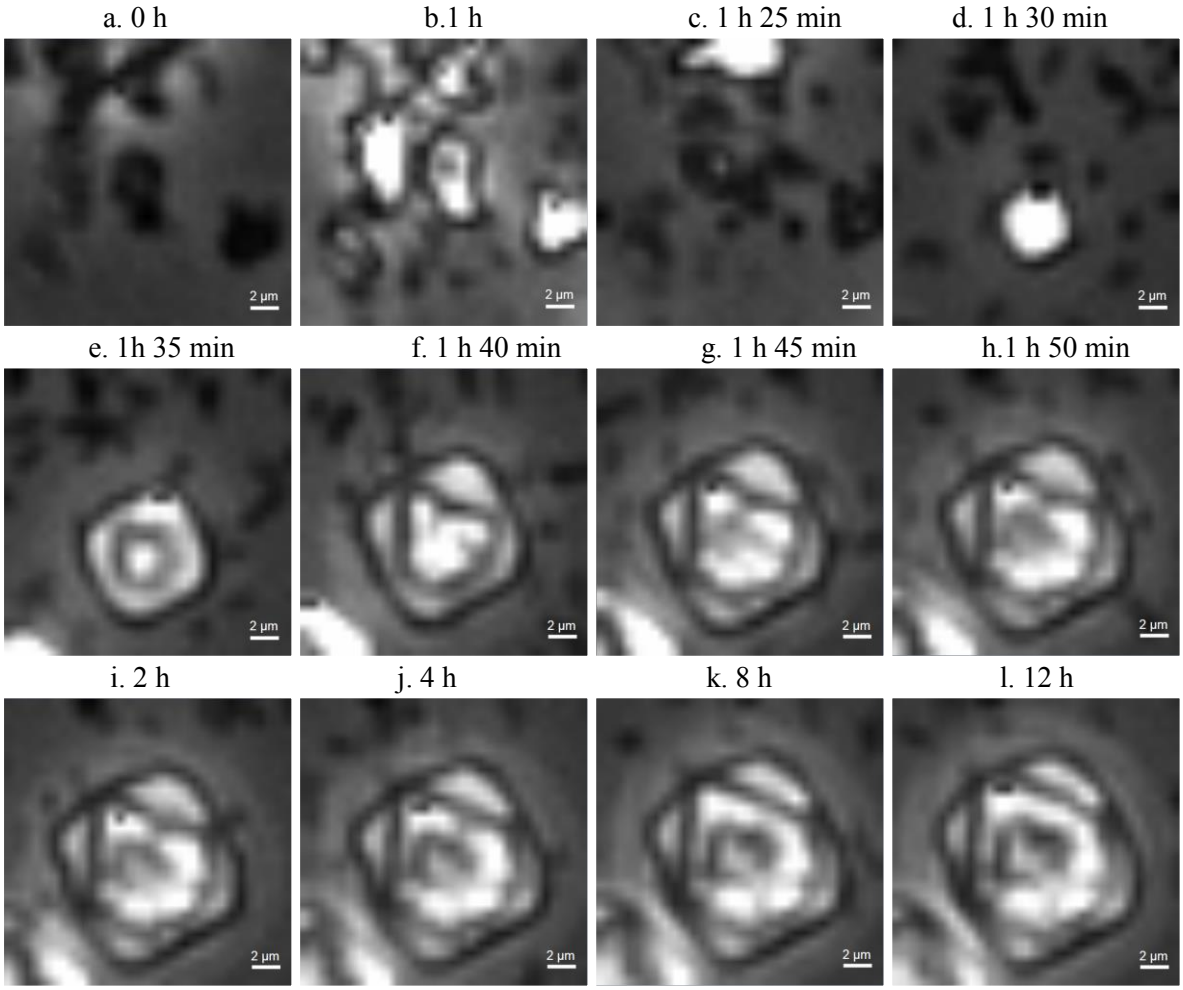

Figure 5.7 Microscope images showing growth of a rhombohedral $CaCO_3$ crystal. **(a-c)** events preceding the formation of the crystal; **(d-l)** crystal formation and growth.

5.4 MICP processes occurring in a porous medium during a staged injection procedure

The effects of bacterial aggregates and individual bacterial cells on the MICP process were explored in the glass slide experiment, and it was shown that bacterial aggregates have an effect on the initial stage of $CaCO_3$ precipitation. The glass slide experiment also revealed that the $CaCO_3$ phases formed during the initial stage were not stable and dissolved after more stable $CaCO_3$ crystals formed. However, as stated previously, the glass slide experiment cannot manipulate the injection of bacterial suspension and cementation solution, whereas real-world MICP applications normally involve multiple injections of cementation solution. In addition,

the presence of a soil matrix as a porous medium may affect the distribution of bacterial aggregates and individual bacterial cells, which may consequently affect the MICP process. Therefore, after the glass slide experiment, a microfluidic chip experiment was conducted to further explore the effects of individual bacterial cells and bacterial aggregates on MICP processes and the changes in shape and size of the $CaCO_3$ precipitates in a porous medium during a staged injection MICP procedure.

Representative images taken immediately after and 24 hrs after the injection of bacterial suspension are shown in **Figure 5.8**. Bacterial cells continued to multiply after being injected as shown by the difference in bacterial number between **Figure 5.8b** and **Figure 5.8a**. Counting the number of bacteria present in three pores of the microfluidic chip revealed that the number of bacteria increased by about 5 times [from $(3.8 \pm 0.2)\times10^8$ to $(2.0 \pm 0.1)\times10^9$ cells per ml] during the 24-hour settling period.

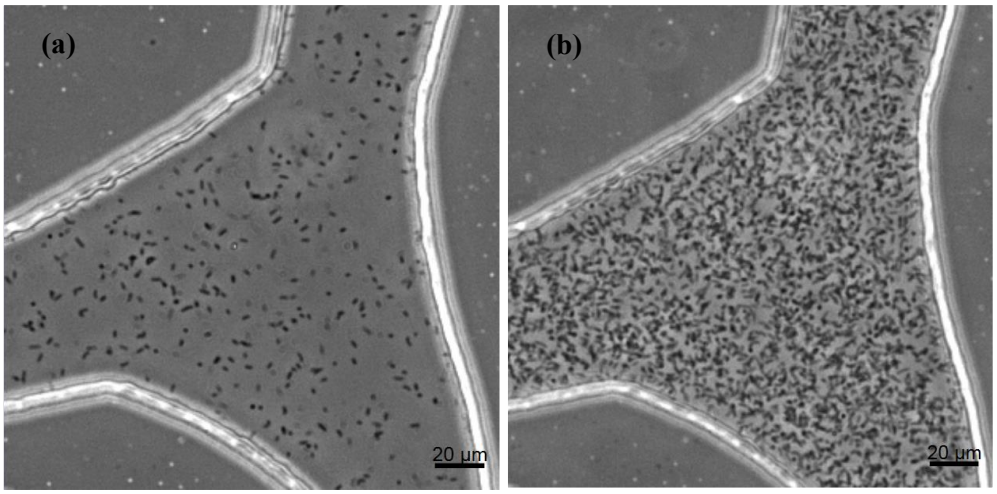

Figure 5.8 Microscope images of a pore in the middle of the microfluidic chip taken immediately after the injection of a bacterial suspension with an OD_{600} of 1.0 **(a)** and 24 hours after allowing the bacteria to settle **(b)**

5.4.1 MICP processes after the first injection of cementation solution

To observe the MICP processes after the first injection of cementation solution, time series images of five pores in the microfluidic chip taken directly after the first injection of

cementation solution, and at 1 hr, 3 hrs, and 24 hrs are shown in **Figure 5.9**. As expected, the higher bacterial density in this experiment (compared with Test 5 in *Chapter 4*), resulted in more bacterial aggregates being formed after the injection of cementation solution. In addition, this experiment suggests that bacterial aggregation and the formation of irregular-shaped $CaCO_3$ fix the bacterial cells and reduce their ability to move. However, because *S. pasteurii* bacteria can swim and irregular-shaped $CaCO_3$ eventually dissolved, the bacteria became more homogeneously distributed at 24 hr compared with 0 hr. Furthermore, these observations suggest that the distribution of bacterial aggregates may affect the distribution of crystals. For example, the crystals formed closer to the bacterial aggregates and irregular-shaped precipitates in pores II, III and V (shown by the circles). These observations are consistent with those obtained in Test 5 in *Chapter 4*. In addition, these observations also suggest that the distribution of bacterial aggregates is not the only factor that affects the distribution of the crystals. This is because many irregularly-shaped precipitates dissolved without forming crystals closer to them, such can be seen in pores I, III and V (shown by the arrows). As it still difficult to predict the positions within the pores where crystals form, more investigations on the nucleation processes are needed to improve our understanding of these events.

The main events occurring during the MICP process in the microfluidic chip were also in general consistent with the events observed in the glass slide experiment. Bacterial cells aggregated after the injection of cementation solution (see **Figure 5.9**, pore I, II, III and V, 0 hr photos). Irregular-shaped $CaCO_3$ precipitates were formed on the bacterial aggregates or individual bacterial cells (see **Figure 5.9**, pore I, II, III and V, 0 hr photos). Irregular-shaped $CaCO_3$ precipitates continued to grow from 0 to 1 hour (see **Figure 5.9**, pore I, II, III and V, 1 hr photos compared with 0 hr photos) and then dissolved (see **Figure 5.9,** pore I, II 3 hr photos; pores III V 24 hr photos compared with 0 hr photos). With the dissolution of the irregular-shaped $CaCO_3$ precipitates, the bacterial cells that were enclosed became dispersed (see **Figure 5.9**, pore I, II 3 hr phots). $CaCO_3$ crystals appeared with the dissolution of the irregular-shaped $CaCO_3$ precipitates (such as pore V, 3 hr photo compared with 1 hr photo). Finally, the spherical crystals dissolved but the other crystals remained (such as pore IV, 24 hrs photo).

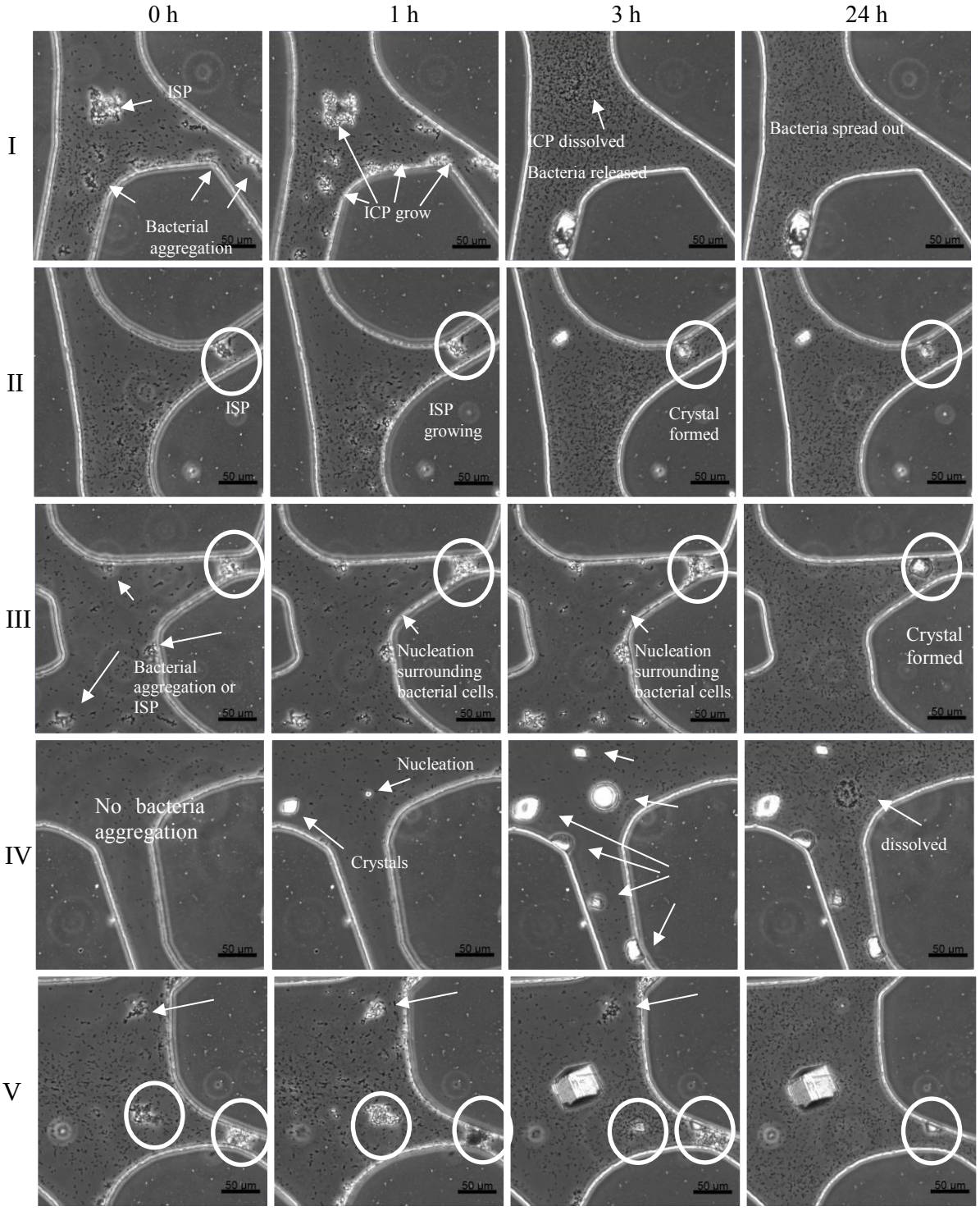

Figure 5.9 Microscope images of five pores in the microfluidic chip at 0, 1, 3 and 24 hours after the first injection of cementation solution

5.4.2 MICP processes after the second injection of cementation solution

To observe the MICP processes after the second injection of cementation solution, images of Pore V at 0, 1, 3 and 24 hours after the completion of the second injection of cementation solution are shown in **Figure 5.10**. The two crystals formed after the first cementation solution injection were still at the same place inside the pore after the second injection of cementation solution. This suggests that the crystals were stable inside the porous medium and could not be flushed out at a flow rate of 5.6 PV/h. At 3 hours, small crystals formed (light dots in **Figure 5.10**). However, by 24 hours, the small crystals dissolved. The big crystals in these two pores continued to grow during the first 24 hours, after which only the big crystals and several newly formed crystals remained.

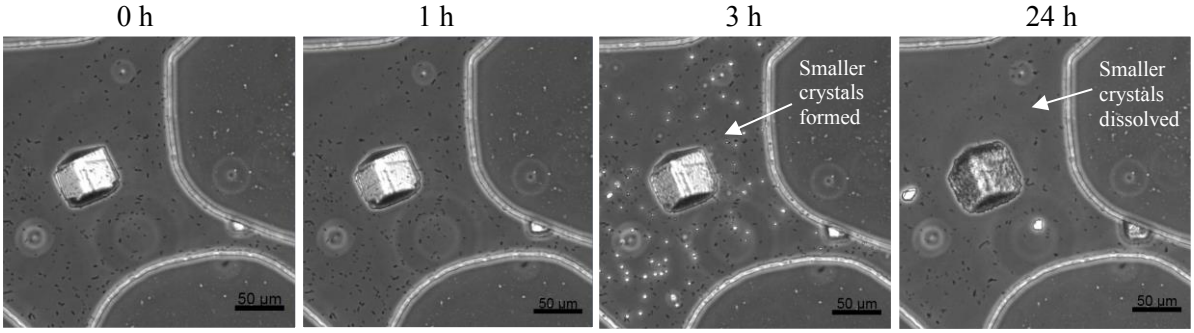

Figure 5.10 Microscope images of pore V in the microfluidic chip at 0, 1, 3 and 24 hours after the second injection of cementation solution

This observation suggests that the dissolution of less stable $CaCO_3$ crystals at the expense of growth of more stable crystals not only occurred after mixing the bacterial suspension and cementation solution but could also occur after the second injection of cementation solution. This implies that when the interval between cementation solution injections is long enough for smaller and unstable crystals to dissolve and larger, more stable crystals to grow, the larger crystals become larger and more stable as the number of cementation solution injections increases. By contrast, when the injection interval is not long enough for the small crystals to dissolve, they may continue growing during subsequent injections. It would therefore be interesting to conduct further experiments to study the effect of the interval between cementation solution injections in stage-injection procedures on the size and number of the crystals. In addition, as the size and number of the crystals may affect the mechanical properties

of the MICP-treated sand, further experiments could be conducted to study the effect of injection interval on the mechanical properties of MICP-treated sand.

5.5 Conclusions

In this study, MICP processes were visualised at the microscale by conducting both glass slide experiments and microfluidic chip experiments in order to understand the effects of bacterial cells/aggregates on $CaCO_3$ precipitation and changes in the shape and size of the $CaCO_3$ precipitates during the MICP process. The main findings of this study are summarised as follows.

Bacteria aggregated after the mixing of bacterial suspension and cementation solution in the glass slide experiments and after the injection of the cementation solution in the staged-injection microfluidic chip experiments, even though less aggregation was observed in the latter case. Bacterial aggregation resulted in $CaCO_3$ precipitates growing on top of bacterial aggregates and the bacterial cells becoming trapped inside them. Comparisons between the bacterial aggregates produced in the staged injection experiment in this *Chapter* with Test 5 in *Chapter 4* suggest that bacterial density may affect the number of bacterial aggregates formed. Further work is warranted to investigate the effect of bacterial density on the formation of bacterial aggregates and the effects that this has on the MICP process. In addition, bacterial aggregates fix bacterial cells, and the transport and filtration of bacterial aggregates in a porous medium might affect the distribution of bacteria in a soil matrix, which may consequently affect the MICP process and the properties of the $CaCO_3$ crystals formed. Further work would be useful to study the effects of factors such as the size of bacterial aggregates, the injection flow rate of cementation and the pore size of the porous medium on the transport and distribution of bacterial aggregates in soil matrices.

The shape and size of the $CaCO_3$ precipitates changed during the MICP process. Irregular-shaped $CaCO_3$ precipitates formed during the initial stage of the precipitation process but dissolved when new $CaCO_3$ crystals formed. In addition, with the dissolution of irregular-shaped $CaCO_3$, spherical and rhombohedral $CaCO_3$ crystals formed. Furthermore, spherical

$CaCO_3$ crystals and smaller $CaCO_3$ crystals dissolved at the expense of growth of rhombohedral $CaCO_3$ crystals and larger $CaCO_3$ crystals. Because less stable calcium carbonate crystals may be dissolved at the expense of growth of more stable calcium carbonate crystals, the interval between cementation solution injections during a staged injection MICP treatment process may affect crystal morphology, which in turn would affect the engineering properties of MICP-treated soils. Further work involving translation of these findings to real soil applications will be useful for determining the relationship between the injection protocol used and the effect of this on the engineering properties of MICP-treated soils.

However, it is worth noting that the $CaCO_3$ precipitation during MICP might be affected by many factors such as bacterial density, cementation solution concentration, temperature, pressure and the presence of other ions. The experiments presented in this paper only show the possible effects of phase transformation during MICP at room temperature and normal pressure using a combination of bacterial suspension and cementation solution that are normally used in MICP. Further work can be conducted to investigate the effects of all the above-mentioned factors on the MICP process and the final properties of $CaCO_3$ produced.

Chapter 6 Effects of bacterial density on growth kinetics and characteristics of microbial-induced calcium carbonate crystals

6.1 Research aims

Understanding the growth kinetics of $CaCO_3$ precipitates is essential for predicting the time needed for $CaCO_3$ precipitation to complete and for designing an appropriate MICP protocol for engineering applications. Zhang et al. (2018) presented $CaCO_3$ crystal growth kinetics induced by *S. pasteurii* in a liquid medium which was placed in a petri dish or on an agar pad which was immobilised with *S. pasteurii* cells and contained Ca^{2+} and urea. However, the kinetics of $CaCO_3$ crystal growth obtained in the study by Zhang and colleagues (2018) might have limited implications for real MICP applications, as the experimental conditions in these two methods do not mimic real MICP conditions occurring in the pore fluid of a porous soil matrix. As shown in *Chapter 4*, the use of a microfluidic chip in this PhD study enables the MICP process to be simulated under conditions which more closely resemble MICP conditions found in real soils. In addition, the use of a microfluidic chip enables both the density of bacteria and the main parameters of $CaCO_3$ crystals such as size, shape and number to be quantified. Therefore, microfluidic chip experiments could be used to develop a better understanding of the kinetics of $CaCO_3$ precipitation which might occur during MICP processes in real soils.

As reviewed in *Chapter 2*, bacterial density has a positive effect on the ureolysis rate. Previous work has shown that the rate of ureolysis increases linearly from 50 mM/h to 300 mM/h as the bacterial density increases from 1×10^7 to 2×10^8 colony-forming units per millilitre of cell

suspension (CFU/ml) (Lauchnor et al., 2015). Ureolysis rate increases the rate of formation of CO_3^{2-} in the solution, which consequently affects the supersaturation state of the solute and the growth kinetics of $CaCO_3$ crystals. However, no research has yet been conducted to study the effect of bacterial density on the kinetics of microbial-induced $CaCO_3$ crystal growth.

Understanding the factors affecting the growth kinetics of $CaCO_3$ crystals is essential for designing appropriate MICP protocols. In addition, the effects of these factors on the micro-scale characteristics of $CaCO_3$ crystals should also be considered. As shown in *Chapter 5*, the phase, shape, and size of the $CaCO_3$ precipitates might change with time during an MICP process. Therefore, when the total amount of $CaCO_3$ is the same, the engineering properties of MICP-treated soils can vary significantly due to differences in the micro-scale properties of $CaCO_3$ crystals. As reviewed in *Section 2.3.2.2*, bacterial density might affect the size and number of $CaCO_3$ crystals. Based on observations that larger carbonate crystals were generated in the presence of ureolytic bacterial cells, whereas smaller crystals were produced in the absence of ureolytic bacterial cells, it was proposed that higher bacterial concentrations may generate larger carbonate crystals (Mitchell and Ferris, 2006). Others have found that the higher the ureolysis rate, the smaller the size of the crystals which formed. For example, Cuthbert et al. (2012) found that the average size of $CaCO_3$ crystals decreased from 100 μm to 10 μm when the ureolysis rate increased from 0.1 to 10 mM/d. Similarly, Cheng et al. (2017) found that crystal sizes decreased from 20-50 μm to 2-5 μm when the ureolysis rate increased from 300 mM/h to 3000 mM/h. As the ureolysis rate is positively correlated to bacterial density (Lauchnor et al., 2015), the conclusions of Cuthbert et al. (2012) and Cheng et al. (2017) seem to contradict those proposed by Mitchell and Ferris (2006). As a result, the precise effects of bacterial density on the characteristics of microbial-induced $CaCO_3$ crystals are still largely unknown.

Therefore, in this Chapter a microfluidic chip experiment was conducted to investigate the effects of bacterial density on the growth kinetics and characteristics of microbial-induced $CaCO_3$ crystals. In addition, having shown that bacterial density may also affect the formation of bacterial aggregates which in turn affect the MICP process and the properties of the $CaCO_3$ formed, the effects of bacterial density on the formation of bacterial aggregates and the

characteristics of $CaCO_3$ were also investigated in these experiments. Furthermore, depending on the application, injections of cementation solution are normally repeated multiple times to increase the level of $CaCO_3$ content. In this Chapter, 12 injections of cementation solution were conducted, and the effects of bacterial density on crystal growth and characteristics during these 12 injections were investigated.

6.2 Experimental protocols

Sporosarcina pasteurii (DSM 33) bacteria were used in all experiments. The bacterial suspension was cultivated as described in *Chapter 3* to reach an OD_{600} of 3.0. Five bacterial suspensions were then prepared from this bacterial suspension (OD_{600} = 3.0) by diluting this bacterial suspension using autoclaved NH_4-YE liquid medium at dilution ratios, v (bacterial suspension): v (NH_4-YE liquid medium) of 1:14, 1:5, 1:2, 2:1 and 1:0. 1.25 PV of the bacterial suspensions were then injected into five microfluidic chips at an injection flow rate of 56 PV/h (same as to those in Test 6 described in *Chapter 4)*, to quantify bacterial density and to determine the correlation between bacterial cell density and optical density. Microscope images of these five microfluidic chips were taken at 10 minutes after the completion of the injection of bacterial suspension, after bacteria were left to settle for 2 hours, and immediately after injecting the cementation solution. The cementation solution contained 0.25 M of $CaCl_2$, 0.375 M of urea and 3 g/L of nutrient broth.

To investigate the effects of bacterial density on the growth kinetics and characteristics of microbial-induced $CaCO_3$ crystals inside the microfluidic chips during MICP, bacterial suspensions with dilution ratios of 1:14, 1:2 and 1:0 were chosen to represent low, medium and high bacterial density conditions. The injection of cementation solution was repeated for twelve times at an injection interval of 24 hours to increase the content of $CaCO_3$ formed. Time-series images were taken at an imaging interval of 15 minutes after each of the 12 injections. The main parameters of bacterial suspension and cementation solution together with their injection parameters in these protocols are summarised in **Table 6.1**.

Table 6.1 Summary of bacterial, chemical and injection parameters associated with the microfluidic chip experiments

Protocol No.	Volume proportion *	Bacterial OD_{600}	Injection number	Injection interval (day)
1	1:14	0.2	12	1
2	1:5	0.5	1	-
3	1:2	1.0	12	1
4	2:1	2.0	1	-
5	1:0	3.0	12	1

Note: Volume proportion refers to *v* (bacterial suspension): *v* (nutrient liquid)

In parallel to the microfluidic chip experiment, a set of liquid batch experiments were conducted to examine the influence of bacterial density on ureolysis kinetics and to compare the findings with the results obtained from the microfluidic chip experiments to determine the correlation between the kinetics of ureolysis and precipitation. The experimental setup was described in *Section 3.2*. The concentration of urea and the optical density of bacterial suspension in each bacteria-urea mixture were designed to be in a similar range compared to the concentrations and densities used in the microfluidic experiments.

6.3 Results and discussion

6.3.1 Bacterial quantification

Microscope images taken at the centre of the microfluidic chip at 10 min after the injection of bacterial suspensions, after the two-hour settling period, and after the first injection of cementation solution are shown in **Figure 6.1a**. The bacterial densities were correlated with the initial OD_{600} of bacterial suspension and the results are shown in **Figure 6.1b**. After bacterial injection, the bacterial density was linearly correlated with OD_{600}. The correlation is:

$$Bacterial\ \ density\ (cells/ml) = (0.18 + OD_{600} \times 3.60) \times 10^8 \qquad 6.1$$

The bacterial densities after bacterial settling and after the injection of cementation solution were also linearly correlated with the initial OD_{600} of bacterial suspension. The R^2 values of the all three linear regression lines in **Figure 6.1 b** were higher than 0.98. The bacterial densities which were present 10 mins after the injection of bacteria varied between 1.0×10^8 and 1.20×10^9 cells/ml (**Figure 6.1b**), and after two-hours of settling, the bacterial densities increased to 2.0×10^8 -1.55×10^9 cells/ml due to bacterial growth *in situ* (**Figure 6.1b**). This suggests that bacteria grew in all of the five protocols, although the growth rate varied. The highest growth rate was obtained from Protocol 1 (in which the initial bacterial OD_{600} was 0.2) where the cell density doubled after two hours of settling. The lowest growth rate was obtained from Protocols 4 and 5, where the bacterial densities after two-hours of settling were about 1.25 times higher than the initial densities (OD_{600} was 2.0 and 3.0). The growth rate of bacteria in Protocols 2 and 3 was about 1.5 times higher than the initial densities (OD_{600} was 0.5 and 1.0). The difference in bacterial growth rate might be because the relative abundance of nutrients available to the bacterial population varied depending on the initial bacterial density, with individual bacteria in more concentrated bacterial suspensions being exposed to a smaller share of the total nutrients available.

About 30% of the bacteria (0.5×10^8 to 5.2×10^8 ml^{-1}) remained attached to the inner surface of the porous medium after the injection of cementation solution compared to the number of bacteria present after bacterial settling (**Figure 6.1b**). As bacterial aggregates also occurred after the injection of cementation solution, especially when the bacterial density was high, and the number of bacteria present in bacterial aggregates was not counted, the actual bacterial density should be higher than 30 % of their amount after bacterial settling.

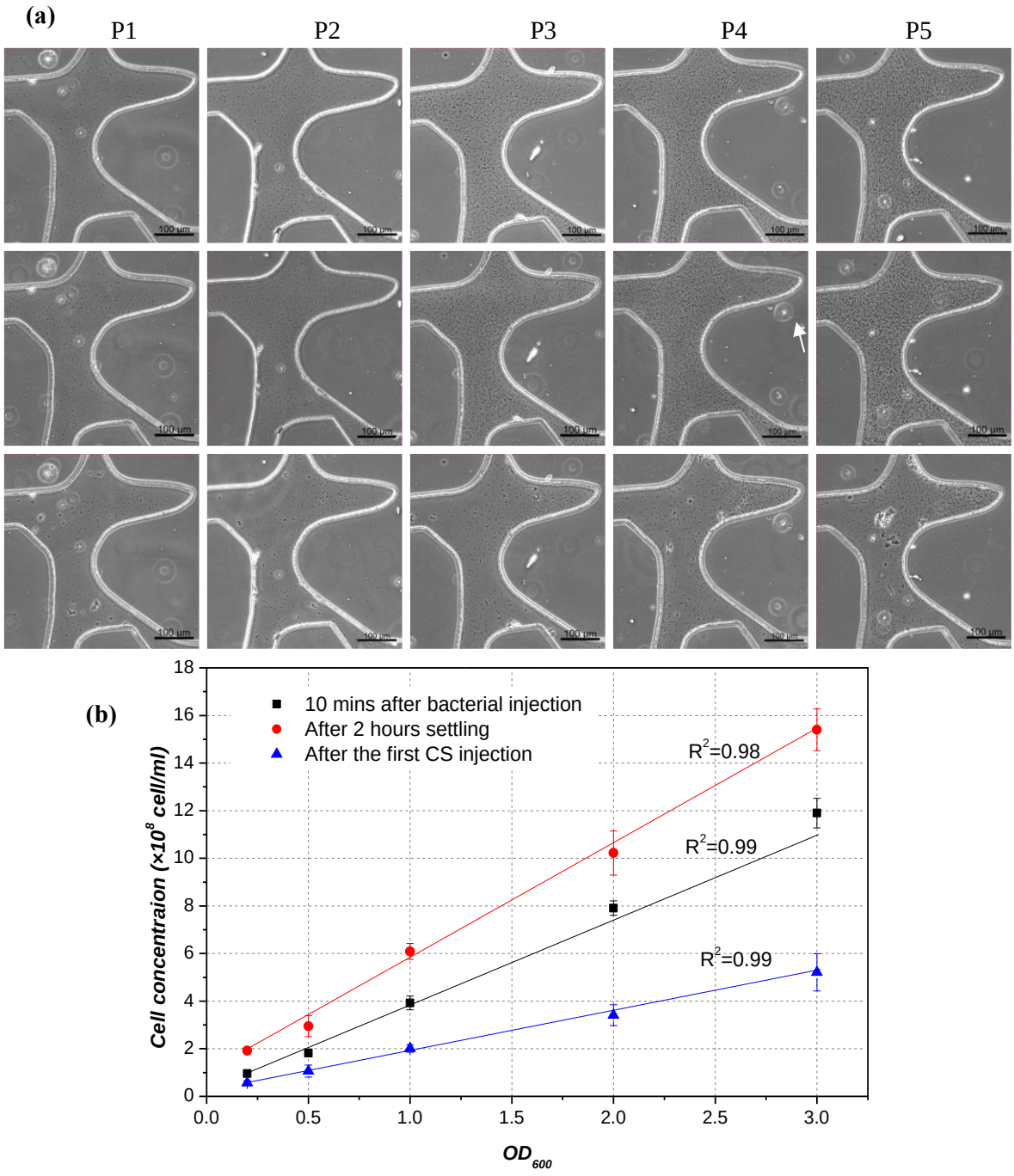

Figure 6.1 (a) Microscope images of one pore at the centre of the microfluidic chip taken ten mins after bacterial injection (first row), after two hours of settling (second row) and after the first injection of cementation solution (third row); **(b)** correlations between the initial OD_{600} of the bacterial suspensions and bacterial density at ten mins after bacterial injection (black squares), after settling (red circles) and after the first injection of cementation solution (blue triangles). Data are presented as mean ± standard error, and each measurement was repeated three times.

6.3.2 Effect of bacterial density on the kinetics of ureolysis

In parallel to the microfluidic experiments, the ureolysis rate in mixtures of bacterial suspensions with various bacterial densities and urea solution at constant concentration (0.375 M in the mixture). The results are shown in **Figure 6.2**. The ureolysis rate increased with the increase of bacterial density until the bacterial density reached 4×10^8 cells per ml, beyond which the ureolysis rate stopped increasing (**Figure 6.2**). The increase in ureolysis rate associated with a bacterial density in the range of 1×10^7 - 2×10^8 per ml is consistent with the results obtained by (Lauchnor et al., 2015). In addition, for bacterial densities exceeding around 4×10^8 cells per ml, the ureolysis rate no longer increased as the bacterial density increases, which is also consistent with the hypothesis made by Lauchnor et al. (2015). Specific bacterial activity decreased as the bacterial density increased, suggesting that there was a competing effect among bacteria to hydrolyse the urea, and the higher the bacterial density, the lower the specific ureolysis rate became. This is also consistent with the results of Stocks-Fisher et al. (1999) which showed that the specific ureolysis rate decreases with the increase in bacterial density in the range of 2×10^6 - 2×10^8 cells per ml.

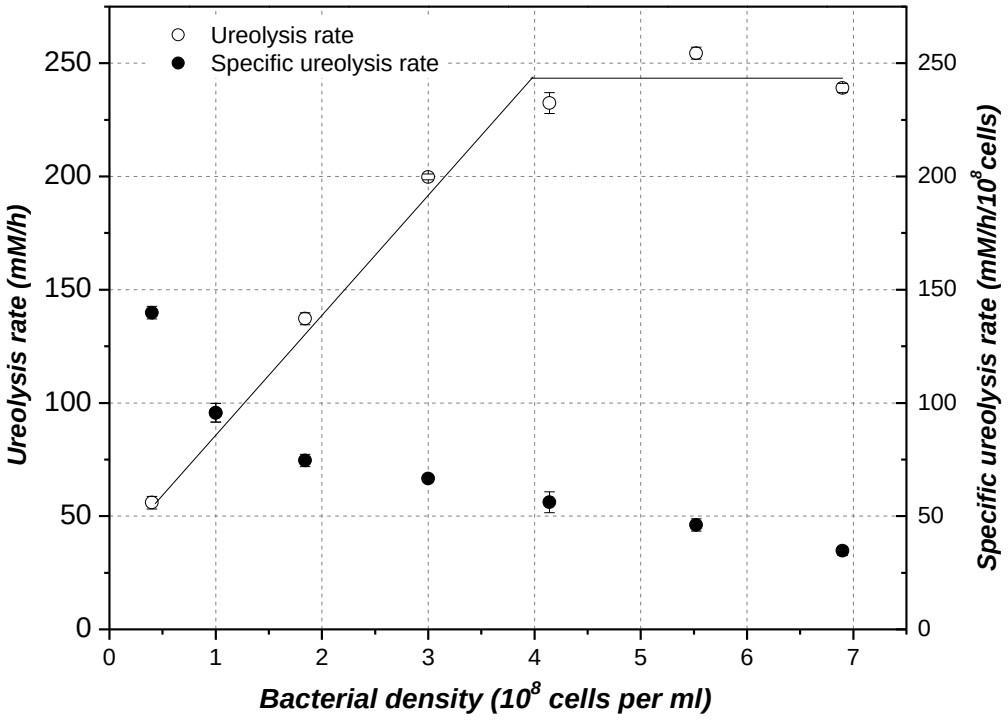

Figure 6.2 Ureolysis rate and specific ureolysis rate plotted against bacterial density

6.3.3 Effect of bacterial density on overall precipitation kinetics

To observe the kinetics of $CaCO_3$ precipitation after a single injection of cementation solution, images showing the 2 mm by 2 mm squares at the centre of the microfluidic chips containing $CaCO_3$ crystals (appearing as white dots) were captured at an imaging interval of 15 mins for 24 hours. The images taken at 0.5 hr, 1 hr, 3 hr and 24 hr after the injection of cementation solution are presented in **Figure 6.3**. The mean intensity values and normalised mean intensity values of all images taken during the 24-hour period after injection of cementation solution, were plotted against time (**Figure 6.3 b, c**). The mean intensity of the images here represents the relative areas which were occupied by the precipitates. The time when the image intensity stops changing is clear and represents the completion of precipitation. The $CaCO_3$ precipitated at different rates as the bacterial density was varied, with a higher bacterial density resulting in a higher overall precipitation rate. When the bacterial densities after the completion of the cementation solution injections were 0.5×10^8, 2.0×10^8, or 5.2×10^8 cells per ml, the time taken for $CaCO_3$ precipitation to complete was about 15 hrs, 3 hrs and 1.5 hrs, respectively. At 24 hrs, the areas occupied by $CaCO_3$ crystals in these three cases were also different; a higher initial bacterial density resulted in the precipitated crystals occupying a larger area.

These results suggest that bacterial density has an effect on the overall precipitation rate of $CaCO_3$ crystals. For bacterial densities between 0.5×10^8 and 5.2×10^8 cells per ml, the overall precipitation rate was higher when the bacterial density was higher. This might be explained by the fact that bacteria hydrolyse urea into CO_3^{2-} and NH_4^+, thereby increasing the local supersaturation for $CaCO_3$ precipitation. Therefore, at higher bacterial densities, bacteria hydrolyse more urea over the same amount of time, which consequently causes more local supersaturation zones to emerge, thus promoting the nucleation and growth of $CaCO_3$ crystals.

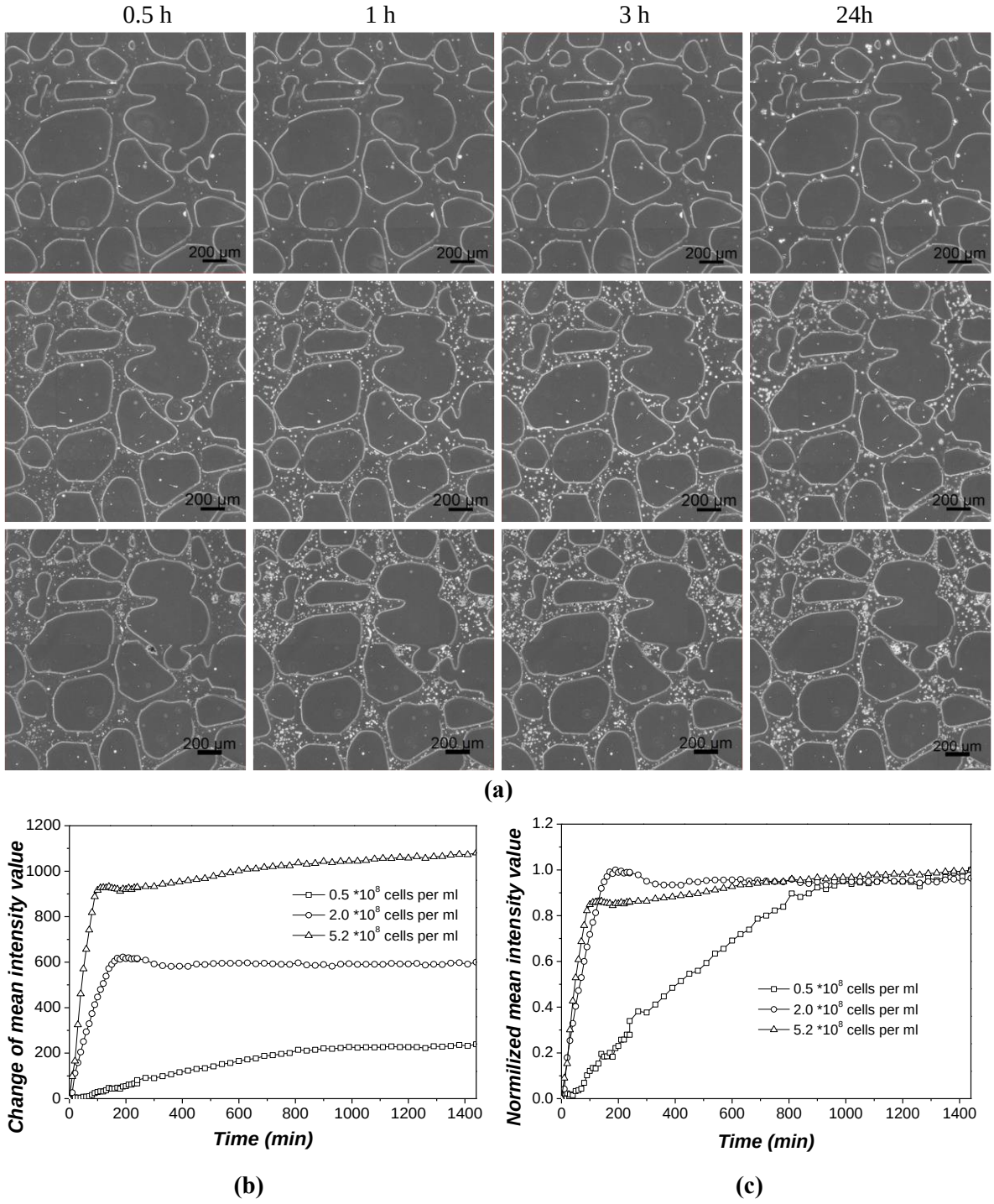

Figure 6.3 (a) Microscope images at the centre of the microfluidic chip taken 0.5, 1, 3 and 24 hours after the first injection of cementation solution, the bacterial densities were 0.5×10^{8} cells/ml, 2.0×10^{8} cells/ml and 5.2×10^{8} cells/ml in the first row, second row and third row, respectively; **(b)** the mean intensity value of the pictures vs. time; **(c)** mean intensity values of the images normalised to the highest mean intensity of the images vs. time; white dots in (a) represent the $CaCO_3$ crystals.

The bacterial density present at the ten minutes after injection, after settling, and after the injection of cementation solution in the three protocols, together with the overall precipitation time and the maximum input rate calculated by dividing the concentration of Ca^{2+} in the cementation solution by the overall precipitation time, are summarised in **Table 6.2**. By conducting soil column tests in which the concentration and interval between cementation solution injections were varied and the $CaCO_3$ content within the soil columns was measured after the MICP treatment process was completed, Al Qabany et al. (2012) suggested that the input rate of urea and $CaCl_2$ should not be higher than 0.042 M/h to achieve high chemical efficiency (result also shown in **Table 6.2**). However, the effects of bacterial density on chemical efficiency were not considered in the study of Qabany et al. (2012).

Because the difference in the overall precipitation rate was due to differences in bacterial density, the maximum input rates required to achieve high efficiency were 0.016 M/h, 0.083 M/h and 0.160 M/h for the protocols when bacterial densities after the injection of cementation solution were 0.5×10^8, 2×10^8 and 5.2×10^8 cells per ml, respectively. The initial bacterial density in the study by Al Qabany et al. (2012) was 1.0, which is the same as the bacterial density in protocol 3 in this study. However, the maximum input rates obtained by Al Qabany and colleagues were different from the maximum input rate for protocol 3 in this study. This might be because even though the initial bacterial density is the same, the number of bacteria present may change during the injection of bacterial suspension and cementation solution. It is therefore difficult to quantify the change in bacterial density within the porous soil matrix during this procedure. In addition, the ureolysis rate in this study was about 140 mM/h when the bacterial density was 1.0, which was also much higher compared to the activity of bacteria (20 mM/h) reported by Al Qabany et al. (2012). The difference in bacterial activity may also affect the overall precipitation rate and thus affects the input rate required to achieve a high chemical transformation efficiency.

Table 6.2 Summary of the changes in bacterial density during MICP treatment and associated overall precipitation times

OD_{600} Before injection	Bacterial density ($\times 10^8$ cells per ml)			Overall Precipitation		Reference
	After BS injection	After settling	After CS injection	Time (h)	Rate M/h	
0.2	1	1.9	0.5	15	0.016	P1, this study
1.0	4	8.1	2.0	3	0.083	P3, this study
3.0	12	17.4	5.2	1.5	0.160	P5, this study
1.0	-	-	-	-	0.042	Al Qabany et al., 2012

Note: BS-bacterial suspension; CS-cementation solution

6.3.4 Effect of bacterial density on growth kinetics of individual calcium carbonate crystals

To observe the growth kinetics of individual $CaCO_3$ crystals, magnified images of one pore taken at 0.5 hour, 1 hour, 1.5 hours and 2 hours after the first injection of cementation solution in each protocol are shown in **Figure 6.4**. To quantify the growth rate of the crystals in the three protocols during the two-hour period after the first injection of cementation solution, each crystal was assumed to be a hemisphere growing on the surface of the microfluidic channel, with the volume of the crystal being calculated based on its measured diameter. The average crystal volumes of individual crystals were plotted against time between 0 - 2 hrs in **Figure 6.5.** The bacterial density was found to have a limited effect on the growth rate of individual crystals during the first two hours because the crystals grew steadily at the same growth rate even though the bacterial density varied (**Figure 6.5**). The growth rate of the crystals over the two-hours was about 240 $\mu m^3/h$.

Comparing **Figure 6.5** with **Figure 6.3**, it can be seen that a higher bacterial density resulted in a higher overall precipitation rate (**Figure 6.3**) but did not increase the growth rate of individual crystals (**Figure 6.5**). This is because bacterial density has an effect on the number of the crystals produced in this pore, the higher the bacterial density, the larger number of

crystals formed in this area (see **Figure 6.5**). A more detailed discussion of the effect of bacterial density on the number of crystals formed is presented in the next section.

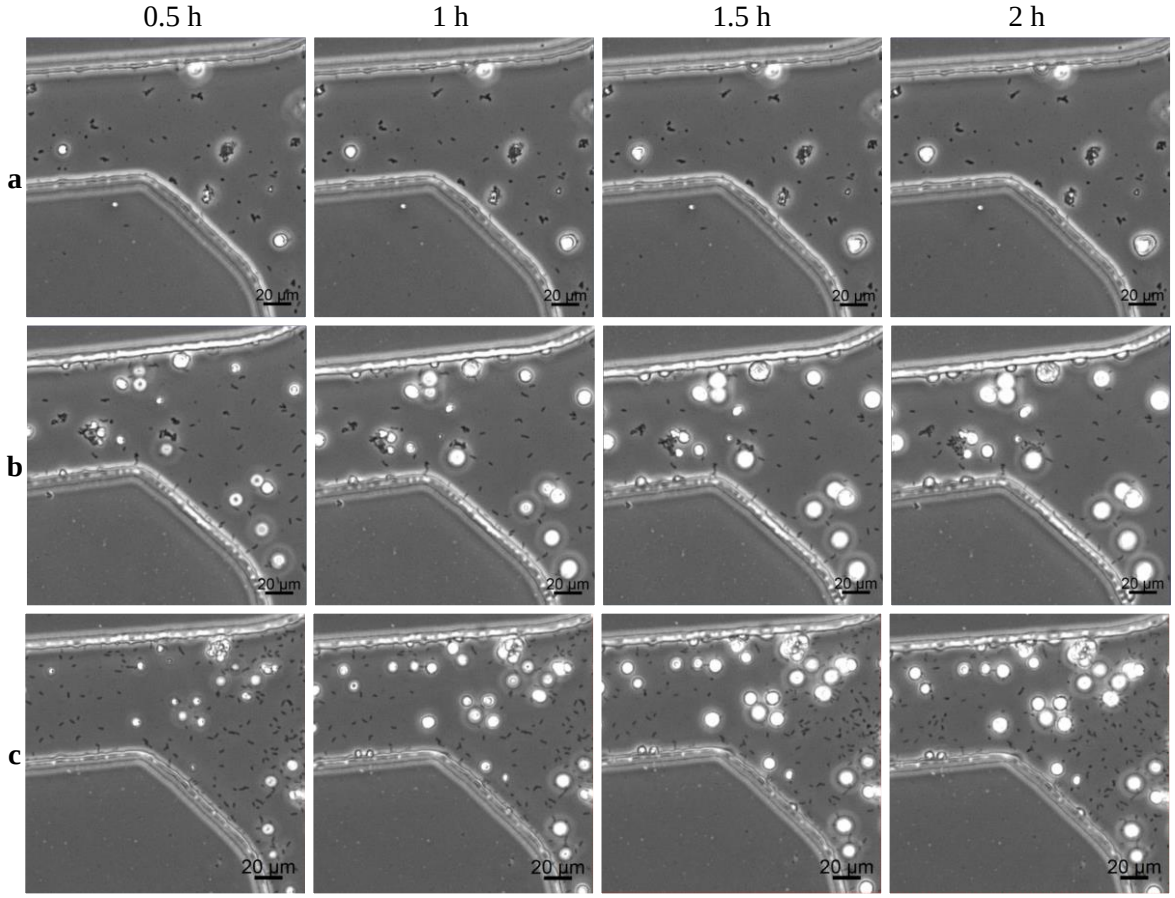

Figure 6.4 Microscope images of three protocols captured at 0.5, 1, 1.5 and 2 hours after the first injection of cementation solution. The bacterial densities in the protocols were 0.5×10^8 cells per ml **(a)**, 2.0×10^8 cells per ml **(b)**, and 5.2×10^8 cells per ml **(c)**

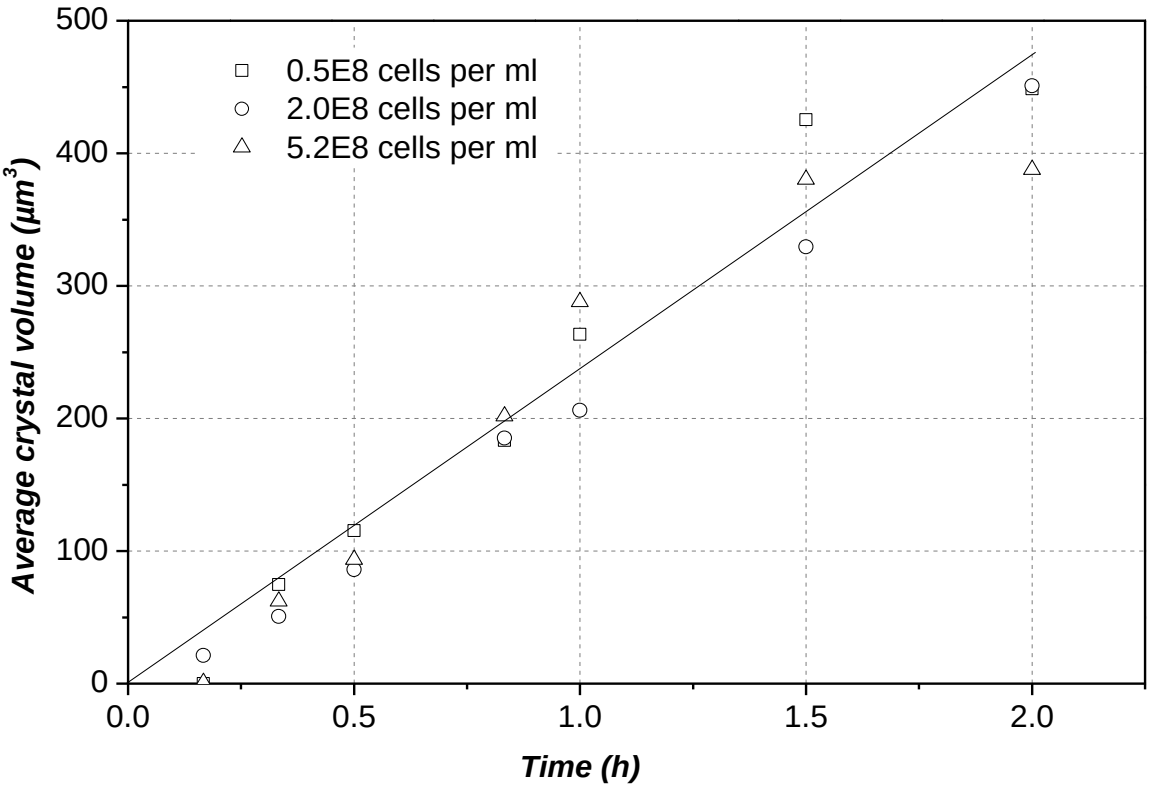

Figure 6.5 Average crystal volume vs time

To observe the growth individual crystal over a longer period of time after the first injection of cementation solution, microscope images of the same pores, as shown in **Figure 6.4**, at different time points taken between 2 hours and 24 hours after the first injection of cementation solution are shown in **Figure 6.6**. To quantify the growth rate of individual crystals during the 24-hour period after the first injection of cementation solution, average crystal volumes in the three protocols, 1, 3, and 5, were plotted against different time for different time points between 0 and 24 hours, with the results presented in **Figure 6.7**.

After 2 hours, the crystals in the protocol which contained the lowest concentration of bacteria (0.5×10^{8} cells per ml) continued growing at a rate that was similar to their growth rate during the first 2 hours and stopped growing after 15 hours. The time taken for the average crystal volume to stop increasing was the same as the time required for their overall precipitation to stop. Similarly, crystals in the protocol which contained the highest concentration of bacteria (5.2×10^{8} cells per ml) continued growing for about 1.5 hours, which is the same as the overall

precipitation time. However, for the protocol with a bacterial density of 2×10^8 cells per ml, the time taken for the average crystal to stop growing was about 10 hours, which is different than the time required for the overall precipitation to stop (3 hours) (**Figure 6.3**). It is shown in **Figure 6.7** that some of the crystals in Protocol 3 continued growing between 3 and 10 hours at the expense of the dissolution of other crystals. The dissolution of the crystals is discussed in more detail in the next section.

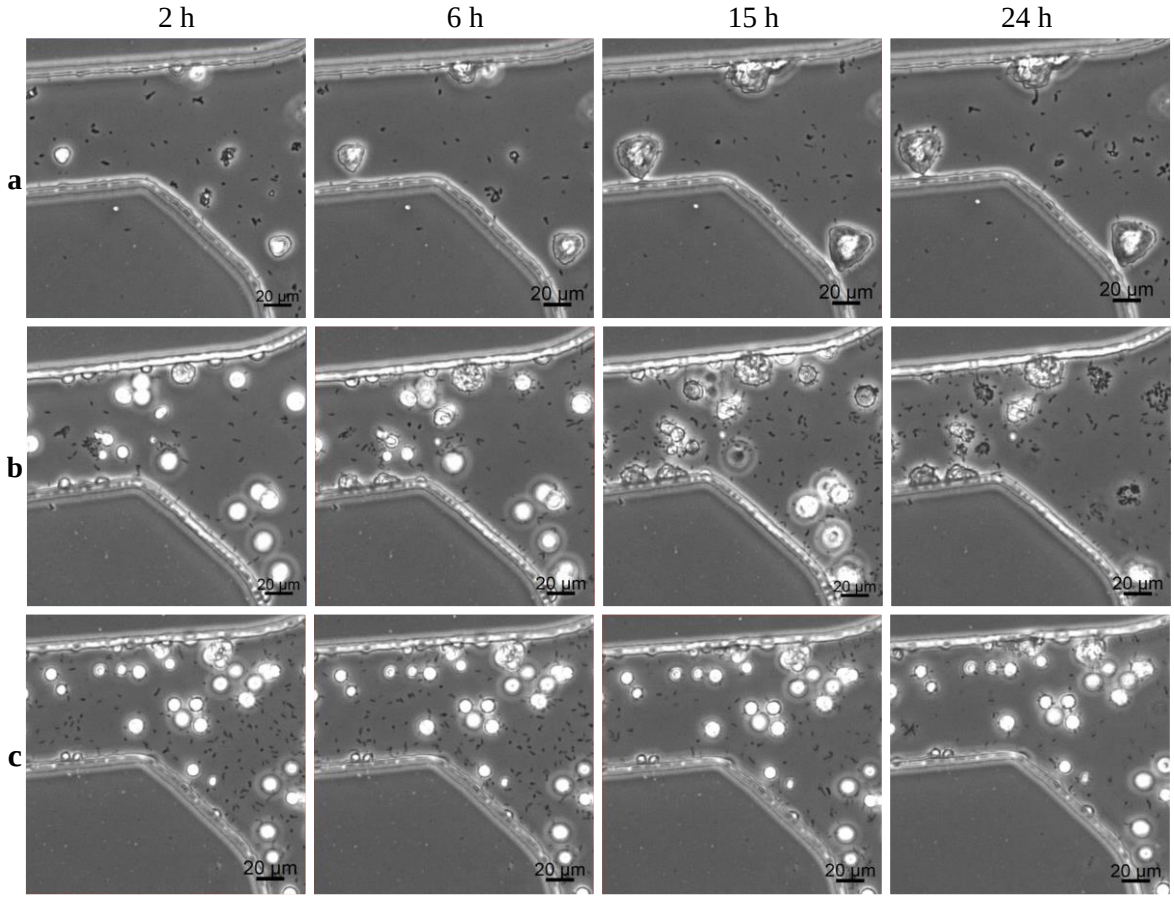

Figure 6.6 Microscope images of three protocols captured at 2 h, 6 h, 15 h and 24 h after the first injection of cementation solution. The bacterial densities in the protocols were 0.5×10^8 cells per ml **(a)**, 2.0×10^8 cells per ml **(b)**, and 5.2×10^8 cells per ml **(c)**

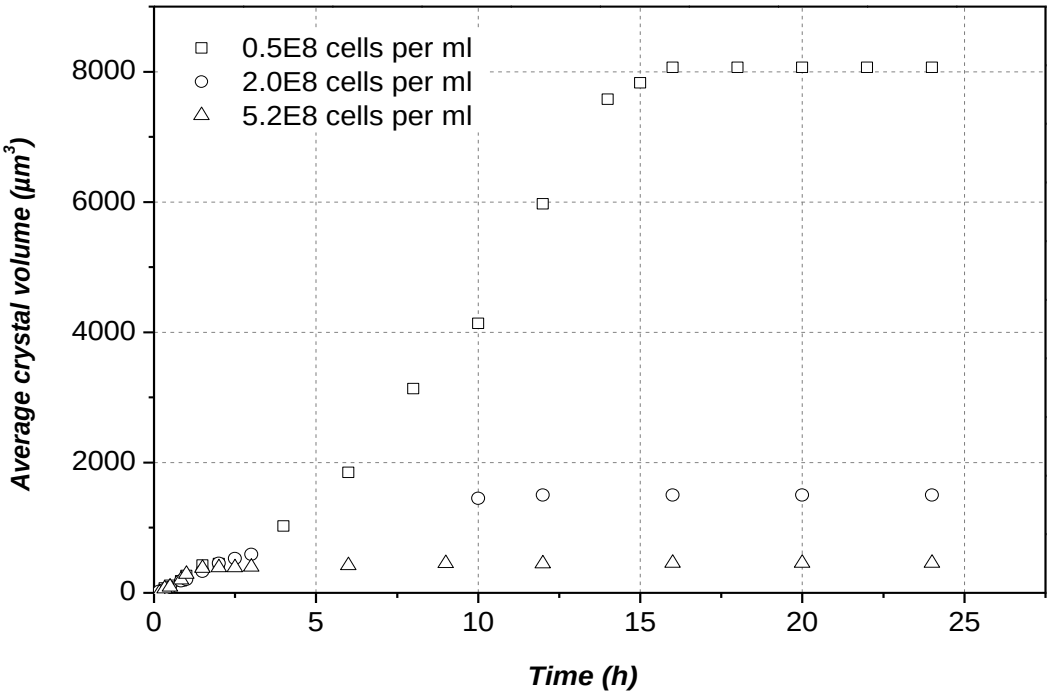

Figure 6.7 Scatter plot of average crystal size vs time

The $CaCO_3$ precipitation rate was estimated by measuring the rate of decrease in Ca^{2+} concentration in liquids processed by batch tests. It was found that in the presence of 10^6 -10^8 cells/ml of S. pasteurii, the concentration of insoluble Ca^{2+} ions increased to about 25 mM within about 16 hours (Stocks-Fischer et al., 1999). In this thesis study, in the presence of 0.5, 2 and 5 $\times 10^8$ cells/ml of S. pasteurii, the time taken for 250 mM of Ca^{2+} to precipitate was about 15, 3 and 1.5 hours, respectively, with an overall precipitation rate of 0.016, 0.083 and 0.16 M/h, respectively (see **Table 6.2**). Based on the linear correlation between bacterial density and precipitation rate, when bacterial density is 10^6 cells/ml, the estimated precipitation rate is 0.00032 M/h, with the estimated time to complete the precipitation being 78 h. Similarly, when the bacterial density is 10^8 cells/ml, the estimated precipitation rate is 0.032 M/h, with the estimated time to complete the precipitation being 0.78 h. The range is consistent with the results of Stocks-Fischer et al. (1999). Apart from being estimated by measuring the rate of decrease in Ca^{2+} concentration in liquids, precipitation rate was also estimated by measuring the rate of increase in the volume of individual crystals. Experimental studies on MICP were normally conducted in real soils where the growth of individual crystals cannot be observed, or under conditions such as on agar pads (Zhang et al., 2018), where the individual crystal

growth can be observed, but cannot be simulated under real MICP conditions. This thesis study presents the first results which demonstrate the growth rate of microbial-induced $CaCO_3$ crystals under the conditions similar to those present in real soils, as well as the effect of bacterial density on this process, thereby providing useful insights to inform further MICP studies.

These results demonstrate that, even though the total amount of $CaCO_3$ might be the same, the size of $CaCO_3$ crystals may be different when different bacterial densities are used. In turn this difference would affect the engineering properties of the MICP-treated samples such as permeability, stiffness, and strength. All of the cementation inside soils decreases permeability, and large crystals at the open pore throat might correspond to the effective $CaCO_3$ required to reduce soil permeability (Al Qabany and Soga, 2013). The production of larger crystals at narrow pore throats that are able to bond soil particles might be more efficient in increasing the stiffness/strength of MICP-treated soils (DeJong et al., 2010). Further work involving translation of these findings to real soil applications will be useful for determining a relationship between the treatment process and the engineering properties of MICP-treated soils.

6.3.5 Effect of bacterial density on crystal dissolution

As shown in the second row of **Figure 6.6**, crystals formed may be unstable and can dissolve. To observe the effect of bacterial density on crystal dissolution in more detail, 0.5 mm by 0.5 mm microscope images captured at a central pore at 3 h, 6 h, 12 h and 24 h after the first injection of cementation solution during the three protocols are shown in **Figure 6.8**. The images in the second row of **Figure 6.8** show that crystal dissolution occurred in the protocol containing bacteria with a density of 2×10^{8} cells per ml (Protocol 3). For example, crystals were no longer visible in the circled area of the image taken at 12 hours compared with the existence of the crystals in the same area in the image taken at 6 hours. In addition, the third row of **Figure 6.8** shows that in the protocol containing bacterial cells with a high bacterial density (Protocol 5, 5.2×10^{8} cells per ml), dissolution occurred at a later time point during the 24 hour imaging period (crystals circled at 12 h disappeared by 24 h) compared to the

dissolution observed when the bacterial density was medium (second row in **Figure 6.8**). However, crystals in the first row of **Figure 6.4**, **Figure 6.6** and **Figure 6.8** continued growing once formed when the bacterial density was low (Protocol 1, 0.5 × 10 ^{8} cells per ml). These observations suggest that bacterial density has an effect on the formation and dissolution of $CaCO_3$ crystals.

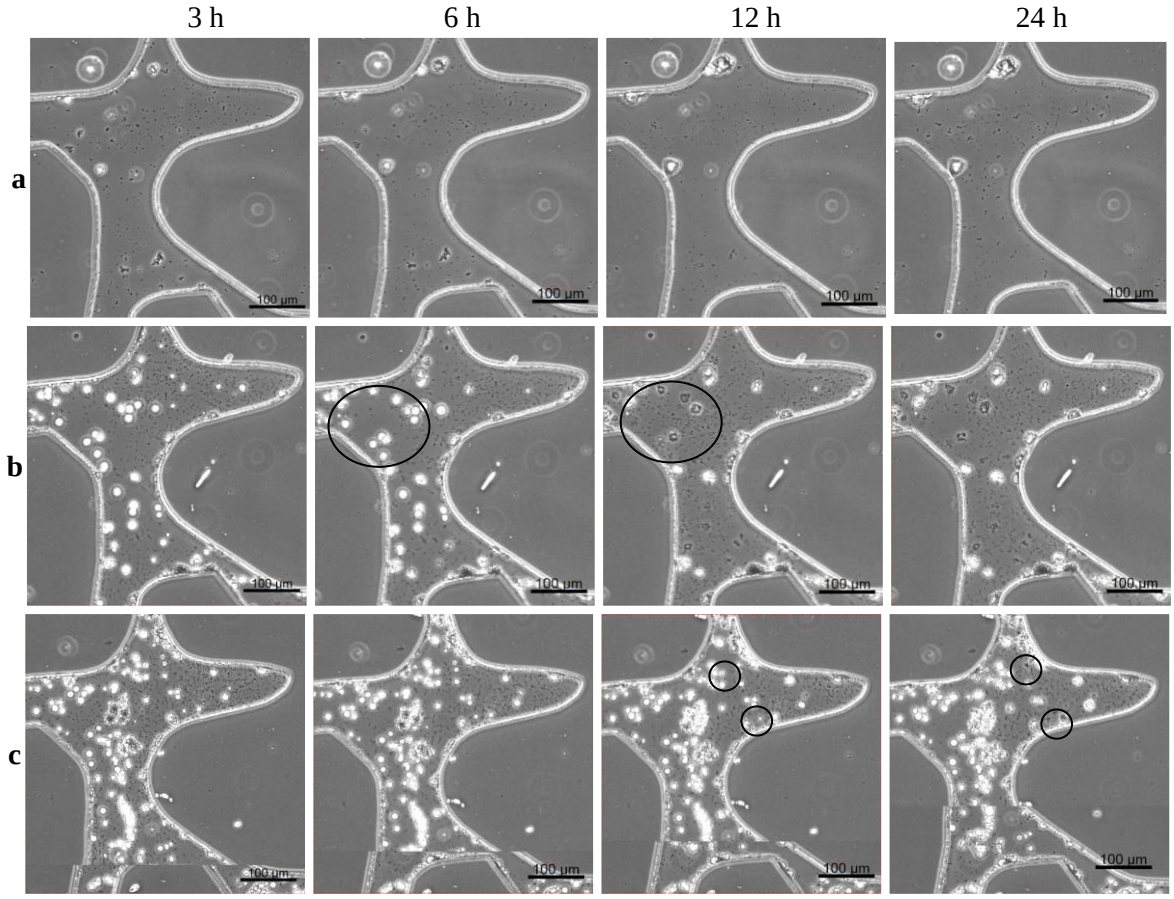

Figure 6.8 Microscope images captured at 3 h, 6 h, 12 h and 24 h after the first injection of cementation solution in the three protocols in which the bacterial densities used were 0.5×10^{8} cells per ml **(a)**, 2.0×10^{8} cells per ml **(b)**, or 5.2×10^{8} cells per ml **(c)**

As reviewed in *Section 2.2.2*, many studies have found that during the reaction between $CaCl_2$ and Na_2CO_3 in aqueous solutions, the $CaCO_3$ precipitation process tends to follow Ostwald's step rule (Kawano et al., 2002; Wei et al., 2003; Rodriguez-Blanco et al., 2011). A diagram illustrating the relationship between precipitation-dissolution, phase transformation and the initial supersaturation state associated with this process is shown in **Figure 6.9**. The

equilibrium $CaCO_3$ solubility products of amorphous $CaCO_3$, vaterite and calcite at 25°C are $10^{-6.4}$, $10^{-7.91}$, and $10^{-8.48}$ M^2, respectively (Plummer and Busenberg, 1982; Brečevic and Nielsen, 1990). This means that, assuming the concentration of Ca^{2+} is 1 M, the formation of these types of $CaCO_3$ requires local concentrations of CO_3^{2-} to be higher than $10^{-6.4}$, $10^{-7.91}$, and $10^{-8.48}$ M to achieve the supersaturation states (based on *Equation 2.5* in *Chapter 2*), which are above the red, blue and black lines in **Figure 6.9**, respectively.

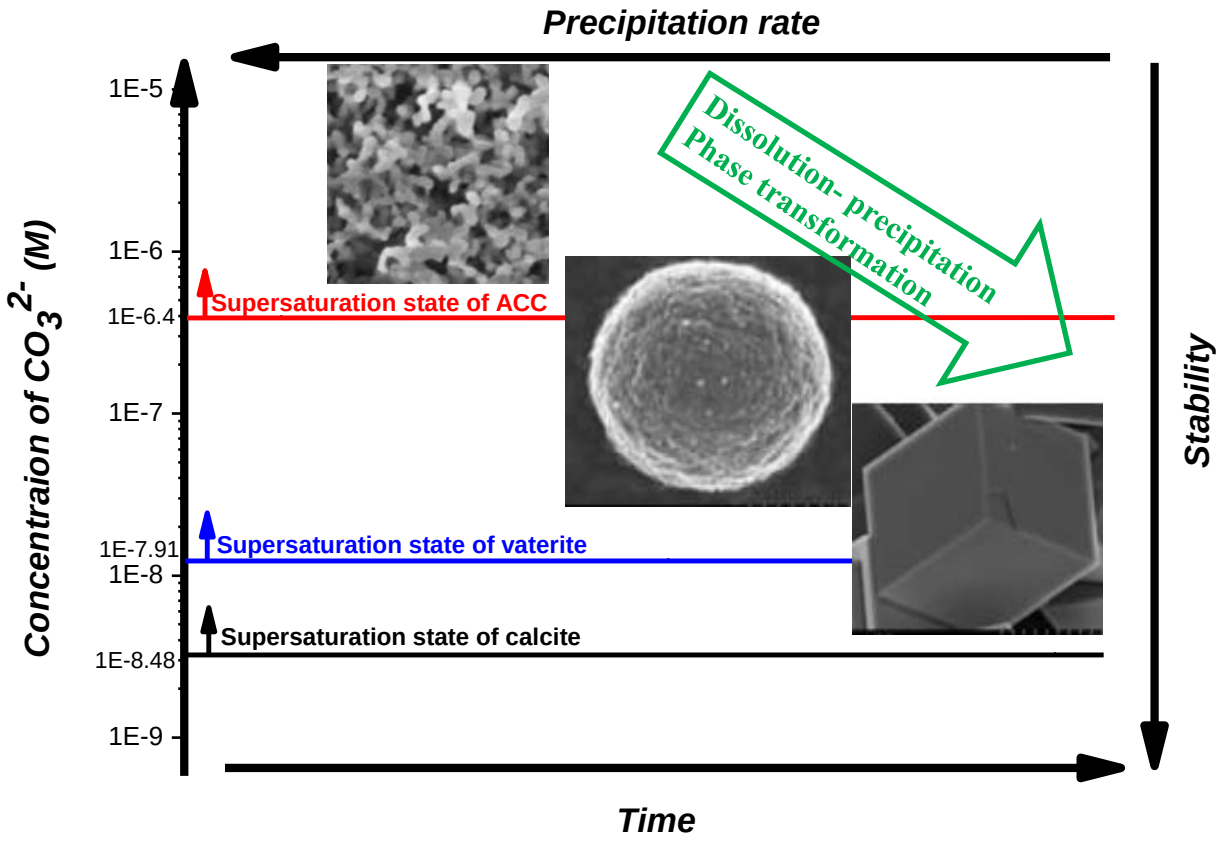

Figure 6.9 Scheme illustrating the precipitation-dissolution and phase transformation, assuming the concentration of Ca^{2+} is constantly 1.0 M

During the MICP process, Ca^{2+} ions are normally present at concentrations in the range of 0.1 M-1.5 M (Whiffin et al., 2007; van Paassen et al., 2010; Al Qabany and Soga, 2013; Cheng et al., 2017) from the beginning of $CaCO_3$ precipitation process, whereas the initial concentration of CO_3^{2-} is zero. The concentration of CO_3^{2-} only starts increasing after ureolysis occurs.

Therefore, the MICP process is affected by the balance between the ureolysis rate and precipitation rate.

When the bacterial density is low, which causes the rate of urea hydrolysis to be low, the amount of CO_3^{2-} hydrolysed from urea increases slowly up to the black line in **Figure 6.9**, after which calcite starts forming. With the formation of more and more CO_3^{2-}, the calcite crystals continued growing. This might explain the case shown in the first row of **Figure 6.6** and **Figure 6.8**, where when the bacterial density was low (5×10^7cells per ml), stable $CaCO_3$ crystals formed slowly with during the MICP process.

When the bacterial density is higher, the overall rate of urea hydrolysis is higher, resulting in more urea being hydrolysed into CO_3^{2-} over the same period of time. When the rate of CO_3^{2-} production is higher than the precipitation rate of calcite, the concentration of CO_3^{2-} in the system accumulates until the concentration of CO_3^{2-} exceeds the threshold denoted by the blue line in **Figure 6.9**, after which vaterite can form as well. When the concentration of CO_3^{2-} is between $10^{-8.48}$ and 2.5×10^{-8} M in the case when the concentration of Ca^{2+} is 1 M based on **Figure 2.7**, the precipitation rate of calcite is higher than that of vaterite; when the concentration of CO_3^{2-} is higher than 2.5×10^{-8} M (in the case when the concentration of Ca^{2+} is 1 M), the precipitation rate of vaterite is higher than that of calcite. Therefore, there would be a combination growth of calcite and vaterite until the concentrations of CO_3^{2-} and Ca^{2+} drop below the blue line, at which point vaterite starts dissolving while calcite can still precipitate. As the precipitation –dissolution –re-precipitation process progresses, the stability of $CaCO_3$ crystals increases. This might explain the case shown in the second row of **Figure 6.6** and **Figure 6.8**, where when the bacterial density was medium (2×10^8 cells per ml), both stable and unstable $CaCO_3$ crystals and the unstable form of $CaCO_3$ crystals form and growth at the beginning of the precipitation process, until around 6 hours, after which the unstable $CaCO_3$ crystals dissolved whilst the stable form of $CaCO_3$ crystals can still grow.

Similarly, if the rate of CO_3^{2-} production is higher than the precipitation rate of vaterite, the concentration of CO_3^{2-} in the system accumulates until it exceeds the threshold denoted by the red line in **Figure 6.9**, after which ACC can form. Subsequently, the dissolution-reprecipitation process was governed by the concentration of CO_3^{2-} in the system according to

the same process as described above. This might explain the case shown in the third row of **Figure 6.6** and **Figure 6.8**, as well as the results shown in *Chapter 5*, where irregular-shaped $CaCO_3$ formed first, but later on transformed into more stable phases. The relative abundance of each $CaCO_3$ crystal phase varies depending on how fast the ureolysis rate is relative to the precipitation rate. The higher the ureolysis rate, the higher the likelihood that a greater number of less stable $CaCO_3$ crystals can precipitate. This is the case shown in the third row of **Figure 6.8**.

To further explore the reason behind the dissolution, microscope images taken 0, 3, 6, 12 and 24 hours after the completion of the second injection of cementation solution in the three protocols containing low, medium and high bacterial concentrations are shown in **Figure 6.10**. As predicted, in the protocol containing low bacterial density, the crystals which formed after the first injection of cementation solution continued growing after the second injection of cementation solution (**Figure 6.10b)**. In addition, new crystals formed during the 24-hour injection interval, shown by the arrows in **Figure 6.10a**. Existing crystals formed after the first injection of cementation solution and new crystals which were formed after the second injection of cementation solution continued growing during the 24-hour period, whilst no crystals dissolved during this time period.

When a medium bacterial density was used, as expected, the formation and dissolution of unstable crystals was observed after the second injection of cementation solution during the 24 hours injection interval (**Figure 6.10b)**. However, the pattern of crystal formation/dissolution in Protocol 3 (**Figure 6.10b)** was very different to the pattern observed in Protocol 1 (**Figure 6.10a)**. In the medium bacterial density (2.0×10^{8} cells per ml) protocol, a considerably large proportion of the small crystals formed a continuous coating on the surfaces of the microfluidic chip after the second injection of cementation solution. Small crystals continued growing after being formed until around 3 hours, as shown by the increase in the intensity of the images. Small crystals were not stable and dissolved, as shown by their dissolution at 6 hours. By 12 hours after the second injection of cementation solution, the newly formed crystals, which were relatively unstable, disappeared. By 24 hours, most of the crystals which remained were larger

crystals which were formed after the first injection of cementation solution. These results are consistent with the results obtained in *Chapter 5*.

Using the high bacterial density protocol (5.2×10^8 cells per ml), small crystals, which look the same as those which formed when a medium bacterial density was used, were also observed after the second injection of cementation solution, but unlike in medium bacterial density protocol, these crystals did not dissolve by 24 hours (**Figure 6.10c)**. Nevertheless, the trend that unstable crystals do not dissolve within 24 hours after the second injection of cementation solution was the same as the trend in crystal dissolution after the first injection.

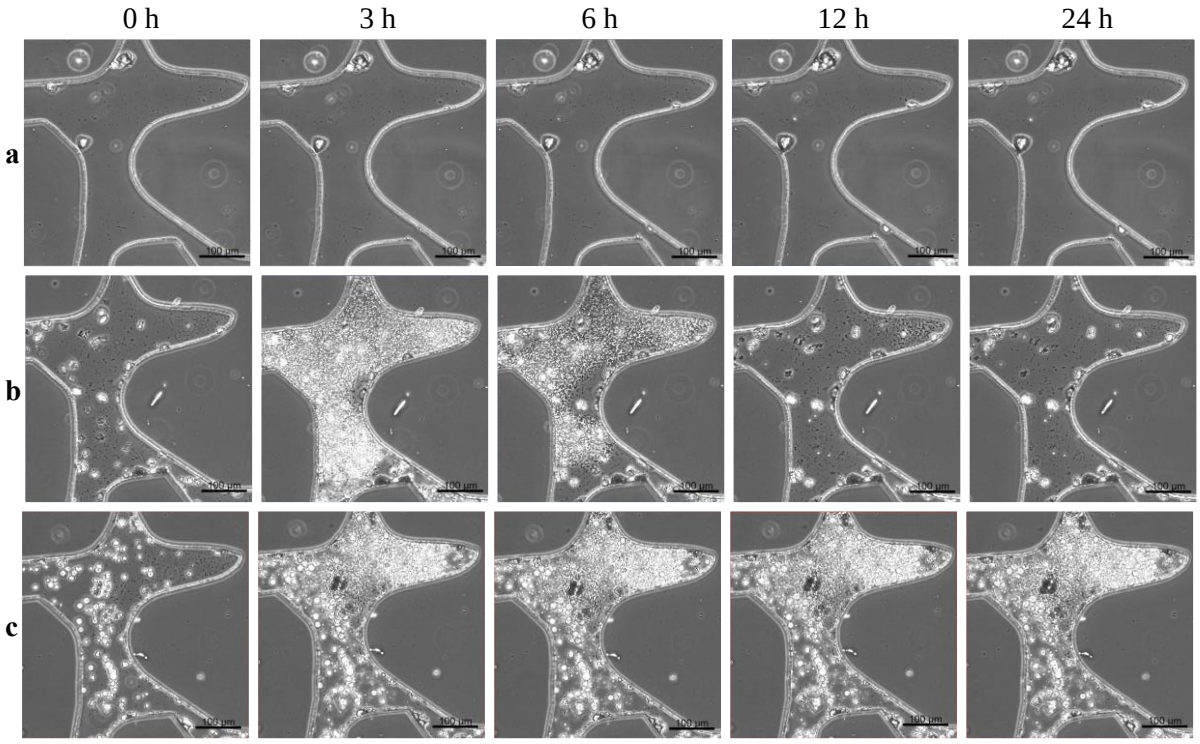

Figure 6.10 Microscope images captured at 0 h, 3 h, 6 h, 12 h and 24 h after the second injection of cementation solution in protocols involving bacterial densities of 0.5×10^8 cells per ml **(a)**, 2.0×10^8 cells per ml **(b)**, or 5.2×10^8 cells per ml **(c)**

These observations are to some extent consistent with the explanations related to the effects of bacterial density on the crystal solubility described previously. However, unlike after the first injection of cementation solution, a larger amount of small unstable crystals coated the inner surface of the microfluidic chip after the second injection. The surfaces of the microfluidic

channels were treated to be negatively charged, which might adsorb some Ca^{2+} cations after the injections of cementation solution and hence contribute to $CaCO_3$ crystal nucleation on the surface of the porous medium. In addition, the surfaces of bacterial cell walls and calcite crystals are also negatively charged, which might adsorb Ca^{2+} cations as well. Compared to the number of bacteria present after the first injection of cementation solution, fewer bacterial cells were present inside the porous medium after the second injection of cementation solution, therefore contributing less to the adsorption of Ca^{2+}, which might consequently cause more Ca^{2+} to be adsorbed to the surface of the porous medium. However, the nucleation of $CaCO_3$ itself is a very complex process which is affected by many factors and is so far largely unknown (De Yoreo et al., 2015).

As was found in *Chapter 4* the bacterial density in the microfluidic chip progressively decreased with each subsequent injection of cementation solution that was performed. Based on this observation, it can be predicted that as the number of injections increases, the ureolysis rate decreases. Therefore, the use of a low bacterial density and a 24-hour interval between injections might not be suitable for fully transforming the injected chemicals into crystals. However, as the injection interval in this experiment was kept constant at 24 hours, this may result in a decrease in crystal growth rate with each subsequent injection. On the other hand, if using the protocol with a high bacterial density, the ureolysis rate may decrease to a point where more stable crystals start forming and unstable crystals dissolve at the expense of the growth of more stable crystals. To test whether these scenarios were indeed the case, microscope images during the three protocols taken after the 3rd, 6th, 9th and 12th injections of cementation solution are shown in **Figure 6.11**.

It is shown in **Figure 6.11a** that the crystals which formed in the low bacterial density protocol after the 3rd to 12th injections of cementation solution were stable, which is consistent with the observations obtained after the first and second injections of cementation solution. In addition, this was also consistent with the prediction that a decrease in bacterial density may cause rate of crystal growth to decrease. It is shown in **Figure 6.11c** that by the 6th injection of cementation solution, dissolution of the unstable crystals can be observed, and after 9th injection of cementation solution, the crystals which remained were relative large and stable.

The tendency for relatively unstable crystals to dissolve after the 3rd to the 12th injections of cementation solution when higher bacterial densities are used being slower was the same as the events observed after the first and second injections of cementation solution.

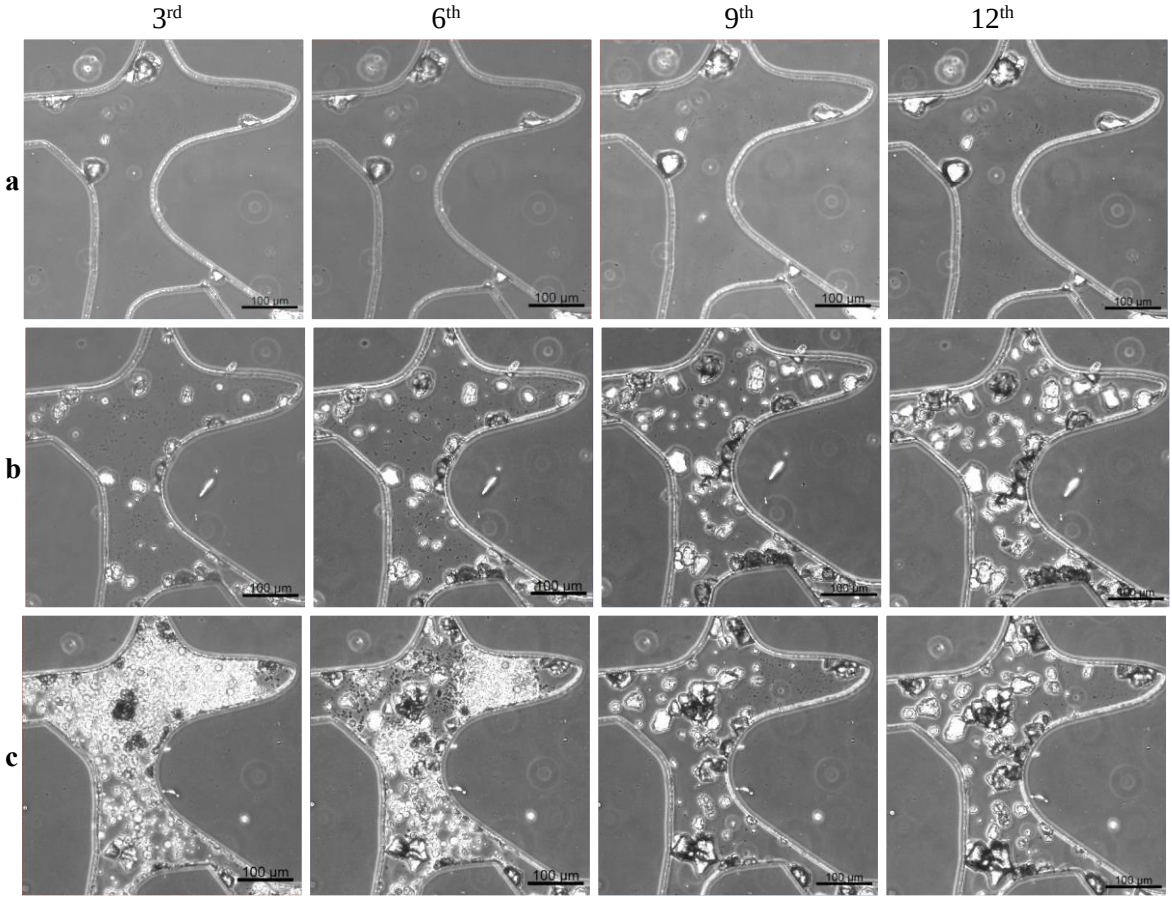

Figure 6.11 Microscope images during three protocols captured after the 3rd, 6th, 9th and 12th injections of cementation solution. The bacterial densities in the protocols were **(a)** 0.5×10^8 cells per ml, **(b)** 2.0×10^8 cells per ml, and **(c)** 5.2×10^8 cells per ml

6.3.6 Effect of bacterial density on crystal number

It is shown in **Figure 6.3**, **Figure 6.4**, **Figure 6.6** and **Figure 6.8** that bacterial density had an effect on the concentration of $CaCO_3$ crystals (i.e. the number of $CaCO_3$ crystals formed per unit volume (per ml)). The quantification of crystal concentration at different time points in the three protocols where the bacterial density varied is shown in **Figure 6.12**. In the protocol involving the lowest bacterial density, the crystal concentration increased with time to about 1-2 $\times$ 10^6 per ml during the initial stages after the injection of cementation solution. Together

with the images shown in **Figure 6.4**, the results of this experiment suggest that the time taken for the crystal number to reach a plateau was less than 0.5 hours. In the protocol involving the use of a medium bacterial density, the number of crystals increased with time until about 2 hours, and then decreased with time until about 10 hours. The highest crystal concentration was about 1.4×10^7 per ml, and the concentration of stabilised crystals was about 7×10^6 per ml. In the protocol which contained the highest concentration of bacteria, the crystal concentration increased with time until about 2 hours, after which the concentration remained relatively constant. The concentration of crystals in this case was about 2.1×10^7 per ml between 2 to 24 hours. As previously discussed, dissolution of unstable crystals also occurred in this case, and the time taken for the crystal number to reach a stabilised plateau should be higher than 24 hours. However, because the interval between injections was kept constant at 24 hours in this experiment, the time for the crystals to transform into more stable crystals after the first injection of cementation solution was not investigated in this case. However, in general, this experiment suggests that the higher the bacterial density, the higher the number of crystals which formed, and as the crystal formed are not stable when the bacterial density is high, the time required for crystal number to reach a plateau increases with bacterial density.

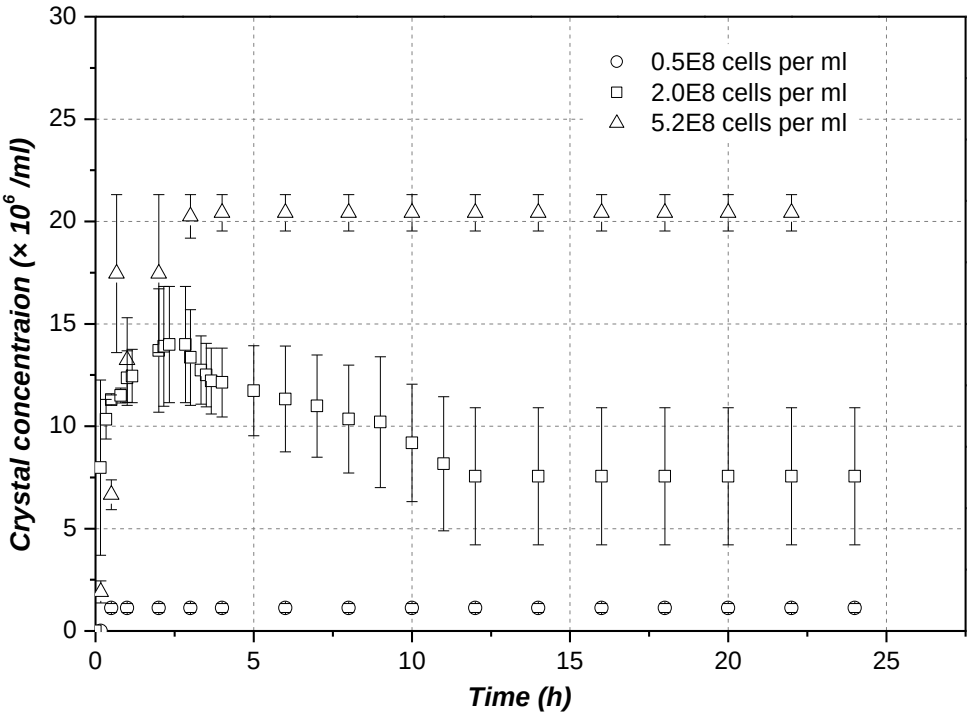

Figure 6.12 Scatter plot showing the change in the concentration of $CaCO_3$ crystals with time

6.3.7 Effect of bacterial density on crystal morphology

As described in the previous sections of this Chapter, bacterial density has an effect on $CaCO_3$ morphology. More stable crystals tend to form when the bacterial density is lower. In this thesis study, when the bacterial density was low (0.5×10^8 cells per ml), the crystals present 24 hours after the injection of cementation solution were mainly prismatic, suggesting that the crystals might be calcite (Al Qabany et al. 2012; Zhao et al. 2014). These crystals continued growing during the intervals between injections, and the size of these crystals increased with each subsequent injection. They did not dissolve during the whole MICP process.

When the bacterial density was 2×10^8 cells per ml, the crystals formed at the beginning of each of the first few injections of cementation solution were mainly spherical, which is consistent with the shape of vaterite (van Paassen, 2009; Al Qabany et al., 2012; Zhao et al., 2014). However, more stable crystal types were also observed in this protocol after each of the injections, and more stable crystals continued growing even after the unstable crystals started to dissolve. The solubility and the shapes of these crystals are consistent with those of calcite and vaterite.

When the bacterial density was high (5×10^8 cells per ml), bacterial aggregates formed after the first injection of cementation solution and irregular-shaped crystals formed on top of them (**Figure 6.8c**). This observation is consistent with the observations obtained in *Chapter 5*. Concomitantly, spherical crystals were also observed. Even though these two forms of $CaCO_3$ precipitates remained present after several initial injections of cementation solution (**Figure 6.8c**, **Figure 6.10c and Figure 6.11c**), they were eventually replaced by the more stable form of $CaCO_3$ crystals. The stability and shapes of these forms of $CaCO_3$ suggests that when bacterial density is high, the formation of $CaCO_3$ follows the ACC-vaterite-calcite sequence described in *Chapter 5*.

Using the high bacterial density protocol, bacterial aggregates were observed after the first injection of cementation solution, as shown in **Figure 6.13a**. In the same spot, crystal aggregates were observed after the 12^{th} injection of cementation solution, as shown in **Figure 6.13b**.

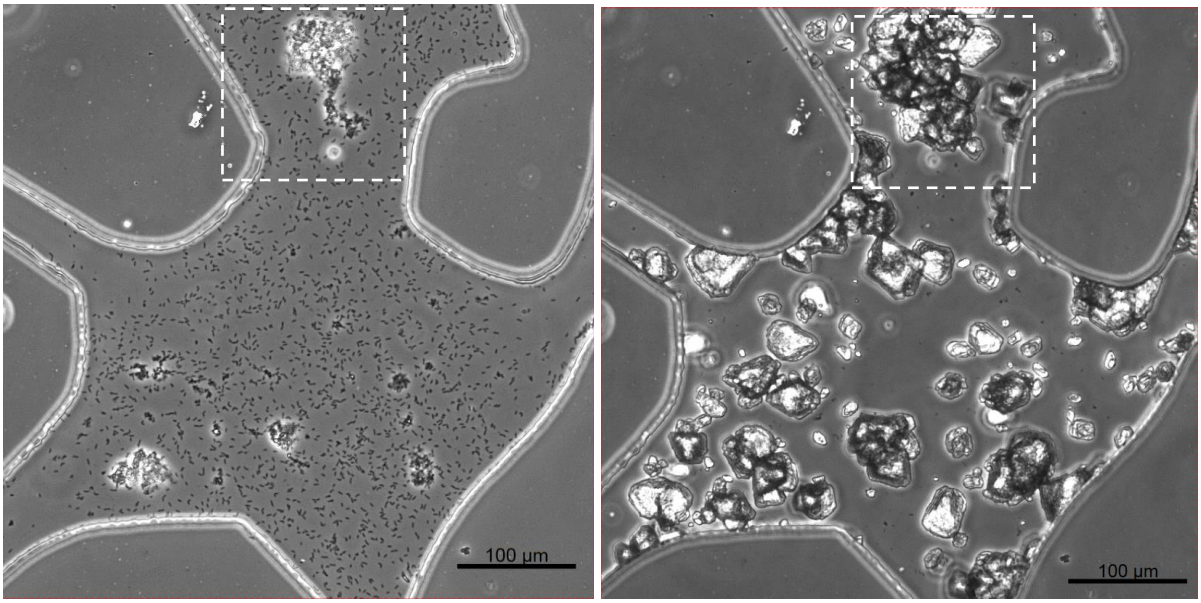

(a) **(b)**

Figure 6.13 Bacterial aggregates formed after the first injection of cementation solution **(a)**; crystal aggregates formed 24 hours after the 12th injection of cementation solution **(b)**.

To observe the effect of bacterial aggregates on the formation of $CaCO_3$ crystals in more detail, magnified images of the squares in **Figure 6.13** taken 0, 20 min, 1 h and 1 day after the first injection of cementation solution are shown in **Figure 6.14a**, and images taken 24 hours after the 2nd, 3rd, 5th and 7th injections of cementation solution are shown in **Figure 6.14b**. After the first injection of cementation solution, bacteria aggregated and irregular-shaped $CaCO_3$ crystals formed on the bacterial aggregate (**Figure 6.14a**, 0 min image). The bacterial aggregate continued growing, shown by the increase in image intensity at 20 min compared with 0 min (**Figure 6.14 a**, 20 min image). At 20 mins, however, spherical crystals formed on the bacterial aggregates (**Figure 6.14a**, 20 min image). The spherical crystals continued growing in size during the first hour after injection (**Figure 6.14a**, 1 h image). In addition, more spherical crystals also formed, but not on the bacterial aggregates (**Figure 6.14a**, 1 h image). The spherical crystals were not stable and some dissolved by 24 hours after injection (**Figure 6.14 a**, 1 d image). During the following injections from the 2nd to the 7th, even though more unstable crystals appeared and disappeared, the crystals which were formed on the bacterial aggregates continued growing. Because the crystals are so close to each other, they merged into one large crystal aggregate as they grew (**Figure 6.14b**, 7th injection image).

Crystal aggregates have been observed in many MICP studies (van Paassen, 2009; Cheng et al., 2017). This experiment suggests that the crystal aggregates may have formed due to crystal nucleation points being close to each other, and as the crystals grew, they merged into one big aggregate. As the number of bacteria has an effect on the number of nucleation sites, more crystals formed when more bacterial cells were present in a given volume. Therefore, the crystals are more likely to be located closer to each other. In addition, because bacterial aggregates contain a high density of bacterial cells, the likelihood of crystals growing on or surrounding them may also be higher than for single bacterial cells. In this particular case, the crystal aggregates present within the pores occurred at a similar location to the bacterial aggregates.

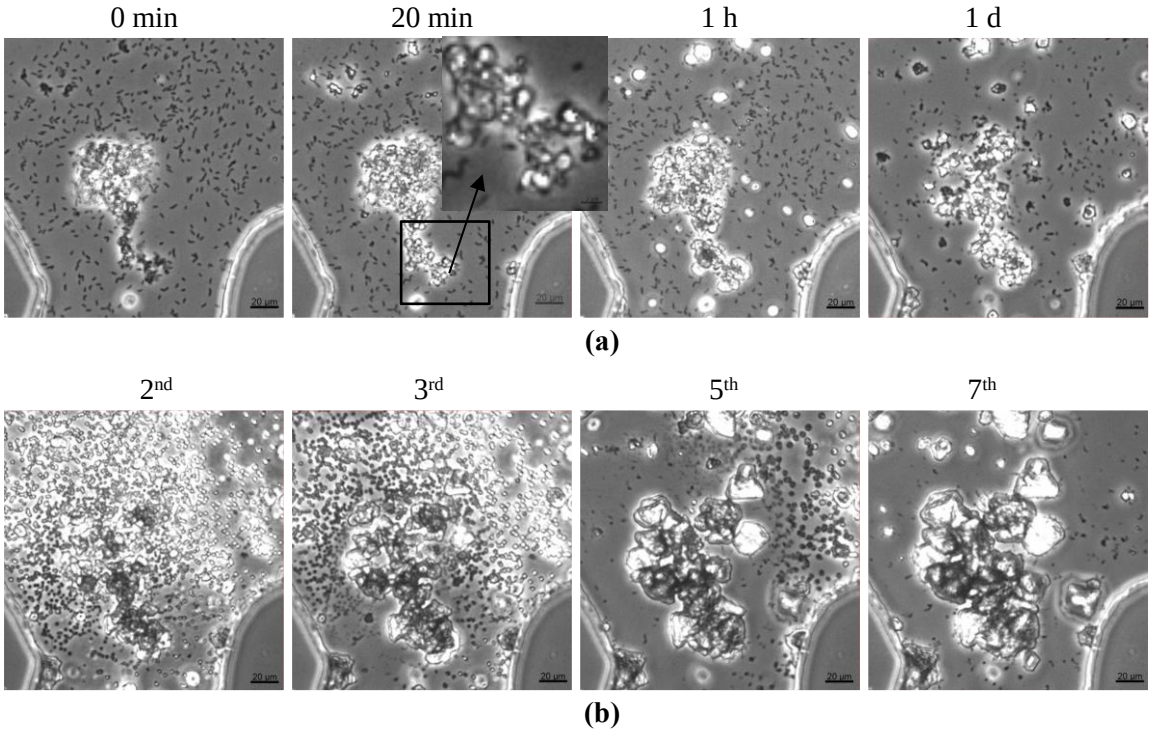

Figure 6.14 Magnified images of the squares in Figure 6.13 taken at **(a)** 0 min, 10 min, 20 min, 1 hr, 1 day after the 1st injection of cementation; **(b)** at 24 hours after the 2nd, 3rd, 5th and 7th injections of cementation solution

6.4 Conclusions

Microfluidic chip experiments were conducted in this study to investigate the effects of bacterial density on the kinetics and characteristics of $CaCO_3$ formation during MICP. The main findings of the study are summarised as follows.

In addition to affecting the rate of ureolysis, bacterial density also affected the overall precipitation rate, with the time required for $CaCO_3$ precipitation to complete decreasing as the bacterial density was increased, provided that the same bacterial strain was used and the bacterial density was less than 4×10^8 cells per ml. Therefore, the use of higher bacterial densities makes the MICP treatment protocol more time-efficient.

However, in addition to affecting the precipitation rate, bacterial density also affected the characteristics of $CaCO_3$ crystals. Bacterial density affected crystal density (the number of crystals formed within a given volume), with a higher bacterial concentration resulting in a larger number of crystals being formed in the same volume. Therefore, when crystals are given enough time to grow and when the bacterial activity and the concentration and volume of the injected cementation solution are kept constant, a lower bacterial density produces fewer but larger crystals and vice versa. This suggests that a lower bacterial density could be useful for treating sand containing large particles, which has so far been a challenge for MICP applications. Assuming two types of sand have the same particle shape, surface properties, and packing level, larger sand particles would result in a smaller number of particle contacts but with larger gaps between the particles. Therefore, fewer but larger $CaCO_3$ crystals would be required to bond the soil particles together in this case. However, it should be noted that when the bacterial density is low, maintaining bacterial activity might be a problem. For example, as shown in **Figure 6.11a,** crystal size did not increase from the 9^{th} to the 12^{th} injection of cementation solution, which might be because the bacterial activity was not high enough to maintain the precipitation.

In addition, the crystals which formed when the bacterial density was low were more stable, continued growing after being formed and did not dissolve. However, when the bacterial density was higher, less stable crystals formed first, followed by the formation of more stable crystals at the expense of growth of less stable crystals. The higher the bacterial density, the longer the less stable crystals remained before dissolving. Based on solubility and density, calcite is the most stable form of $CaCO_3$ both physically and chemically, and it has been suggested that the precipitation of calcite is preferred for a permanent stable cementation (van Paassen, 2009). Therefore, when designing an MICP treatment protocol, the effect of bacterial density on the phase transformation and the time required for the crystals to become stable need to be considered.

Furthermore, bacterial density affects the formation of bacterial aggregates after the injection of cementation solution, which in turn affects the formation of crystal aggregates. As bacterial aggregates are notably larger compared with individual bacteria, bacterial aggregates might be less likely to become homogenously distributed within the soil matrix, especially when they are large enough to clog the pores which prevents the transport of other bacteria and bacterial aggregates with flow. As the formation of crystal aggregates is affected by bacterial aggregates, a non-homogenous distribution of bacteria within a soil matrix also results in a non-homogenous distribution of $CaCO_3$. Further work would be useful to investigate the effect of bacterial density on the distribution of bacteria and the resulting effect this has on the distribution of $CaCO_3$ content.

Chapter 7 Enhancing strength of MICP-treated sandy soils: from micro to macro

7.1 Research aims

In the tests described in *Chapter 5*, unstable $CaCO_3$ crystals dissolved at the expense of the growth of more stable crystals after the first and second injections of cementation solution. The crystals that appeared three hours after the second injection of cementation solution were predominantly large crystals, with some small crystals also being observed. However, all the small crystals disappeared, and only large crystals remained 24 hours after the second injection of cementation solution. Therefore, even though the total $CaCO_3$ content between three hours and 24 hours was the same, the distribution of crystal sizes was different between these two time points.

In the study described in this chapter, micro-scale experiments were conducted by using microfluidic chips to observe the formation of calcium carbonate crystals with time during a staged-injection MICP process and to investigate the effects of injection intervals on the properties of calcium carbonate crystals. In the first two microfluidic chip experiments, the main variable was injection interval between two successive injections of cementation solution during the treatment procedure, in an attempt to establish a correlation between the $CaCO_3$ precipitation process and the final size of $CaCO_3$ crystals. The third microfluidic chip experiment was conducted to test whether the dissolution of unstable and smaller $CaCO_3$ crystals at an expense of more stable and larger crystals also occurred when the concentration of cementation solution was either 0.5 M or 1.0 M.

Based on the findings from the micro-scale experiments, macro-scale experiments were conducted using sandy soil columns by injecting cementation solution at various concentrations and injection intervals during MICP treatment. The parameters of MICP-treated sandy samples that were evaluated included their compressive strength, $CaCO_3$ content, and the micro-scale properties of $CaCO_3$ after MICP treatment. The objectives of this series of experiments were to investigate (i) the effects of injection interval on the chemical transformation efficiency of MICP and the strength of MICP-treated sand; (ii) the correlation between $CaCO_3$ content and strength of MICP-treated sand; and (iii) the correlation between the micro-scale properties of $CaCO_3$ crystals and the strength of MICP-treated sand.

7.2 Experimental procedures

7.2.1 Micro-scale MICP experiments

Three micro-scale experiments were conducted using microfluidic chips to observe the formation of calcium carbonate crystals over time during a staged-injection MICP processes. The first two experiments were conducted to assess the effects of injection interval on the properties of calcium carbonate crystals. In these two experiments, the staged-injection MICP processes involved a single injection of bacterial suspension followed by twelve injections of cementation solution with an injection interval of either 4 or 24 hours. In experiment 1, cementation solution was injected 2-4 times per day over a total period of 4 days in the experiment involving a short injection interval (4 hours). In experiment 2, the cementation solution was injected only once per day over 12 days in the experiment where the interval between injections was 24 hours. Experiment 3 was conducted to test whether the crystal dissolution observed when the concentration of cementation solution was 0.25 M (*Chapter 5*) could also occur when the concentrations of cementation solution were either 0.5 M or 1.0 M. The parameters of bacteria, bacterial injection, cementation solution and the injection of cementation solution in the three experiments are summarised in **Table 7.1**.

Table 7.1 Parameters of microfluidic chip experiments

Experiment No.		1	2	3	
Microfluidic chip No.		1-3	4-6	7	8
Bacterial suspension and injection	OD_{600}	1.0	1.0	1.0	1.0
	Flow rate (PV/h)	56	56	56	56
	Injection PV	1.25	1.25	1.25	1.25
	Number of injections	12	12	1	1
	Settling duration (h)	18-24		24	24
Cementation solution and injection	Content	0.25 M*	0.25 M*	0.5 M**	1 M ***
	Flow rate (PV/h)	5.6	5.6	5.6	5.6
	Injection PV	1.25	1.25	1.25	1.25
	Number of injections	12	12	2	2
	Injection interval (h)	4	24	24	24
	Number of injections per day	2-4	1	1	1
	Total treatment duration (days)	4	12	2	2

Note: PV-pore volume of the microfluidic chip; *0.25 M $CaCl_2$, 0.375 M urea, and 3 g/L nutrient broth; **0.5 M $CaCl_2$, 0.75 M urea, and 3 g/L nutrient broth; ***1.0 M $CaCl_2$, 1.5 M urea, and 3 g/L nutrient broth

7.2.2 Macro-scale MICP experiments

Six MICP treatment procedures at varied concentrations and injection intervals of cementation solution were applied to eighteen soil columns prepared in syringe tubes. The total amount of cementation solution injected was kept constant in these eighteen columns. The parameters of bacterial suspension, bacterial injection, cementation solution and the injection of cementation solution in this macro-scale experiment are summarised in **Table 7.2**.

After performing MICP treatment, the treated sand samples were flushed with at least two pore volumes of DI water to wash away all excess soluble salts. The sand samples were then dried at 100.5 °C for at least 24 hours. Subsequently, the unconfined compressive strength (UCS) of the treated samples and the total calcium carbonate content present in the MICP-treated soil columns were measured as described in *Section 3.4*. The chemical transformation efficiencies of $CaCO_3$ in these specimens were evaluated based on the relationship between $CaCO_3$ content

and the amount of chemicals injected. It should be noted that the concentration of urea was 1.5 times higher than the concentration of $CaCl_2$, and when evaluating the chemical transformation efficiency, the extra urea that could not transform into $CaCO_3$ was not accounted for. Scanning electron microscopy (SEM) was used to observe the microscale parameters of the calcium carbonate crystals (such as size and distribution) which formed in inside the soil columns. The samples are assumed to be homogeneous from top to bottom and samples for SEM analysis were selected at around the centre of each of the soil columns as representative to examine the micro-scale properties of the whole sample.

Table 7.2 Parameters of macro-scale experiments

		Short interval			Long interval		
Treatment protocol No.		1	2	3	4	5	6
Soil column No.		1~3	4~6	7~9	13~15	10~12	16~18
Bacterial suspension and injection	OD_{600}	1.0	1.0	1.0	1.0	1.0	1.0
	Number of injections	1	1	1	1	1	1
	Injection PV number	1.2	1.2	1.2	1.2	1.2	1.2
	Settling duration (h)	24	24	24	24	24	24
Cementation solution and injection	Concentration (M)	0.25	0.5	1.0	0.25	0.5	1.0
	Number of injections	12	6	3	12	6	3
	Injection interval (h)	12	24	48	24	48	96
	Number of injections per day	2	1	0.5*	1	0.5	0.25
	Total treatment duration (days)	6	6	6	12	12	12

Note: Concentration of cementation solution were indicated by the concentration of $CaCl_2$ in the cementation solution; the concentration of urea is 1.5 times of CaC_2; 3 g/L nutrient broth was contained in the cementation solution; * 0.5 injection per day means 1 injection in two days.

7.3 Results of micro-scale experiments

7.3.1 Short injection interval (4 h) experiment

Images of one pore containing $CaCO_3$ crystals at the centre of microfluidic chip No.1 taken at the completion of the retention period (the time in between two adjacent injections given to the

crystals to grow) of each of the cementation solution injections are shown in **Figure 7.1**. When the injection interval of cementation solution was 4 hours, the crystals continued growing once formed. This observation is quite different from the case of a 24-h injection interval where dissolution of unstable $CaCO_3$ crystals at the expense of more stable crystals after either the first or the second injection of cementation solution (*Chapters 5* and *6*). Taken together, this finding suggests that an injection interval of 4 hours was not long enough for unstable crystals to dissolve.

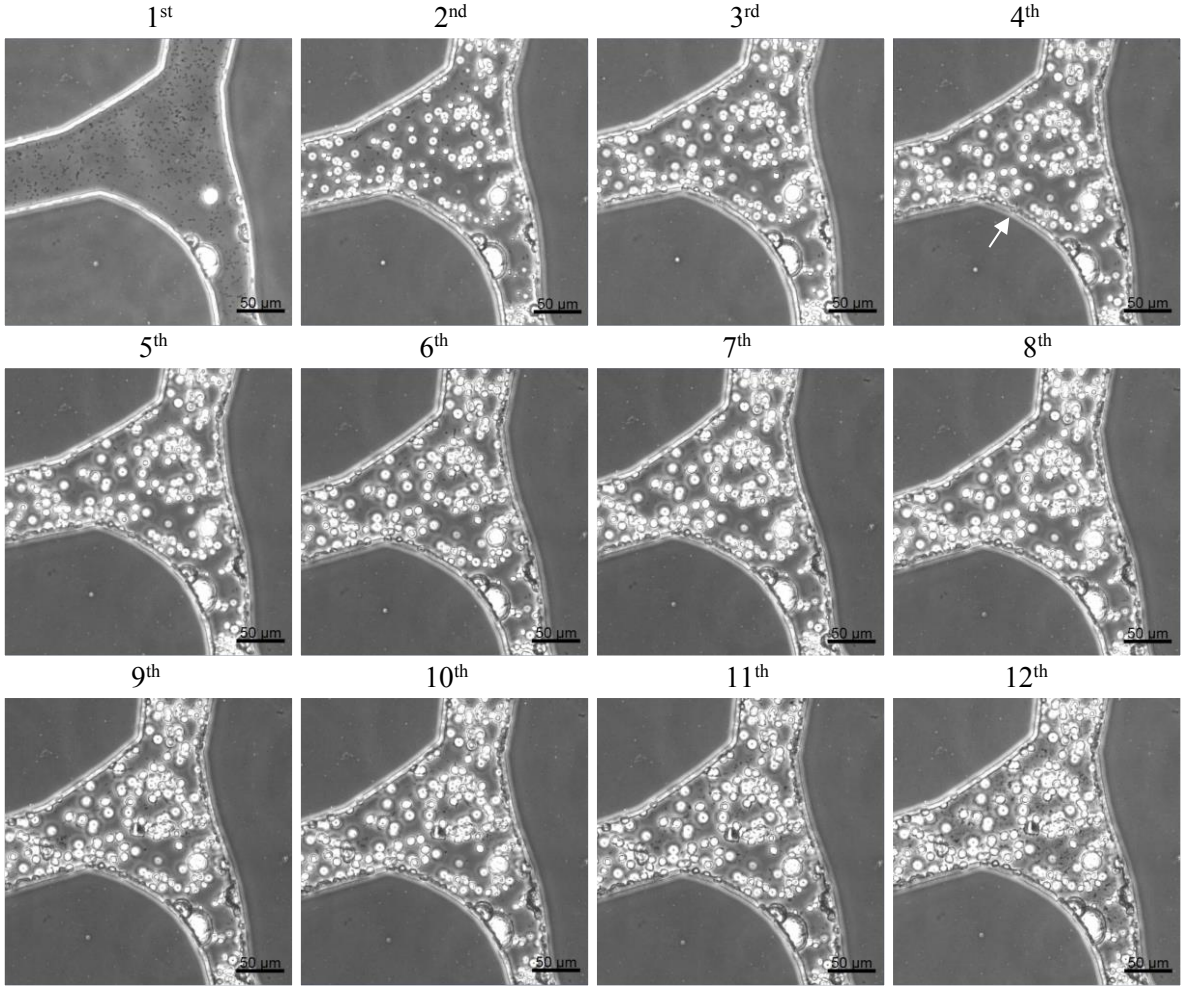

Figure 7.1 Microscope images of the centre pore of microfluidic chip No.1 (4 h injection interval) at the completion of the retention period of all the 12 injections of cementation solution

To quantify the growth of the crystals in the images shown in **Figure 7.1**, the diameters of three randomly selected crystals were measured and the volumes of the crystals were calculated based on their shapes assumed to be half-sphere. The bar chart of the volumes of the three

crystals in the images are presented in **Figure 7.2**. The three crystals selected were also shown in **Figure 7.2**. These three crystals occurred after the second injection of cementation solution. They grew during the twelve injections of cementation solution treatment, while the growth rate over the time frame between the 2nd and the 5th injections was greater than that between the 5th and the 12th injections. The decreasing growing rate of these crystals might be due to the formation of new crystals, which consume the $CaCl_2$ and urea injected. The sizes of the three crystals were between 30 and 60 μm^3 after the second injection of cementation solution, increased by about 4-5 times after the 5th injection of cementation solution, and became between 220 to 350 μm^3 after the 12th injection of cementation solution. The growth rate and the final sizes of the three crystals varied. The growing of the crystals is affected by many factors such as the local concentration of bacterial cells, and the local concentration of urea and $CaCl_2$, which are time dependent and are affected by the existence and growth of the surrounding crystals.

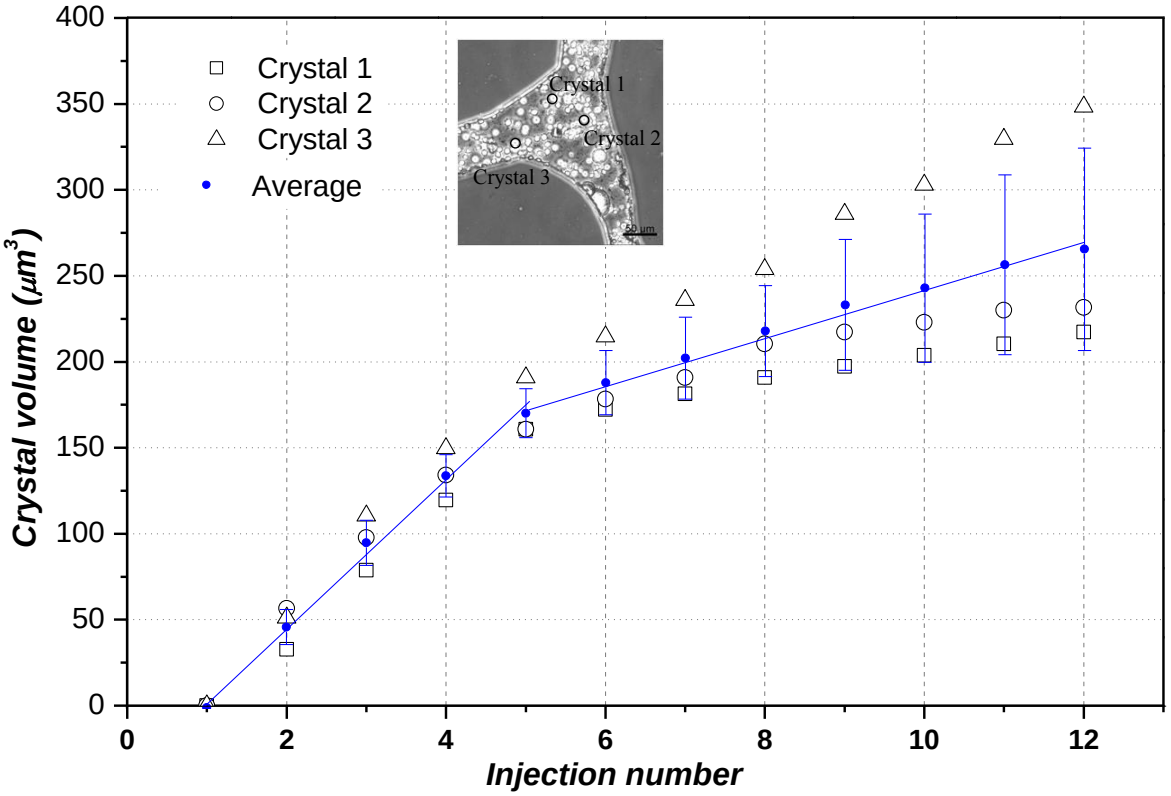

Figure 7.2 Increase in volume of three crystals with injection; the average volume of the three crystals was also plotted with time, and data presented as mean ± standard error

Images of the middle squares with areas of 2 mm by 2 mm of microfluidic chip No. 1, 2 and 3, taken at the completion of the retention time of the last injection of cementation solution are shown in **Figure 7.3a**. Magnified images of the central pores of the squares in the images shown in **Figure 7.3a** are presented in **Figure 7.3b**. The crystals coated the inner surface of the microfluidic chip. The crystals formed after MICP treatment with short injection intervals (4 h) were 5 - 10 μm in size, spherical in shape, with 200 - 1000 crystals being present per 10^6 μm^3. As stated earlier, small crystals remained inside the pores because a 4 -hour retention time was not long enough for small crystals to dissolve. The results of the three parallel samples are consistent with each other, in which the $CaCO_3$ crystals were generally small and coated the surface of the chip, even though the number of crystals in the third sample was less than the number of crystals present in the first two samples.

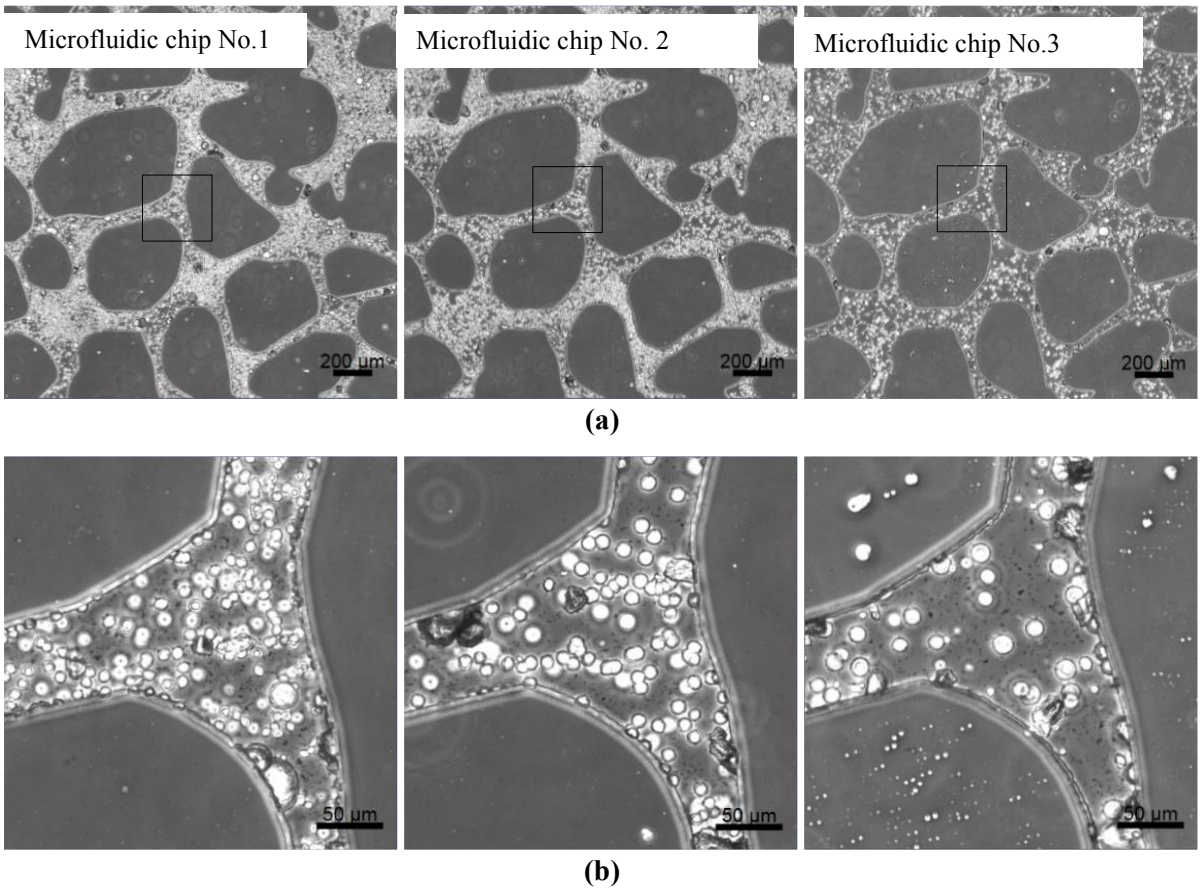

Figure 7.3 Microscope images of microfluidic chip No. 1-3 (4 h injection interval) at the completion of the retention period of the final injection of cementation solution. **(a)** images of the centre 2 mm by 2 mm squares; **(b)** magnified images of pores marked by black squares in (a)

7.3.2 Long injection interval (24 hr) experiment

Images of one pore containing $CaCO_3$ crystals at the centre of microfluidic chip No.4 (long injection interval of 24 hr) taken at the completion of retention period of each of the 12 injections of cementation solution are shown in **Figure 7.4.** Three crystals formed in the pore shown in **Figure 7.4** after the first injection of the cementation and then continued growing after subsequent injections. New crystals were formed after the 4^{th} injection, and the sizes of the new crystals were shown to increase with the injections. At the completion of the retention period (24 hr) of each injection of cementation solution, the crystals formed were larger but fewer in number compared with the crystals formed in the same stage in microfluidic chip No.1 (shown in **Figure 7.1**).

The crystals formed after the first injection of cementation solution in this sample were in the shape of a rhombohedron (**Figure 7.4**), which is consistent with the shape of calcite. However, the morphology of crystals 2 and 3 after the second injection of cementation solution and the morphology of crystal 1 after the sixth injection could not be clearly distinguished. Similar phenomena were observed in a previous study (Mitchell and Ferris, 2006) in which SEM was used to assess crystal morphology. It was found that crystal morphology was not clear, and often appeared poorly ordered, with a stepped surface topography which resulted in somewhat rounded crystal edges (Mitchell and Ferris, 2006). Apart from these three crystals, some other crystals formed between the 6^{th} and 12^{th} injections of cementation solution. The crystals formed during this time period were rhombohedral in shape.

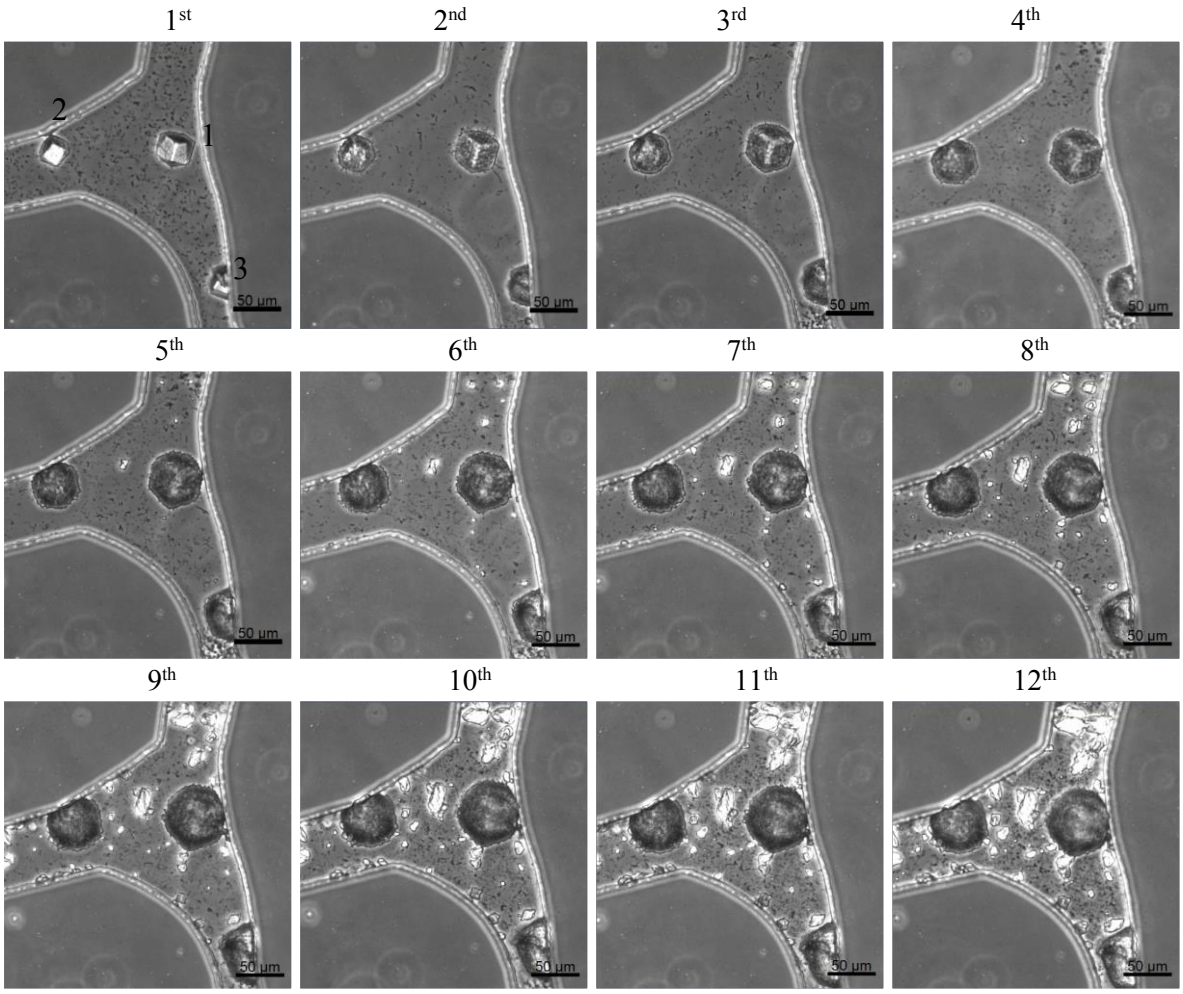

Figure 7.4 Microscope images of the centre pore of sample 1 (24 h injection interval) at the completion of the retention period of each injection of cementation solution

The increase in crystal size with respect to the injection number is presented in **Figure 7.5**. From the first to the 12th injection of cementation solution, the average crystal size increased from about 1 × 10^4 µm^3 to about 5-8 × 10^4 µm^3. The growth rate decreased after about the 6th injection, which is similar as sample 1, and also possibly because the other crystals which formed after the 6th injection of cementation solution also consumed the cementation solution.

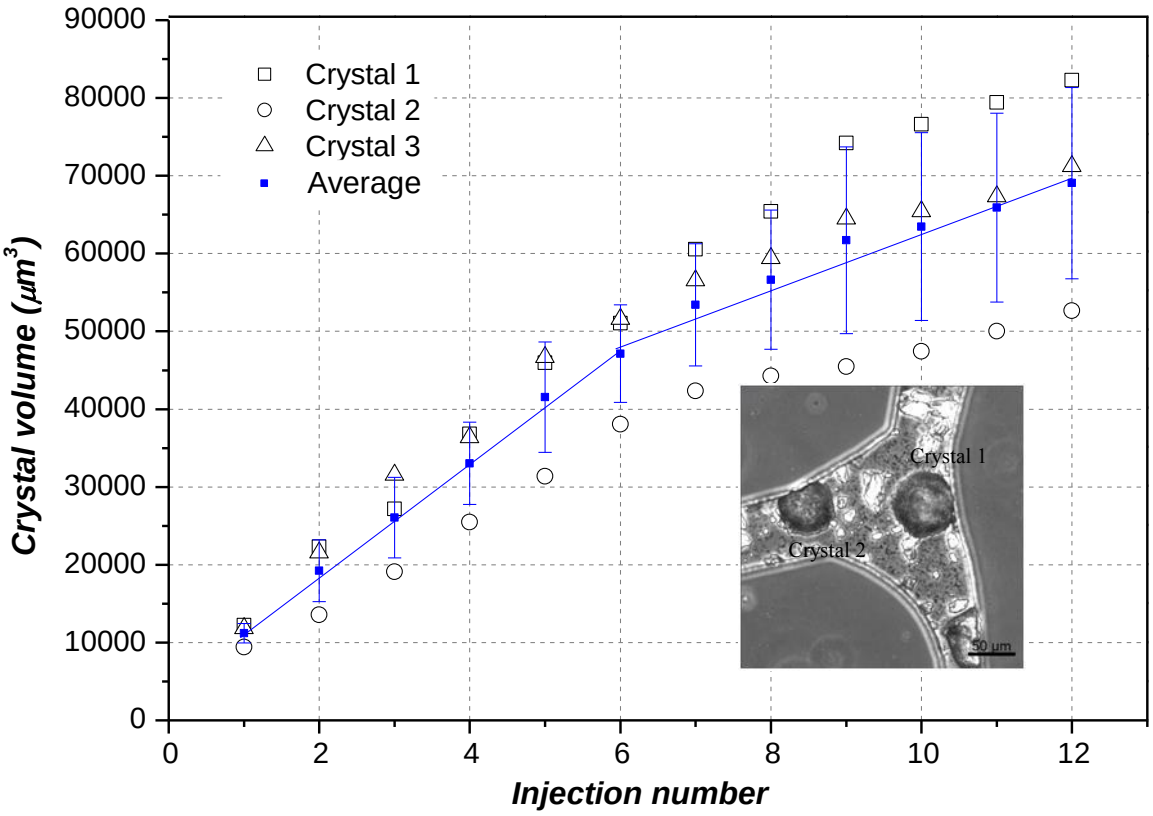

Figure 7.5 Crystal sizes after each injection of cementation solution; the average volume of the three crystals was also plotted with time, and data presented as mean ± standard error

Images of the middle squares with areas of 2 mm by 2 mm of microfluidic chip No. 4 to 6, taken at the completion of the retention time of the last injection of cementation solution are shown in **Figure 7.6a**. Magnified images of the central pores of the squares are shown in **Figure 7.6b**. The sizes of crystals are larger (10 - 80 μm) than those in microfluidic chip No. 1-3 experiment 1. The shapes of the crystals are rhombohedral, which is consistent with the shape of calcite. The number of crystals inside the pores is small (5 - 20 per 10^6 um^3), which is about 40 times smaller than the number of crystals observed in microfluidic chip No. 1-3. Although the number of crystals in the three samples varied, each sample showed a similar trend in crystals size and distribution.

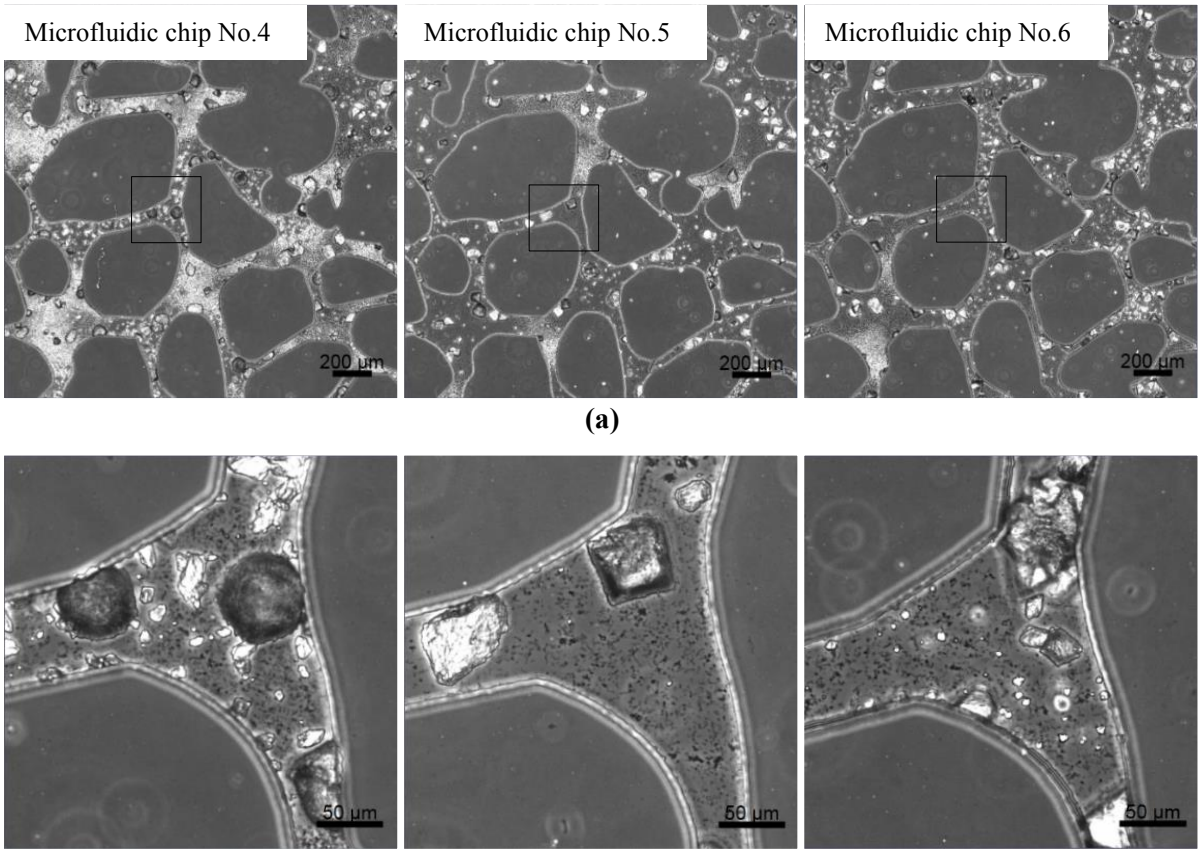

Figure 7.6 Microscope images of microfluidic chip No. 4-6 (24 h injection interval) at the completion of the retention period of the final injection of cementation solution. **(a)** images of the centre 2 mm by 2 mm squares; **(b)** magnified images of the pores marked by black squares in (a).

Consistent with the results shown in *Chapter* 5, unstable $CaCO_3$ crystals dissolved at the expense of the growth of more stable crystals after the second and third injections of cementation solution (**Figure 7.7**). The dissolution of the unstable crystals occurred between the 4^{th} and 24^{th} hour after each of the injections. A 24 -hour retention time resulted in smaller spherical crystals being dissolved, and the dissolved calcium and carbonate ions from the small crystals formed into bigger crystals.

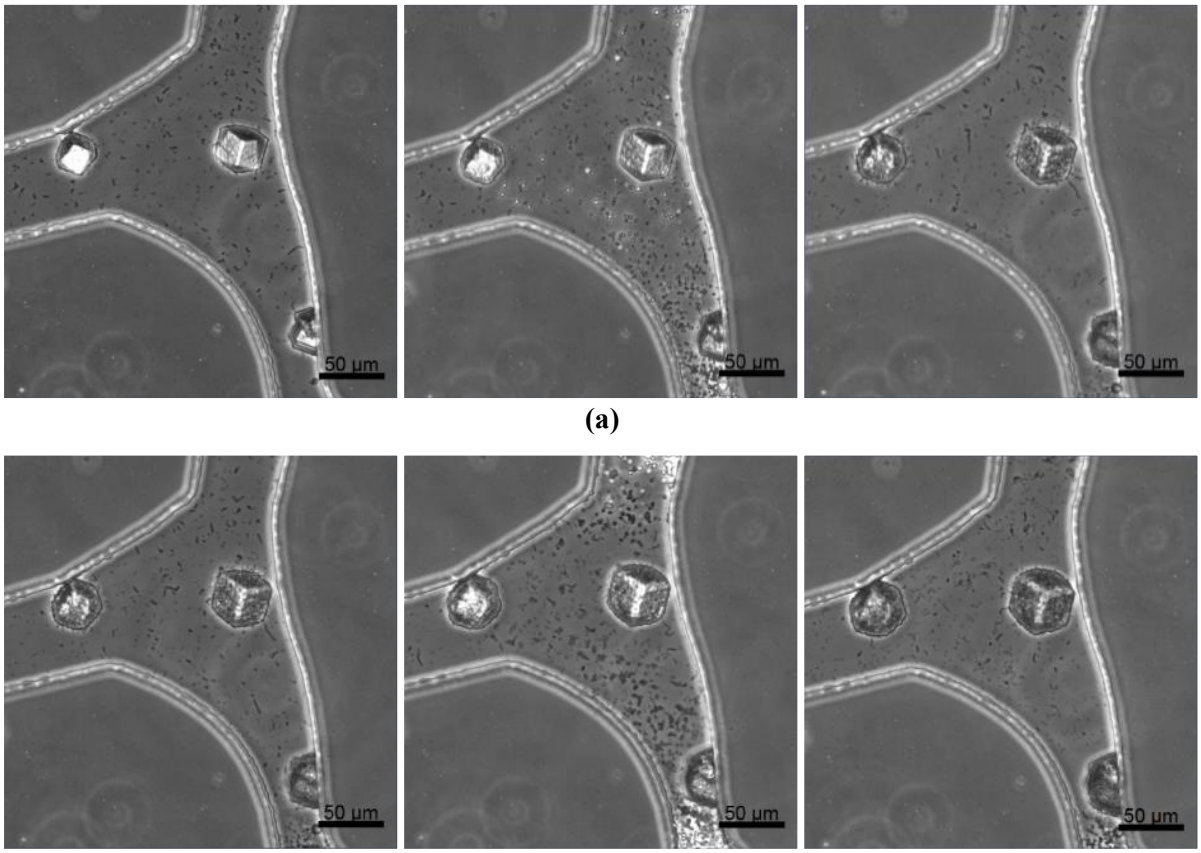

Figure 7.7 Microscope images of microfluidic chip No. 4 (24 h injection interval) at 0, 4, and 24 h after the second **(a)** and third **(b)** injection of cementation solution.

Al Qabany et al. (2012) concluded that the size of $CaCO_3$ crystals formed was smaller when soil samples were treated more frequently with a lower concentration of cementation solution compared with soil samples that were treated less frequently with a higher concentration of cementation solution. In light of this finding, the results presented in this thesis suggest that when the concentration of cementation solution is constant, the treatment frequency or injection interval also affect the final size of the crystals. In this sense, longer injection intervals (24 hours), compared with 4 hours, result in larger crystals being formed. Because crystal size may affect engineering properties such as strength, this might be the reason why the strength of the MICP-treated samples varied when the properties and the $CaCO_3$ content of the treated soils were the same. Additionally, previous research suggests that the formation of stable $CaCO_3$ crystals is important for improving the stability of MICP-treated soils (van Paassen, 2009).

Therefore, based on these results, a long injection interval (24 hours) might be better compared with a shorter injection interval (4 hours).

7.3.3 Effect of higher concentrations of cementation solution (0.5 M and 1.0 M)

Concentrations of cementation solution that have been normally used are between 0.25 M and 1.0 M. Another microfluidic chip experiment (Experiment 3) was conducted to investigate whether the dissolution of smaller or relatively unstable crystals occurs as an expense of larger or more stable crystals when the concentration of cementation solution is 0.5 M or 1.0 M. Microscope images of 250 μm by 250 μm squares at 1, 3, 6 and 24 hours after the completion of the second injection of cementation solution with a concentration of 0.5 M are shown in **Figure 7.8**. Similar to what was observed when the concentration of cementation solution is 0.25 M, small crystals also formed after the second injection of cementation solution and subsequently dissolved to then be replaced by larger crystals.

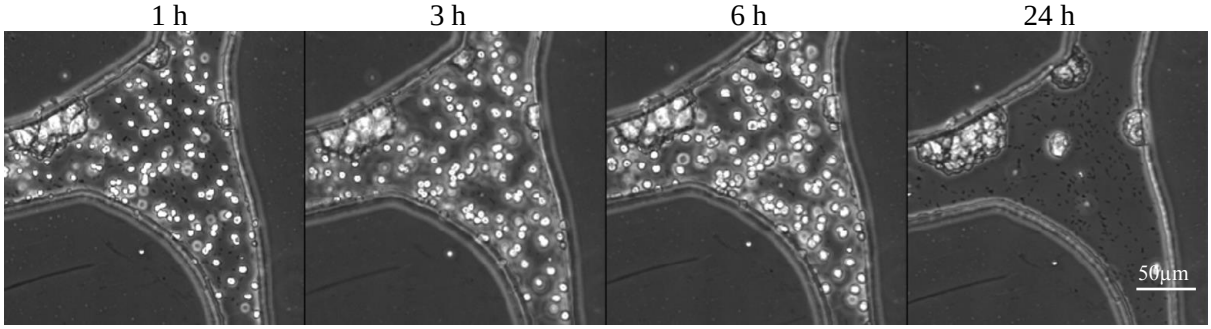

Figure 7.8 Microscope images of 250 μm by 250 μm square at the centre of microfluidic chip No. 7 at 1, 3, 6 and 24 hours after the completion of the second injection of cementation solution

The dissolution of unstable crystals at the expense of growth of more stable crystals was also observed after the first injection of cementation solution when the concentration of cementation solution was 1 M (**Figure 7.9**). During the 1st hour, irregular-shaped $CaCO_3$ crystals and spherical $CaCO_3$ crystals were observed in the pore as shown in **Figure 7.9**. The irregular-shaped $CaCO_3$ dissolved and the spherical $CaCO_3$ continued growing during the next 3 hrs. At 6 hrs, three more crystals appeared, while the regular-shaped $CaCO_3$ observed previously

almost disappeared, and the spherical $CaCO_3$ was larger compared to its size at 3 hrs. By 24 hrs, the spherical-shaped $CaCO_3$ crystal dissolved while the three rhombohedral crystals became larger. This result is consistent with the observations mentioned in *Chapter 5*, even though the concentration of cementation solution is this experiment was 1.0 M, which is higher than the concentration used in *Chapter 5* (0.25 M).

In summary, the growth of more stable crystals at the expense of the dissolution of less stable crystals seems to be the trend during MICP processes, regardless of whether the concentration of cementation solution is 0.25 M, 0.5 M or 1.0 M. Therefore, in general, as long as the interval between injections does not result in a decrease in bacterial activity, longer intervals between injections result in more stable $CaCO_3$ crystals being produced.

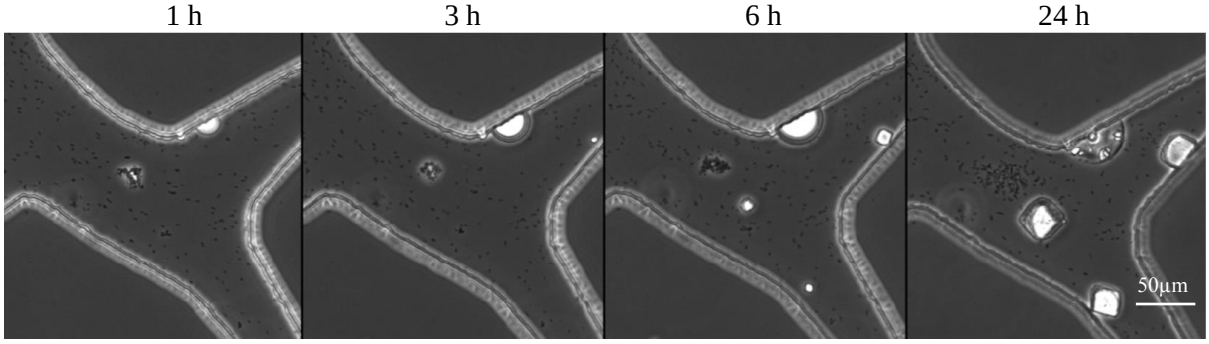

Figure 7.9 Microscope images of 250 μm by 250 μm square at the centre of microfluidic chip No. 8 taken at 1, 3, 6 and 24 hours after the completion of the first injection of cementation solution

7.4 Results of macro-scale experiments

As shown by the results of the micro-scale experiments, the time interval between injections of cementation solution affects the micro-scale properties of the $CaCO_3$ crystals such as size, shape, number, and stability. A smaller number of larger and more stable rhombohedral $CaCO_3$ crystals formed during the MICP process when a longer injection interval (24 h) was used, whereas a larger number of smaller and less stable rhombohedral $CaCO_3$ crystals formed during the MICP process with a shorter injection interval (4 h). As stated before, the micro-scale properties of $CaCO_3$ crystals have significant effects on the macro-scale mechanical properties of MICP-tread sandy soils, such as strength. Therefore, after performing micro-scale MICP

experiments, macro-scale experiments were conducted to explore the effect of injection interval on the mechanical properties of MICP-treated sand. Six experimental conditions of MICP treatment with combinations of various concentrations of cementation solution and injection intervals were used (**Table 7.2**). Three parallel samples were prepared for each of the six conditions. Photos of one of the three parallel samples after each of the six different treatment protocols are shown in **Figure 7.10**. Samples processed using protocols 1, 2, 4, and 5 (0.25 M and 0.5 M) were well extracted from the moulds, while samples processed using protocols 3 and 6 (1.0 M) were found to break at points where they were relatively weakly cemented. The other two samples from each of the six different experimental conditions were consistent with these six samples. These results are consistent with the results presented in Al Qabany et al. (2012), which showed that that a 1.0 M cementation solution produced weaker samples compared to 0.25 M and 0.5 M cementation solutions. To analyse the strength of each sample, UCS tests were conducted on these samples, with the results presented in the following section.

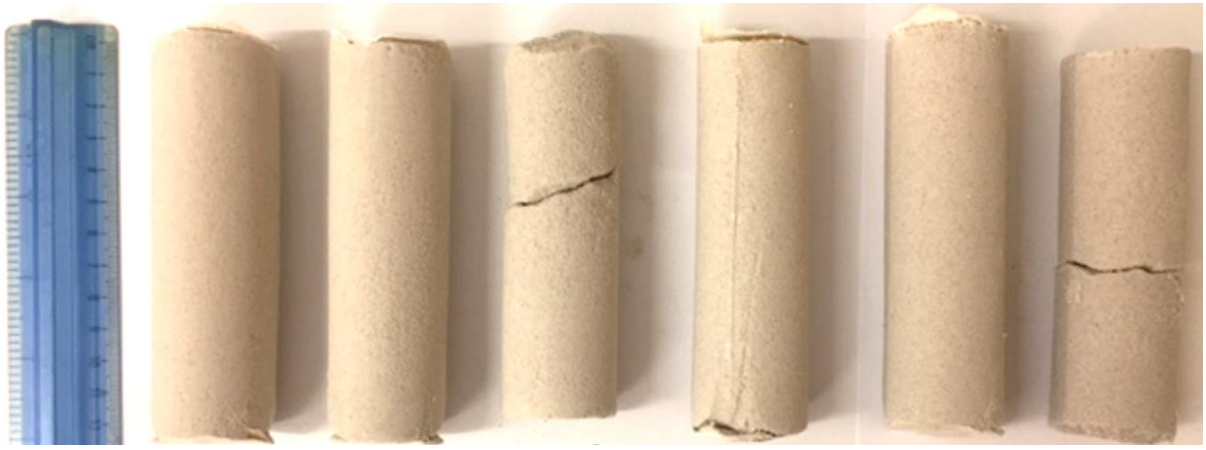

Figure 7.10 Exemplary photos of samples in the six macro-scale MICP experiments

7.4.1 Unconfined compressive strength (UCS)

A photo of a MICP-treated specimen in a UCS test is shown in **Figure 7.11a**, and a photo of the sample after being broken in the UCS test is shown in **Figure 7.11b**. Typical tensile failure pattern appeared from top to bottom along the sample were observed in the UCS tests, which

was similar to the previous observation by van Paassen et al. (2009), Al Qabany et al. (2012) and Cheng et al. (2012).

(a) **(b)**

Figure 7.11 (a) a photo of an MICP-treated specimen in a UCS test; **(b)** a photo of the sample after being broken during the UCS test

Large variations in the UCS values (from 1000 kPa to 5500 kPa) of the samples occurred when the concentration of cementation solution or treatment duration was varied (Figure 7.12), even though the total amount of reactant (urea and $CaCl_2$) injected was the same for all of the samples (3 M *1.1 PV). Samples treated with 0.25 M and 0.5 M of cementation solution had higher average UCS values than samples treated with 1 M cementation solution. When the concentration of cementation solution was kept constant, samples treated over longer treatment intervals had higher UCS values than samples treated over shorter intervals. For example, samples treated with 0.25 M cementation solution over 12 days had higher UCS values than samples treated with the same concentration of cementation solution over 6 days, whereas samples treated with 0.5 M cementation solution had higher UCS values when treated over 12 days instead of 6 days. It should be noticed that because the 1 M samples were broken (**Figure 7.10**), the UCS values of samples treated with 1.0 M cementation solution shown in **Figure 7.12** were calculated by testing the larger part of the two broken parts of each of the samples. Al Qabany et al. (2012) also present the UCS results of MICP-samples when the concentration of cementation is 1.0, while as the samples were very weak, the UCS could not be conducted, and therefore the UCS values was presented as having null strength. However, in the experiment

present here, the samples treated with cementation solution with a concentration of 1.0 were broken into two pieces during the extraction process from the column cells, the strength of the samples obtained in this experiment are higher than the strength obtained in the study of Al Qabany et al. (2012).

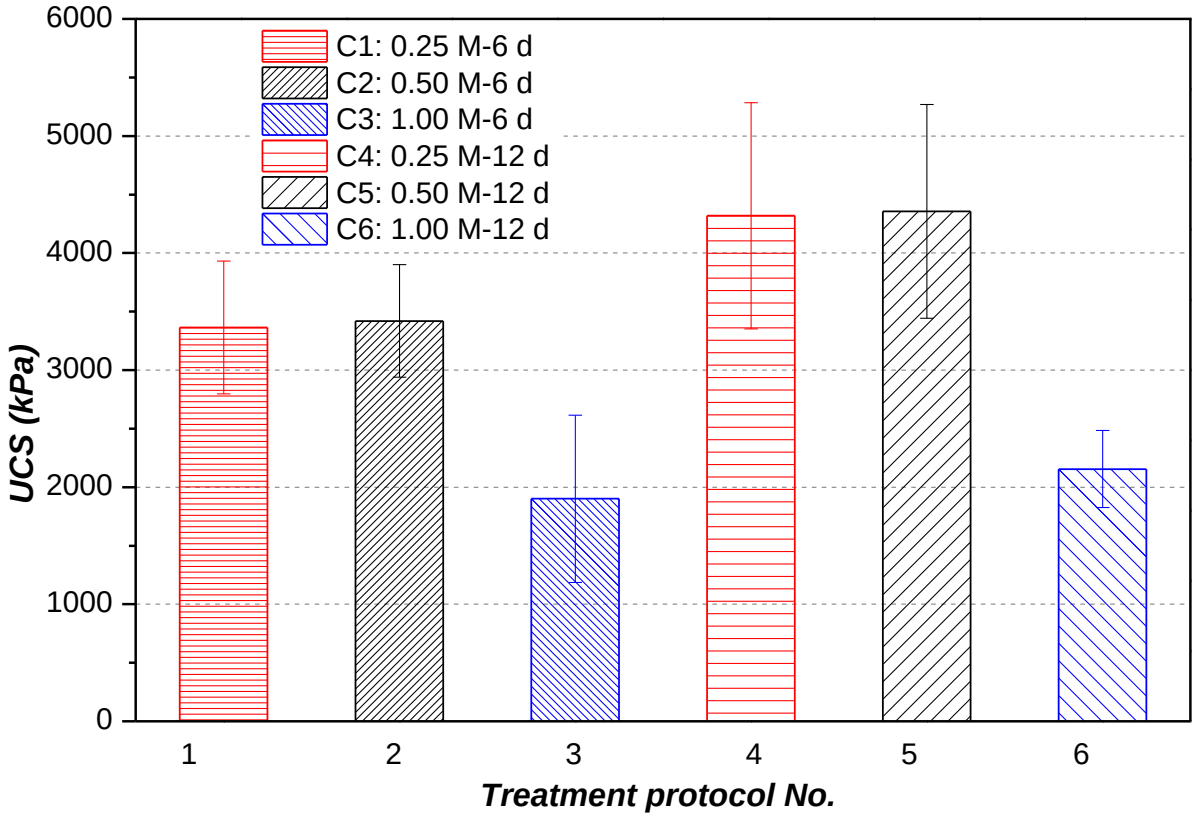

Figure 7.12 Unconfined compressive strength (UCS) values of MICP-treated sand samples. Data presented as mean ± standard error, n=3 (n is the number of times each treatment condition and the relative measurement was repeated)

7.4.2 Chemical efficiency

Following the study conducted by Al Qabany et al. (2012), chemical efficiency was defined as the percentage of tested mass of $CaCO_3$ in relative to the calculated mass of $CaCO_3$ if all of the $CaCl_2$ injected into the soil pores transform into $CaCO_3$. The equation is given as,

$$Efficiency(\%) = \frac{m(CaCO_3)/m_1(sand)}{C(CaCl_2)\times PV\times IN\times M(CaCO_3)/m_2(sand)}\times 100\% \qquad 7.1$$

where $m(CaCO_3)/m_1(sand)$ is the measured $CaCO_3$ content; $C(CaCl_2)$ (mol/L) is the concentration of $CaCl_2$ in the cementation solution; PV (L) is the pore volume of the soil column; IN is the injection number of cementation solution; $M(CaCO_3)$ is the molar mass of $CaCO_3$, which is a constant 100 g/mol; $m_2\ (sand)$ is the dry mass of the total sand in the column.

The chemical efficiencies of the samples are shown in **Figure 7.13**. In general, when the concentration of cementation solution was either 0.25 M or 0.5 M, the chemical efficiency was relatively high (higher than 75 %). By contrast, when the concentration of cementation solution was 1 M, the mean chemical efficiency was lower, which are 71 % and 64% for 6 day treatment and 12 day treatment, respectively. The variation in chemical efficiency was also smaller when the concentration of cementation solution was lower (0.25 M or 0.5 M) compared to the chemical efficiency when the concentration of cementation solution was 1.0 M. The sample treated with 1 M cementation solution over 12 days had the lowest average efficiency (64 %) and efficiency range of 53 % - 69 %, which might be because the intervals between injections being 4 days caused a decrease in bacterial activity. During the 4-day retention time, only 3 g/L nutrient broth was injected to maintain bacterial activity. However, as the bacterial activity inside the soil was difficult to measure, this can only be speculated. The variations in the efficiencies of samples 1.0 M - 6 d and 1.0 M - 12 d were about 42% and 16%, respectively, which were the largest among all the samples tested. Together with the appearance of the samples shown in **Figure 7.10**, the large variations in the chemical efficiency of these 1.0 M samples suggest that the samples treated with 1.0 M cementation solution were in-homogeneously cemented. It was suggested by Al Qabany et al. (2012) that to achieve a chemically efficient condition, the time interval between each injection of cementation solution (retention time) should be long enough to allow sufficient time for the urea and $CaCl_2$ to react and form $CaCO_3$. However, in addition to this suggestion, the results obtained from this PhD study suggested that the retention time should not be too long because the bacterial activity may decrease as the nutrient resources become limited.

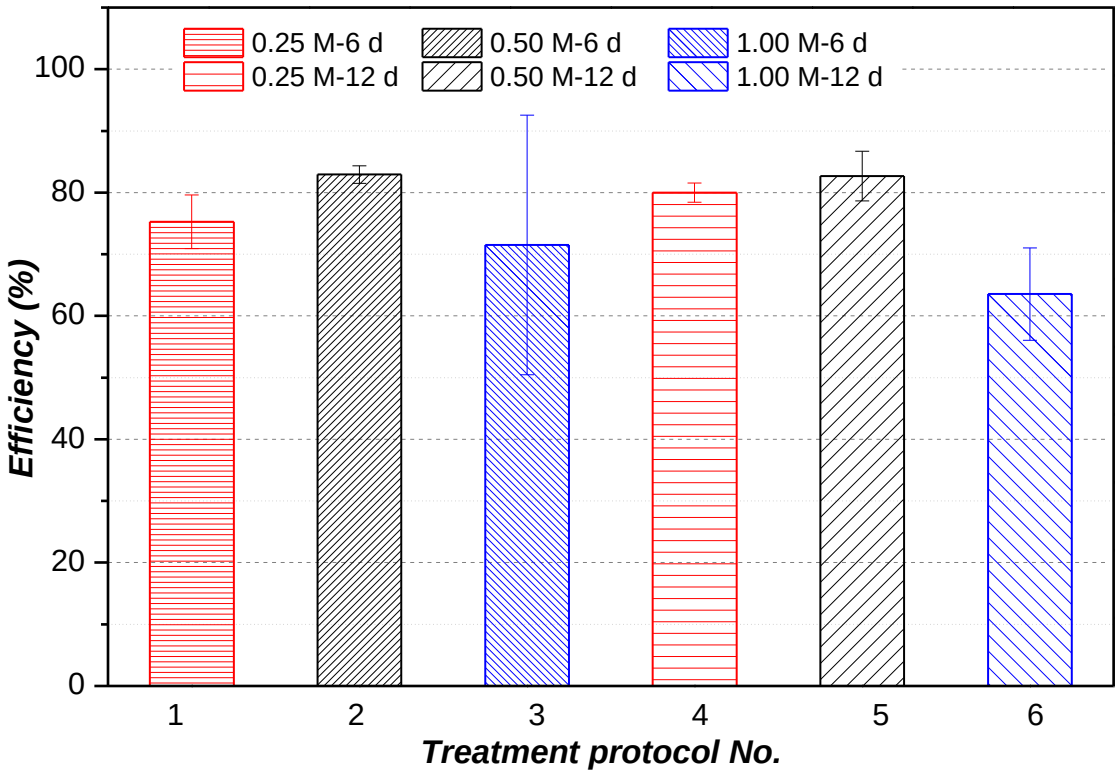

Figure 7.13 Chemical efficiencies of the MICP-treated sand samples. Data presented as mean ± standard error, n=3 (n is the number of times each treatment condition and the relative measurement was repeated)

7.4.3 Relationship between $CaCO_3$ content and unconfined compressive strength

UCS values of the samples were plotted against $CaCO_3$ content, with the results shown in **Figure 7.14**. For comparison, the results of Al Qabany and Soga (2013) were also plotted in the same figure. Large variations in the UCS values from 0 to 5.5 MPa were observed even when the $CaCO_3$ content was the same. This large variation in UCS values at a given $CaCO_3$ content is consistent with the summary of the results reported in literature made by the author of this thesis and colleagues (Wang et al., 2017). For the samples treated with cementation solution with a concentration of either 0.25 M or 0.5 M, higher UCS values were obtained when the treatment interval was longer. The UCS values of samples treated with 1.0 M cementation solution were in general lower than the UCS values of samples treated with 0.25 M or 0.5 M, which is consistent with the results presented in Al Qabany and Soga (2013).

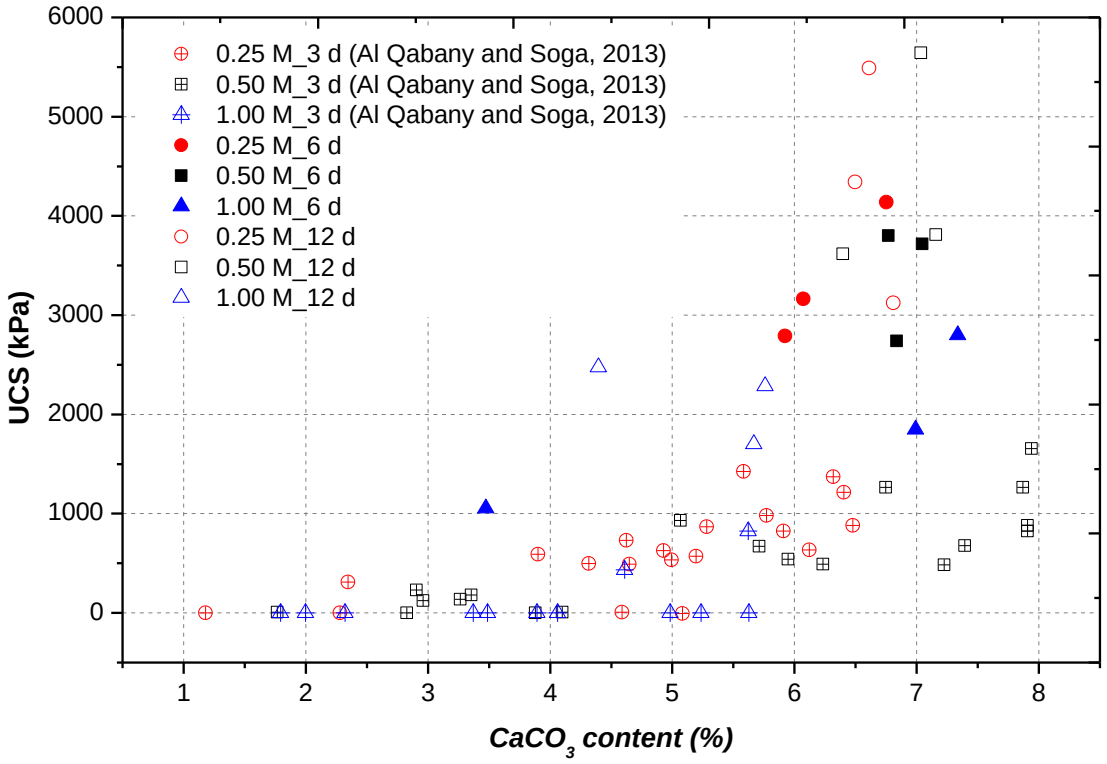

Figure 7.14 $CaCO_3$ content vs UCS (comparison with the results of Al Qabany and Soga, 2013)

7.4.4 Performance efficiency

A higher chemical efficiency enables the desired amount of $CaCO_3$ to be produced using lower amounts of $CaCl_2$ and urea. However, the engineering properties of MICP-treated sandy soils do not only depend on the $CaCO_3$ content, but are also highly dependent on the micro-scale properties of $CaCO_3$ crystals. The $CaCO_3$ crystals that efficiently bond soil particles contribute to the increase in the strength of MICP-treated sandy soils. Therefore, apart from calcium carbonate content, the microscale properties of the $CaCO_3$ precipitates have also been suggested to play an important role in determining the engineering properties of MICP-treatment soils (Al Qabany and Soga, 2013; Wang et al., 2017). In this study, another factor considered to be important for designing MICP processes is the performance efficiency, which refers to the effectiveness with which $CaCO_3$ crystals are able to bond soil particles for increasing strength and is quantified as the ratio of the strength of the MICP-treated sandy specimen to the $CaCO_3$ content formed in the specimen. It is shown in **Figure 7.15** that when the concentration of cementation solution is kept as constant, the performance efficiency was higher when the injection intervals were longer. The performance efficiency is 22 % higher in

Protocol 4 (0.25 M-12 day treatment) than in Protocol 1 (0.25 M-6day treatment); 27% higher in Protocol 5 (0.50 M-12 day treatment) than in Protocol 2 (0.50 M-6 day treatment); and 33 % higher in Protocol 6 (1.00 M-12 day treatment) than in Protocol 3 (1.00 M-6 day treatment). In addition, when the total duration of the injection procedure was the same, the average performance efficiency was higher when a lower concentration of cementation solution was injected more times. For example, the average performance efficiency of Protocol 1 was higher than Protocol 2, which in turn was higher than Protocol 3; and the average performance efficiency of Protocol 4 was higher than Protocol 5, which was higher than Protocol 6 (**Figure 7.15**). The performance efficiency of Protocol 6 is 69 % higher than Protocol 3; the performance efficiency of Protocol 4 is 55% higher than Protocol 6. These results are consistent with the results presented in Al Qabany and Soga (2013), which showed that performing multiple injections of cementation solution with a lower concentration over a longer period of time can produce samples with higher unconfined compressive strength.

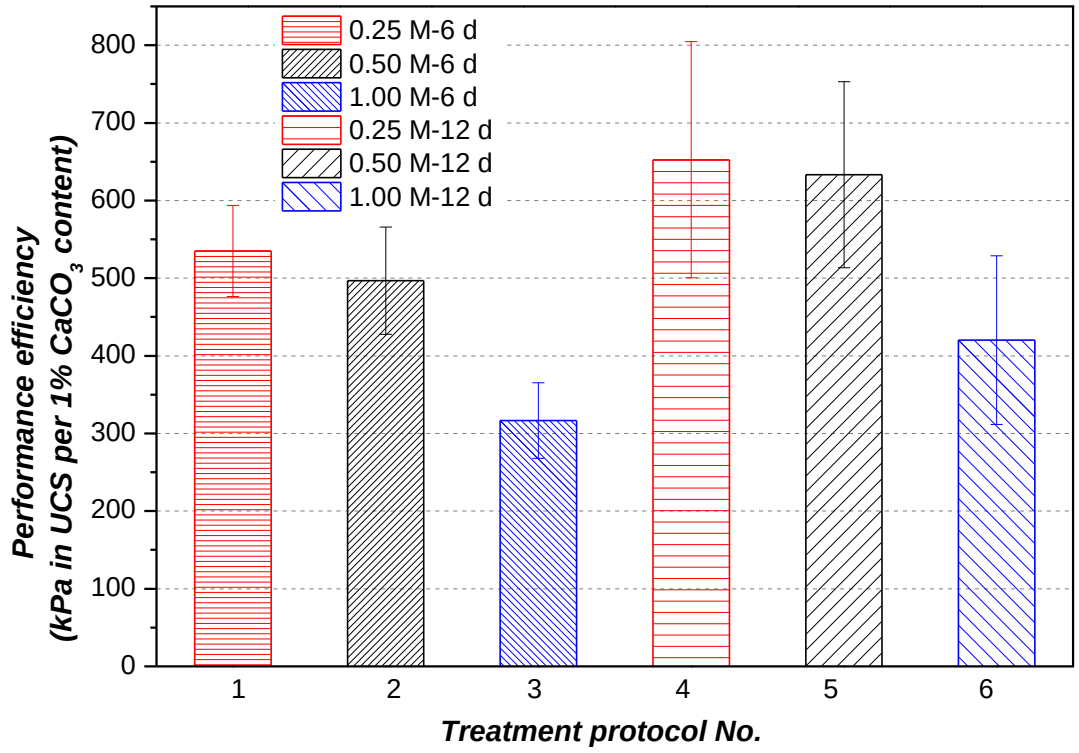

Figure 7.15 Performance efficiency of MICP-treated sand samples. Performance efficiency was obtained by dividing the UCS values by the $CaCO_3$ contents. Data presented as mean ± standard error, n=3 (n is the number of times each treatment condition and the relative measurement was repeated)

7.4.5 Micro-scale properties of $CaCO_3$ crystals observed by SEM

As described previously, increasing the interval time between injections can increase the performance efficiency. Together with the findings that the micro-scale properties of $CaCO_3$ are affected by the injection interval, these results support the observation that a smaller number of larger and more stable $CaCO_3$ formed when the interval between cementation solution injections was increased. To observe the micro-scale properties of $CaCO_3$ crystals after the MICP treatment, SEM images of the samples were taken, with the results presented in **Figure 7.16**. When the concentrations of cementation solution were the same, the crystals in the samples treated by a staged-injection procedure with a longer interval between cementation solution injections treatment were larger than that in the samples treated over a shorter time interval. Compared to the samples when the concentration of cementation solution was 0.25 M, it can be found that when increasing the injection interval from 3 hours, to 6 hours and then to 24 hours, the average size of the crystals formed after the 12^{th} injection of cementation solution increased from about 5 μm (**Figure 2.16a**, Al Qabany et al., 2012) to 30 μm (**Figure 7.16 a**) and then to 50 μm (**Figure 7.16 d**), respectively. These results are also consistent with the results obtained in the micro-scale experiments. When the concentration of cementation solution was 0.25 M and the injection interval was increased from 4 hours to 24 hours, the crystal size after the 12^{th} injection of cementation solution increased from about 10 μm to 50 μm (see **Figures 7.3** and **7.6**).

The observation that the samples with a higher strength tend to have larger $CaCO_3$ crystals is also consistent with the results presented by Cheng et al. (2012) which showed that when the $CaCO_3$ content is similar, the UCS values of the MICP-treated samples tend to be higher when the $CaCO_3$ crystals are larger.

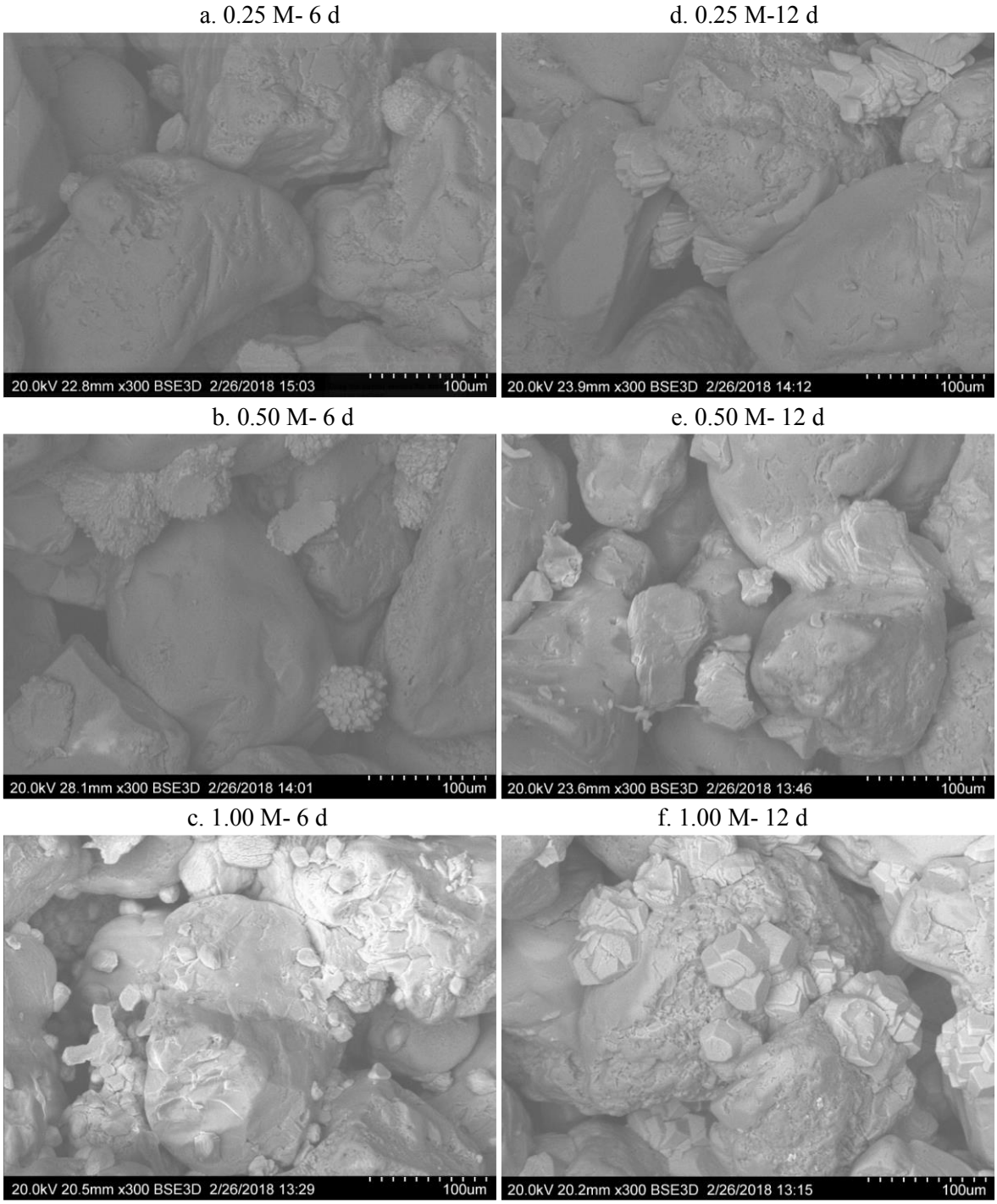

Figure 7.16 SEM images of $CaCO_3$ crystals inside MICP-treated sand samples after MICP treatments. **a**. 0.25 M-6 day treatment, $CaCO_3$ content is 6.1 %; **b**. 0.50 M- 6 day treatment, $CaCO_3$ content is 7.0 %; **c**. 1.00 M-6 day treatment, $CaCO_3$ content is 7.0 %; **d**. 0.25 M-12 day treatment, $CaCO_3$ content is 6.6 %; **e**. 0.50 M-12 day treatment, $CaCO_3$ content is 7.0 %; **f**. 1.00 M-12 day treatment, $CaCO_3$ content is 5.8 %

Research has shown that many factors such as the concentration of cementation solution and the bacterial activity affect the size and type of $CaCO_3$ precipitates formed. This thesis study suggests that the interval between cementation solution injections also has an effect on the size of $CaCO_3$ crystals, with the size of the $CaCO_3$ being larger when the interval between injections of cementation solution is longer. In the experimental setup described in this research, samples treated with an injection interval of 1 day using 0.25 M cementation solution, as well as samples treated with an injection interval of 2 days using 0.5 M cementation solution, had higher UCS values than when the injection intervals were shorter. A possible explanation for the effect of crystals size on increasing the performance efficiency of MICP-treated samples might be that the crystals should be large enough to fill the gaps between soil particles to sufficiently bond them (**Figure 7.17**). In addition, when the $CaCO_3$ crystals are large, the soil particles may be more difficult to rotate during shearing (Zhao et al., 2018). The experiments presented in this study provide a way to increase the percentage of larger and more stable $CaCO_3$ crystals by increasing the injection interval of cementation solution and thus increase the compressive strength.

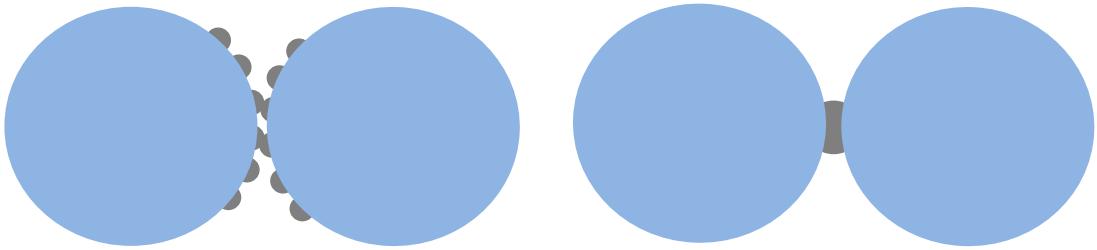

Figure 7.17 Proposed schematic of inefficient **(a)** and efficient (**b**) $CaCO_3$-mediated bonding of soil particles

7.5 Conclusions

In this study, both micro-scale and macro-scale experiments were conducted to investigate the effect of changing the interval between cementation solution injections on the size of $CaCO_3$ crystals formed after MICP treatment and the strength of MICP-treated sandy soils. The findings of this study are summarised as follows.

The interval between cementation solution injections was found to have an effect on the $CaCO_3$ precipitation process. When the injection interval was long enough (24 hours for 0.25 M cementation solution), unstable and smaller $CaCO_3$ crystals dissolved at an expense of the growth of more stable and larger $CaCO_3$ crystals. However, in the case of shorter injection intervals (4 hours for 0.25 M cementation solution), the unstable and smaller $CaCO_3$ crystals formed, did not have enough time to dissolve and promote the growth larger and more stable $CaCO_3$ crystals. The interval between cementation solution injections therefore affects crystal size and the strength of MICP-treated samples. By varying the interval between cementation solution injections in a staged-injection procedure, a larger number of crystals (200 - 1000 per 10^6 μm^3) with smaller sizes (5 - 10 μm) were produced when the interval was 4 hours, whereas the crystals were larger (10 - 80 μm) and fewer in number (5 - 20 per 10^6 um^3) when the interval was 24 hours. The dissolution of unstable or smaller $CaCO_3$ crystals at the expense of growth of more stable or larger $CaCO_3$ crystals also occurred when the concentration of cementation solution was 0.5 M or 1.0 M.

The results of the macro-scale experiments showed that the injection interval and concentration of cementation solution had an effect on the chemical efficiency of $CaCO_3$ formation. The $CaCO_3$ transformation efficiency in the six treatment procedures was generally high (75% -83 %) with a smaller variation (1.5% - 4.5%) when the concentration of cementation solution was either 0.25 M or 0.5 M. Samples treated with 0.25 M cementation solution injected at intervals of either 12 hours or 24 hours, or with 0.5 M cementation solution injected at intervals of 24 hours or 48 hours, had high $CaCO_3$ transformation efficiencies. However, the $CaCO_3$ transformation efficiency was lower with a larger variation in range when the concentration of cementation solution was 1.0 M. The mean transformation efficiencies in Protocols 3 and 6, when the concentration of cementation solution was 1.0, were 71 ± 29 % and 64 ± 12%, respectively. Together with the observation that samples treated with 1.0 M cementation solution broke after being taken out from the columns, these findings suggest that $CaCO_3$ content is not uniformly distributed in the soil columns and is thus not as effective at binding soil particles together when the concentration of cementation solution is 1.0 M.

Despite the similarities observed in $CaCO_3$ transformation efficiency, the strength of MICP-treated soils varied considerably. The variation in the strength of MICP-treated sandy soils in relative to $CaCO_3$ content varied. It was found that by increasing the total treatment duration from 6 days to 12 days, the performance efficiency increased by 22 %, 27 % and 33 % when the concentration of cementation was 0.25 M, 0.50 M and 1.00 M, respectively. In addition, when $CaCO_3$ content were the same, the unconfined compressive strength of the samples obtained in this study, where the total treatment duration was either 6 days or 12 days, were higher than the UCS values of samples when the treatment duration was 3 days. Considering together with the results obtained in micro-scale experiment, and from the SEM imaging on the soil samples after MICP treatment, this may be due to differences in the micro-scale properties of $CaCO_3$ crystals. When the treatment duration is longer, larger and more stable crystals tend to be the dominant crystals which tend to be able to bond soil particles and be more efficient in increasing the strength of the MICP-treatment samples.

Chapter 8 Enhancing the homogeneity of MICP-treated sandy soils: from micro to macro

8.1 Research aims

Homogeneity in MICP treatment (i.e. uniform distribution of $CaCO_3$ within a soil matrix after MICP treatment) is critical to the success of MICP soil improvement procedures but remains poorly studied (Mujah et al., 2017). As described in *Chapters 4-5*, bacterial aggregation occurred after injecting bacterial suspension and cementation solution into the medium, and it was found that bacterial aggregation was induced by the $CaCl_2$ present in the cementation solution. Therefore, the concentration of $CaCl_2$ in the cementation solution and the density of bacterial cells inside the bacterial suspension would affect the size of bacterial aggregates. Compared with individual bacterial cells, bacterial aggregates are notably larger and are hence more likely to become trapped in pore throats. Therefore, when the MICP process is applied in a soil matrix, the bacterial distribution might be affected by the filtration of the bacterial aggregates along the injection path, which in turn affects the distribution of $CaCO_3$ inside the soil matrix. It was also found from the experiment presented in *Chapter 6* that bacterial density has an effect on crystal size and number. Therefore, if the bacteria are not distributed homogeneously throughout the soil matrix, the micro-scale properties of $CaCO_3$ crystals formed would vary between different areas, thus affecting the uniformity and strength of MICP-treated soils.

The aim of the research described in this chapter was to investigate the effects of bacterial density and the concentration of cementation solution on the homogeneity of MICP-treated sandy soils, including the distribution homogeneity of the macro-scale $CaCO_3$ content and the

micro-scale properties of $CaCO_3$ crystals. In addition, the strength, stiffness, rigidity and uniformity of MICP-treated sandy soil were also investigated.

First, a microscope slide experiment was conducted to investigate the effects of bacterial density and the concentration of cementation solution on the size of bacterial aggregates. Subsequently, macro-scale experiments were conducted by applying MICP treatment in six one-metre-long soil columns using various bacterial densities and cementation solution concentrations whilst keeping the total amount of cementation solution injected (calculated by multiplying the injection volume of cementation solution by its concentration) the same. The $CaCO_3$ content, the strength and stiffness of the MICP-treatment soil specimen along the soil columns were measured, in order to evaluate the homogeneity of MICP along the soil columns. Soil samples at selected points along the soil columns were also imaged using scanning electron microscopy (SEM) to investigate the relationship between the macro-scale mechanical behaviour of MICP-treated soils and the micro-scale properties of $CaCO_3$ crystals (such as size and distribution) inside the soil pores.

8.2 Experimental procedures

8.2.1 Micro-scale MICP experiments

A glass slide experiment was conducted to investigate the effects of bacterial density and the concentration of cementation solution on the size of bacterial aggregates. The experimental setup and the procedure associated with the glass slide experiment was described in *Chapter 3*. Microscopic images of the glass slide samples containing mixtures of equal volumes of bacterial suspension and cementation solution were taken immediately after mixing the bacterial suspension with cementation solution. When testing the effect of bacterial density on the size of the bacterial aggregates, the concentration of cementation solution was kept constant at 1.00 M, and the OD_{600} values of bacterial suspensions trialled were 0.1, 0.3, 1.0 and 3.0. When testing the effect of the concentration of cementation solution on the size of bacterial aggregates, the OD_{600} of bacterial suspension was kept constant at 1.0, and the concentrations of cementation solution trialled were 0.10 M, 0.25 M, 0.50 M, and 1.00 M. It is worth noting

that the optical density values of bacterial suspension and the concentrations of cementation solution mentioned here refer to their initial values before mixing.

8.2.2 Macro-scale MICP experiments

A soil column experiment was conducted to investigate the effects of bacterial density and the concentration of cementation solution on the homogeneity of MICP-treated soils. The soil columns were one-metre long, with the experimental setup described in Chapter 3. Six soil columns were treated using different bacterial densities and concentrations of cementation solution whilst keeping the total amount of cementation solution injected constant. The experimental parameters are summarised in **Table 8.1.** During the injection of cementation solution, the duration of each injection was measured, and the average injection flow rate was calculated as

$$v(m/s) = \frac{V(m^3)}{n \times A(m^2) \times t(s)} \quad 8.1$$

where v is the injection flow rate, V is the volume of cementation solution injected through the soil columns in each injection (2.2×10^{-3} m^3), A is the cross-sectional area of the soil samples (0.0038 m^2), n is the porosity of the soil matrix (0.4), and t is the duration of each injection. It should be noted that the porosities of the soil matrices decreased during MICP treatment due to an increase in $CaCO_3$ content during the injection events. However, for simplification, n was assumed to be constant. After MICP treatment, the cemented sands were removed from the moulds to test unconfined compressive strength (UCS), to measure $CaCO_3$ content, and to be analysed by SEM.

Table 8.1 Parameters of macro-scale MICP experiments

Column number	OD_{600} of BS	Concentration of CS	Number of injections	Injection interval (days)	Volume injected each time (L)	Molar mass of CS injection each time (mol)
1	0.1	0.125 M	20	0.5	2.2	0.275
2	1.0	0.125 M	20	0.5	2.2	0.275
3	0.1	0.25 M	10	1	2.2	0.55
4	1.0	0.25 M	10	1	2.2	0.55
5	0.1	0.5 M	5	2	2.2	1.1
6	1.0	0.5 M	5	2	2.2	1.1

Note: BS-bacterial suspension; CS-cementation solution; In the cementation solution, 0.125 M, 0.25 M and 0.5 M refer to the concentrations of $CaCl_2$ present in the cementation solution; Apart from $CaCl_2$, urea with a concentration of 1.5 times of $CaCl_2$ and nutrient broth with a concentration of 3 g/L were also contained in the cementation solution.

8.3 Results and discussion

8.3.1 Bacterial aggregates

The optical microscope images of glass slide samples containing mixtures of bacterial suspension with different densities and cementation solution with different concentrations are shown in **Figure 8.1**. Bacterial aggregates formed in all of the samples, while the sizes of the bacterial aggregates varied between different samples. Within each individual sample, the size of bacterial aggregates also varied.

The quantification of the sizes of the bacterial aggregates is shown in **Figure 8.2**. When the OD_{600} of bacterial suspension was kept constant at 1.0, the effect of the concentration cementation solution on the size of bacterial aggregates was not obvious when the concentration of cementation solution was gradually increased from 0.10 M to 0.50 M, but was more pronounced when the concentration of cementation solution was 1.00 M. At this concentration, the average size of bacterial aggregates was more than two times larger than the size of bacterial aggregates when the concentration of cementation solution was 0.10 - 0.50 M. When the concentration of cementation solution was kept constant at 1.00 M, the average size

of bacteria increased as the optical density of the bacterial suspension increased. As the optical density increased from 1.0 to 3.0, the average size of bacterial aggregates increased by more than two-fold, from 1672 μm^2 to 4882 μm^2. It is worth noting that the size of the bacterial aggregates in the glass slide experiment cannot represent the size of the bacterial aggregates in a soil column experiment. This is because in the soil column experiment, the bacterial suspension and cementation solution are injected into the soil at different times rather than being mixed and then injected together. However, this glass slide experiment was conducted to estimate the effect of changing the bacterial density or the concentration of cementation solution on the size of the bacterial aggregates formed.

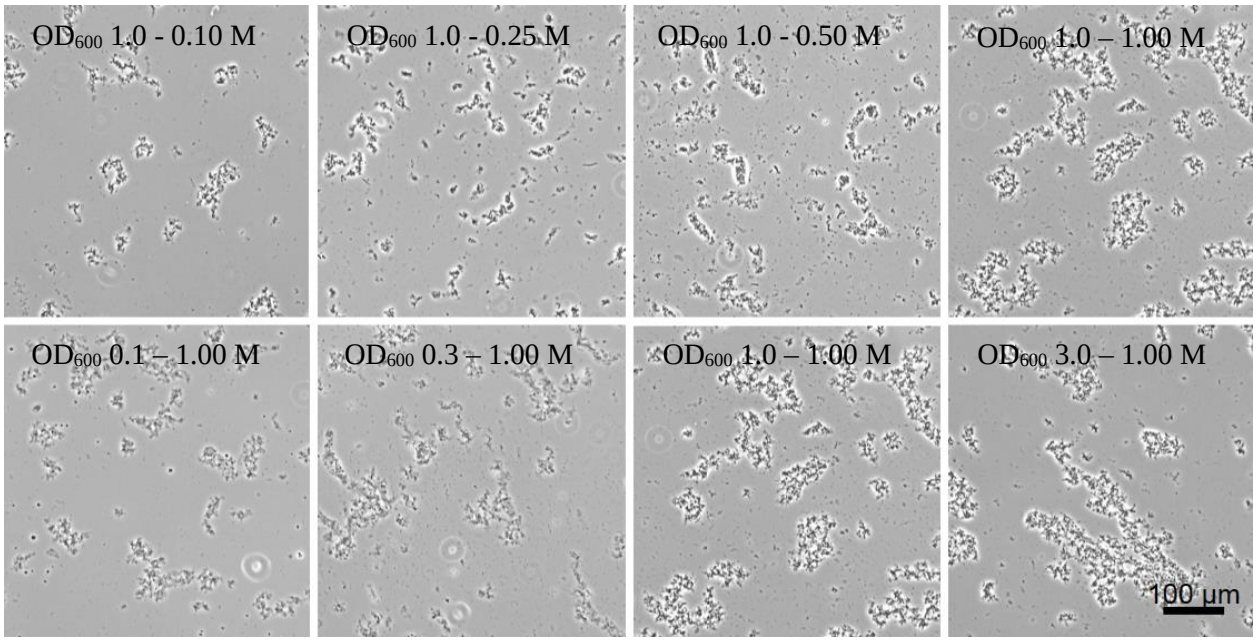

Figure 8.1 Microscope images of the mixtures of bacterial suspension and cementation solution with various optical densities and concentrations

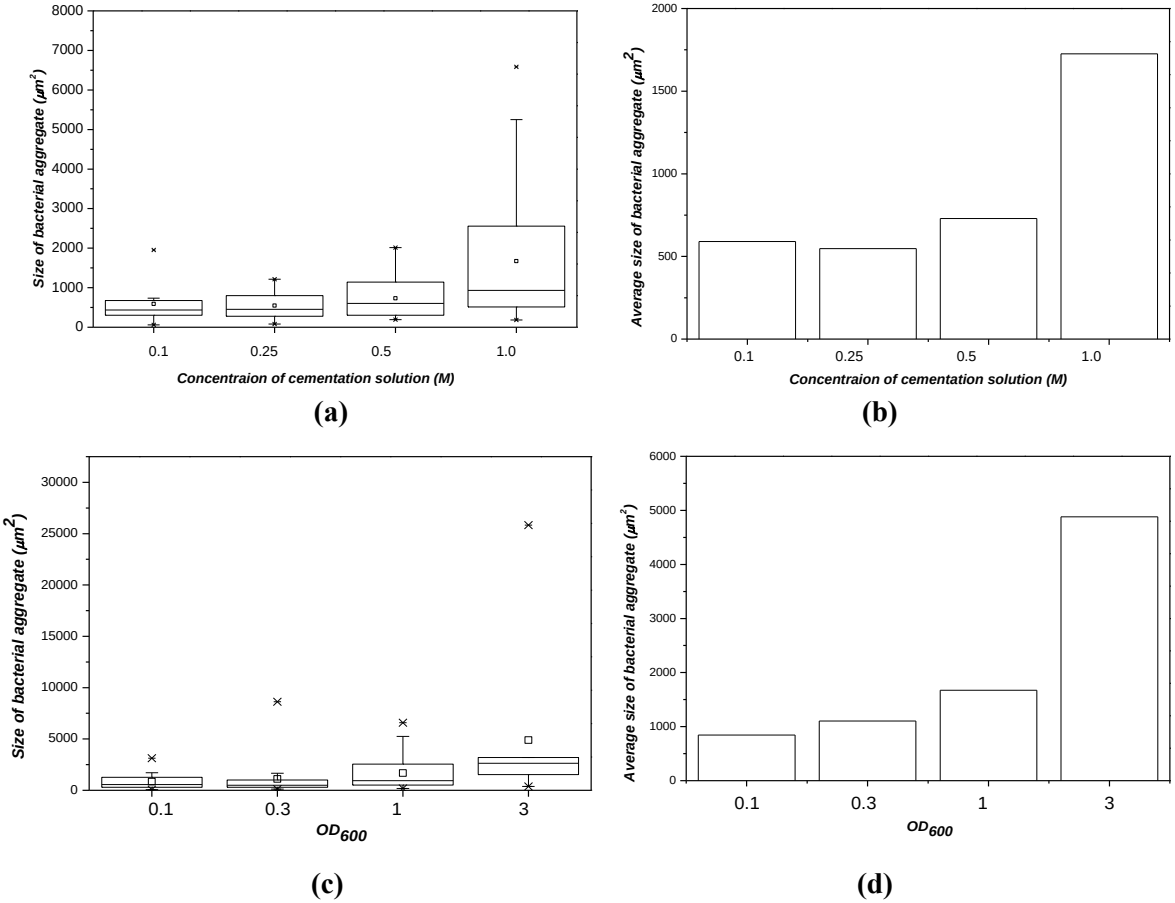

Figure 8.2 Quantification of sizes of bacterial aggregates in Figure 8.1. **(a)** and **(b)**, depict the relationship between the size of bacterial aggregates and the concentration of cementation solution when the OD_{600} of bacterial suspension was 1.0. **(c)** and **(d)** depict the effect of the optical density of bacterial suspension on the size of bacterial aggregates formed when the concentration of cementation solution was 1.0 M

8.3.2 Injection flow rate

The average injection flow rates during each injection of cementation solution in the six columns were plotted against the injection number of cementation solution (**Figure 8.3**). For columns 1 to 5, the injection flow rate decreased gradually as the number of injection increased, suggesting that $CaCO_3$ crystals are formed gradually during the MICP treatment. However, for column 2, during the second injection, the injection flow decreased from about 3×10^{-4} m/s to 1×10^{-5} m/s, whereas the injection flow rates of the other columns were still above 1×10^{-4} m/s. The rapid reduction in the injection flow rate suggests that local clogging by $CaCO_3$ due

to the large bacterial aggregates is caused by the combined effect of a high bacterial density (OD_{600} 1.0) and a high concentration of cementation solution (0.50 M).

This result is consistent with the experimental result of Al Qabany and Soga (2013), which showed that the use of a cementation solution with a high concentration of urea and calcium chloride resulted in a rapid drop in permeability at the early stage of calcite precipitation, whereas the use of a cementation solution with a low concentration of urea and calcium chloride resulted in a more gradual and uniform decrease in permeability. However, following this finding, the results presented here suggest that not only the concentration of cementation solution but also the density of bacterial suspension has an effect on the reduction of permeability at the early stage of MICP treatments. The use of a high-calcium chloride (0.50 M) and urea (0.75 M) together with a bacterial suspension with a high bacterial density (OD_{600} = 1.0) resulted in a rapid drop in permeability at the early stage of calcite precipitation. However, the use of a solution with a high concentration of calcium chloride (0.50 M) and urea (0.75 M) together with a bacterial suspension with abut low bacterial density (OD_{600} = 0.1) did not result in a rapid drop in permeability at the early stage of calcite precipitation.

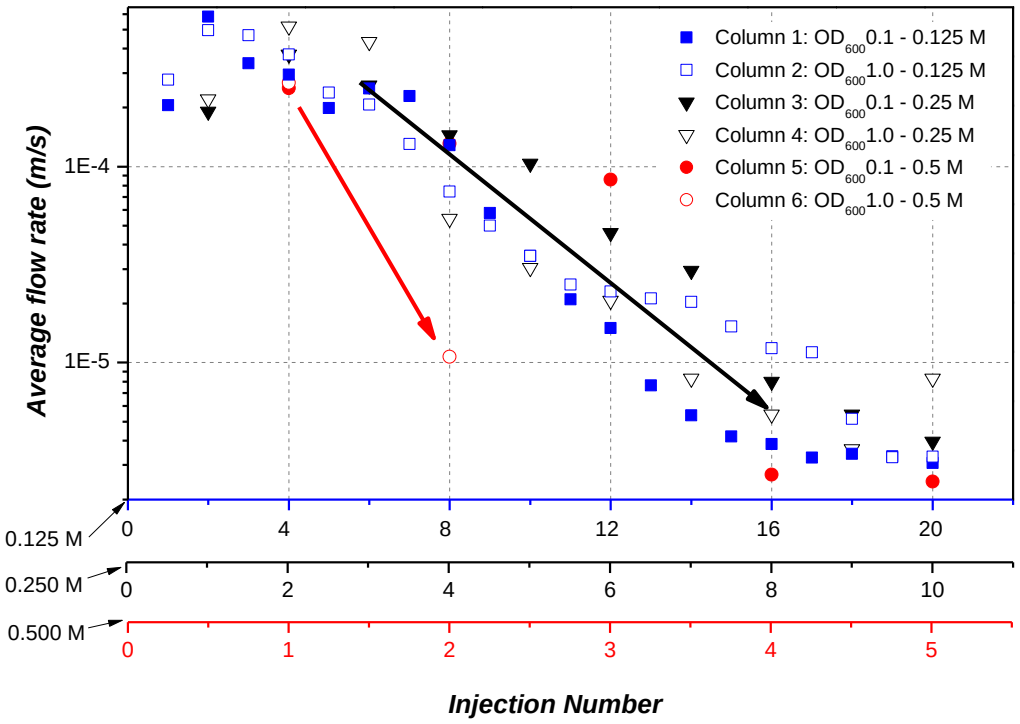

Figure 8.3 Relationship between average flow rate and injection number of cementation solution

8.3.3 Distribution of $CaCO_3$ content and transformation efficiency

After the MICP-treated process, the cemented soil samples were removed from the moulds. After visual inspection, they were found to be fully cemented (**Figure 8.4**). However, the extraction of the soil specimen from the column cells caused the samples to break at points where they were found to be weakly cemented. Based on the number of the fractures, it appears that samples 1, 3 and 5 have higher strength compared with samples 2, 4 and 6. Additionally, sample 4 seems stronger than samples 2 and 6. The difference in the strength along different parts of the columns might due to differences in the distribution and micro-scale properties of $CaCO_3$ crystals. Further information about the $CaCO_3$ content and the strength of these samples is described in the next two sections.

Figure 8.4 Cemented samples after extraction from rigid columns. From left to right the column numbers are 1 to 6

The distribution of $CaCO_3$ content along the soil columns from the top to the bottom is shown in **Figure 8.5**. An experiment was conducted to estimate the measurement error of $CaCO_3$

content. The $CaCO_3$ content of three samples processed from the long column test was measured three times for each sample, and it was found that average $CaCO_3$ content in these three samples were 3.87±0.12%, 10.86±0.05% and 3.63±0.05%. Because the error associated with these measurements was found to be small, samples at each point of the columns were therefore assumed to be homogeneous. When comparing the results for the six columns, apart from column 6, in which the total amount of cementation solution injected was 60% lower than the total amount injected in the other columns, the $CaCO_3$ distribution in the other five columns varied considerably from column to column even though the total amount of cementation solution injected was the same. The amount of cementation solution injected into the five columns apart from column 6 were 5.5 mol. Both bacterial density and the concentration of cementation solution affect the distribution of $CaCO_3$ content.

Columns 1, 2, 4 and 6 show relatively good homogeneity in the distribution of $CaCO_3$ throughout each column, and among these four columns, column 4 has the highest overall $CaCO_3$ content. Columns 3 and 5 show large variations in $CaCO_3$ content. These results suggest that, irrespective of the concentration of cementation solution, $CaCO_3$ was relatively homogeneously distributed along the height of the column when the bacterial suspension of OD_{600} 1.0. On the other hand, when the optical density of the bacterial suspension was 0.1, only the column treated with a low concentration of cementation solution (0.125 M) produced a homogenous distribution of $CaCO_3$, while in the case of 0.25 M or 0.5 M, $CaCO_3$ was heterogeneously distributed. Taken together, these results suggest that a homogenous distribution of $CaCO_3$ can be achieved when the bacterial density is 1.0 or when the bacterial density is 0.1 and a low concentration of calcium chloride is used.

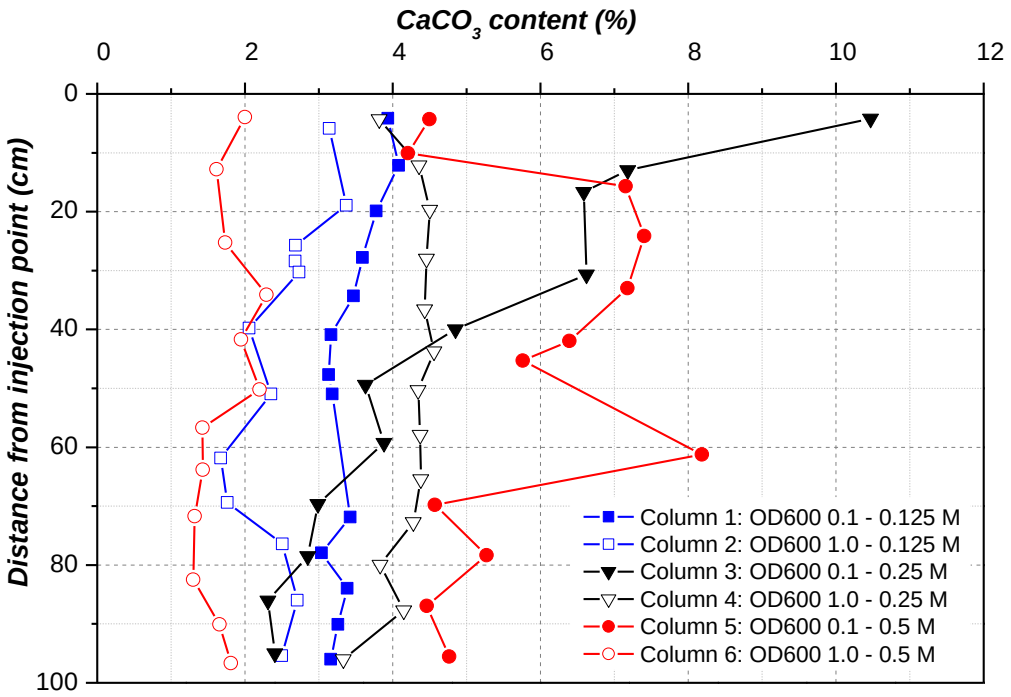

Figure 8.5 Distribution of $CaCO_3$ content along 1 metre-long columns of MICP-treated sandy soil

To analyse $CaCO_3$ content in more detail, box plots were produced to visualise the range and distribution of $CaCO_3$ content and the associated transformation efficiencies (**Figure 8.6**). The mean and median values are represented as lines and square dots inside the box, respectively; the other lines are the lower quartile (25^{th} percentile) and upper quartile (75^{th} percentile); the height of the box (difference between the lower and upper quartile) being referred to as the interquartile range (IQR). When comparing Columns 1 and 2 for which the concentration of cementation solution introduced was 0.125 M, the soil column treated with the higher bacterial density (OD_{600} = 1.0, Column 2) had a lower average $CaCO_3$ content and a lower transformation efficiency compared with Column 1 which was treated with a lower bacterial density (OD_{600} = 0.1) (**Figure 8.6**). The same phenomenon was observed when comparing Columns 3 and 4, or Columns 5 and 6. Comparisons between Columns 1, 3 and 5, all of which were treated with bacterial suspension with an OD_{600} of 0.1, revealed that increasing the concentration of cementation solution resulted in an increased average transformation efficiency. The same conclusions can also be drawn when comparing the average transformation efficiencies of Columns 2, 4 and 6. Taken together, these results suggest that within the range of bacterial density and concentration of cementation solution tested in this

study, a higher bacterial optical density decreases the transformation efficiency, while a higher concentration of cementation solution increases transformation efficiency.

As has been described in the glass slide experiment in this chapter and the results shown in *Chapters 4*, *5* and *6*, bacterial aggregates formed after the bacterial suspension and cementation solution were mixed. Bacterial aggregates adsorb Ca^{2+} and are capable of being flushed out of the column if their size is not large enough for them to be trapped in pore throats. When the bacterial density is higher (OD_{600} = 1.0 compared with OD_{600} = 0.1), more bacterial aggregates tend to form. Bacterial aggregates were also observed during the injection of cementation solution in Columns 2, 4 and 6 (see **Figure 8.7**), but were not observed in Columns 1, 3 and 5. Therefore, because of the adsorption of Ca^{2+} to the bacterial aggregates that were then flushed out from the soil matrix during injections, the amount of Ca^{2+} that remained in the soil columns decreased, thus reducing $CaCO_3$ content and transformation efficiency after MICP treatment.

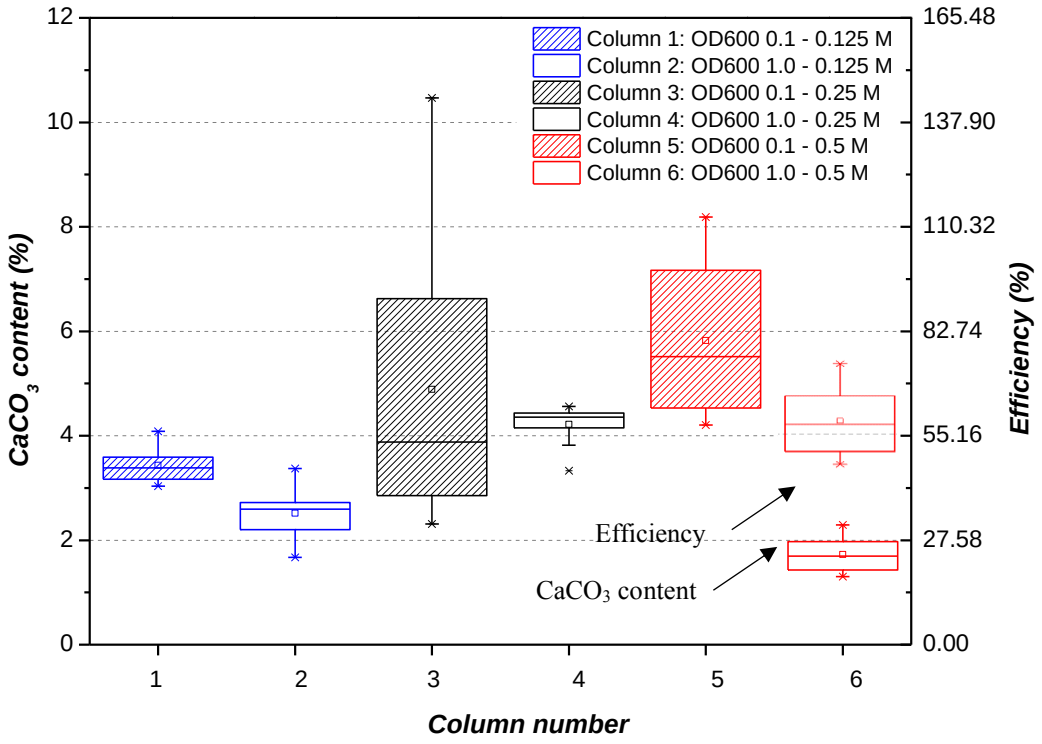

Figure 8.6 Box plots of $CaCO_3$ content and transformation efficiency. The square dot inside the box is the mean value; the line inside the box is the median value; the other lines are the lower quartile (25th percentile) and upper quartile (75th percentile); the height of the box (difference between the lower and upper quartile) being referred to as the interquartile range (IQR)

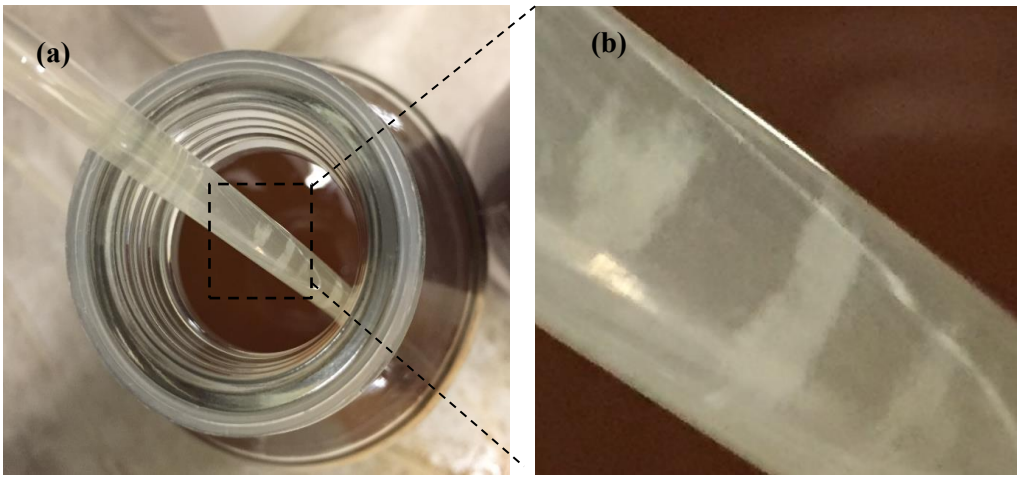

Figure 8.7 Bacterial aggregates in the outflow of Column 4. (**a**) the outflow tube and outflow container; (**b**) magnified image of the square shown in (**a**)

When the bacterial density was 1.0, compared with the other columns, the injection flow rate decreased substantially during the second injection of cementation solution in Column 6, in which the concentration of cementation solution used was 0.50 M. This suggests that the column was clogged locally due to the formation of large bacterial aggregates. The glass slide experiment showed that the size of bacterial aggregates is affected by both the density of bacterial suspension and the concentration of cementation solution. When both the bacterial density and concentration of cementation solution are high (Column 6: OD_{600} 1.0-0.50 M), the bacterial aggregates are large and therefore can be trapped inside the column. This may explain the large reduction in the injection rate.

These results are consistent with the results obtained by Al Qabany and Soga (2013), who stated that inhomogeneity along the sand column samples is a result of localised clogging, especially when the concentration of cementation solution is high. It should be noted that the concentration of cementation solution that caused inhomogeneity was 1.0 M in Al Qabany and Soga (2013) while in this thesis project the concentration was 0.5 M. However, the sand columns in this experiment were much longer than the columns used by Al Qabany and Soga (2013), meaning that the bacterial aggregates had a longer distance to travel and accumulate during the injection of cementation solution, which might have caused the bacterial aggregates to become large enough to cause local clogging. However, since the effect of the concentration of cementation solution and the scale of experimental samples on the transport of bacterial

aggregates was not the focus of this study, further work related to this needs to be conducted to confirm whether this is indeed the case.

8.3.4 Distribution of strength and stiffness obtained from UCS tests

The soil columns were divided into around 10 pieces for UCS test. A typical tensile failure pattern appeared from top to bottom along the sample during the UCS tests (shown in **Figure 8.8a**), which was similar to previous observations made by van Paassen et al. (2010), Al Qabany et al. (2012) and Cheng et al. (2012). A typical stress-strain curve obtained from one of the UCS tests on the MICP-treated specimen is shown in **Figure 8.8b**. The unconfined compressive strength (UCS) value is defined as the highest stress value along stress-strain curve, and the stiffness (Young's modulus) is determined by calculating the slope of the loading curves at 50 % of maximum stress.

In **Figure 8.9a**, the UCS values of MICP-treated soils are plotted against the distances from the top of the soil columns at which these values were measured. The distribution of UCS values for each column is presented as box plots in **Figure 8.9b**. The trends observed here are similar to the trends observed for the distribution of $CaCO_3$ content along the soil columns. Higher average UCS values (higher than 600 kPa) were obtained in Columns 3, 4 and 5. Among these three columns, Column 4 was the most homogenous (less than 600 kPa difference between the highest and lowest UCS value) whilst it also had the lowest average UCS values (about 600 kPa); Columns 3 and 5 had higher average UCS values (800 kPa and 1300 kPa, respectively) with a higher range of UCS values (the difference between the highest and lowest UCS values was higher than 1800 kPa and 2200 kPa, respectively). Relatively good homogeneity in the distribution of UCS values was also obtained in Columns 1, 2 and 6, with the average UCS values of these three columns being relatively low (lower than 300 kPa) (**Figure 8.9 a**, **b)**. In general, higher UCS values were obtained closer to the injection point, whereas lower UCS values were obtained further closer to the outlet, even though occasionally the highest UCS value was obtained further away from the injection point, such as in Column 5.

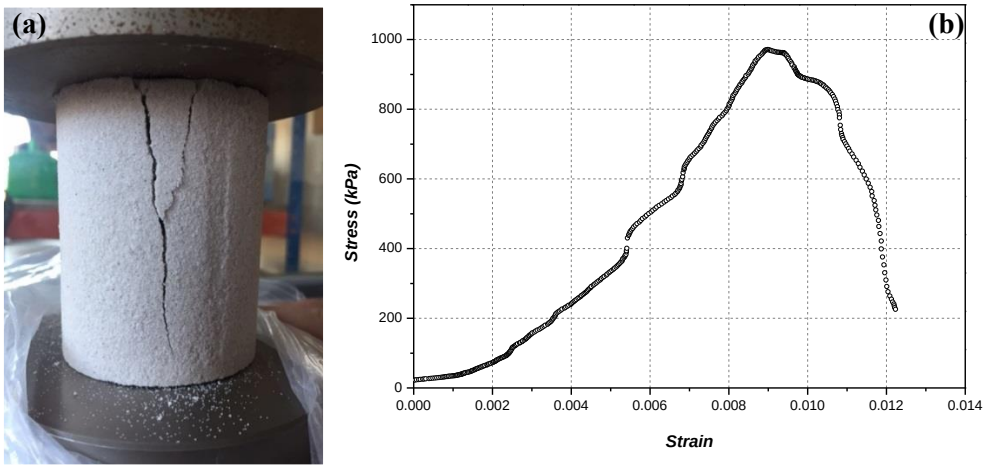

Figure 8.8 (a) Photo showing a typical tensile failure pattern during a UCS test; **(b)** Typical stress-strain curve of an unconfined compressive strength test. The elastic Young's modulus are derived from the slope of the tangent to the stress-strain curve at 50% of the maximum stress value reached

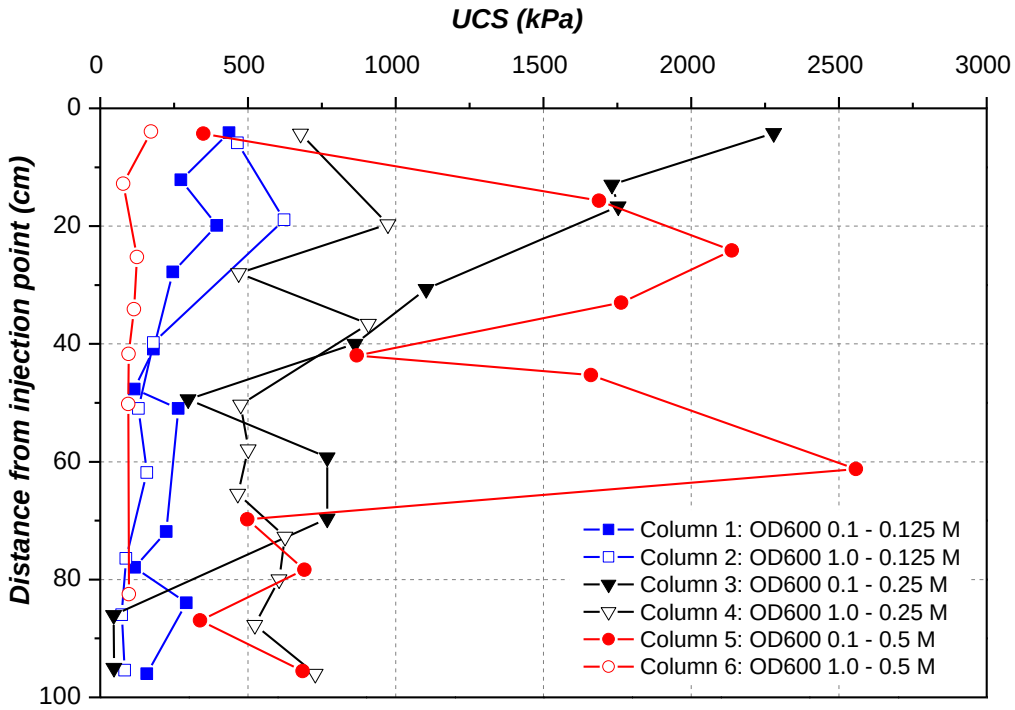

(a)

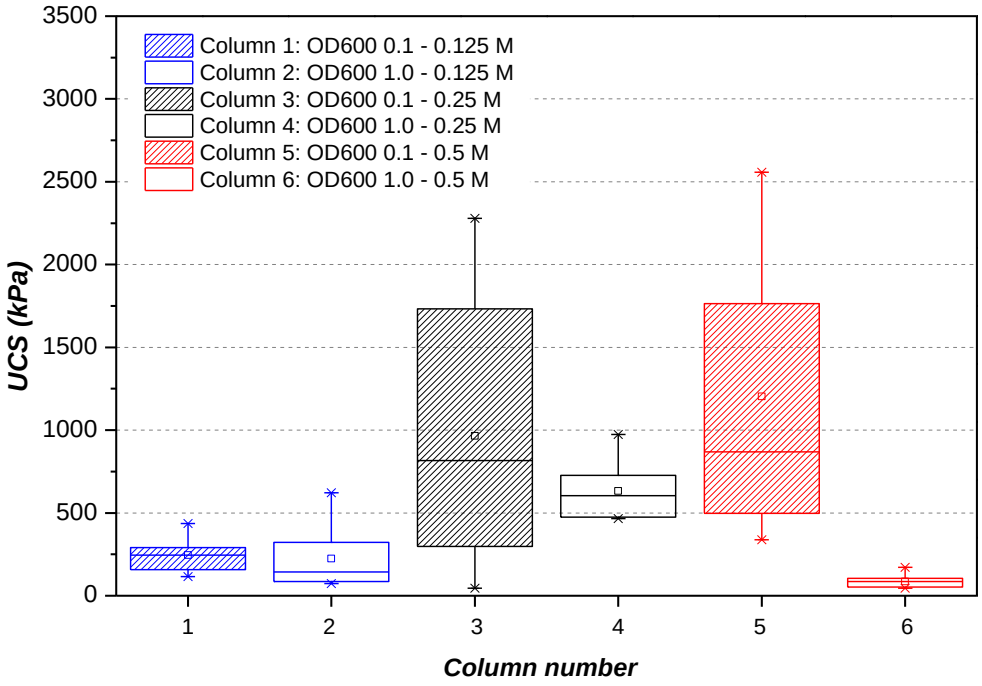

(b)

Figure 8.9 (**a**) Distribution of unconfined compressive strength (UCS) values along the length of each of the six soil columns; (**b**) box plots of UCS values of each sample

In **Figure 8.10a**, the stiffness of MICP-treated soils, expressed as elastic modulus values, is plotted against the distance from the top of the soil columns at which these values were measured. The distribution of stiffness values for each column being presented as box plots in **Figure 8.10b**. Similar to the trend in the average UCS values and the distribution of UCS values presented earlier, the highest average elastic modulus (stiffness, 1300 MPa) was obtained in Column 5, followed by the average elastic modulus of Column 3 (1000 MPa), which is higher than the average elastic modulus of Column 4 (700 MPa) (**Figure 8.10**). In addition, larger variations in the values of the elastic modulus (about 2300 MPa) were also observed in Columns 3 and 5. In comparison, the variation in the elastic modulus in Column 4 (about 500 MPa) is much smaller. Columns 1, 2, and 4 have good homogeneity in the elastic modulus (about 500 MPa), with the average elastic modulus of these three samples being around 250-300 MPa.

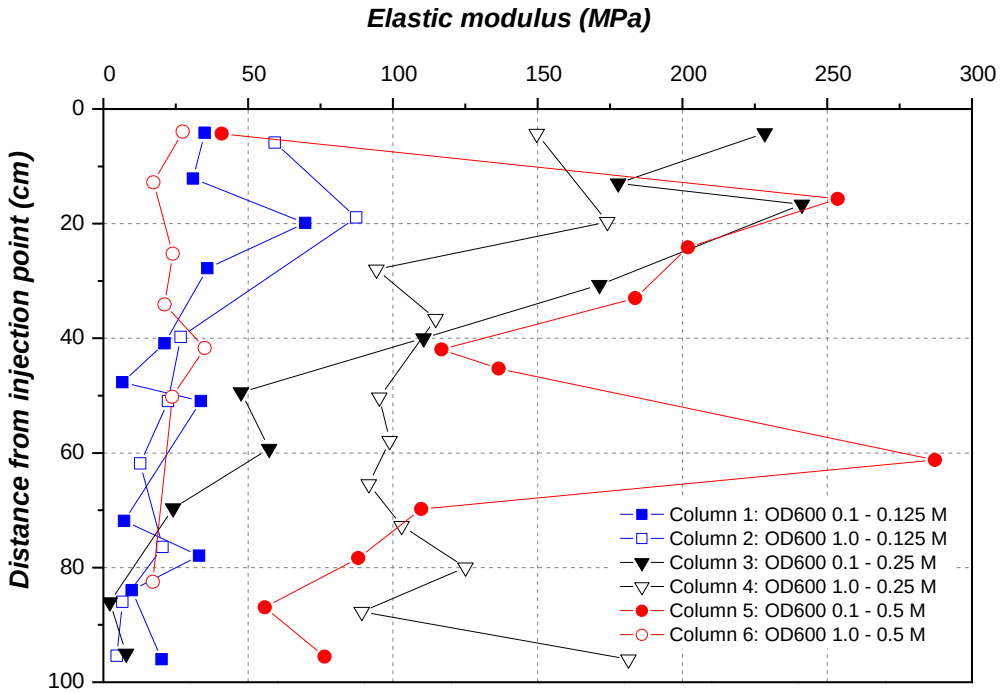

(a)

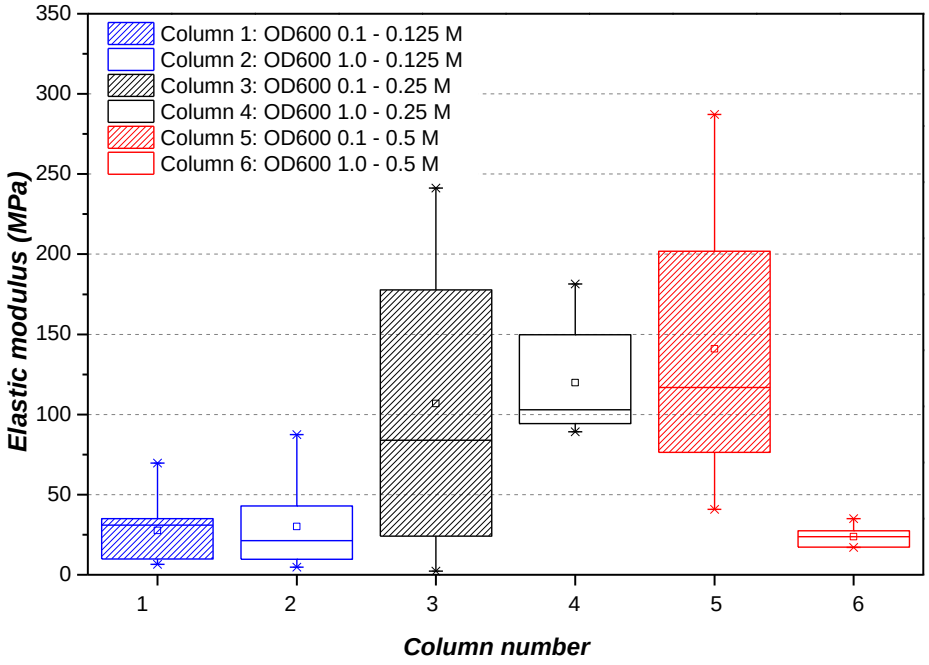

(b)

Figure 8.10 (a) distributions of elastic modulus; **(b)** box plot of elastic modulus

Research has shown that the unconfined compressive strength and stiffness of MICP-treated soils is not only affected by the $CaCO_3$ content (Whiffin et al., 2007; van Paassen et al., 2010;

Qabany and Soga, 2013; Cheng and Shahin, 2013; Zhao et al., 2014), but also affected by the microscale properties of $CaCO_3$ crystals (Qabany and Soga, 2013; Cheng and Shahin, 2013; Zhao et al., 2014). The effects of $CaCO_3$ content and $CaCO_3$ micro-scale properties on the mechanical performance of MICP-treated soils will be described in the next two sections.

8.3.5 Effects of $CaCO_3$ content on the mechanical performance of MICP-treated soils

To observe the effects of $CaCO_3$ content on the strength and stiffness of MICP-treated soils, the UCS (represents strength) and rigidity values (represents stiffness) of all the specimens obtained from the six soil columns were plotted against the $CaCO_3$ content (shown in **Figure 8.11)**. Rigidity is calculated according to the following equation:

$$Rigidity = Elastic\ modulus / UCS = 1/\varepsilon_f \quad 8.2$$

where ε_f is the axial strain at failure.

In general, UCS values increased with the increase in $CaCO_3$ content, with huge variations in UCS values being observed when the $CaCO_3$ content was the same, as shown in **Figure 8.11a**. This trend is consistent with several studies (such as Whiffin et al., 2007; van Paassen et al., 2010, Al Qabany and Soga, 2013; Cheng and Shahin, 2013; Zhao et al., 2014). When comparing the UCS-$CaCO_3$ content relations obtained from the six columns, it can be seen that Columns 3 and 5, which are treated with low bacterial densities and medium to high concentrations of cementations solution, have larger variations in $CaCO_3$ content and therefore, larger ranges in the UCS values. $CaCO_3$ contents that were higher than 6 % and UCS values that were higher than 1000 kPa were obtained from these two columns. The uniformity of $CaCO_3$ formation along the soil columns affect the uniformity of the mechanical performance of the MICP-treated soils. With the exception of three points circled in **Figure 8.11b**, and the points between the two lines in this figure, it can be seen that, when the $CaCO_3$ content is similar, the rigidity of the samples cemented using a bacterial suspension with an optical density of 1.0 is higher than that of the samples treated at a bacterial optical density of 0.1. Compared with the effects of bacterial density on the rigidity of MICP-treated sand, the effect of the concentration of cementation solution on rigidity is not very obvious.

As reviewed in *Chapter 2*, MICP treatment is a reactive transport process during which $CaCO_3$ may precipitate. As shown in *Chapters 4-6*, irregular-shaped $CaCO_3$ may form during the injection of cementation solution. The formation of irregular-shaped $CaCO_3$ delays the formation of $CaCO_3$ crystals which are formed with the dissolution of irregular-shaped $CaCO_3$. The solubility and morphology of the irregular-shaped $CaCO_3$ crystals are consistent with properties of amorphous phase $CaCO_3$ (ACC). During the injection of cementation solution, as long as the concentration of CO_3^{2-} and Ca^{2+} in the cementation solution is higher than the supersaturation state of ACC, the ACC tends to be stable. After the completion of the injection of cementation solution, the concentration of CO_3^{2-} and Ca^{2+} in the cementation solution may decrease due to the formation of crystals. When the concentration of CO_3^{2-} and Ca^{2+} drop below the supersaturation state of ACC, ACC crystals start to dissolve.

The ACC forms on bacterial aggregates whose size is affected by the concentration of cementation solution and the density of bacterial suspension. As shown in *Chapter 5*, ACC has been shown to be able to move with the flow, while the movement might be affected by the size of ACC crystals. If ACC is formed and the distribution of ACC is relatively homogenous, $CaCO_3$ is more likely to be uniformly distributed throughout the columns.

If no ACC is formed, the crystals might form directly and keep growing during the injection of cementation solution. As shown in *Chapter 4*, $CaCO_3$ crystals formed and kept growing during a procedure involving a continuous injection of cementation solution (6 PV for 1 hour). During the injection of cementation solution, more cementation solution flows past crystals located closer to the injection point compared to crystals located closer to the outlet. Therefore, if crystals continue to grow during the injection of cementation solution, the $CaCO_3$ content would be expected to be higher closer to the injection point and lower closer to the outlet, which would therefore result in a non-uniform distribution of $CaCO_3$ content and mechanical properties.

In this study, ACC was formed when the bacterial density was 1.0 (**Figure 8.7)**, but was not formed when the bacterial density was 0.1. Consistent with the hypothesis, the soil columns in which the bacterial density 1.0 were contained a relatively uniform distribution of $CaCO_3$ crystals after MICP treatment.

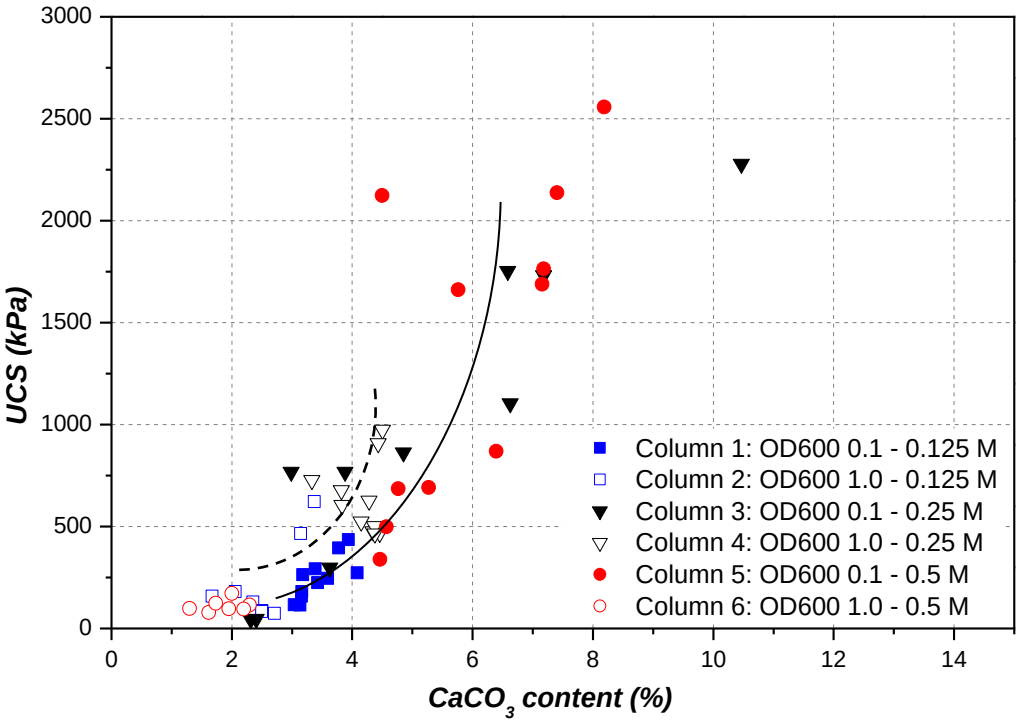

(a)

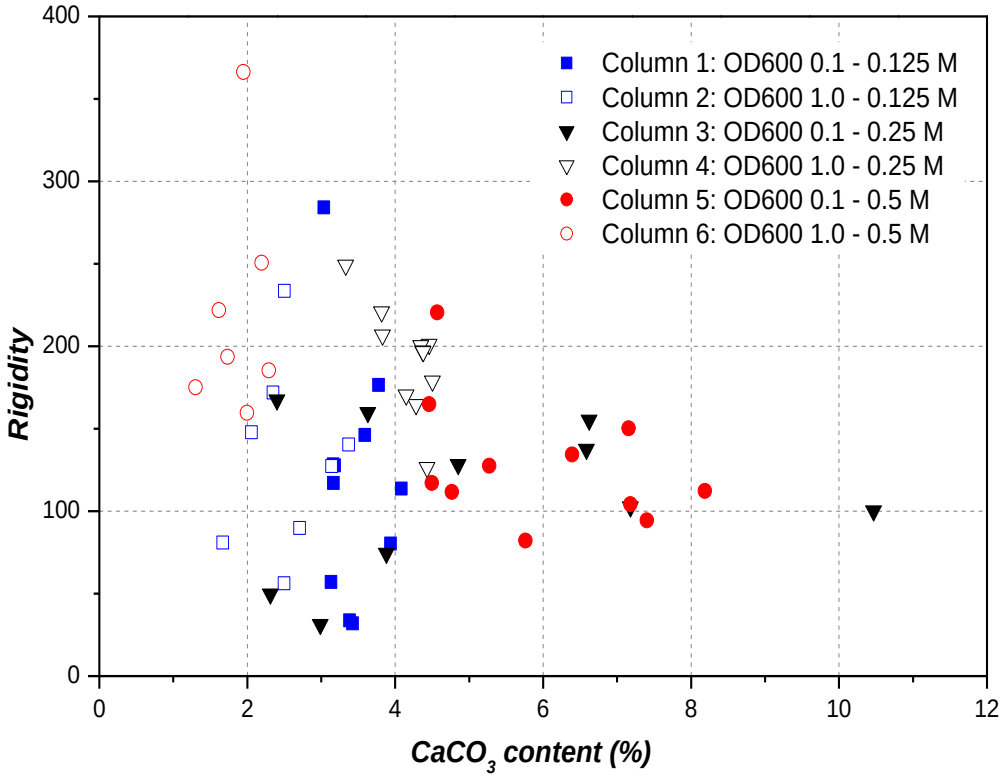

(b)

Figure 8.11 (a) UCS vs $CaCO_3$ Content; **(b)** $CaCO_3$ content vs rigidity (elastic modulus / UCS)

As shown in *Chapter 6*, the size and number of crystals formed are both affected by bacterial density. In addition, when the $CaCO_3$ content are the same, the size and number of crystals would affect the mechanical properties of MICP-treated sand. Therefore, to discuss the mechanical properties of the MICP-treated soils in more detail, the performance efficiency of MICP (the stiffness of MICP-treated soil divided by the percentage of soil containing $CaCO_3$ content) is plotted against $CaCO_3$ content in **Figure 8.12a**, and the box plot of the performance of each columns is shown in **Figure 8.12b**. With the exception of three points circled in **Figure 8.12a**, when the $CaCO_3$ content was similar, the performance efficiency of the samples cemented at a bacterial optical density of 1.0 was higher than that of the samples treated at a bacterial optical density of 0.1.

It is also shown in **Figure 8.12b** that, apart from column 6, in which the injection amount of cementation solution was 60 % lower than the others, column 2 had higher average performance efficiency than column 1, and column 4 had higher average performance efficiency than column 3. Comparisons between columns 1, 3 and 5, where the samples were treated at a bacterial density of 0.1, suggest that a higher concentration of cementation solution results in a higher the average performance efficiency (**Figure 8.12b)**. Similarly, when comparing columns 2, 4 and 6 where the samples were treated a bacterial density of 1.0, again apart from column 6, the highest average performance efficiency was obtained in Column 4, where the concentration of cementation solution was 0.25 M, which is higher than that in column 3 (0.125 M) (**Figure 8.12b)**.

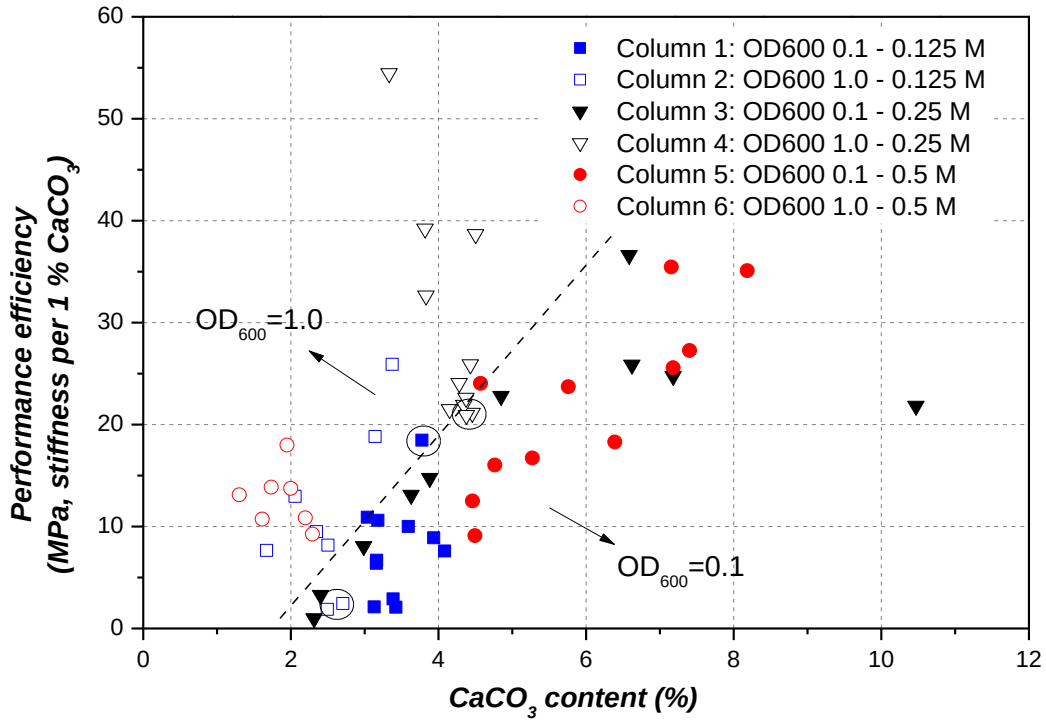

(a)

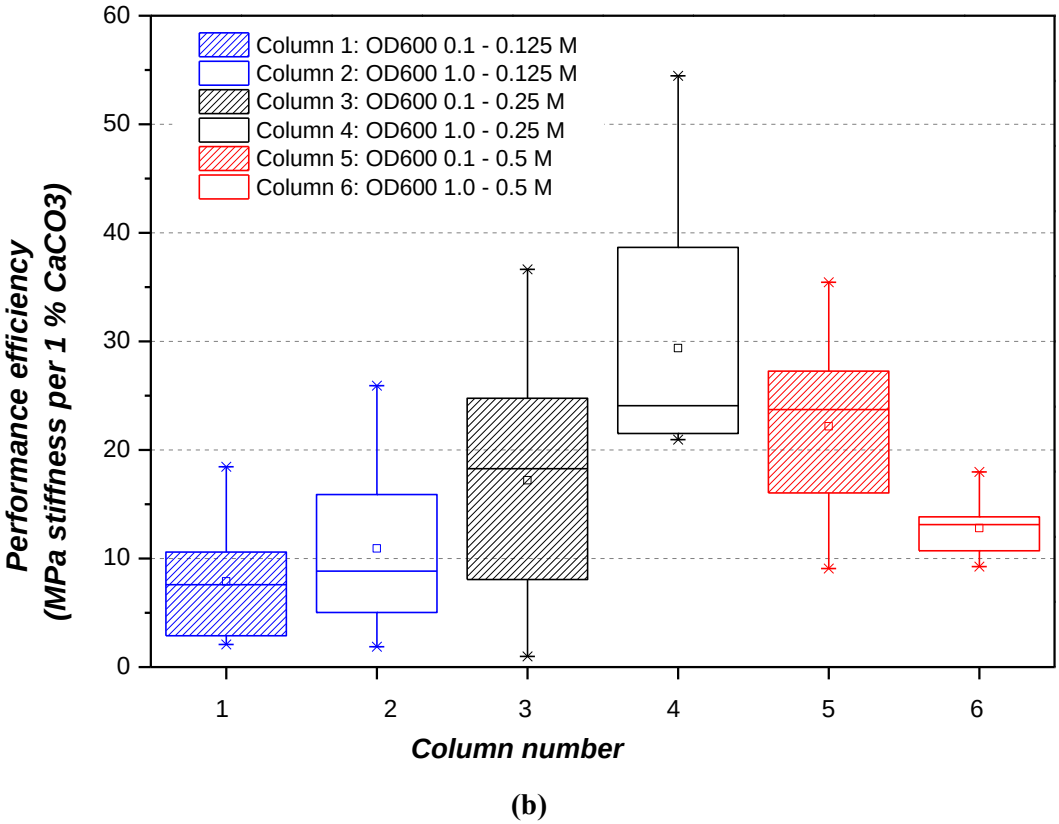

(b)

Figure 8.12 (a) $CaCO_3$ content vs performance efficiency; **(b)** box plots of performance efficiency

The above-mentioned results suggest that the $CaCO_3$ formed when the bacterial density was 1.0 (compared with being 0.1) or when the concentration of cementation solution was higher are more likely to be more efficient in increasing the stiffness of MICP-treated soil. However, this does not mean that, the higher the bacterial density is and/or the higher the concentration of cementation solution is, the better the stiffness becomes. This is because when the bacterial density was 1.0, the concentration of cementation being high (0.5 M) caused clogging and became difficult to be injected further after 2nd injection. Research has suggested that crystals size, number and distribution all affect the efficiency of crystals in increasing the strength/stiffness of MICP-treated soils. To further discuss the reason behind the difference in the performance efficiency, the microscale properties of the $CaCO_3$ crystals are discussed in the next section.

8.3.6 $CaCO_3$ crystal properties and the relationship between micro-scale and macro-scale properties

To investigate the micro-scale properties of $CaCO_3$ crystals, SEM images of three selected locations (close to the top, in the middle and towards the bottom) along the six MICP-treated sand column samples are shown in **Figure 8.13**. Box plots showing the variation in crystal sizes obtained from nine images taken at top, middle and bottom of each of the columns, including the three images shown in **Figure 8.13,** are presented in **Figure 8.14**. The crystal size varied from column to column and from top to bottom within the same column. The crystal sizes in Column 1 were larger than those in Column 2. Similarly, crystals were larger in Column 3 than in Column 4, and were larger in Column 5 compared to Column 6. When the concentration of cementation solution was the same, a higher bacterial density resulted in the formation of smaller crystals. These results are consistent with the results obtained in the micro-scale experiment shown in *Chapter 6*. For Columns 1, 3, and 5, the average crystal size increased with the increase in the concentration of cementation solution. These results are consistent with the results obtained by Al Qabany et al., 2012.

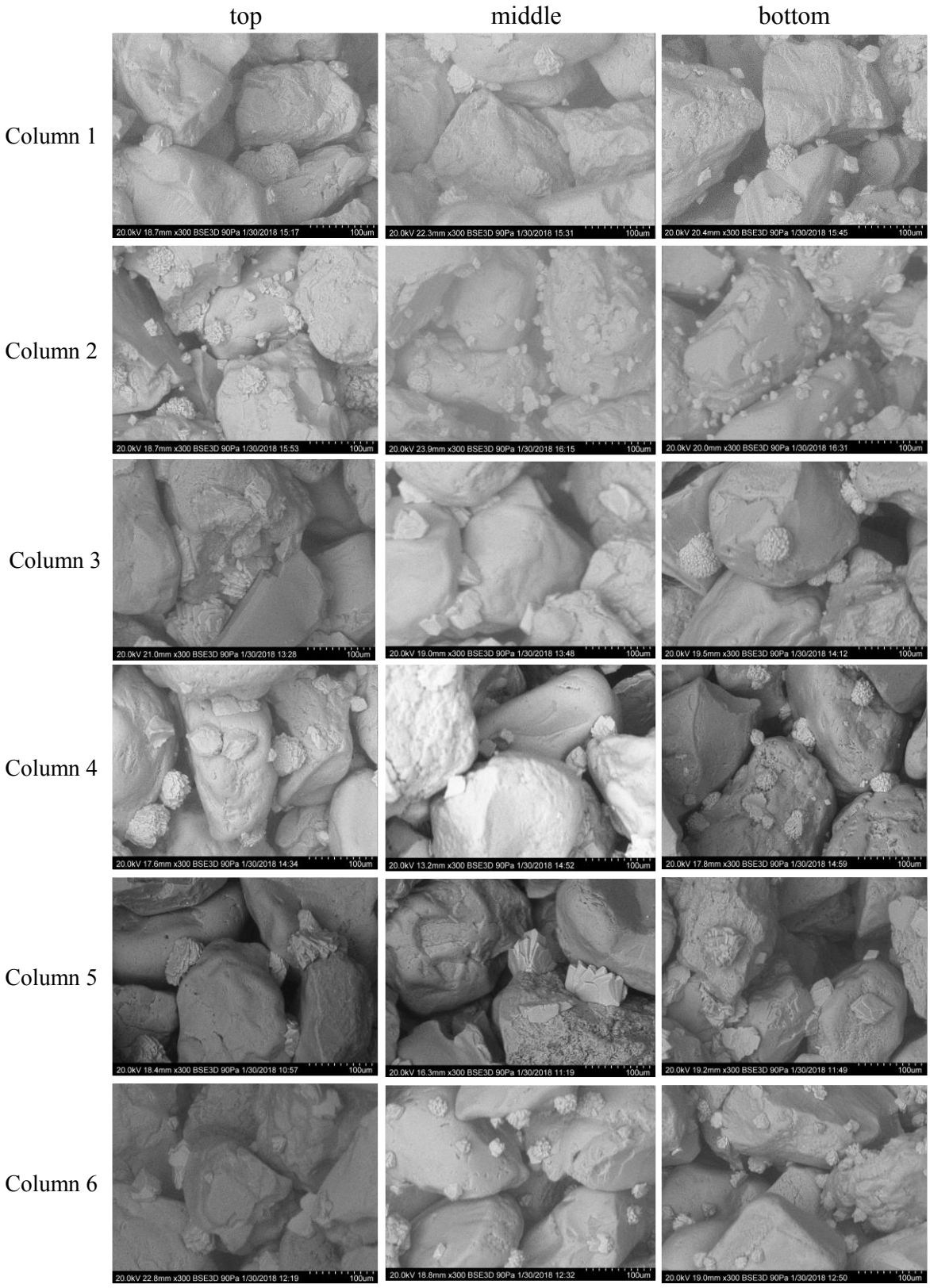

Figure 8.13 SEM images of samples obtained in the six columns at around top, middle and bottom along their length

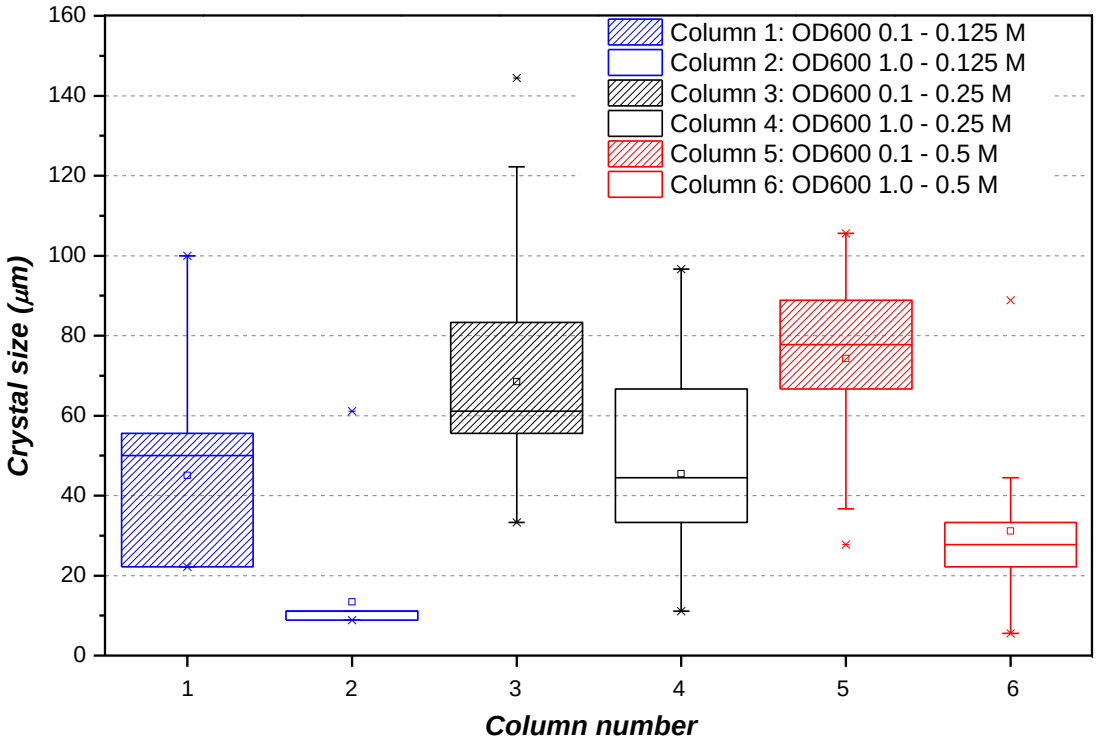

Figure 8.14 Box plots of crystals size. Data were obtained from nine images taken at top, middle and bottom of each of the columns

To investigate the effect of micro-scale properties of $CaCO_3$ crystals on the macro-scale properties of MICP-treated sand, the data associated with Columns 2, 3 and 4 were picked as examples to correlate the micro-scale properties of $CaCO_3$ crystals to the macro-scale mechanical properties of MICP-treated sandy specimens. The elastic modulus values of the soil specimen were normalized with respect to the average values of all of the six columns and are plotted against distance from the injection point (**Figure 8.16**). In the same figure, the efficiencies were also plotted against depths. SEM images of the samples are shown in the figure as well. Apart from one point tested, the stiffness values in Column 2 are all below average (**Figure 8.15**). It has been suggested that those crystals filling the gaps between the sand grains and forming effective bridges contribute to the pathway where the load transferred from particle to particle, and thus improve soil stiffness and strength (Martinez and DeJong, 2009). The crystals formed in Column 2 are small and cannot fill the gaps of between the sand grains, which consequently caused an overall low stiffness of the MICP-treated soils.

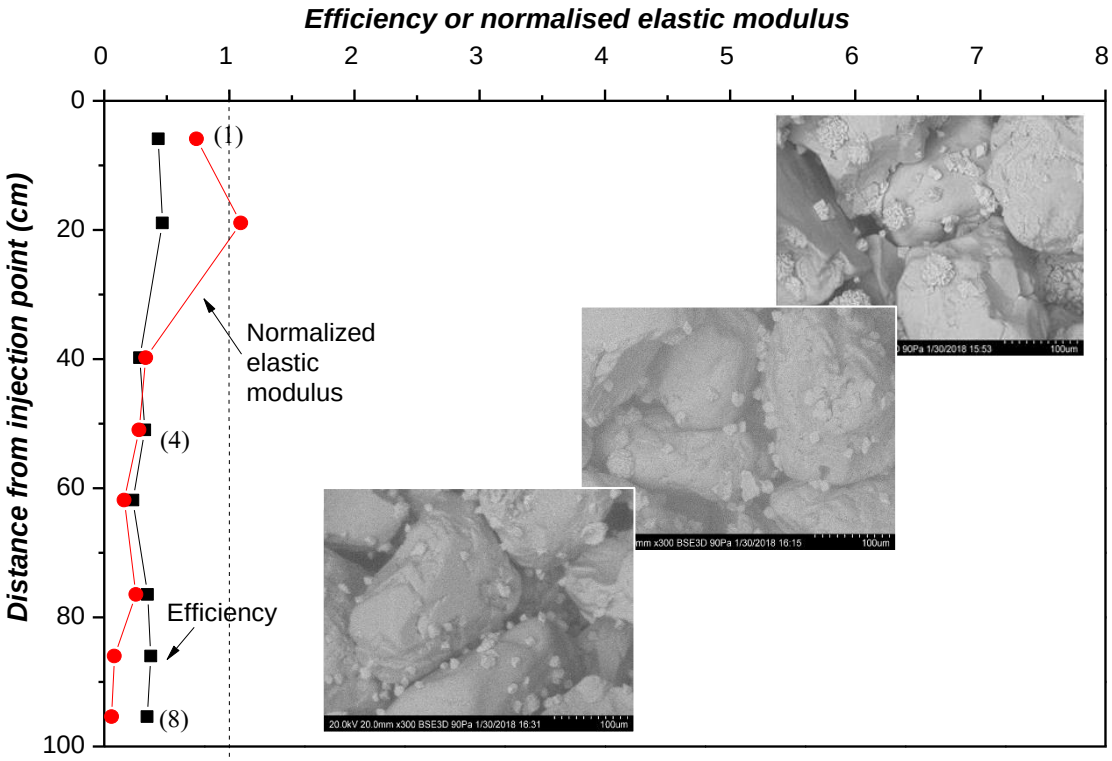

Figure 8.15 Effect of $CaCO_3$ crystals on the mechanical properties of MICP-treated sand, Column 2

The stiffness results for Column 3 are above average at the top (point 1), whilst being below average at the middle and bottom (points 7 and 11) (**Figure 8.16**). When looking at the SEM photos of the three points, the size of the crystals decreases from top to bottom, which correlates with the decrease in stiffness from top to bottom along the column. It has been stated that large crystals located at the gaps between the sand grains are deemed to be effective crystals which contribute the most to the strength gain of bio-cemented soils (Cheng et al., 2017). Similarly, in this study, the large crystals contribute the increase in stiffness.

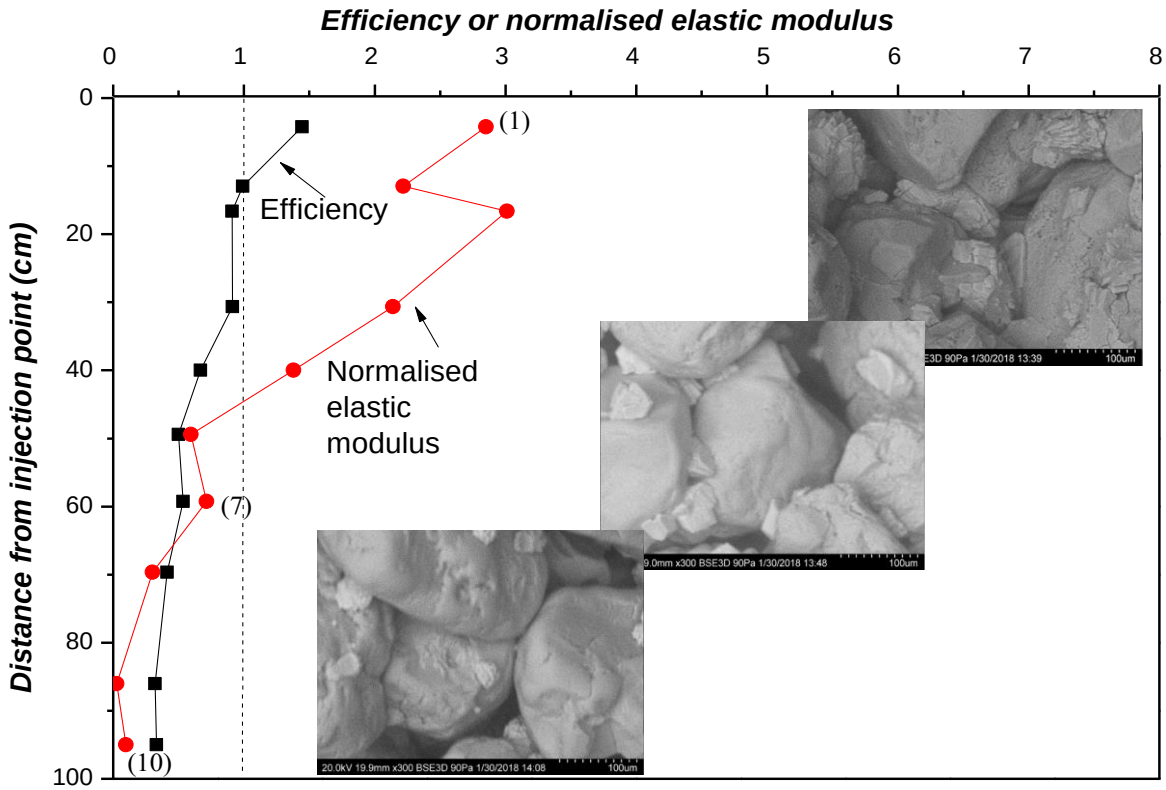

Figure 8.16 Effect of $CaCO_3$ crystals on the mechanical properties of MICP-treated sand, Column 3

The stiffness values in Column 4 were all above average (**Figure 8.17**). Compared with Column 3, the crystals are smaller, but larger in number. Compared with Column 2, the crystals are larger in size but smaller in number. It is shown in **Figure 8.12b** that the performance efficiency of Column 4 is higher than both Columns 2 and 3.

Previous work has shown that the efficiency (strength per mass of $CaCO_3$) of larger calcite crystals precipitated at the gaps between the sand grains is higher than the efficiency obtained from smaller crystals being randomly precipitated throughout the sand matrix (Cheng et al., 2017). Consistent with this study, considering together with the results shown in **Figure 8.12b**, this thesis study suggests that the crystals that bond soil particles should be large enough to sufficiently increase the mechanical performance of MICP-treated soils (Column 3 compared with 2), but once they are large enough, further increase in crystals size might decrease performance efficiency. This might be because although larger crystals are more likely to sufficiently bond soil particles, for the same amount of $CaCO_3$, the larger crystal size would

result in the smaller crystal number. If the number of crystals is much smaller than the number of contacts between soil particles, even though big crystals can sufficiently bond soil particles at some contacts, there would be not enough crystals available to bond all the soil particles together, thus resulting in an overall lower performance efficiency. Therefore, there needs to be a balance between the size and number of crystals to maximize the performance efficiency of MICP-treated soils.

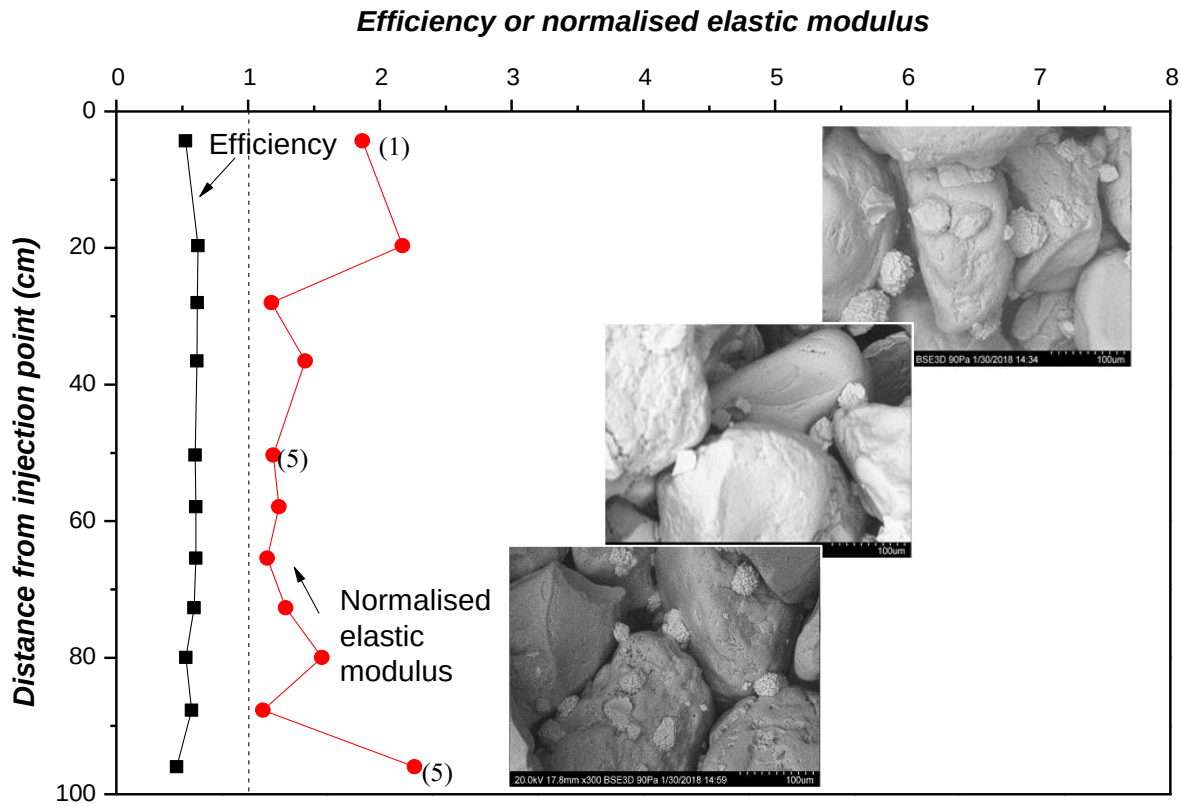

Figure 8.17 Effect of $CaCO_3$ crystals on the mechanical properties of MICP-treated sand, Column 4

8.4 Implications for engineering applications

The findings from this study show that different micro-scale distributions of $CaCO_3$ precipitation that form as a result of using different bacterial densities and different concentrations of cementation solution affect the macro-scale strength, stiffness, efficiency, and homogeneity of MICP-treated soils. This finding potentially has implications for how MICP could be applied in engineering practice.

A bacterial optical density OD_{600} of 1.0 resulted in the precipitation of calcium carbonate crystals with a similar size along the length of the column together with homogeneous carbonate precipitation, but with weaker efficiency, stiffness and UCS values. A bacterial optical density OD_{600} of 0.1 resulted in the precipitation of calcium carbonate crystals with a larger variation in size, with crystals located closer to the injection point being larger and those located closer to the outlet of the column, being smaller. In this case the crystals were less homogeneous overall but the MICP-treated soils had higher efficiency, stiffness and UCS values.

When the OD_{600} of the bacterial suspension was 1.0, the cementation solution with a concentration of 0.5 M could only be injected twice, which was due to the large bacterial aggregates causing clogging during the injection. However, when bacterial optical density was 1.0, a cementation solution with a concentration of 0.125 M could be injected 20 times, with the resulting efficiency being low. This might be because the bacterial aggregates were small in size and could not be trapped inside the column, therefore being flushed out together with Ca^{2+} that formed on the bacterial aggregates. For field applications that require an increase in homogeneity, a bacterial suspension with an OD_{600} of 1.0, and cementation solution with a concentration of 0.25 M could therefore be used.

To achieve the same amount of calcium carbonate precipitation, a greater number of injections would be required when a solution with a lower concentration of chemicals is used. However, for practical reasons, the number of injections should preferably be minimised. One possible approach that could be examined is to start with a 0.25 M solution for an initial homogeneous distribution of precipitation, then increase the chemical concentration of the solution to 0.5 M or 1.0 M in order to reduce the subsequent number of injections. Such an approach could be applicable, yet further research is needed to prove its effectiveness.

8.5 Conclusions

The results presented in *Chapter 5* showed that bacteria aggregated in response to the presence of calcium chloride in the cementation solution, and the results in *Chapter 6* showed that the

size of $CaCO_3$ crystals at the pore scale was affected by the bacterial density used to induce MICP. Following the micro-scale experiment, a macro-scale experiment on one-meter soil columns were then conducted to investigate the effects of bacterial number and concentration of cementation solution on the engineering properties and homogeneity of MICP-treated soils. The main findings are summarised as follows.

Results of microscopic glass slide experiments show that both bacterial density and the concentration of cementation solution affect the size of bacterial aggregates. When the bacterial density was 1.0 M (0.5 M in the mixture of bacterial density and cementation solution) and the concentration of cementation solution was increased from 0.5 M (0.25 M in the mixture) to 1.0 M (0.5 M in the mixture), the average size of bacterial aggregates increased by a factor of higher than two. When the concentration of cementation solution was 1.0 M (0.5 M in the mixture), the average size of bacterial aggregates increased as the bacterial density increased from OD_{600} of 0.1 to 3.0.

Results show that the distribution of $CaCO_3$ content, as well as the distribution of strength and stiffness of MICP-treated soil columns were more homogenous when the bacterial density used was 1.0 M compared with 0.1 M. Additionally, when the optical density (OD_{600}) of bacterial suspension was 1.0, a lower concentration of cementation solution (0.25 M) resulted in higher strength and stiffness of MICP-treated specimens. When the concentration of cementation solution was 0.5 M, a large reduction in injection flow rate occurred after only two injections of cementation solution. This suggests that some of the pores within the soil columns which the chemical solution could access were reduced in size due to bacterial aggregates being formed together with adsorbed amorphous $CaCO_3$. When the concentration of cementation solution was 0.125 M, the efficiency of the MICP treatment was only 35 %, which was the lowest amongst the six columns tested. This suggests that the size of bacterial aggregates and amorphous $CaCO_3$ were too small to be trapped inside the soil columns, resulting in them being flushed out during the injection of cementation solution, thus reducing the chemical efficiency of MICP treatment.

When a bacterial density OD_{600} of 0.1 was used, larger crystals precipitated closer to the top of the columns and bonded the sandy soil particles, thus increasing the strength and stiffness of

the soil. By contrast, smaller crystals were produced closer to the bottom of the column and were therefore not as efficient in increasing the strength and stiffness of the soils. Therefore, the treatment homogeneity of the columns was lower than when a bacterial suspension with an OD_{600} of 1.0 was used. Larger crystals which formed closer to the top of the columns decreased in size as the depth of the column increased, possibly because there were fewer bacterial cells at the top than at the bottom due to the accumulation of bacteria at the bottom of the column with flow. However, when the bacterial density was 1.0, the bacterial aggregates formed in the column can help to fix bacterial cells throughout the whole length of the column. Further research needs to be conducted to investigate the transport of bacterial cells and aggregates.

Chapter 9 General conclusions and recommendations for further work

9.1 Summary of findings and implications

In this PhD research project, both micro-scale and macro-scale experiments were conducted to develop a better understanding of the fundamental mechanisms of MICP at the micro-scale, which can be applied to improve the engineering properties including both mechanical properties and the uniformity of MICP-treated soils at the macro-scale.

At the micro-scale, *Chapter 4* describes the design and fabrication of a microfluidic chip to model a sandy soil specimen and to study MICP under conditions which mimic fluid flow through soil matrices. The utility of the microfluidic chip in characterising the micro-scale properties of MICP, including the quantification of bacteria and the sizes and shapes of $CaCO_3$ crystals, was also investigated. In *Chapter 5*, micro-scale experiments were conducted to improve insights into the effects of bacterial cells/aggregates on $CaCO_3$ precipitation and the changes in shape and size of the $CaCO_3$ precipitates during the MICP process under real MICP conditions. *Chapter 6* presented a quantitative study which investigated the effects of bacterial density on both the growth kinetics and characteristics of $CaCO_3$ during MICP. At the macro-scale, the effects of the interval between cementation solution injections on the micro-scale properties of $CaCO_3$ crystals such as size and number, as well as the effects on the strength of MICP-treated sand, were investigated, with the results presented in *Chapter 7*. In *Chapter 8*, a macro-scale experimental study was performed by using one-metre-long soil columns to investigate the effects of bacterial density and concentration of cementation solution on the strength and homogeneity of MICP-treated soils.

These micro- and macro-scale experiments provided new insights into fundamental mechanisms of MICP such as the behaviour of both bacteria and $CaCO_3$ crystals and the effects of bacteria on $CaCO_3$ growth. In addition, this thesis study suggests possible ways in which MICP treatment protocols can be optimised to improve the mechanical properties and homogeneity of MICP-treated sand. The main findings and implications of this PhD study are summarised as follows.

9.1.1 A microfluidic chip is a useful tool to study the micro-scale mechanisms of MICP

This study revealed that the microfluidic chip is a useful tool to study the micro-scale mechanisms of MICP, including the behaviour of both bacteria and $CaCO_3$ crystals. The microfluidic chip designed in this study was based on a cross-sectional image of a solidified and sectioned sandy soil matrix to model its main features including shape, size and distribution of both soil particles and soil pores. By using the combination of transparent microfluidic chips and a phase-contrast microscope, this study revealed that bacterial cells and $CaCO_3$ crystals can be observed under a saturated condition at the particle-scale throughout the entire MICP processes, which has not been possible before.

9.1.2 Phase transformation of $CaCO_3$ during MICP processes

An important observation in this study was that when the bacterial density (OD_{600}) used was 1.0 or higher which is common in other MICP studies (Al Qabany et al., 2012; Feng and Montoya, 2015; Lin et al., 2017; Cheng et al., 2017; Cardoso et al., 2018), the phase transformation of $CaCO_3$ which occurred during MICP followed Ostwald's step rule. During this transformation process, irregular-shaped $CaCO_3$ precipitated at the beginning of the MICP process and subsequently dissolved at the expense of growth of spherical and rhombohedral $CaCO_3$ crystals. With time, spherical $CaCO_3$ crystals dissolved and re-precipitated as rhombohedral $CaCO_3$ crystals. The shapes, precipitation rates and stabilities of the irregular-shaped, spherical and rhombohedral $CaCO_3$ crystals are all consistent with those of the three main phases of $CaCO_3$ - ACC, vaterite and calcite. The transformation of these phases with time is consistent with Ostwald's step rule, which states that less stable phases of $CaCO_3$ form

quickly and first, after which they become transformed into more stable phases of $CaCO_3$ with time by dissolution and reprecipitation. This study provided the first direct observations which revealed that the phase transformation of $CaCO_3$ not only occurs during the chemical precipitation of $CaCO_3$ induced by chemicals such as $CaCl_2$ and Na_2CO_3 (Rodriguez-Blanco et al., 2011), but also occurs during MICP processes. These observations are important as they suggest that the phase transformation of $CaCO_3$ should be considered when designing MICP protocols as it affects the type, number and size of $CaCO_3$ crystals and thus the engineering properties of MICP-treated sand.

9.1.3 Aggregation of *S. pasteurii* during MICP processes

Another important observation in this study is that *S. pasteurii* cells aggregate after being mixed with cementation solution or after the injection of cementation solution during staged-injection procedures. In addition, this study showed that the sizes of bacterial aggregates are affected by both bacterial density and the concentration of cementation solution, with a higher bacterial density and concentration of cementation solution generally resulting in the formation of larger bacterial aggregates. This suggests that depending on the pore size and the flow rate, the size of bacterial aggregates may affect their transport through the soil matrix. This is because larger bacterial aggregates are more likely to become trapped within the soil matrix, which would prevent the transport of other bacteria and bacterial aggregates and may result in a heterogeneous distribution of bacteria and $CaCO_3$. However, as long as the bacterial aggregates are not too large, in which case they clog the soil pores, the bacterial aggregates helped bacteria to be retained inside the porous medium. Therefore, bacterial density and the concentration of cementation solution may affect both the distribution and amount of bacteria inside the soil matrix, which consequently affects the MICP process and $CaCO_3$ properties at the micro-scale and the uniformity and mechanical properties of MICP-treated sand at the macro-scale.

9.1.4 Bacterial density affects the kinetics of $CaCO_3$ crystal growth and the characteristics of $CaCO_3$ formed during MICP

Another key finding of this study was that bacterial density affects both the kinetics of $CaCO_3$ growth and the characteristics of $CaCO_3$ formed during MICP. Although the effects of bacterial

density on the precipitation rate of $CaCO_3$ have previously been investigated indirectly in batch test conditions by measuring the change in Ca^{2+} concentration with time in the liquid (Ferris et al., 2003), the effects of bacterial density on the changes in crystals number and size could not be investigated using this method. This PhD study provided the first direct micro-scale observations of the effects of bacterial density on the kinetics of $CaCO_3$ crystal growth. Direct real-time observations of crystal growth revealed that the number of crystals formed increased as the bacterial density was increased from 5×10^7 to 5×10^8 cells per ml, while each of the crystals grew at the same rate. Therefore, when the crystals are given sufficient time to grow and when the concentration and volume of the injected cementation solution are kept constant, a lower bacterial density produces fewer but larger crystals and vice versa. This observation suggests that a lower bacterial density could be useful for treating sand containing large particles, which has so far been a challenge for MICP applications. Assuming two types of sand have the same particle shape, surface properties, and packing level, larger sand particles would result in a smaller number of particle contacts but with larger gaps between the particles. Therefore, fewer but larger $CaCO_3$ crystals would be required to bond the soil particles together in this case. However, it should be noted that when the bacterial density is low, maintaining bacterial activity might be a problem. For example, as shown in **Figure 6.11a,** crystal size did not increase from the 9^{th} to the 12^{th} injection of cementation solution, which might be because the bacterial activity was not high enough to maintain the precipitation.

9.1.5 Strength of MICP-treated sand can be enhanced by increasing the intervals between cementation solution injections

Following the improved understanding of the phase transformation of $CaCO_3$ during the MICP process at the micro-scale, the interval between cementation solution injections was found to have an effect on the number and size of the $CaCO_3$ crystals, as well as on the strength of MICP-treated sand. This study found that a larger number (200 - 1000 per 10^6 μm^3) of small crystals (5 - 10 μm) were produced when the interval was 4 hours, whereas the crystals were larger (10 - 80 μm) and fewer in number (5 - 20 per 10^6 μm^3) when the interval was 24 hours. At the micro-scale, the strength of MICP-treated soils increased by 200 % when the total duration of the injection protocol was 12 days compared to 3 days.

9.1.6 Homogeneity of MICP-treated sand can be improved by optimising bacterial density and the concentration of cementation solution

Macro-scale experiments performed using one-metre long soil columns revealed that the homogeneity of MICP-treated sand can be improved by optimising bacterial density and the concentration of cementation solution used. It was found that the treatment homogeneity of the columns in terms of both mechanical properties and $CaCO_3$ concentration was higher when a bacterial suspension with an OD_{600} of 1.0 was used compared to a bacterial suspension with an OD_{600} of 0.1. Together with the observations of crystals properties along the length of the columns, these observations are consistent with the hypothesis of this study that an optimised bacterial density and concentration of cementation solution can help fix bacteria inside the soil column and create a uniform distribution of bacteria. When a bacterial density OD_{600} of 0.1 was used, larger crystals precipitated closer to the top (inlet) of the columns, while smaller crystals were produced closer to the bottom (outlet) of the column, possibly because there were fewer bacterial cells at the top than at the bottom due to the accumulation of bacteria at the bottom of the column with flow. However, when an OD_{600} of 1.0 was used and the size of the bacterial aggregates was moderate, bacteria distributed along the whole length of the column. This might be because fewer bacteria accumulated at the bottom of the column with flow as some of the aggregates became trapped between the sand particles further towards the top of the column.

In addition, when the bacterial density was 1.0, a large reduction in injection flow rate occurred after only two injections of cementation solution when the concentration of cementation solution was 0.5 M, which is also consistent with the hypothesis that large bacterial aggregates cause local clogging and impede flow. When the concentration of cementation solution was 0.125 M, the efficiency of MICP treatment was only 35 %, which was the lowest amongst the six columns tested. This suggests that the size of bacterial aggregates and amorphous $CaCO_3$ crystals were too small to be trapped inside the soil columns, resulting in them being flushed out during the injection of cementation solution, thus reducing the chemical efficiency of MICP treatment. A cementation solution with a concentration of 0.25 M resulted in a relatively high strength and stiffness of MICP-treated specimens.

These observations suggested that the combination of a moderate concentration of cementation solution and density of bacterial suspension can generate bacterial aggregates with moderate sizes, thereby helping to retain bacteria inside the soil column and resulting in a homogenous distribution of bacteria and $CaCO_3$ content. However, the optimal size of the bacterial aggregates required to treat different types of sand might be different. Further work to investigate the transport of bacterial aggregates in porous media with different pore parameters, such as the size of the pores and pore throats, might aid the development of optimised MICP treatment protocols for treating different types of sands.

9.1.7 Implications for applications

The results of the micro-scale to macro-scale experiments conducted in this PhD study suggest that the micro-scale MICP processes greatly affect the micro-scale properties of $CaCO_3$ formed such as size and number of $CaCO_3$ crystals. In turn, this affects the macro-scale engineering properties of MICP-treated sand, such as strength, permeability and uniformity. Micro-scale MICP processes involve time-dependent precipitation of $CaCO_3$, including the possibility of formation of $CaCO_3$ polymorphs and phase transformation, which are highly affected by bacterial density, concentration of cementation solution, as well as by the interval between injections and the number of cementation solution injections used.

Based on the results of this study, for engineering practice it is suggested that a combination of OD_{600} of 1.0, bacterial activity of 200-300 mM/h, concentration of cementation solution of 0.25 M and injection Darcy flow velocity of about 3×10^{-4} m/s can produce relatively uniform one metre columns of MICP-treated silica sand with size of d_{50} 160 μm and d_{90} 250 μm, and compaction of 95% of maximum dry density. To increase the strength of the MICP-treated sand under these conditions, the results of this thesis study suggest that the injection interval should be 24 hours, even though the chemical efficiency can be higher than 80% when the injection interval is three hours. The reason behind this is because the phase transformation coupled with a longer injection interval can produce larger and more stable $CaCO_3$ crystals, thereby increasing the strength of MICP-treated sand. The UCS of the sand obtained when 10 injections of cementation solution were applied was 500 to 1000 kPa. If a higher UCS is needed, the number of cementation solution injections can be increased accordingly. If this

process was to be scaled up for a field trial, similar conclusions might be expected, but conditions might need to be altered due to the impact of outdoor temperatures, soil properties, and native bacteria.

9.2 Recommendations for further work

- **Improve microfluidic porous medium from 2-D to 3-D**

The microfluidic chip designed and fabricated in this PhD project enabled the study of the fundamental mechanisms of MICP including the behaviour of both bacteria and $CaCO_3$, and has shed new light on the process and the kinetics of MICP. The improved understanding obtained from the micro-scale experiments was helpful for optimising MICP protocols at the macro-scale in order to improve the strength and uniformity of MICP-treated soils. However, even though the current design of the microfluidic chip can represent the main features of a soil matrix such as the surface properties of the soil particles, the size and the distributions of the pore throats, the design is still a simplified version of a real three-dimensional soil matrix. Improving the design of a microfluidic chip by making it three-dimensional might help improve the understanding of the distribution of bacteria, bacterial aggregates and $CaCO_3$ crystals in real soils. This will further aid our understanding of how to predict where and how the $CaCO_3$ would bond the soil particles, which will consequently be helpful for designing more effective MICP protocols. However, the fabrication of a 3-D porous matrix, as well as the observation of bacteria and $CaCO_3$ in a 3-D porous matrix are still very challenging. The 3-D fabrication of the 3-D porous medium cannot be achieved using the fabrication procedure described in this study. Other techniques such as 3-D printing might therefore be worth considering. In addition, the observation of bacteria and crystals in the 3-D porous medium would be technically challenging, and would therefore require further exploration.

- **Explore the effects of surface properties and pore size on the MICP process and upscaling studies**

The properties of a soil matrix, such as size, shape and distribution of sand particles and pores, and the surface properties of the sand particles such as roughness and surface charge may affect

the transport, attachment and detachment of bacteria, which consequently affect the process and kinetics of MICP and the characteristics of the $CaCO_3$ crystals formed. As the geometric design of the porous medium of the microfluidic chip is flexible, the surface properties of the porous medium could be modified using certain chemical and physical surface treatment methods to simulate different types of sand. Micro-scale MICP experiments can be conducted using these different porous media to investigate the effects of sand type on MICP processes, and upscaling studies can be conducted accordingly to optimise MICP protocols.

- **Explore the effects of experimental factors such as temperature and oxygen levels on the MICP process at the micro-scale**

Many experimental factors such as temperature and oxygen level might affect the ureolysis activity of bacteria, which in turn affects the ureolysis rate and the process and kinetics of $CaCO_3$ precipitation. In addition, apart from the effect of bacteria, environmental factors such as temperature also affect $CaCO_3$ growth kinetics. The MICP process and kinetic studies were conducted in the lab at 20-25°C and normal room air conditions. When MICP is applied in real environments, the environmental temperature and oxygen level may vary, and their effects on the MICP process are still largely unknown. Therefore, it would be interesting to conduct further work to study the process and kinetics of $CaCO_3$ precipitation and the characteristics of $CaCO_3$ at different temperatures and oxygen levels.

- **Optimise the protocols for MICP applications such as clogging: from micro- to macro-scale**

Bacteria were found to aggregate when mixed with cementation solution, and the size of the aggregates is dependent on both the density of bacterial suspension and the concentration of cementation solution. Bacterial aggregates also occurred after the injection of cementation solution in a staged-injection procedure, during which bacterial suspension and cementation solution are injected into a soil matrix sequentially. The size of bacterial aggregates during the staged injections are smaller than in the mixtures of bacterial suspension and cementation solution where the densities of bacterial suspension and concentration of cementation are the same. This explains why the staged-injection procedure has been suggested to be more

effective at delivering bacterial suspension and cementation solution over longer distances compared with injecting the mixture of bacterial suspension and cementations solution. The staged-injection procedure is therefore a more effective injection protocol for soil stabilisation. However, for some other applications, such as for bio-clogging in a shallow zone, which requires the formation of a large amount of $CaCO_3$ crystals over a shorter period of time, a protocol involving the injection of a mixture of bacterial suspension and cementation solution might be preferable. Further work using the microfluidic chip and upscaling studies to investigate the suitability of different MICP treatment protocols for different applications might help improve the MICP design for applications beyond soil stabilisation, such as bio-clogging.

- **Explore the micro-scale MICP process involving bacterial strains other than *S. pasteurii***

The results presented in this thesis study showed that bacterial properties such as mobility, aggregation, attachment, detachment, and activity affect MICP processes. These properties may vary depending on the bacterial strain used in the experiments. In addition to *S. pasteurii*, many other types of bacteria have also been applied in MICP studies, especially for different applications of MICP. For example, the use of *Bacillus sphaericus* has been shown to result in a higher treatment efficiency compared to *S. pasteurii* for treating concrete surfaces. Furthermore, bacteria isolated from local environments might suit the local environmental conditions such as temperature, pH, pressure, and oxygen levels more than *S. pasteurii*. Further micro-scale experiments could therefore be performed to investigate MICP processes involving different bacterial strains for different MICP applications.

References

Achal, V., Mukerjee, A., & Sudhakara Reddy, M. (2013). Biogenic treatment improves the durability and remediates the cracks of concrete structures. Construction and Building Materials, 48, 1–5.

Al Qabany, A. (2011). Microbial Carbonate Precipitation in Soils. University of Cambridge.

Al Qabany, A., & Soga, K. (2013). Effect of chemical treatment used in MICP on engineering properties of cemented soils. Géotechnique, 63(4), 331–339.

Al Qabany, A., Soga, K., & Santamarina, C. (2012). Factors Affecting Efficiency of Microbially Induced Calcite Precipitation. Journal of Geotechnical and Geoenvironmental Engineering, 138(8), 992–1001.

Auset, M., & Keller, A. A. (2006). Pore-scale visualization of colloid straining and filtration in saturated porous media using micromodels. Water Resources Research, 42(12), 1–9.

Bang, S. S., Galinat, J. K., & Ramakrishnan, V. (2001). Calcite precipitation induced by polyurethane-immobilized Bacillus pasteurii. Enzyme and Microbial Technology, 28, 404–409.

Bang, S. S., Lippert, J. J., Yerra, U., Mulukutla, S., & Ramakrishnan, V. (2010). Microbial calcite, a bio-based smart nanomaterial in concrete remediation. International Journal of Smart and Nano Materials, 1(1), 28–39.

Berkowitz, B., & Zhou, J. (1996). Reactive solute transport in a single fracture. Water Resources Research, 32, 901–913.

Bodas, D., & Khan-Malek, C. (2007). Hydrophilization and hydrophobic recovery of PDMS by oxygen plasma and chemical treatment-An SEM investigation. Sensors and Actuators, B: Chemical, 123(1), 368–373.

Bots, P., Benning, L. G., Rodriguez-Blanco, J.-D., Roncal-Herrero, T., & Shaw, S. (2012). Mechanistic insights into the crystallization of amorphous calcium carbonate (ACC). Crystal Growth and Design, 12(7), 3806–3814.

Brečević, L., & Nielsen, A. E. (1989). Solubility of amorphous calcium carbonate. J. Cryst. Growth, 98, 504−510.

Burbank, M. B., Weaver, T. J., Green, T. L., Williams, B. C., & Crawford, R. L. (2011). Precipitation of calcite by indigenous microorganisms to strengthen liquefiablesoils. Geomicrobiology Journal, 28(4), 301–312.

Cardoso, R., Pires, I., Duarte, S. O. D., & Monteiro, G. A. (2018). Effects of clay's chemical interactions on biocementation. Applied Clay Science, 156, 96–103.

Carteret, C., Dandeu, A., Moussaoui, S., Muhr, H., Humbert, B., & Plasari, E. (2009). Polymorphism Studied by Lattice Phonon Raman Spectroscopy and Statistical Mixture Analysis Method. Application to Calcium Carbonate Polymorphs during Batch Crystallization. Crystal Growth and Design, 9(2), 807–812.

Chen, G., Hong, Y., & Walker, S. L. (2010). Colloidal and bacterial deposition: Role of gravity. Langmuir, 26(1), 314–319.

Cheng, L., & Cord-Ruwisch, R. (2012). In situ soil cementation with ureolytic bacteria by surface percolation. Ecological Engineering, 42, 64–72.

Cheng, L., Cord-Ruwisch, R., & Shahin, M. A. (2013). Cementation of sand soil by microbially induced calcite precipitation at various degrees of saturation. Canadian Geotechnical Journal, 50(1), 81–90.

Cheng, L., Shahin, M. A., & Mujah, D. (2017). Influence of Key Environmental Conditions on Microbially Induced Cementation for Soil Stabilization. Journal of Geotechnical and Geoenvironmental Engineering, 143(1), 04016083.

Chou, C.-W., Seagren, E. A., Aydilek, A. H., & Lai, M. (2011). Biocalcification of Sand through Ureolysis. Journal of Geotechnical and Geoenvironmental Engineering, 137(12), 1179–1189.

Chou, C.-W., Seagren, E., Aydilek, A. H., & Lai, M. (2011). Biocalcification of Sand through Ureolysis. Journal of Geotechnical and Geoenvironmental Engineering, 137(12), 1179–1189.

Cöelfen, H., & Antonietti, M. (2008). Mesocrystals and nonclassical crystallization. John Widley & Sons, Ltd.

Chu, D. H., Vinoba, M., Bhagiyalakshmi, M., Hyun Baek, I., Nam, S. C., Yoon, Y., & Jeong, S. K. (2013). CO_2 mineralization into different polymorphs of $CaCO_3$ using an aqueous-CO_2 system. RSC Advances, 3(44), 21722-21729.

Cuthbert, M. O., Riley, M. S., Handley-Sidhu, S., Renshaw, J. C., Tobler, D. J., Phoenix, V. R., & MacKay, R. (2012). Controls on the rate of ureolysis and the morphology of carbonate precipitated by S. Pasteurii biofilms and limits due to bacterial encapsulation. Ecological Engineering, 41, 32–40.

Dalas, E., Kallitsis, J., & Koutsoukos, P.G. (1988). The crystallization of calcium carbonate on polymeric substrates. Journal of Crystal Growth, 89(2-3): 287-294.

Dawoud, O. (2015). The Applicability of Microbially Induced Calcite Precipitation (MICP) for Soil Treatment. PhD Thesis, University of Cambridge.

Dawoud, O., Chen, C. Y., & Soga, K. (2014a). Microbial induced calcite precipitation for geotechnical and environmental applications. Proceedings of GeoShanghai International Congress.

Dawoud, O., Chen, C. Y., & Soga, K. (2014b). Microbial-induced calcite precipitation (MICP) using surfactants. Proc., Geo-Congress 2014 Technical Papers: Geo-Characterization and Modeling for Sustain- ability, M. Abu-Farsakh and L. R. Hoyos, eds., ASTM, Atlanta, 1635–1643.

De Muynck, W., Cox, K., Belie, N. De, & Verstraete, W. (2008). Bacterial carbonate precipitation as an alternative surface treatment for concrete. Construction and Building Materials, 22(5), 875–885.

De Muynck, W., De Belie, N., & Verstraete, W. (2010). Microbial carbonate precipitation in construction materials: A review. Ecological Engineering, 36(2), 118–136.

De Muynck, W., Leuridan, S., Van Loo, D., Verbeken, K., Cnudde, V., De Belie, N., & Verstraete, W. (2011). Influence of Pore Structure on the Effectiveness of a Biogenic Carbonate Surface Treatment for Limestone Conservation. Applied and Environmental Microbiology, 77(19), 6808–6820.

De Yoreo, J. J., Gilbert, P. U. P. A., Sommerdijk, N. A. J. M., Penn, R. L., Whitelam, S., Joester, D., & Dove, P. M. (2015). Crystallization by particle attachment in synthetic, biogenic, and geologic environments. Science, 349(6247).

DeJong, J. T., Fritzges, M. B., & Nüsslein, K. (2006). Microbially Induced Cementation to Control Sand Response to Undrained Shear. Journal of Geotechnical and Geoenvironmental Engineering, 132(11), 1381–1392

DeJong, J. T., Martinez, B. C., Ginn, T. R., Hunt, C., Major, D., & Tanyu, B. (2014). Development of a scaled repeated five-spot treatment model for examining microbial induced calcite precipitation feasibility in field applications. Geotechnical Testing Journal, 37(3), 424–435.

DeJong, J. T., Mortensen, B. M., Martinez, B. C., & Nelson, D. C. (2010). Bio-mediated soil improvement. Ecological Engineering, 36(2), 197–210.

DeJong, J. T., Soga, K., & Kavazanjian, E. (2013). Biogeochemical processes and geotechnical applications: progress, opportunities and challenges. Geotechnique, 63(4), 287–301.

Dhami, N. K., Reddy, M. S., & Mukherjee, A. (2013). Biomineralization of calcium carbonates and their engineered applications: a review. Frontiers in Microbiology, 4(October), 314.

Dijk, P., & Berkowitz, B. (1998). Precipitation and dissolution of reactive solutes in fractures. Water Resour Res. 34, 457–470.

Domenico, P. S., & Schwartz, F. W. (1998). Physical and chemical hydrogeology, 2nd ed. New York: Wiley.

Drescher, K., Shen, Y., Bassler, B. L., & Stone, H. A. (2013). Biofilm streamers cause catastrophic disruption offlow with consequences for environmental and medical systems. Proc. Natl. Acad. Sci. USA 110, 4345–50

Durham, W.M., Tranzer, O., Leombruni, A., & Stocker, R. (2012). Division by fluid incision: biofilm patch development in porous media. Phys. Fluids 24, 091107

Dunne, W. M. (2002). Bacterial Adhesion: Seen Any Good Biofilms Lately? Clinical Microbiology Reviews. 15(2), 155–166.

Dupraz, S., Parmentier, M., Ménez, B., & Guyot, F. (2009). Experimental and numerical modeling of bacterially induced pH increase and calcite precipitation in saline aquifers. Chemical Geology, 265(1–2), 44–53.

El Mountassir, G., Lunn, R. J., Moir, H., & MacLachlan, E. (2014). Hydrodynamic coupling in microbially mediated fracture mineralization: Formation of self-organized groundwater flow channels. Water Resources Research, 50 (1), 1–16.

Fauriel, S., & Laloui, L. (2012). A bio-chemo-hydro-mechanical model for microbially induced calcite precipitation in soils. Computers and Geotechnics, 46, 104–120.

Feng, K., & Montoya, B. M. (2015). Influence of confinement and cementation level on the behavior of microbial-induced calcite precipitated sands under monotonic drained loading. Journal of Geotechnical and Geoenvironmental Engineering, 2(Atcc 11859), 04015057.

Ferris, F. G., Phoenix, V., Fujita, Y., & Smith, R. W. (2003). Kinetics of calcite precipitation induced by ureolytic bacteria at 10 to 20 °C in artificial groundwater. Geochimica et Cosmochimica Acta, 67(8), 1701–1722.

Fujita, Y., Grant Ferris, F., Daniel Lawson, R., Colwell, F. S., & Smith, R. W. (2000). Calcium carbonate precipitation by ureolytic subsurface bacteria. Geomicrobiology Journal, 17(4), 305–318.

Fujita, Y., Taylor, J. L., Gresham, T. L. T., Delwiche, M. E., Colwell, F. S., Mcling, T. L., & Smith, R. W. (2008). Stimulation of microbial urea hydrolysis in groundwater to enhance calcite precipitation. Environmental Science &Technology, 42(8), 3025–3032.

Fujita, Y., Taylor, J. L., Wendt, L. M., Reed, D. W., & Smith, R. W. (2010). Evaluating the potential of native ureolytic microbes to remediate a 90Sr contaminated environment. Environmental Science &Technology, 44(19), 7652–7658.

Ganendra, G., De Muynck, W., Ho, A., Arvaniti, E. C., Hosseinkhani, B., Ramos, J. A., & Boon, N. (2014). Formate oxidation-driven calcium carbonate precipitation by Methylocystis parvus OBBP. Applied and Environmental Microbiology, 80(15), 4659–67.

Garrett, T. R., Bhakoo, M., & Zhang, Z. (2008). Bacterial adhesion and biofilms on surfaces. Progress in Natural Science, 18(9), 1049–1056.

Gebauer, D., Völkel, A., & Cölfen, H. (2008). Stable prenucleation calcium carbonate clusters. Science (New York, N.Y.), 322(5909), 1819–22.

Hammes, F., & Verstraete, W. (2002). Key roles of pH and calcium metabolism in microbial carbonate precipitation. Re/Views in Environmental Science & Bio/Technology 1, 1(Morita 1980), 3–7.

Harkes, M. P., van Paassen, L. A., Booster, J. L., Whiffin, V. S., & van Loosdrecht, M. C. M. (2010). Fixation and distribution of bacterial activity in sand to induce carbonate precipitation for ground reinforcement. Ecological Engineering, 36(2), 112–117.

Jaho, S., Athanasakou, G. D., Sygouni, V., Lioliou, M. G., Koutsoukos, P. G., & Paraskeva, C. A. (2015). Experimental Investigation of Calcium Carbonate Precipitation and Crystal Growth in One- and Two-Dimensional Porous Media. Crystal Growth & Design, acs.cgd.5b01321.

Jiang, N.-J., Soga, K., & Kuo, M. (2017). Microbially Induced Carbonate Precipitation for Seepage-Induced Internal Erosion Control in Sand–Clay Mixtures. Journal of Geotechnical and Geoenvironmental Engineering, 143(3), 04016100.

Joshi, S., Goyal, S., Mukherjee, A., & Reddy, M. S. (2017). Microbial healing of cracks in concrete: a review. Journal of Industrial Microbiology and Biotechnology, 44(11), 1511–1525.

Kawano, J., Shimobayashi, N., Kitamura, M., Shinoda, K., & Aikawa, N. (2002). Formation process of calcium carbonate from highly supersaturated solution. Journal of Crystal Growth, 237–239(1–4 I), 419–423.

Keykha, H. A., Zareian, M., Huat, B. B. K., Asadi, A., & Kawasaki, S. (2013). Electrokinetic properties of pasteurii and aquimarina bacteria, 1–8.

Kim, D., Chung, S., Sang-Hyup, L., & Choi, J. (2012). Relation of microbial biomass to counting units for Pseudomonas aeruginosa. African Journal of Microbiology Research, 6(21), 4620–4622.

Kim, H. K., Park, S. J., Han, J. I., & Lee, H. K. (2013). Microbially mediated calcium carbonate precipitation on normal and lightweight concrete. Construction and Building Materials, 38, 1073–1082.

Kralj, D., Brečević, L., & Nielsen, A. E. (1990). Vaterite growth and dissolution in aqueous solution I. Kinetics of crystal growth. Journal of Crystal Growth, 104(4), 793–800.

Kralj, D., Brecević, L., & Nielsen, A. E. (1994). Vaterite growth and dissolution in aqueous solution II. Kinetics of dissolution. Journal of Crystal Growth, 143(3–4), 269–276.

Kralj, D., Brecević, L., & Kontrec, J. (1997). Vaterite growth and dissolution in aqueous solution III. Kinetics of transformation. Journal of Crystal Growth, 177(3–4), 248–257.

Lanning, L. M., & Ford, R. M. (2002). Glass micromodel study of bacterial dispersion in spatially periodic porous networks. Biotechnology and Bioengineering, 78(5), 556–66.

Lasaga, A. C. (1998). Theory of Crystal Growth and Dissolution. Kinetic Theory in the Earth Sciences, 2, 581–712.

Lauchnor, E. G., Schultz, L. N., Bugni, S., Mitchell, A. C., Cunningham, A., Gerlach, R., & Sciences, E. (2013). Bacterially Induced Calcium Carbonate Precipitation and Strontium Co-Precipitation in a Porous Media Flow System. Environmental Science & Technology, 47, 1557–1564.

Lauchnor, E. G., Topp, D. M., Parker, A. E., & Gerlach, R. (2015). Whole cell kinetics of ureolysis by Sporosarcina pasteurii. Journal of Applied Microbiology, 118(6), 1321–1332.

Leclerc, E., Sakai, Y., & Fujii, T. (2003). Cell culture in 3-dimensional microfluidic structure of PDMS (polydimenthylsiloxane). Biomedical Microdevices, 5(2), 109–114.

Lecuyer, S., Rusconi, R., Shen, Y., Forsyth, A., Vlamakis, H., Kolter, R., & Stone, H. A. (2011). Shear stress increases the residence time of adhesion of Pseudomonas aeruginosa. Biophysical Journal, 100(2), 341–350.

Lian, B., Hu, Q., Chen, J., Ji, J., & Teng, H. H. (2006). Carbonate biomineralization induced by soil bacterium Bacillus megaterium. Geochim. Cosmochim. Acta, 70(22), 5522–5535.

Lin, H., Suleiman, M. T., Jabbour, H. M., & Brown, D. G. (2017). Bio-grouting to enhance axial pull-out response of pervious concrete ground improvement piles. Canadian Geotechnical Journal, 12(June), 1–12.

Liu, J., Ford, R. M., & Smith, J. A. (2011). Idling time of motile bacteria contributes to retardation and dispersion in sand porous medium. Environmental Science &Technology, 45(9), 3945–3951.

Long, Z., Nugent, E., Javer, A., Cicuta, P., Sclavi, B., Cosentino Lagomarsino, M., & Dorfman, K. D. (2013). Microfluidic chemostat for measuring single cell dynamics in bacteria. Lab on a Chip, 13(5), 947-954.

Mannik, J., Driessen, R., Galajda ,P., Keymer, J. E. & Dekker, C. (2009). Bacterial growth and motility in submicron constrictions. Proc. Natl. Acad. Sci. USA 106:14861–66.

Mitchell, J., & Santamarina, J. (2005). Biological considerations in geotechnical engineering. Journal of Geotechnical and, (October), 1222–1233.

Martin, D., Dodds, K., Ngwenya, B. T., Butler, I. B., & Elphick, S. C. (2012). Inhibition of sporosarcina pasteurii under anoxic conditions: Implications for subsurface carbonate precipitation and remediation via ureolysis. Environmental Science & Technology, 46(15), 8351–8355.

Martinez, B. C., DeJong, J. T., Ginn, T. R., Montoya, B. M., Barkouki, T. H., Hunt, C., & Major, D. (2013). Experimental Optimization of Microbial-Induced Carbonate Precipitation for Soil Improvement. Journal of Geotechnical and Geoenvironmental Engineering, 139(4), 587–598.

Mitchell, A. C., & Ferris, F. G. (2005). The coprecipitation of Sr into calcite precipitates induced by bacterial ureolysis in artificial groundwater: Temperature and kinetic dependence. Geochimica et Cosmochimica Acta, 69(17), 4199–4210.

Mitchell, A. C., & Ferris, F. G. (2006). The Influence of Bacillus pasteurii on the Nucleation and Growth of Calcium Carbonate. Geomicrobiology Journal, 23(November), 213–226.

Mitchell, A. C., Dideriksen, K., Spangler, L. H., Cunningham, A. B., & Gerlach, R. (2010). Microbially enhanced carbon capture and storage by mineral-trapping and solubility-trapping. Environmental Science & Technology, 44(13), 5270–5276.

Montoya, B., DeJong, J., & Boulanger, R. (2013). Dynamic response of liquefiable sand improved by microbial-induced calcite precipitation. Géotechnique, 63(4), 302–312.

Morse, J. W., Arvidson, R. S., & Lüttge, A. (2007). Calcium carbonate formation and dissolution. Chemical Reviews, 107(979), 342–381.

Mortensen, B. M., Haber, M. J., DeJong, J. T., Caslake, L. F., & Nelson, D. C. (2011). Effects of environmental factors on microbial induced calcium carbonate precipitation. Journal of Applied Microbiology, 111(2), 338–49.

Mujah, D., Shahin, M. A., & Cheng, L. (2017). State-of-the-Art Review of Biocementation by Microbially Induced Calcite Precipitation (MICP) for Soil Stabilization. Geomicrobiology Journal, 34(6), 524–537.

Mullin, J. W. (2001). Crystallization. Butterworth-Heinemannm, Oxford.

Ogino, T., Suzuki, T., & Sawada, K. (1987). The formation and transformation mechanism of calcium carbonate in water. Geochim. Cosmochim. Acta, 51(10), 2757–2767.

Omoregie, A. I., Khoshdelnezamiha, G., Senian, N., Ong, D. E. L., & Nissom, P. M. (2017). Experimental optimisation of various cultural conditions on urease activity for isolated Sporosarcina pasteurii strains and evaluation of their biocement potentials. Ecological Engineering, 109(September), 65–75.

Persat, A., Nadell, C. D., Kim, M. K., Ingremeau, F., Siryaporn, A., Drescher, K., & Stone, H. A. (2015). The mechanical world of bacteria. Cell, 161(5), 988–997.

Phillips, A. J., Gerlach, R., Lauchnor, E., Mitchell, A. C., Cunningham, A. B., & Spangler, L. (2013a). Engineered applications of ureolytic biomineralization: a review. Biofouling, 29(6), 715–33.

Phillips, A. J., Lauchnor, E., Eldring, J., Esposito, R., Mitchell, A. C., Gerlach, R., & Spangler, L. H. (2013b). Potential CO_2 leakage reduction through biofilm-induced calcium carbonate precipitation. Environmental Science & Technology, 47(1), 142–149.

Plummer, L. N. & Busenberg, G. E. (1982). The solubilities of calcite, aragonite and vaterite in CO_2–H_2O solutions between 0 and 90 °C and an evaluation of the aqueous model for the system $CaCO_3$–CO_2–H_2O. Geochimica et Cosmochimica Acta, 46, 1011–1040.

Rebata-Landa, V. (2007). Microbial Activity in Sediments: Effects on Soil Behavior. PhD Thesis, Georgia Institute of Technology.

Rodriguez-Blanco, H., Shen, Q., Zhao, Y., Wang, D. J., & Xu, D. F. (2003). Influence of polyvinylpyrrolidone on the precipitation of calcium carbonate and on the transformation of vaterite to calcite. Journal of Crystal Growth, 250 (3–4), 516–524.

Rodriguez-Blanco, J. D., Shaw, S., & Benning, L. G. (2011). The kinetics and mechanisms of amorphous calcium carbonate (ACC) crystallization to calcite, via vaterite. Nanoscale, 3(1), 265–271.

Rodriguez-Navarro, C., Jimenez-Lopez, C., Rodriguez-Navarro, A., Gonzalez-Muñoz, M. T., & Rodriguez-Gallego, M. (2007). Bacterially mediated mineralization of vaterite. Geochimica et Cosmochimica Acta, 71, No. 5, 1197–1213.

Rowshanbakht, K., Khamehchiyan, M., Sajedi, R. H., & Nikudel, M. R. (2016). Effect of injected bacterial suspension volume and relative density on carbonate precipitation resulting from microbial treatment. Ecological Engineering, 89, 49–55.

Sarda, D., Choonia, H. S., Sarode, D. D., & Lele, S. S. (2009). Biocalcification by Bacillus pasteurii urease: A novel application. Journal of Industrial Microbiology and Biotechnology, 36(8), 1111–1115.

Shahrokhi-Shahraki, R., Zomorodian, S. M. A., Niazi, A., & O'Kelly, B. C. (2015). Improving sand with microbial-induced carbonate precipitation. Proceedings of the Institution of Civil Engineers - Ground Improvement, 168(3), 217–230.

Sia, S. K., & Whitesides, G. M. (2003). Microfluidic devices fabricated in poly(dimethylsiloxane) for biological studies. Electrophoresis, 24(21), 3563–3576.

Siddique, R., & Chahal, N. K. (2011). Effect of ureolytic bacteria on concrete properties. Construction and Building Materials, 25(10), 3791–3801.

Smeets, P. J. M., Finney, A. R., Habraken, W. J. E. M., Nudelman, F., Friedrich, H., Laven, J., & Sommerdijk, N. A. J. M. (2017). A classical view on nonclassical nucleation. Proceedings of the National Academy of Sciences, 201700342.

Söhnel, O. & Mullin, J.W. (1982). Precipitation of calcium carbonate. Journal of Crystal Growth, 60(2), 239.

Soon, N. W., Lee, L. M., Khun, T. C., & Ling, H. S. (2014). Factors Affecting Improvement in Engineering Properties of Residual Soil through Microbial-Induced Calcite Precipitation. Journal of Geotechnical and Geoenvironmental Engineering, 04014006-1-11

Stocks-Fischer, S., Galinat, J. K., & Bang, S. S. (1999). Microbiological precipitation of $CaCO_3$. Soil Biology and Biochemistry, 31(11), 1563–1571.

Stumm, W., Morgan, J. J. (1981). Aquatic Chemistry. John Wiley, New York.

Stumm, W., Morgan, J. J. (1996). Aquatic chemistry, 3rd edition. New York: Wiley.

Teng, H. H., Dove P. M., & DeYoreo, J. J. (2000). Kinetics of calcite growth: surface processes and relationships to macroscopic rate laws. Geochim. Cosmochim. Acta 64, 2255–2266.

Tobler, D. J., Cuthbert, M. O., & Phoenix, V. R. (2014). Transport of Sporosarcina pasteurii in sandstone and its significance for subsurface engineering technologies. Applied Geochemistry, 42, 38–44.

Tobler, D. J., Cuthbert, M. O., Greswell, R. B., Riley, M. S., Renshaw, J. C., Handley-SidhuS., & Phoenix, V. R. (2011). Comparison of rates of ureolysis between Sporosarcina pasteurii and an indigenous groundwater community under conditions required to precipitate large volumes of calcite. Geochimica et Cosmochimica Acta, 75(11), 3290–3301.

Tobler, D. J., Maclachlan, E., & Phoenix, V. R. (2012). Microbially mediated plugging of porous media and the impact of differing injection strategies. Ecological Engineering, 42, 270–278.

Tohidi, B., Anderson, R., Clennell, M. Ben, Burgass, R. W., & Biderkab, A. B. (2002). Visual observation of gas-hydrate formation and dissociation in synthetic porous media by means of glass micromodels. Geology, 29(9), 867–870.

Tufenkji, N. (2007). Modeling microbial transport in porous media: Traditional approaches and recent developments. Advances in Water Resources, 30(6–7), 1455–1469.

van Paassen, L. (2009). Biogrout: Ground Improvement by Microbially Induced Carbonate Precipitation. PhD Thesis, Delft University of Technology.

van Paassen, L., Ghose, R., van der Linden, T. J. M., van der Star, W. R. L., & van Loosdrecht, M. C. M. (2010). Quantifying Biomediated Ground Improvement by Ureolysis: Large-Scale Biogrout Experiment. Journal of Geotechnical and Geoenvironmental Engineering, 136(12), 1721–1728.

van Paassen, L. A., Harkes, M. P., van Zwieten, G. A., van Der Zon, W. H., van Der Star, W. R. L., & van Loosdrecht, M. C. M. (2009). Scale up of BioGrout: A biological ground reinforcement method. Proceedings of the 17th International Conference on Soil Mechanics and Geotechnical Engineering: The Academia and Practice of Geotechnical Engineering, 3, 2328–2333.

Wang, Y., Soga, K. & Jiang, N-J. (2017). Microbial induced carbonate precipitation (MICP): the case for microscale prespective. Proceedings of the 19th International Conference on Soil Mechanics and Geotechnical Engineering, 1099-1102.

Warren, L. A., Maurice, P. A., Parmar, N., & Ferris, F. G. (2001). Microbially mediated calcium carbonate precipitation: Implications for Interpreting calcite precipitation and for solid-phase capture of inorganic contaminants. Geomicrobiology Journal, 18(1), 93–115.

Weibel, D. B., Diluzio, W. R., & Whitesides, G. M. (2007). Microfabrication meets microbiology. Nature Reviews, 5, 209–218.

Whiffin, V. S. (2004). Microbial $CaCO_3$ Precipitation for the production of Biocement. PhD Thesis, Murdoch University.

Whiffin, V. S., van Paassen, L. A., & Harkes, M. P. (2007). Microbial Carbonate Precipitation as a Soil Improvement Technique. Geomicrobiology Journal, 24(5), 417–423.

Whitesides, G. M. (2006). The origins and the future of microfluidics. Nature, 442(7101), 368–373.

Widdel, F. (2007). Theory and measurement of bacterial growth. Di Dalam Grundpraktikum Mikrobiologie, 1–11.

Wojtowicz, J. A. (1998). Factors affecting precipitation of calcium carbonate. J. Swimming Pool Spa Ind., 3(1), 18–23.

Wolthers, M., Nehrke, G., Gustafsson, J. P., & Van Cappellen, P. (2012). Calcite growth kinetics: Modeling the effect of solution stoichiometry. Geochimica et Cosmochimica Acta, 77, 121–134.

Wong, I., & Ho, C. M. (2009). Surface molecular property modifications for poly(dimethylsiloxane) (PDMS) based microfluidic devices. Microfluidics and Nanofluidics, 7(3), 291–306.

Yang, X. (2005). Three-Dimensional Characterization of Inherent and Induced Sand Microstructure, PhD thesis, Georgia Institute of Technology.

Yoon, J. H., Lee, K. C., Weiss, N., Kho, Y. H., Kang, K. H., & Park, Y. H. (2001). Sporosarcina aquimarina sp. nov., a bacterium isolated from seawater in Korea, and transfer of Bacillus globisporus (larkin and stokes 1967), Bacillus psychrophilus (Nakamura 1984) and Bacillus pasteurii (Chester 1898) to the genus Sporosarcina as Sporosa. International Journal of Systematic and Evolutionary Microbiology, 51(3), 1079–1086.

Yoon, H., Valocchi, A. J., Werth, C. J., & Dewers, T. (2012). Pore-scale simulation of mixing-induced calcium carbonate precipitation and dissolution in a microfluidic pore network. Water Resources Research, 48(February), 1–11.

Zapata, A., & Ramirez-Arcos, S. (2015). A Comparative Study of McFarland Turbidity Standards and the Densimat Photometer to Determine Bacterial Cell Density. Current Microbiology, 70(6), 907–909.

Zhang, C., Kang, Q., Wang, X., Zilles, J. L., Müller, R. H., & Werth, C. J. (2010). Effects of pore-scale heterogeneity and transverse mixing on bacterial growth in porous media. Environmental Science & Technology, 44(8), 3085–3092.

Zhang, W., Ju, Y., Zong, Y., Qi, H., & Zhao, K. (2018). In situ real-time study on dynamics of microbially induced calcium carbonate precipitation at a single-cell level. Environmental Science & Technology, acs.est.8b02660.

Zhao, Q., Li, L., Li, C., Li, M., Amini, F., & Zhang, H. (2014). Factors Affecting Improvement of Engineering Properties of MICP-Treated Soil Catalyzed by Bacteria and Urease. Journal of Materials in Civil Engineering, 26(12), 04014094.

Zhao, S., Evans, T. M., & Zhou, X. (2018). Shear-induced anisotropy of granular materials with rolling resistance and particle shape effects. International Journal of Solids and Structures, 150, 268–281.

Zhou, G. T., Yu, J. C., Wang, X. C., & Zhang, L. Z. (2004). Sonochemical synthesis of aragonite-type calcium carbonate with different morphologies. New Journal of Chemistry, 28(8), 1027–1031.

Zhou, J., Ellis, A. V., & Voelcker, N. H. (2010). Recent developments in PDMS surface modification for microfluidic devices. Electrophoresis, 31(1), 2–16.

Zhou, J., Khodakov, D. A., Ellis, A. V., & Voelcker, N. H. (2012). Surface modification for PDMS-based microfluidic devices. Electrophoresis, 33(1), 89–104.